Characteristics of turbulence in free convection flow past a vertical plate.

Smith, Ronald Robin

CHARACTERISTICS OF TURBULENCE IN FREE CONVECTION FLOW PAST A VERTICAL PLATE

A Thesis submitted for the
Degree of
Doctor of Philosophy
in the
Faculty of Engineering
of the
University of London

by

Ronald Robin Smith

Queen Mary College

December 1972

ABSTRACT

An experimental and theoretical investigation of the turbulent free convection boundary layer on a vertical plane surface in air has been conducted.

The experimental investigation comprised observations of both the streamwise development from alaminar state to a 'fully developed' turbulent flow and the lateral structure of the turbulent flow at Grashof numbers up to 7×10^{10}. Measurements were taken of the probability density distributions of temperature and streamwise velocity as well as power spectra of these quantities. The results show that a periodic flow structure, present in the early stages of the transition, disappears as the intensities of temperature and velocity increase to a maximum in the mid-stage of the transition and then decay.

Observations in the 'fully turbulent' flow suggest that the flow has a lateral structure similar to that of a forced convection flow: a viscous sublayer with mean temperature profiles linearly dependent on the distance from the plate, a buffer layer which includes the maximum of mean velocity profiles, and a turbulent layer where the power spectra of temperature and velocity contain an inertial subrange.

The theoretical investigation comprised a study of the governing equations and the application of several turbulence hypotheses to the prediction of the boundary layer flow. Solutions for lateral profiles and for the streamwise development of velocity and temperature fields agreed reasonably well with experimental data although there was some disagreement on the heat-transfer rates. Energy balances of the mean kinetic energy and turbulence kinetic energy of the turbulent flow were also predicted.

Measurements of the flow were performed with a hot-wire anemometer and thermocouple sensor in conjunction with digital data processing. A large part of the work was devoted to the development of suitable data processing techniques.

ACKNOWLEDGEMENTS

The work reported in this thesis was carried out in the Department of Mechanical Engineering, Queen Mary College, University of London. It has been most satisfying to have the opportunity to learn through a stimulating research programme. Throughout the work I have benefited from the talents and counsel of many individuals.

I am grateful to Dr.R.Cheesewright who initiated this programme. His kind consideration, particularly in the later stages of this study, is warmly acknowledged.

I sincerely appreciate the friendship of Mr.G.Langer and the many refreshing discussions we have had. The advice that Dr.W.Jones offered during the early stages of the theoretical work is gratefully recognized.

I wish to express my thanks to Messrs.A.Thurston and H.Gray for their help in manufacturing the apparatus. The moral support which these men and Mr.I.Cartledge provided will be warmly remembered. I am also grateful to T.Storey and A.Thurston for preparing the photographs and to Mrs.G.Green for tracing several of the figures.

The help of Miss A.Davis in the reception of the Queen Mary College Computer Centre and the assistance of Miss G.Hall who designed the program control for the datalogger are sincerely appreciated.

I am very grateful to Mrs.Lynn Parry who so willingly typed this thesis.

I am most indebted to my parents for their love, for the inspiration that their lives have given me, and for their consistent encouragement throughout my education.

Much credit for the completion of this programme must be given to my wife who not only edited and typed the drafts of the thesis but also traced several of the figures. She has shared with me the valleys of discouragement found in research as well as the strange peaks of exultation.

TO MY PARENTS

AND

MY WIFE

LIST OF CONTENTS

LIST OF SYMBOLS

a	constant in Chapter 3
B	bandwidth defined in section 3.5.3.2
c	constant in Chapter 9
C	capacitance (section 6.4)
f	frequency
f_c	cut off frequency defined in section 3.4.2
f_x	function defined in section 9.3
F	flatness factor defined in section 3.5.2.
g	gravity
Gr	local Grashof number = $\frac{\rho^2 g\beta(T_w-T_G)x^3}{\mu^2}$
h	heat-transfer coefficient
J	variance of temperature defined in section 3.2
k	(i) Hinze's constant defined in equation (3.4)
	(ii) turbulence kinetic energy defined in section 9.2
K	(i) degrees of freedom (section 3.5.3.2)
	(ii) mean kinetic energy (Chapters 9 and 10)
l	(i) length of wire (Chapter 6)
	(ii) turbulence length scale (Chapter 9)
Nu	(i) Nusselt number of a wire defined in section 6.4
	(ii) Nusselt number of a plate defined in section 8.1
p(n)	probability density distribution (section 3.5.2)
Pr	Prandtl number
$P_{xx}(n)$	Power spectral density distribution defined in section 3.5.3.2
$\dot{Q}$	heat transfer from a hot wire
R	(i) resistance of a wire (section 6.4)
	(ii) turbulence Reynolds number (Chapter 9)
Ra^+	function of a Rayleigh number defined in section 2.3

Re	Reynolds number
$R_{x'y'}$	correlation coefficient $\overline{x'y'}/\sqrt{\overline{x'^2}}\sqrt{\overline{y'^2}}$
s(j)	data sequence defined in section 3.5.1
S	skewness defined in section 3.5.2
St	Strouhal number defined in section 3.6.1
t	time
T, T'	mean and fluctuating component of temperature
U, u'	mean and fluctuating components of velocity in x direction
U_B	buoyancy velocity $\equiv \sqrt{g(T_w-T_\infty)x/T_\infty}$
U_x, u_x'	velocity where x designates direction (Chapters 3, 6 and 9)
V	variance defined in section 3.5.2
V+v'	velocity in y direction (Chapter 8, 10)
w(j)	data window defined in section 3.5.3.2
W(n)	spectral window defined in section 3.5.3.2
x, y	coordinates
x_i	coordinates (Chapters 3, 6 and 9)
X(n)	linear Fourier coefficient sequence defined in section 3.5.3.1
X^P	probability moment defined in section 3.5.2
β	(i) yaw angle defined in section 3.3.2 (ii) non-dimensional mean temperature $\equiv (T-T_\infty)/(T_w-T_\infty)$
β'	non-dimensional deviation of temperature $\equiv \sqrt{\overline{T'^2}}/(T_w-T_\infty)$
γ	non-dimensional velocity in x direction $\equiv U/U_B$
γ'	non-dimensional deviation of velocity in x direction $\equiv \sqrt{\overline{u'^2}}/U_B$
δ_m	momentum thickness (Chapter 2)
ε	dissipation defined in section 9.2
ζ	non-dimensional distance defined in section 8.1
θ	phase angle defined in section 8.1.3

κ	velocity ratio defined in section 2.2.2
μ	viscosity
μ_t	turbulent viscosity (Chapters 9, 10)
ρ	density
σ	Prandtl number
σ_ϕ	turbulent Prandtl-Schmidt number defined in section 9.3
τ	shear stress
ϕ	non-dimensional power spectral density distribution defined in section 8.1.2

Subscripts

f	film
g	local condition
i	instantaneous
m	maximum
n	normal (section 3.3.2)
t	tangential (section 3.3.2)
w	plate
β	yaw
*	non-dimensional function of τ_w

LIST OF FIGURES

LIST OF TABLES

LIST OF PLATES

Note on Presentation

All Figures and Plates may be found at the end of the presentation unless they immediately accompany the text.

Tables are included at the end of the appropriate chapter.

CHAPTER 1

INTRODUCTION

Free convection, often called natural convection, is a common phenomenon in our world. In the flow of cold air from a window in winter or the steam rising from a cup of coffee, density differences within the fluid induce motion in a direction that tends to re-establish equilibrium. Many such motions involve both laminar and turbulent flow; for example, a plume of smoke can be seen to follow a short trajectory of organized motion before it undergoes a transition to the random motion of turbulence. Most laminar free convection flows have been adequately analysed, but turbulent motion, often present in the phenomena of interest to the engineer, presents a much more complicated problem. Although turbulent free convection flows have been studied since early in this century when they were considered in the design of refrigerated food storage, it is only recently that the design of heat exchangers in nuclear reactors, containers for liquefied gases, and cooling towers for power plants has demanded more detailed information on the behaviour of such flows.

The free convection flow past a vertical surface immersed in a stagnant pool of fluid represents one of the simplest configurations in which the characteristics of the flow may be observed. However, the flow structure is very complex since it is bounded by a solid surface and by a stagnant fluid. Furthermore, many of the significant processes which govern the structure of the flow occur near the solid boundary and are thus affected by both the solid surface and the main body of turbulent motion. Predictions of the flow in this important region are impaired because neither theoretical solutions founded on hypotheses of fully developed turbulence nor those for laminar flow are adequate. Moreover, in this

region very few experimental observations exist against which the accuracy of the predictions can be measured.

Extensive measurements of the velocities in this flow have not been made in the past, possibly because the very small magnitude of the velocities renders many anemometer techniques unsuitable and other anemometer techniques either possess undesirable temperature sensitivity characteristics or are labour intensive. The recent development of digital computing facilities does provide the opportunity to employ a thermoanemometer together with a thermometer for estimating the velocities. Moreover, the use of such a measuring system facilitates an extensive survey of the structure of the turbulent flow, because it provides the facilities to monitor the flow continuously and also several analyses can be performed on the same recorded data.

During the development of this project, the extent of the measurements was governed by the parallel development of the digital data acquisition system and associated data processing methods. For example, in the earlier stages of the work, only the measurement of temperature was possible because the velocity data could not be processed in real time and data recording facilities were not available. Later in the programme the spectral analysis was postponed until difficulties in the processing software had been removed. The final work comprised extensive measurements of the temperature and streamwise velocity in the free convection turbulent flow and also in the laminar and transitional states of the flow. These measurements included estimates of the probability density distributions and the power spectra of temperature, velocity and some of the covariances of these quantities.

In addition to the experimental examination of the flow, a theoretical investigation was conducted. Several turbulence hypotheses, two of which had been successfully used for the prediction of forced convection flows, were applied to the solution of the equations governing turbulent free convection flow. This work allowed the prediction both of quantities that could be compared to data observed in the experimental programme and of important processes that were too difficult to measure.

A review of the current knowledge of the turbulent free convection boundary layer and a formulation of the aims of the present experimental work are contained in the second chapter of this presentation.

Chapter 3 deals with the methods of measurement for free convection flow. The decisions leading to the selection of a thermometer and a thermoanemometer are given. Several methods of using digital data processing in conjunction with thermoanemometer techniques are examined and general principles of digital data acquisition are presented. Also included in this chapter is an extensive study of statistical analysis methods appropriate for use with digital processing.

Following the description of the experimental apparatus (Chapter 4), the instrumentation required for the study is set forth in Chapter 5. Also included is a consideration of those aspects of the analogue instrumentation, the digital instrumentation and the data processing programs which were pertinent to this research.

The development of a wind tunnel and a special anemometer suitable for the calibration of a thermoanemometer is recorded in Chapter 6. An assessment of the accuracy of the calibration is also given there.

The description of a typical set of experiments (Chapter 7) is followed by the results of the experimental investigation in Chapter 8. These findings are incorporated in two themes: the streamwise development of the flow and the lateral structure of the turbulent boundary layer. An overall summary of experimental results is also included.

The theoretical description of the boundary layer is next considered. Chapter 9 contains a review of past investigations, equations which describe the flow, and an assessment of turbulence models applicable to the flow. The results of the predictions are given in Chapter 10.

The conclusions of this presentation are summarized in Chapter 11.

CHAPTER 2

LITERATURE REVIEW

2.1. Introduction

The study of the free convection boundary layer along a vertical surface represents one of the classical problems of heat transfer. The laminar boundary layer flow for the case of constant surface temperature was experimentally investigated by Schmidt and Beckman in 1930 and the solution of the governing equations by Polhausen and by Ostrach (1952) confirmed their results. The first experiments on the turbulent boundary layer were conducted by Griffith and Davis (1922) who measured lateral profiles of temperature and of velocity as well as the local heat-transfer rates. However, the main interest of subsequent experimenters centred on the heat-transfer rates to the bulk fluid (Saunders (1936), Fujii (1959a)). Further details of the turbulent boundary layer were not available until Cheesewright (1968) measured the mean velocity and temperature profiles and Warner and Arpaci (1968) observed the mean temperature profiles. That the velocity measurements of Griffith and Davis show a remarkable agreement to those of Cheesewright is a tribute to their pioneer investigation.

Ede (1956) gave a comprehensive survey of the available knowledge of this boundary layer and Cheesewright (1966) extended the review to 1962. Although there was very little literature on the structure of the turbulent boundary layer when the author commenced this research programme (1969), several reports have now become available (1972). In order to present an effective summary of these reports, the following work is divided into discussions of the lateral profile characteristics of (a) time-averaged

temperature and velocity and (b) the fluctuations of these quantities. The chapter concludes with a review of some criteria which have been used to identify the beginning of 'fully turbulent flow'.

2.2. Lateral Profile Characteristics

2.2.1. Time-Mean Temperature Profiles

Most recent experimental investigations of the turbulent free convection boundary layer on a vertical surface have yielded data on the thermal characteristics. Mean temperature profiles on a boundary layer in air were reported by Cheesewright (1968), Warner and Arpaci, and Coutanceau (1969), and in water by Lock and Trotter (1968) and Vliet and Lui (1969). Fujii et al. (1970) have presented measurements in boundary layers of three fluids: water, a light spindle oil and a heavy lubrication oil. Although Pirvano et al. (1970) did not report their data for the mean temperature profiles of a boundary layer in air, they did claim substantial agreement with Cheesewright.

In general, there is good agreement between independent observations of mean temperature profiles in any particular fluid. However, it appears that the lateral distributions are influenced by the properties of the fluid (Fujii et al., Warner and Arpaci). The trend of this effect is analogous to the Prandtl number dependency observed in the profiles in a laminar boundary layer.

Measurements in the region very near the plate are of interest as there is some uncertainty about the transfer mechanisms for momentum and heat flux. Some investigators (Cheesewright (1968), Lock and Trotter) have doubted whether the concept of a sub-layer which is dominated by molecular transfers can be applied to free convection boundary layers. Others such as Fujii et al. have supported the concept because they observed that although

there were fairly large thermal fluctuations in the near-plate region, mean temperature profiles were linear. In a theoretical analysis of the boundary layer, Yang and Nee (1970) suggested that a viscous sub-layer with a non-linear velocity profile should exist. Kutateladze et al. (1972) have expressed a similar view.

Experimental evidence of the local structure of the flow near the plate is scarce; in fact, the only available measurements from which we can deduce the nature of this flow are those of the mean temperature (Warner and Arpaci, Cheesewright (1968), Fujii (1959), Vliet and Lui). The collation of these data by Vliet and Lui indicates that the region near the plate is not truly dominated by viscous mechanisms. However, because the only detailed study in this region was that of Warner and Arpaci and, because that data exhibit certain inconsistencies (discussion, Cheesewright (1968)), these conclusions are questionable. In two more recent studies, Fujii et al. and Pirvano et al. both observed linear time averaged temperature profiles which suggest that this flow region is governed by molecular action.

Measurements of temperature near the plate are prone to at least two experimental errors: the distance of the sensor from the plate is highly uncertain, and spurious responses of the sensor may be caused by the steep thermal gradients near the plate. In regard to the latter, constructional details of the probes may be important. Whereas most investigators decided to take the leads from the temperature sensor directly downstream, parallel to the plate for a short distance before guiding them through the layer, Warner and Arpaci chose to place the leads laterally along the isotherm for a short distance before mounting the wires on the ends of an 'L'-shaped boundary layer probe. Whether the differences in the various

correlations can be accounted for by these distinctions in probe configuration is difficult to assess. It is evident, however, that further detailed investigations of the near-plate region are required.

Even if the concept of a viscous sub-layer is applicable to free convection, the lateral extent of the layer and the stability of its structure are likely to be very dependent on the properties of both the fluid and the plate. There are several observations which indicate that variations of the plate conditions affect the flow conditions.

Fujii et al. observed that the fluctuations of plate surface temperature were maximum in the transition region, and then decreased to a level of $\pm$10% of the boundary layer temperature difference in the turbulent region. It appeared that these fluctuations were affected by large scale fluid movements in the flow. A similar observation was made by Vliet and Lui. They suggested that the slowly fluctuating plate temperature in the transition region indicated that the position of the breakdown of laminar flow was shifting. Fujii et al. suggested that a similar phenomenon would not be detected in a gaseous flow because of the relatively small thermal capacity of these fluids. This assessment concurs with the investigations of Gebhart (1969) in which he noted that the relative thermal capacities of the plate and of the fluid were quite critical in the development of instabilities in the laminar flow. In another study, Pirvano et al. observed that there was a correlation between the temperature fluctuations at 3 mm from a constant temperature plate and the fluctuations of heat flux through the plate.

The apparent correlation between the fluctuations of the plate conditions and of the flow properties indicates that the stability of the plate conditions affects the adjacent flow structure. In turn this suggests

that the physical properties of both the plate and the fluid must be included in any consideration of the characteristics of a viscous sub-layer in a free convection boundary layer.

2.2.2. Mean Velocity Profiles

In recent years there have been several investigations designed to supplement Griffith and Davis' data on the velocities in the turbulent boundary layer. Measurements in a turbulent free convection flow are difficult as the flow is highly non-isothermal having very low dynamic velocities and a possibility of instantaneous negative flow in the outer regions (Kutateladze et al.).

Various techniques have been used to measure the U component of velocity. Cheesewright (1968), Vliet and Lui used thermoanemometers, but whereas Cheesewright had to use non-simultaneous readings of signals from a thermometer and an anemometer, Vliet and Lui were able to record the two signals concurrently. Lock and Trotter used a quartz fibre anemometer similar to that used by Schmidt and Beckmann while Coutanceau was able to detect the flow with a pitot tube and an ultra-sensitive manometer. In contrast to the above techniques, Kutateladze et al. photographed the motion of aluminium tracers in the flow and analysed the loci of the particles.

A comparison of the mean velocity data is difficult because of the different boundary conditions at the vertical surfaces: all the studies in air used a constant temperature plate, while most of the experiments in liquids (Kutateladze et al. was an exception) used a constant flux surface. The absence of an established parameter to correlate the data further complicates any comparison: Coutanceau used a shear stress correlation; Kutateladze et al. proposed a Reynolds number relationship; and both

Cheesewright and Lock and Trotter used a form of the laminar buoyancy correlation. Vliet and Lui did not find any suitable correlation and presented their data normalised to the peak velocity.

Despite these differences, some similarities among the investigators' results are evident. Vliet and Lui have reported remarkably good agreement of the lateral distribution of their data with that of Cheesewright over the outer 90% of the boundary layer. If the data of Kutateladze et al. are presented in a form similar to that of Vliet and Lui (Figure 2.1), a slightly steeper correlation is obtained. Although this disagreement may reflect on the techniques of measurement employed, it is well within experimental error.

In Table 2.1, a collation of the observed values of the maximum velocities (U_m) from various experimental studies is presented together with an appraisal of the data. In order to correlate the data from various investigations, the present analysis follows the one used with laminar flows. The correlation γ_m, defined as

$$\gamma_m = \frac{U_m}{(g\beta\Delta T x)^{0.5}} \quad ,$$

describes the growth of a laminar boundary layer on a constant temperature plate and also on a constant flux plate if the local temperature difference is used for ΔT. However, γ_m is dependent on the Prandtl number of the fluid and in order to achieve a universal comparison, a correlation κ is defined as

$$\kappa = \frac{\gamma_m}{\gamma_\ell}$$

where γ_ℓ is the theoretical value for the maximum velocity of a laminar boundary layer flow if it existed at the conditions that apply to the flow

pertaining to γ_m. That is, κ is a measure of the growth of a free convection boundary layer compared to that of a corresponding laminar flow.

The analysis reveals that for all the available data on the constant temperature surface, the values of γ_m decrease towards 0.5. The only comparable data on the constant flux surface (Lock and Trotter) do not follow this trend.* The author cannot offer any explanation for the difference.

2.2.3. Temperature Fluctuations

Preliminary investigations of the thermal fluctuations were carried out by Cheesewright (1968), Hall and Price (1969), Lock and Trotter, and Fujii et al.

Cheesewright reported that the shape of the lateral profiles of intensity of thermal fluctuations is very similar to that of the mean velocity profiles. The normalised intensity had a peak value of 0.11 slightly to the plate side of the peak of his mean velocity profiles. Hall and Price reported a peak intensity of 0.12 in similar conditions.

Lock and Trotter reported some characteristics of the amplitude distribution. They observed that over the central portion of the layer the maximum and minimum extent of the fluctuations were of the same order of magnitude as the local temperature difference, and that the deficit and excess fluctuations with respect to the mean balanced each other. The symmetry of their probability distributions near the peak velocity confirmed this observation. In the outer region, the probability distribution was

---

*The data of Vliet and Lui could not be included in this analysis because a trip-rod was used to promote a premature development of the turbulent boundary layer.

extremely skewed towards the ambient temperatures while on the inner side of the velocity peak the distribution was very biased toward the plate temperature. The scale of the fluctuations diminished rapidly as the plate was approached.

Fujii et al. presented some data on thermal fluctuations which supported the above observations. These data reveal that over the outer 90% of the boundary layer there is a finite probability that the local temperature at any instance was equal to the ambient temperature, whereas the probability that the local temperature was equal to the plate temperature was only finite over the inner 2-3% of the layer..

2.2.4. Velocity Fluctuations

Examination of the available data for the intensity $\sqrt{\overline{u'_1{}^2}}$ (Kutateladze et al., Vliet and Lui) reveals that the intensity is fairly uniform over the outer region. Vliet and Lui reported that $\sqrt{\overline{u'_1{}^2}}$ grows linearly away from the plate to a peak near the maximum time-averaged velocity. In this region, their value of the correlation γ' equals 0.3*, which correspondsto the data from a forced boundary layer on a flat plate (Klebanoff (1954)). Vliet and Lui's estimate of the flatness revealed a Gaussian distribution over the outer part of the layer and a very peaked distribution near the plate. They cautioned that the data were only qualitative because the length of their samples (30-60s) was not enough to obtain ergodic data. In measurements in ethylene alcohol, Kutateladze et al. reported a maximum value of γ' equal to 0.35.

2.3. Transition from Laminar to Turbulent Flow

In literature on free convection turbulence, there has been only limited agreement about the beginning of 'fully turbulent flow'. For

---

*$\gamma' \equiv \sqrt{\overline{u'_1{}^2}} \Big/ U_m$.

example, the experimental study of Coutanceau was later identified as transition flow (Fujii (1970)).

Moreover, there is no accepted characteristic with which to identify this beginning. Kato et al. (1968) proposed that a ratio of the plate shear velocity (U_*), which is a measure of the energy dissipation at the plate, to the buoyancy velocity (U_B), which represents the potential energy of the flow, would be a suitable criterion. Although this correlation does predict the transition point of some experiments, there is as yet no wide-scale evidence which justifies its usage.

On the other hand, since heat-transfer data are most readily available, and since a transition step is often identifiable, the Nusselt-Grashof relationship has often been used as a measure of the change. However, even this criterion is fallible; Fujii et al. did not observe such a phenomenon in the development of turbulent boundary layers in oil. In Table 2.2 below, the major investigations and their upper limit of the reported data are tabulated. The heat-transfer data of Vliet and Lui and of Fujii et al. for constant flux conditions in water agreed that the transition region extended from Ra^+ = 3.0E+10 to 4.0E+10[/]. Vliet and Lui reported that Ra^+ did not give a good correlation of the transition data. For constant plate temperature the data of Fujii et al. suggested that the transition region extended from Gr*Pr = 1.0E+10 to 8.0E+10 (1.0E+9 < Gr < 8.0E+9). Other reports (Warner and Arpaci, and Fujii (1959)) detected a transition region given by 1.0E+9 < Gr < 1.0E+10. Finally,

---

/ $Ra^+ \equiv GrPrNu$.

Cheesewright (1968) and Pirvano et al. have both described four regions of the flow based on the local heat-transfer coefficient: the laminar, the transition, a developing turbulent region and a fully turbulent zone. The latter suggested that the transition zone is a function of the Prandtl and Grashof numbers, that the transition and developing turbulence zones overlap, and that the fully developed zone begins at about Gr = 5.0E+10.

It can be seen from this review that the qualitative evidence on the structure of the free convection boundary layer on a vertical plate is quite extensive. However, apart from measurements on the expected values of temperature and velocity and a few isolated observations of their intensities, very few quantitative estimates of the flow structure exist. Neither is there much evidence of the downstream development of the boundary layer nor of the lateral distribution of the amplitude and spectral characteristics of the temperature and velocity. It was the aim of this research programme to provide the experimental data necessary to overcome these deficiencies in our knowledge.

Table 2.1

Comparison of Reported Velocity Data.

Investigator	$Gr \times 10^{-10}$	$Ra \times 10^{-10}$	Pr	$U_m/(m/s)$	γ_L	γ_m	κ
Griffith and Davis (1922)	0.3	0.21	.72	0.60	0.55	0.28	0.51
Cheesewright (1968)	3.0-8.7	2.1-6.2	.72	0.45-0.65	0.55	0.28-0.30	0.53
Coutanceau (1969)	0.1-1.0	0.07-0.72	.72	0.47-0.71	0.55	0.54-0.34	1.0-0.62
Kutateladze (1971)	0.16-0.37	2.1-4.9	13.2	0.032	0.20	0.10	0.5
Lock and Trotter (1968)		0.31-0.68	11.0	0.08	0.22	0.64	2.9

Table 2.2

Comparison of recent investigations

Investigator	Fluid	Plate Condition		Upper Limit Ra	Observations	
		Constant Temp.	Constant Flux		Temperature	Velocity
Griffith and Davis (1922)	Air	✓		<2.1E+9	✓	✓
Cheesewright (1968)	Air	✓		<1.4E+11	✓	✓
Warner and Arpaci (1968)	Air	✓		<1.4E+11	✓	
Lock and Trotter (1968)	Water		✓	<8.4E+9	✓	✓
Coutanceau (1969)	Air	✓		<1.4E+9	✓	✓
Vliet and Lui (1969)	Water	✓		RaNu<1.0E+16	✓	✓
Fujii et al. (1970)	Water Spindle Oil Lubricating Oil	✓	✓	RaNu<1.0E+14	✓	
Pirvano et al.(1970)	Air	✓		<2.1E+9		
Kutateladze (1972)	Ethyl Alcohol		✓	<4.8E+10		✓

CHAPTER 3

METHODS OF MEASUREMENT

3.1. Introduction

Every experimental investigation of the turbulent free convection boundary layer flow is encumbered with difficulties of measurement: the low velocities render many anemometer techniques impractical; the thermal fluctuations complicate the interpretation of the signal from those anemometers which are suitable, and the low frequencies of turbulence demand that the observations be integrated over periods of several minutes.

With the recent development of extensive digital computer facilities, some of these difficulties can be alleviated. It is possible to create digital data records of the signals from both temperature and velocity transducers at rates well in excess of those required to resolve the highest significant frequencies of free convection turbulence. Since the effects of the temperature on the response of the anemometer can be determined for each set of data in the subsequent processing, these data can be transformed into sequences of temperature and velocity. Moreover, with digital methods, the processing can be tailored to suit the specific requirements of the application, which permits the optimum use of interpretive procedures. In addition to these advantages several different analyses can be performed on the same digital data sample*; hence, many hours spent in observing the flow may be eliminated. This is a true bonus which compensates for the frustrations of digital computing.

The present experimental investigation relied heavily upon the use of digital data processing techniques and much of this chapter is concerned

---

*In this thesis the meaning of the term 'sample' is restricted to an ensemble of data acquired in one continuous observation of the time history.

with the ideas underlying the use of such methods. Section 3.2 considers the measurement of temperature and the selection of a thermometer; section 3.3 presents a similar defence for the use of a thermoanemometer in conjunction with digital data processing. The discussion then leads to the general principles of digital data acquisition (section 3.4) and to the statistical analyses of random data sequences (section 3.5).

Section 3.5 is subdivided into two major parts, the first of which deals with the amplitude analysis of a random signal, while the second considers the analysis of the spectral characteristics of such a signal. Both topics are treated in considerable detail because I feel that there is a deficiency of literature (in a form useful to engineers) on these subjects and I hope that this presentation will serve as an introduction to the more difficult statistically-orientated literature which is available.

The chapter concludes (section 3.6) with a brief résumé of those aspects of measuring technique and data processing which are most important to the present investigation.

3.2. Measurement of Temperature

The temperature of a flowing fluid can be measured by many methods but only two need be considered in the present context. The first is to measure the temperature directly with a sensing element which has a small thermal capacity and will therefore quickly assume the local fluid temperature. Two such sensors are the resistance wire and the thermocouple. The resistance wire depends on the thermal sensitivity of the resistance of a filament of fine wire; the thermocouple relies on the e.m.f. generated from the temperature difference between the two junctions of a loop of dissimilar metals.

The second approach is to derive the temperature from a measurement of the convective heat transfer from a heated element to the flow. One example of this approach is the use of a set of parallel hot wires. In order to distinguish between the influences of the fluid velocity and temperature on the convective heat transfer, the wires are operated at different overheat ratios.

The resistance wire and the parallel hot-wire arrangement have both been used in non-isothermal flows because of their relatively high frequency response. However, the significant frequencies of free convection turbulence rarely exceed 100 Hz so that a sensor with a relatively low frequency response could be considered for the present application. The thermocouple is an ideal sensor in several respects: most thermocouples respond linearly; their calibrations are very stable; and a high gain d.c. amplifier is the only instrumentation required to condition the output signal for further data processing.

It was desirable that the thermocouple be as robust as possible, and yet be small enough to respond to the highest frequency of the temperature fluctuations. A simple estimate of the heat transfer from a spherical bead 25 μm in diameter indicated that a thermocouple of this size would have a response well in excess of 200 Hz. Two simple experiments supported these calculations. The first was a measurement of the time response of a thermocouple to a step response in temperature under static conditions. The results agreed with the calculation. The second was the measurement of a spectrum of thermal fluctuations well downstream of a flame from a small bunsen burner. In this experiment the highest frequency detected was 120 Hz which indicated either the absence of spectral distribution above this value or else the presence of attenuation caused by the sensor. In either case,

the choice of chromel-alumel thermocouples with 12.5 μm lead wires to measure the local temperature in a turbulent free convection boundary layer was justified. These thermocouples were mounted in boundary layer probes designed specially for this study (see Appendix A).

3.3. Measurement of Velocity

3.3.1. Selection of a Velocity Sensor

The small magnitude of the velocities (less than 1 m/s) together with the possible occurrence of short periods of negative flow in the free convection boundary layer imposed severe restrictions on the selection of an anemometer. Conventional impact tubes are insensitive to the low dynamic head of the flow and do not respond to instantaneous velocity fluctuations. Techniques such as the photography of tracer particles or the use of a quartz fibre anemometer (an instrument which requires the measurement of the deflection of a fibre cantilever) are labour intensive and are not readily applied to an extensive survey of turbulence.

When this project commenced there were very few anemometers suitable for the measurement of turbulence. (The laser-doppler anemometry technique has developed since that time and is attractive in that its response is insensitive to temperature.) The only anemometer extensively used for the measurement of turbulence was the hot-wire anemometer. Although there have been successful applications of the thermoanemometer to non-isothermal flows (Adriko (1970), Hinze (1959)), its use in free convection flows has been questioned. Warner (1966) and Kutateladze et al. have argued that the turbulence of the flow is too intense and that the velocities are too low for the use of this anemometer. On the other hand, Colak-Antic (1964), Cheesewright (1966), Vliet and Lui (1970) and Dring and Gebhart (1969b) have chosen to employ this instrument. The criticism that the intensities are too

high is probably valid for the outer regions of the flow. However, Vliet and Lui observed an intensity of 0.3 near the maximum mean velocity which would make flow measurement with a single wire sensor just possible (Cheesewright (1972)).

The response of a hot-wire anemometer to low velocities can be considered in the light of two other investigations. From the data of Collis and Williams (1959) on the heat transfer from a hot wire in a horizontal flow, it appears that a wire (5 μm diameter, 200 K overheat) would have adequate sensitivity for use with velocities greater than 0.06 m/s. In another study, Hatton, James and Swire (1970) examined the heat transfer from a cylinder in a flow parallel to the buoyancy forces, as well as in horizontal and downward flows. If their data relating to a 100 μm cylinder in upward flow are extrapolated to include a 5 μm wire, the result suggests that the hot-wire anemometer could be used to sense velocities down to 0.10 m/s. (However, such a large extrapolation must be treated with some reserve.) Although these reports offered an assurance that the response of the hot-wire anemometer would be sufficient, the details of the technique had to be examined for compatibility with the requirements of this project.

The principle of the hot-wire anemometer is that the velocity of the fluid past the hot-wire element can be related to the heat transfer from that element. The wire, which is rigidly fixed between two supports, is usually a few microns in diameter and one or two millimetres in length. Although the anemometer can be operated in a mode where a constant current is passed through a wire and the measurement of the resistance of the wire allows the heat transfer to be calculated, it is most often used in a constant temperature mode with the resistance of the wire (and so the wire temperature) kept constant by controlling the voltage across it. This mode has a better

frequency response (not an important factor in this study) and a greater ease of operation.

Velocity data from the hot-wire response in non-isothermal flows are not easily resolved: a serious disadvantage of the anemometer is that heat transfer from the wire is dependent on the temperature difference between the wire and the flow as well as the flow velocity. The necessary additional information relating to the temperature of the flow may be obtained from either an element sensitive only to the local temperature (e.g. a thermo-couple or a resistance thermometer) or a second hot wire parallel to the first. (These arrangements were discussed in section 3.2.) Thus, with the use of a hot-wire anemometer in non-isothermal flows, each velocity estimate requires the interpretation of at least two signals.

The response of the hot wire is rarely interpreted from theoretical relationships because the unique history of each wire, the possibility of contamination by dirt in the flow and small differences in the wire properties make a general description of the heat transfer from a wire difficult. Instead, the anemometer's signal is interpreted from a calibration in a known flow. The extent of this calibration may range from the measurements of two or three points up to the measurement of tens of points in order that the constants of a characteristic cooling equation can be determined. However, if the response of the anemometer in a non-isothermal flow must be precisely known, a calibration comprising several hundred measurements may be required to cover a desired range of temperature and velocity. Such a process could prove to be very time-consuming. Furthermore, the calibration of a hot wire is difficult over the required range of velocities; hence the need to perform it over a range of temperatures as well bears heavily against the use of this anemometer technique. But

the technique does provide a continuous monitor of the flow. Further, with two or more wire elements, each uniquely orientated in the flow and connected to its own anemometer, it offers a means of resolving the velocity components of the flow (see Hinze). These features encouraged the use of the hot-wire anemometer in the present study; however, another major factor requiring consideration was the compatibility of the signal processing method to the demands of the programme.

Frequently when the hot-wire anemometer is used in isothermal flow, analogue instruments are used to perform arithmetic operations such as addition and multiplication and mathematical procedures such as integration and differentiation. This form of data processing is such an integral part of the hot-wire technique that some of the anemometer practices arise from the requirements of analogue processing. For instance, the calibration data are usually correlated by a power law, a form which is most compatible with analogue linearisers. In another instance, the two wires of a cross-wire array are positioned at angles of $\pm$45 degrees respectively to the mean flow direction in order that calculations of the correlations of the two signals may be simplified.

Such practices do not detract from the accuracy of the hot-wire anemometer measurements in many fluid flows. Indeed, the use of analogue processing is very advantageous to an experimental investigation. Since the signal is monitored continuously, the credibility of the measurements may be assessed, and if an unexpected event is recorded, the set-up can be verified and the peculiar nature of the signal can be immediately examined in more detail. Many of the useful statistical measurements of a random signal (at frequencies > 5Hz) can be made using analogue instrumentation. This includes the calculation of probability distributions, moments, correlation

functions and power spectra. Furthermore, analogue circuitry has been developed to suit specialised analyses.

However, some features of analogue data processing restrict the extent of the analysis and limit the scope of application of the hot-wire technique. For example, the response of analogue instruments to low frequencies (<3Hz) is unsatisfactory for a study in free convection turbulence. Another major difficulty arises because only the time averaged variances of the signals can be measured by analogue techniques. This fact has made it necessary to use linear approximations of the response equations in order to resolve the various flow observations. The use of the small turbulence approximation, as it is often known, is valid for many cases. (For details, see Hinze, Bradshaw.) However, the analysis of non-isothermal flows is severely impeded by this approximation. The combined effects of temperature and velocity on the response of the anemometer must be separated from the time averaged measurements by subsequent calculations; only the double and triple covariances which can be extracted from a set of independent, linear, time averaged response functions can be determined (Hinze, Adriko).

The development of digital equipment has provided an alternative technique for processing the data. Many of the difficulties occurring in the processing of signals by analogue methods are not manifested in digital methods because of the capability to resolve estimates of the 'instantaneous' flow properties from each data set. For measurements in non-isothermal flows, the signals of a hot-wire anemometer and temperature sensor can be sampled over a period long enough to resolve the lowest frequency of interest and subsequently can be transformed into time histories of temperature, effective cooling velocity (if a multiwire system is employed, the velocity components), and any crossproduct of these components. These time histories

can then be analysed by standard statistical techniques. Moreover, since the spectral resolution is governed by only external parameters (the digitization rate and the sample period), there is no difficulty in measuring the low frequencies of the free convection turbulence.

Not only is the ability to analyse the entire signal improved with digital data processing, but the examination of particular features of the time history of the signal is also facilitated. For example, one feature of particular interest in the study of turbulent boundary layers is the irregular interface between the fluid within the layer and the fluid outside; a sensor at a fixed point within this flow region will be intermittently exposed to the turbulence of the flow. In a form of analysis often called conditional or selective sampling, a flow property is sampled and averaged only during that portion of time when the selected condition (usually a threshold level of a flow property) is satisfied. However, it is not the extended features of digital data processing which enabled the use of the hot-wire anemometer in this work, but those features which allowed the ability both to resolve various flow properties from the 'instantaneous' data observations and to integrate over a time scale of several minutes.

In the expectation that the technique would have to be exploited to the lowest limit of its range, the hot-wire anemometer was selected as the velocity sensor in this investigation. The probes designed specifically for this research programme are described in Appendix A.

Several investigators have recently reported the use of digital data processing in conjunction with hot-wire anemometers. Often in such usage the digital processing has simply followed current analogue practice. Details of some of these investigations can be found in reports by Miller

(1966), Bearman (1968) and Luxton et al. (1966). Other investigators have used this form of processing to extend the scope of their analyses of turbulence; three good examples of such work are given by Van Atta and Chen (1969a, 1969b) and Frenkiel and Klebanoff (1967). Still other experimenters have considered the extension of the range of flows to which the hot-wire anemometer in conjunction with the digital data processing can be applied (Singh and Railley (1971), Cheesewright (1972)). From these reports it appears that there are no established methods of digital data processing and, further, that little attention has been given to the possibility of optimizing the processing methods in order to obtain the maximum benefit from their use. The remainder of this section is concerned with various ways of implementing digital data processing techniques with this problem of optimisation in mind.

3.3.2. Heat Transfer from a Hot Wire

With digital data processing in mind, the relationship between the heat transfer from a hot wire and the flow could potentially be expressed in several forms. Before these forms are discussed, however, it may be useful to review the heat-transfer characteristics of a hot wire. In isothermal flows, the heat transfer is effected primarily by the velocity component normal to the wire but also by the flow parallel to the wire. The response of the wire to the direction of the normal component is insignificant and is neglected in this work. With these general features in mind, the overall characteristics of the heat transfer from a single hot wire can be easily visualized (Figure 3.1). In this Figure, Re_n and Re_t are the non-dimensional velocity components, normal and parallel to the wire respectively; Nu is the Nusselt number.

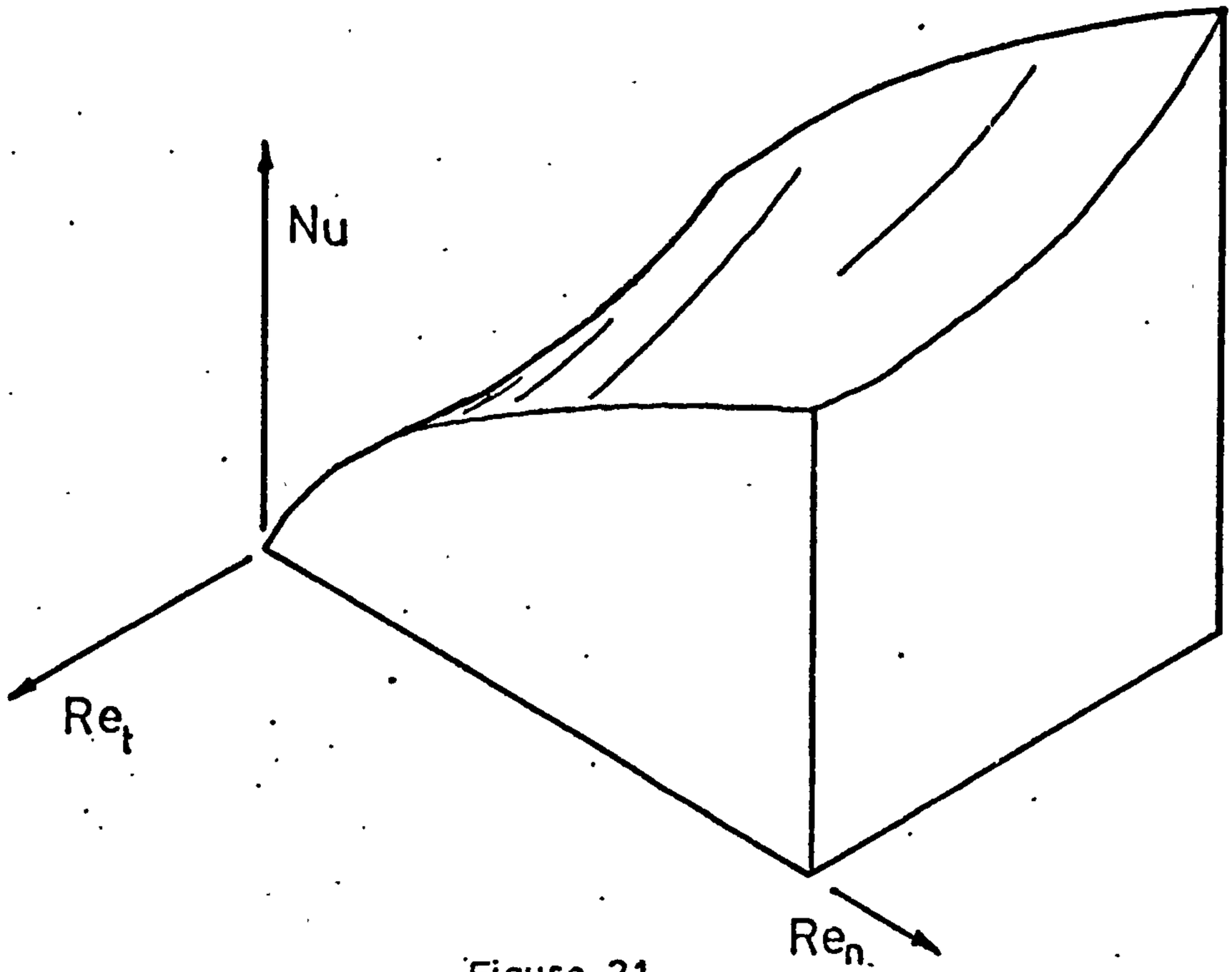

Figure 3-1

The concept is easily extended to include non-isothermal flows: the variations in fluid temperature generate a family of cooling surfaces. The larger the temperature difference between the wire and the fluid, the greater will be the heat transfer. Current practices in hot-wire anemometry employ unique one-dimensional functional representations of the relationship between the heat transfer, the velocity and temperature. With the use of digital techniques, other functional representations, such as multi-dimensional functions or another form of description, may provide a more accurate interpretation of these heat-transfer surfaces. Some possibilities are considered briefly below.

The most direct technique, one which promises an accurate presentation of the hot-wire response, is the creation of an orderly calibration array from the 'raw' data. The nodal points may be determined by the interpolation of the local data points. With such an approach, the

representation of the yaw cooling characteristics for a single wire at all yaw angles $|\beta| < \pi/2$ should be feasible, as disturbances such as interference from supports would be included as part of the calibration. However, such an approach would require an intensive calibration of the sensor over the desired range of velocities, temperatures and yaw angles and, in many cases, the cost would be prohibitive. Limited use of the inter-polation technique in conjunction with other approaches may be feasible where greater flexibility is required to describe the heat-transfer characteristics near conditions of zero velocity and in flow nearly parallel to the wire.

Instead of an interpolation routine, it may be expedient to describe the heat-transfer surfaces (Figure 3.1) by means of a two-dimensional function in the form

$$Nu = f(Re_n, Re_t) .$$

Once an expression of the correct form had been determined, it would only be necessary to use a least square regression to adjust the coefficients of this function for any calibration data set. The author doubts whether this approach would yield a more accurate description than the current use of one-dimensional functions.

Neither of these forms offered sufficient incentive to justify their use in the present investigation; instead, the adoption of current practices, which had received thorough investigation and were readily implemented, was very attractive.

Current practices seek to collapse the family cooling surfaces into a single characteristic shape with the Reynolds number, the Nusselt number and a temperature weighting factor as the parameters. A mark of the success

of this research is that the normal response of an anemometer is correlated by equations such as that proposed by Collis and Williams:

$$Nu\left(\frac{T_f}{T_g}\right)^{-0.17} = A + B\,Re_n^m \quad . \tag{3.1}$$

The present use of the power law correlations of this type is probably based on a similarity to King's law and on the use of analogue linearisers, which often use a presentation of the characteristics in the form of a simple power law. Recent trends (Siddall and Davies (1972)) suggest that the equation

$$Nu\left(\frac{T_f}{T_g}\right)^{-0.17} = a_o + a_1 Re_n^{0.5} + a_2 Re_n \quad , \tag{3.2}$$

where a_i, $i = 0,1,2$ are constant coefficients, represents the data over an extended range. As the operative form of the calibration function is the inverse of the above, an algebraic expression, possibly a polynomial function such as

$$Re_n = a_3 + a_4 Nu_M + a_5 Nu_M^2 + a_6 Nu_M^3 \quad , \tag{3.3}$$

where $Nu_M \equiv Nu\,(T_f/T_g)^{-0.17}$ could be expected to give the same accuracy of fit over a similarly extended velocity range.

Attempts to obtain a universal description of the yaw characteristics by an empirical law have been only partially successful. Several expressions (Cosine, Hinze (1959), Brun and Davies (1968)) purport to describe the heat transfer over the restricted range, $|\beta| < \pi/3$. For larger yaw angles, it is probable that the finite length of the wire and the influence of the probe supports serve to make the calibration of each probe configuration unique. In digital processing, some account for these influences can be taken by making the coefficients in the empirical laws

dependent on the local flow conditions. For example, at very low velocities, the shape of the yaw characteristic is velocity dependent (Baille (1971)). This feature could be incorporated into the empirical cooling law of Hinze* by making the coefficient k a function of velocity (k(u)). (Also see Singh and Railley.)

The way in which a yaw cooling function is employed with digital methods requires closer examination. Hinze, Corrsin (1951) and Klatt (1968) concentrated their studies on the time averaged representation of the hot-wire response. However, with digital processing methods, the representation of the instantaneous response is desired. Furthermore, there may be some advantages in using crossed-wire arrays at angles of inclination other than $\pi/4$ or even in using non-symmetrical arrays (Singh and Railley). The use of tri-wire arrangements requires consideration of the angle of rotation as well as the angle of yaw. For these reasons a unified yaw coding function was developed; the derivation assumed the concept, proposed by Hinze, that the heat transfer is effected by two linear convective modes, that of normal cooling and that of tangential cooling, given by

$$\dot{Q} = \dot{Q}_n + \dot{Q}_t \quad .$$

Although the adoption of this principle does not demand the use of the Hinze cooling law, equation 3.4, it does appear to be the most suitable.

The use of spherical coordinates to describe the orientation of the wire element is given by Klatt. The hot wire is placed at the origin of a cartesian coordinate system orientated in the conventional fashion: the x_1 axis is along the dominant flow direction, U_1, and x_2 is along the secondary

---

* $$\frac{U_\beta}{U_n} = \cos^2\beta + (k \sin\beta)^2 \qquad (3.4)$$

where U_β is the effective cooling velocity, U_n is the normal cooling velocity, k is the Hinze coefficient.

flow U_2. The wire orientation is determined by the angles (α, ϕ). The angle α describes the rotation of the wire with respect to the axis x_1 and the angle ϕ gives the rotation of the wire with respect to the $x_1 - x_2$ plane as shown in Figure 3.2.

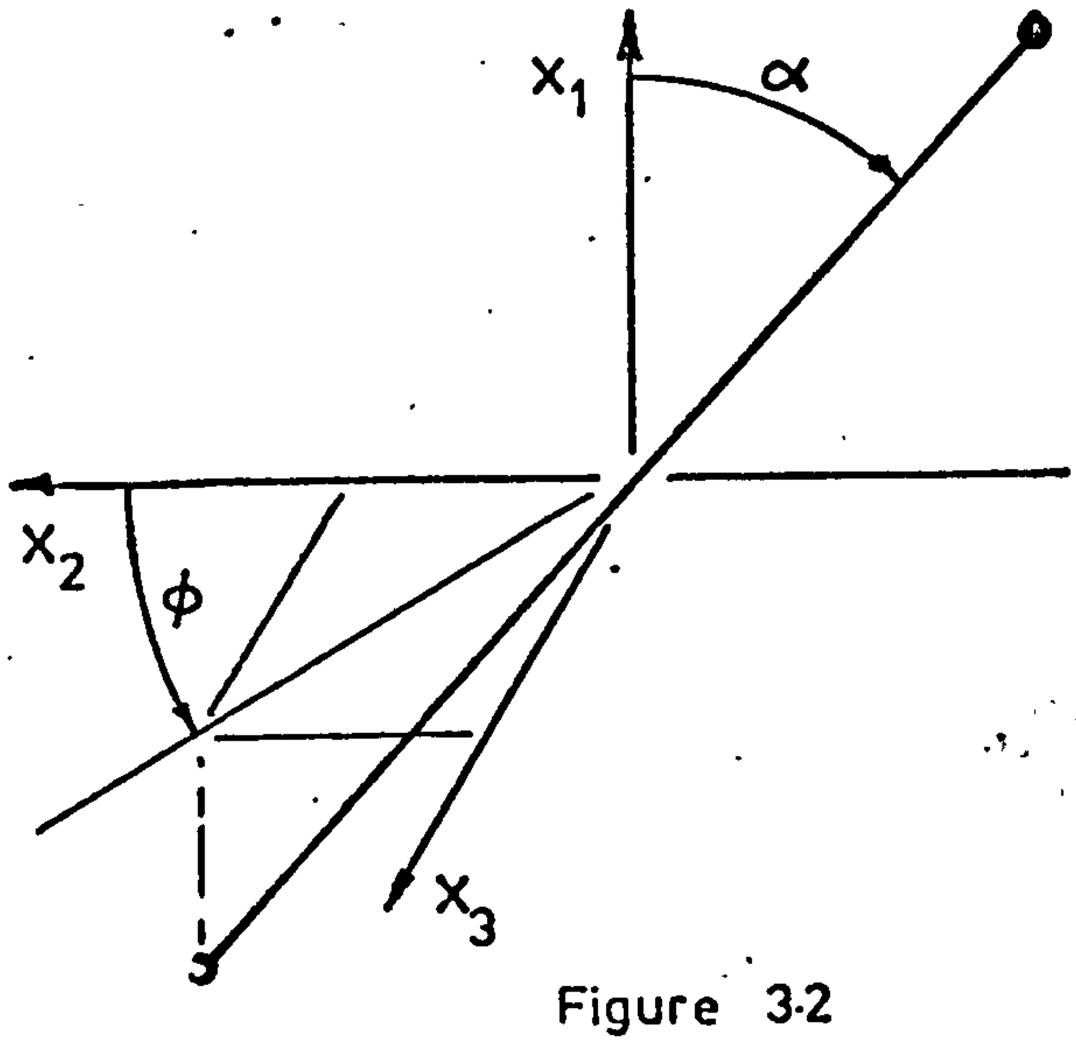

Figure 3.2

Let m be a unit vector in the direction of the instantaneous velocity given by

$$\underline{m} = \frac{U_1}{U_i}\underline{i} + \frac{U_2}{U_i}\underline{j} + \frac{U_3}{U_i}\underline{k} \quad \text{where} \quad U_i = (U_1^2+U_2^2+U_3^2)^{0.5}$$

and let $\underline{\ell}$ be a unit vector along the wire. The yaw angle defined as the angle between the normal plane of the wire and the instantaneous velocity is given by

$$\beta = \cos^{-1}(\underline{\ell}.\underline{m}) \qquad \text{(see Fig.3.3)} \quad .$$

The normal and tangential cooling components U_n and U_t of the velocity are given by

$$U_n = U_i\cos(\beta), \qquad U_t = U_i\sin(\beta) \quad .$$

With the substitution for the angle β, the normal component can be expressed in coordinate components by

$$U_n^2 = (U_1 \sin\alpha \cos\phi - U_2 \cos\alpha)^2 + (U_3 \cos\alpha - U_1 \sin\alpha \sin\phi)^2$$
$$+ (U_2 \sin\alpha \sin\phi - U_3 \sin\alpha \cos\phi)^2 \qquad (3.5)$$

and the tangential component by

$$U_t^2 = (U_1 \cos\alpha + U_2 \sin\alpha \cos\phi + U_3 \sin\alpha \sin\phi) \qquad (3.6)$$

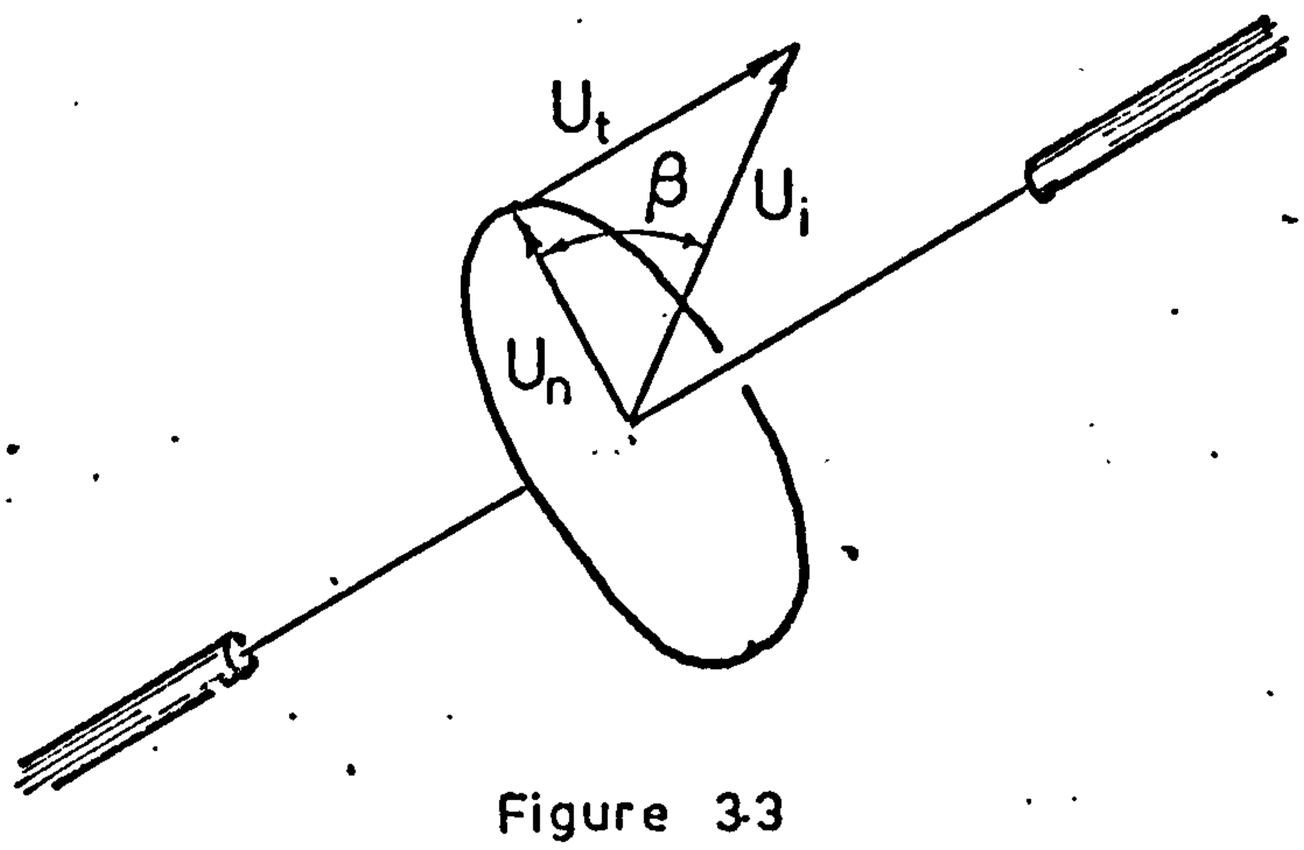

Figure 3.3

Note that in the above equations, no velocity component is neglected as shown by

$$U_i^2 = U_n^2 + U_t^2 = U_1^2 + U_2^2 + U_3^2$$

In accordance with equation (3.4) the estimate of effective cooling velocity is given by

$$U_\beta^2 = U_n^2 + (k\, U_t)^2 \qquad (3.7)$$

where U_β is the effective cooling velocity.

With the appropriate expressions substituted for U_n and U_t, this expression describes the yaw cooling characteristics of a single wire orientated at an arbitrary angle to the flow. It is, however, restricted to the same limited range of values of β as the Hinze law, eq.(3.4).

3.3.3. Interpretation of Hot-Wire Anemometer Signals

From the generalised equation (3.7) for the effective velocity of a hot wire, the response of various combinations of hot-wire sensors can be examined. The wire arrays most commonly used are the single wire (because of its simplicity) and the crossed-wire array (because of its simple directional sensitivity). The interpretation of data from arrays with additional wire elements is an extension of the principles employed in this section.

3.3.3.1. Single Hot Wire

Let a hot wire A be orientated along the x axis ($\alpha_A = \frac{\pi}{2}$, $\phi_A = \frac{\pi}{2}$).

The effective cooling velocity is given by

$$U_{\beta,A}^2 = U_1^2 + U_2^2 + (kU_3)^2 \qquad (3.8)$$

In order that the equation can be solved, normal cooling (i.e., $k = 0$) must be assumed. Then the simplified equation describes a cylinder with its axis along the wire element and may be thought of as the revolution of the normal cooling velocity vector about the wire (Figure 3.4).

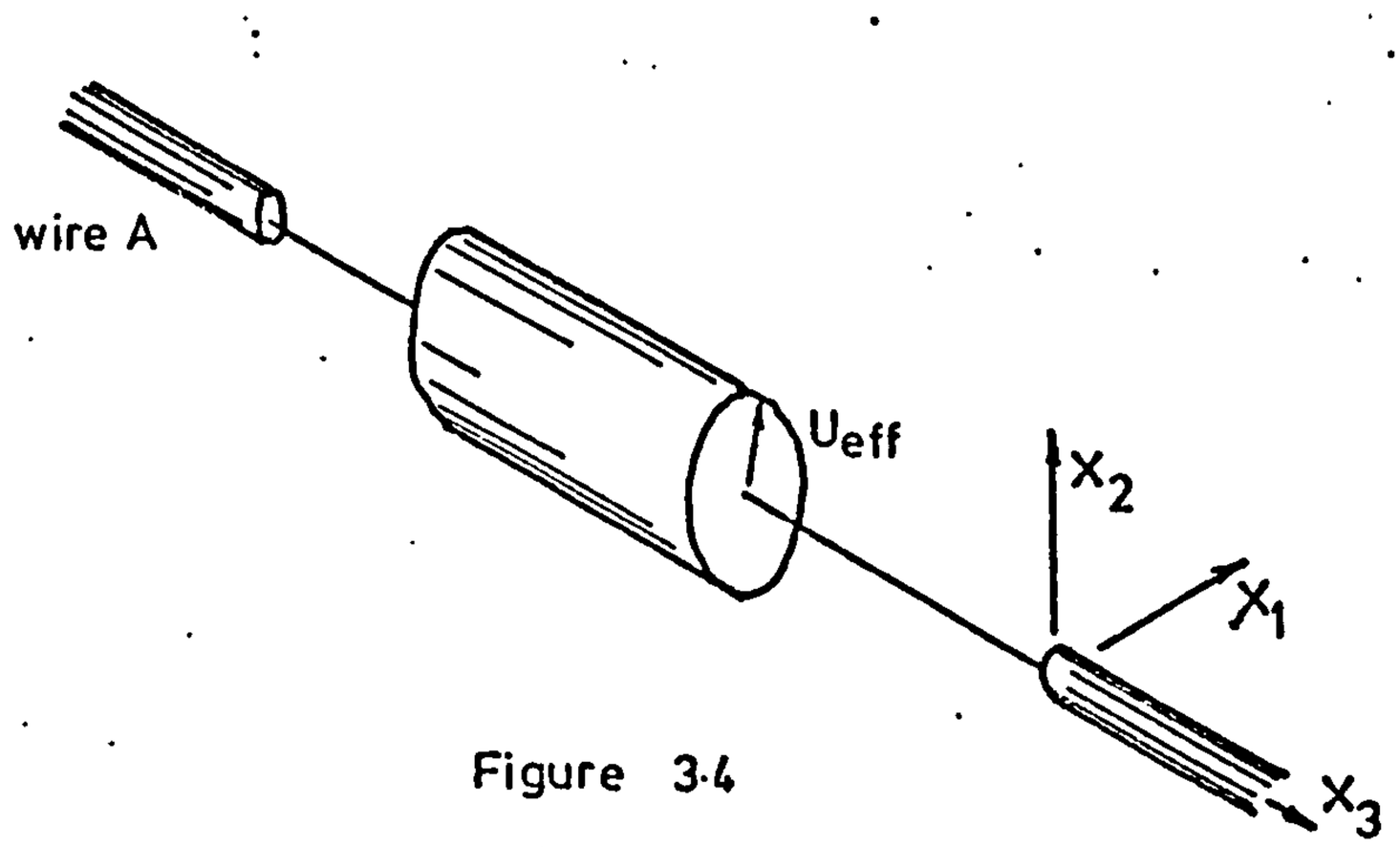

Figure 3.4

This result arises from the assumption that the hot wire is insensitive to the direction of the normal flow. To close the equation, further assumptions about the relative magnitudes of U_1 and U_2 must be made and usually U_2 is neglected. Thus, since assumptions which are identical to those made with analogue signal processing must be employed, digital data processing does not improve the accuracy of the velocity resolution of a single wire anemometer.

3.3.3.2. Crossed-Wire Arrays

For crossed wires B and C in the $X_1 - X_2$ plane ($\phi_B = 0$, $\phi_C = \pi$), two independent equations are generated :

$$U^2_{\beta,B} = (U_1 \sin\alpha_B - U_2 \cos\alpha_B)^2 + U_3^2 + k^2(U_1 \cos\alpha_B + U_2 \sin\alpha_B)^2 \qquad (3.9)$$

$$U^2_{\beta,C} = (U_1 \sin\alpha_C - U_2 \cos\alpha_C)^2 + U_3^2 + k^2(U_1 \cos\alpha_C + U_2 \sin\alpha_C)^2 \quad . \qquad (3.10)$$

In this form, the system is indeterminate; three components cannot be resolved with two equations. If the right-hand side of each equation is expanded, it can be seen that the effective velocities are most strongly affected by the two velocity components in the sensor plane. Thus, with the neglect of the U_3 component, the error of interpretation with digital processing is not identical to the error in analogue processing but is of the same order of magnitude.

With the assumption of normal cooling ($k = 0$), the yaw equations may be simplified to a set of linear equations:

$$U_{\beta,B} = U_1 \sin\alpha_B - U_2 \cos\alpha_B \qquad (3.11)$$

$$U_{\beta,C} = U_1 \sin\alpha_C - U_2 \cos\alpha_C \quad . \qquad (3.12)$$

This set of equations describes the surfaces generated when the two normal cooling components are rotated about their respective wires in the χ_1-χ_2 plane. There are four roots in the solution; if α_B and α_C are equal to $\pi/4$, there are two pairs of symmetrical roots reflected about the wire axes. However, if k is given a finite value, that is, if the Hinze cooling law is employed, then the system becomes a set of well-behaved, homogeneous, second order equations. It may be solved numerically by an extended form of Newton's itinerative technique (see Appendix B). Again, there are four roots to this set of quadratic equations; only one set of the roots, however, portrays the conditions within the flow. The ambiguity rests with the hot wire's insensitivity to the pitch angle: the reflections about the wire axis cannot be distinguished.

The selection of the realistic root must be made on a priori knowledge of the flow. (One criterion may be that U_1 should be positive.) It is possible that an examination of the statistical properties of a short segment of data from each root would distinguish the realistic solution.

3.3.3.3. Data Processing Algorithms

The purpose of the set of response functions is to transform the signals from the set of anemometers into estimates of the flow velocity. At least two algorithms can be used to compute the transformation. A straight-forward approach is to solve the set of equations for each successive point of the heat-transfer data. However, a difficulty exists if an iterative technique such as Newton's method is used. When the solution of a particular root is solved using the information of the previous data as an initial approximation, it is imperative that there be no errors in the recording of the data samples because if a segment of data is discarded (e.g., recording faults), there is no assurance that the same root

will again be selected unless, of course, the sets of roots have contrasting statistical properties.

In an alternative approach this problem is overcome. All the solutions for one particular root are tabulated in a transformation array and then the data are interpreted from these predetermined values. This technique is realisable since the sampled data are discrete and so a finite number of solutions exists. Furthermore, the number of elements in the transformation array may be less than the maximum number of possible combinations of the data, either because the transform of the data may vary slowly and several adjacent elements could be grouped to avoid redundant data, or because the uncertainty of the transformation function is greater than the full accuracy to which discrete data can be resolved. It is probable that an array of up to twenty thousand points would be sufficient for most applications. This value is not unreasonable in view of the large computers available for data processing and it does present a substantial economy in computational time as the total number of transformations used is likely to be in excess of one million.

An efficient retrieval of the information from this array can be achieved if attention is given to the array access routines and the storage of the elements. In place of the popular access routine where the data sample is recursively compared to a sequence until the location of the appropriate solution is determined, an efficient routine can be used in which the array indices are calculated directly from functions that scale the data values*. With this technique, the evaluation of these scaling functions is the only computation necessary for each set of data. Regarding the storage of data, it is possible to store multi-component solutions in one location

---

*c.f. section 3.5.2.1.

for ease of access and economy in storage. This is accomplished by expressing the component values in an integer form, scaling them by an appropriate order of magnitude, and adding the exclusive numbers. In the retrieval of an element, an unscrambling routine may be used that includes division by the scaling factor to obtain a quotient and remainder.

Each algorithm emphasizes a different efficiency of computation. With the use of the tracking algorithm, many repetitious calculations with little demand on core storage are performed; with the use of the calibration array algorithm, there is an economy in calculation but a heavy requirement on core storage. The most appropriate algorithm for an application may be selected in view of machine configuration, cost economy and turn around service.

3.4. Digital Data Acquisition

Having selected a thermometer and an amemometer and considered the methods of interpretation of the 'raw' data, the general principles of digital data acquisition can now be examined. Each digital data point is acquired from the electrical signal of an instrument (i.e., an anemometer) by a high speed analogue-to-digital converter (ADC) which observes the signal for a brief time (a typical aperture time is 10 μs), and then forms a binary representation of the voltage. The accuracy of the binary data is an inverse function of the number of binary bits. (The round off error is given as 2^{-n} where n is the number of binary bits; e.g., for an eight bit binary scale, the signal to noise ratio is 256:1.) The round off error, often called the quantitization error, is included in the data as digital noise. The acquisition of digital data does not require any special alteration to the mode of operation of the anemometer, but it does need a proper conditioning of the analogue signal so that it is compatible with the ADC.

3.4.1. Analogue Signal Preparation

The basic requirement of the analogue conditioning system is that it should adjust the dynamic part of the data signal to span the full scale of the analogue-to-digital converter. Typical conditioning consists of d.c. amplification to scale the signal, zero suppression to remove the constant part of the signal, and frequency filtering to attenuate as much of the extraneous noise as possible. Low pass filtering is used to eliminate electronic noise and other unwanted high frequency signals whereas high pass filtering is employed to remove low frequency signals in cases where only an analysis of the dynamic signal from a sensor having a linear response function is desired.

3.4.2. Digitization Rate

Digital data may be acquired either by observing the continuous analogue signal at irregular intervals according to a random sampling technique or by sampling the signal at equispaced intervals. The latter technique makes subsequent time analysis of the data much easier and is the only method considered here.

Sampling at equispaced intervals, however, may lead to a problem known as aliasing. This problem is not present in analogue processing; it arises because the signals of frequencies at multiples of two may be superimposed on the same equispaced data points (Figure 3.5). If the sampling frequency. is $1/\Delta t$, the spectrum of useful data will be from $\frac{1}{T}$ to $1/2\Delta t$ (where T is the sample period) and the frequencies above this range will appear to be folded into the lower range. The frequency $1/2\Delta t$ is called the Nyquist or cut-off frequency (f_c) (Blackman and Tukey (1958)).

In the digitization of data by this method, an appropriate sampling rate must be selected - one which avoids the acquisition of redundant,

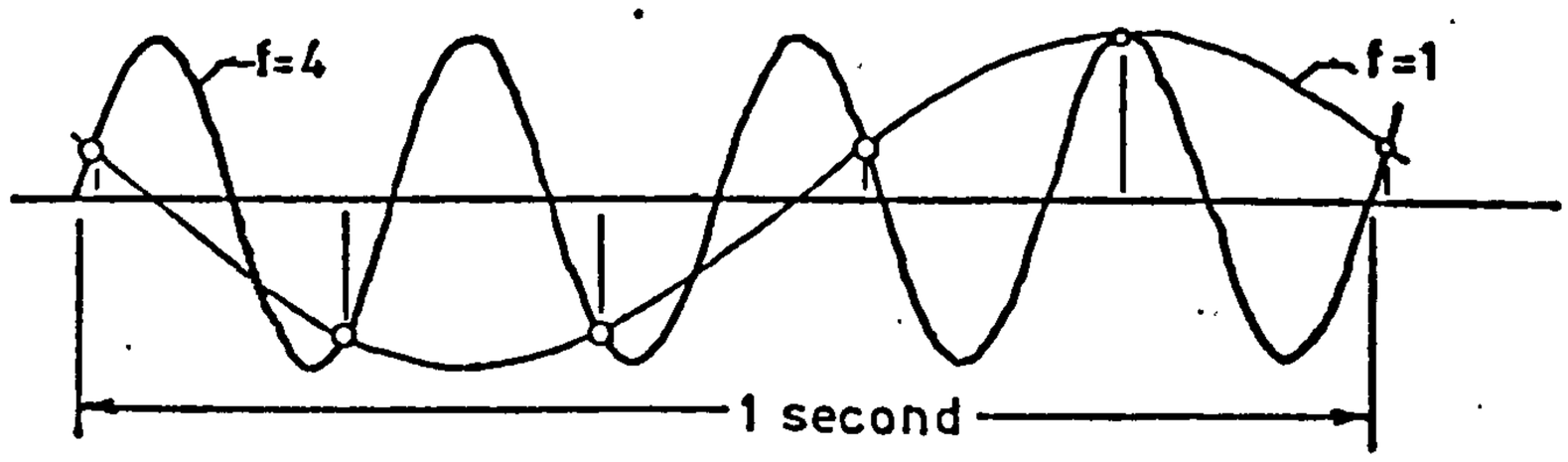

(from Blackman and Tukey)

Figure 3.5

correlated data (by sampling at excessively high rates) and of aliased data (by sampling at very low rates). This rate or its f_c may be determined by one of two methods. According to the first, f_c is chosen to exceed the maximum resolved frequency (f_{max}) in the signal, which avoids the danger of high frequencies folding into the useful spectrum. The alternative approach involves restrictingthe passage of information by low pass filtering. In this case, f_c is set to a value slightly above the low pass filter frequency. No firm relationship between the uppermost resolved signal frequency and f_c is known to exist; however, for the requirements of spectral analysis, f_c may be set very nearly equal to f_{max} (Bendat and Piersol (1966)).

3.5. Statistical Analysis of a Random Scalar Function

3.5.1. Introduction

In contrast to laminar flow which is organised and predictable, turbulent flow is random and unpredictable in detail. Similarly, whereas a signal from laminar flow can be represented by a mathematical function, a signal from turbulence has no recognizable pattern.. Because there is little need at present for information on the details of the turbulence, statistical distributions are used to describe the nature of the flow.

In this section we will consider a random scalar function of time, s(t), which may represent data of either temperature or velocity. The discrete form of s(t) is given by

$$s(j) = s(D + j\Delta t) , \qquad j = 0, 1, 2 \ldots N-1 \tag{3.14}$$

where D is the time datum for the data sample, Δt is the time interval between successive data points, and N is the number of data points. For many analyses it is convenient to consider the deviations x(j) from the ensemble average of s(j). This average, often known as the first amplitude moment, is given by*

$$\overline{s} = \lim_{N\to\infty} \frac{1}{N} \sum_{j=0}^{N-1} s(j) \quad . \tag{3.15}$$

The data sequence x(j) is obtained with a linear transformation

$$x(j) = s(j) - \overline{s} , \quad j = 0, 1, 2 \ldots N-1 \quad . \tag{3.16}$$

In fluid mechanics, this transformation is often known as Reynolds' convention. Both forms of data presentation are used in the following discussion.

The ensemble average is the value to which the arithmetic average of a data sequence converges as the number of observations increases (e.g., equation (3.15)). The concept of ensemble averaging is the essential principle upon which nearly all statistical analyses of a random function are based. The data sequence may be taken from the observations in one sample** of time history or it may be a collation of observations from many independent samples. In cases where the data display a characteristic

---

*In this chapter only, the overbar is used to denote an averaging procedure.

**In this thesis the meaning of the term sample is restricted to an ensemble of data acquired in one continuous observation of the time history.

variation with time (such as data that would be observed from the flow through an internal combustion engine), the statistical description of the flow properties for any particular time must be based on observations taken from many cycles of the flow.

In this instance, where the statistical descriptions are invariant with respect to time, the random process is said to be stationary. Furthermore, if the statistical description of the sample is identical to the description of the continuous process in time, then the process is said to be ergodic. Fortunately, many steady turbulent flows are approximately ergodic and the following description is restricted to the analytical techniques used to examine such processes.

Although a single time history sample is sufficient to describe an ergodic function, the problem of selecting a suitable sample period still remains. For computational efficiency it is desirable to average as few observations as possible while achieving the required accuracy of convergence. One complication in selecting a sample period arises because the convergence of the ensemble average of any of the amplitude moments (i.e., $\overline{X^p}$ where p = 2, 3, 4 ...) depends on the order of the correlation. Generally speaking, if the same degree of accuracy is to be maintained, the sample period must be extended as the order of the sample moment increases. It requires five times the amount of data to determine the fourth moment to a given precision as to estimate the second moment to the same precision (Lumley and Panofsky (1964)). However, the odd ordered moments tend to converge more slowly than do the even ordered ones. Thus there is no one sample length that will satisfy both the criterion of accuracy of convergence and that of computational efficiency. It can be said that the

sample period must be many times larger than the characteristic time scale of the random process but, in general, the selection of an appropriate sample period is still often based on the analyst's intuition.

In the discussion that follows, the statistical analysis of x(j) is considered and the joint analysis of two or more transformed functions is briefly mentioned. Although an exhaustive analysis of the joint probability distribution of amplitude and time would constitute a complete statistical description of x(j), Kawall and Keffer (1971) point out that such an analysis is computationally impractical, and that it would be difficult to interpret. Instead, the analysis of random data is divided into an analysis which is exclusive of time and a second analysis concerned with the time dependency of x(j). For studies in turbulence, the amplitude analysis and the power spectral density analysis are the most useful forms, and attention will be focused on these transformed representations of x(j).

3.5.2. Amplitude Analysis of a Scalar Function

A central concept in the amplitude analysis of a random signal is the probability distribution since it contains a complete description of the amplitude characteristics. The probability distribution may be regarded as a tabulation in a set of class intervals of the frequency with which a specific amplitude value of x(j) occurs. The ratio of the frequency count in each cell (n(k)) to the total number of observations is the probability that x(j) takes a value within the interval width of the cell.

The shape of the probability distribution can be described by the moments $\overline{x^P}$ where

$$\overline{x^P} = \frac{1}{N} \sum_{k=0}^{k=M-1} n(k)\, x^P(k) \quad , \tag{3.17}$$

M is the total number of classes and $x^p(k)$ is the value of the mid-point of the interval. These moments can also be calculated directly from the data sequence x(j) according to the formula

$$\overline{x^P} = \frac{1}{N} \sum_{j=0}^{N-1} x^P(j) \quad . \tag{3.18}$$

The even moments describe the width of the distribution, whereas the odd moments describe its symmetry. Very rarely are moments greater than the fourth order considered (Kendal and Stewart (1963)). The lowest even moment, (p=2) (for data with a zero mean, such as x(j)), is called the variance or the mean square of the fluctuations, and may be calculated from the transformed series by applying one of the above equations or from the data sequence s(j) with the following form:

$$V \equiv \frac{1}{N} \sum_{j=0}^{N-1} s^2(j) - \overline{s}^2 \quad . \tag{3.19}$$

The kurtosis, or flatness factor, is formed by a comparison of the fourth moment to the square of the second moment:

$$F \equiv \overline{x^4}/(\overline{x^2})^2 \quad . \tag{3.20}$$

For a Gaussian distribution, K is equal to three . The third moment, suitably normalised, is called the skewness factor:

$$S \equiv \overline{x^3}/(\overline{x^2})^{3/2} \quad . \tag{3.21}$$

If the distribution is symmetrical, all the odd moments are zero.

The analysis of the correlation functions of two or more data samples is merely an extension of the principles set out for the first order analysis. The joint probability distribution of two simultaneously sampled data sequences (x(j) and y(j)) is two-dimensional. Although the calculation of the joint distribution is simple, the interpretation is not straightforward. The moments of the cross products are given by

$$\overline{x^P y^q} = \frac{1}{N} \sum_{j=0}^{N-1} x^P(j) y^q(j) \qquad (3.22)$$

where q is the order of the moment of the distribution of y(j).

All the above amplitude moments are represented in the biased sample form, that is, they are influenced by the length of the finite sample. Corrections for this biasing are possible; the variance, for example, should be corrected by a factor of N/N-1. However, for data samples of over 1000 points, this particular correction is insignificant.

In computation the probability distribution of one function can be generated by several methods. One possible procedure consists of passing a series of amplitude intervals (i.e., windows) over the data and tabulating the number of points which falls into each interval. A second method involves selecting a data point and searching the class intervals for the appropriate cell. A third algorithm, which is the most efficient means of generating the distribution, eliminates the search routines. In this method, the index to the appropriate window, k, is calculated from a normalising function of the data point given by

$$k = \frac{x(j) - x_{min}}{x_{max} - x_{min}} M \qquad (3.23)$$

where x_{min} is the midvalue of the first cell

x_{max} is the midvalue of the last cell

and k is the nearest integer value of the function.

Then the counter of the class interval of that index would be incremented, viz., n(k) = n(k) + 1.

3.5.3. Power Spectral Density Analysis of a Scalar Function

3.5.3.1. Introduction

One of the most useful forms in which the time dependency of x(j) may be expressed is the power spectral density function (PSD). This function may be computed from x(j) in two basic ways. The first, known as the Blackman-Tukey method, depends upon the computation of the auto-covariance sequence of x(j). Since the auto-covariance sequence and the PSD are Fourier pairs, the PSD estimators can be obtained from the Fourier transformation of the sequence of auto-covariance coefficients. The second method is based on the direct transformation of x(j) to a sequence of linear Fourier coefficients. The PSD estimates are then formed from the squares of these coefficients. Known as the periodogram method, this means of calculating the PSD estimates is rapidly gaining a place of prominence in digital data processing, especially with the recent advent of the fast Fourier transform (FFT) as a method of computation (J.W.Cooley et al. (1967)).

The essence of all discrete power spectral analyses is the discrete fourier transform (DFT) defined by

$$X(n) = \frac{1}{N} \sum_{j=0}^{N-1} x(j) e^{-i(2\pi jn)/N}, \qquad n = 0,1,2 \ldots N-1 \tag{3.24}$$

and the inverse discrete fourier transform given by

$$x(j) = \sum_{n=0}^{N-1} X(n) e^{i(2\pi jn)/N}, \qquad j = 0,1,2 \ldots N-1 \quad . \tag{3.25}$$

Slightly different forms of these definitions are sometimes used but they vary only in the scaling factors.

The basic algorithm for computing the DFT, X(n), of a data sequence x(j) calculates the sum over all the data of the product of the amplitude x(j) and a Fourier weighting factor. Thus

$$X(n) = \sum_{j=0}^{N-1} x(j)\cos(\frac{2\pi jn}{N}) + i \sum_{j=0}^{N-1} x(j)\sin(\frac{2\pi jn}{N}),\ n=0,1,2...N-1 \ . \qquad (3.26)$$

Even though the basic DFT algorithm can be made computationally efficient, it has not been economical to compute the extensive Fourier transforms required by the periodogram method. Thus, in the past this lack of computational ability has hindered the use of the periodogram method although it was the first method to appear.

Instead, the Blackman-Tukey method was preferred in conjunction with the use of the basic algorithm because the method requires only that the Fourier transform be applied to a sequence of covariance coefficients, which is usually less than one-tenth of the length of the data sequence.

However, the recent introduction of the FFT has made practical the implementation of the periodogram method of data processing. Indeed, it can be faster to calculate the covariance coefficient sequence by first computing the PSD coefficients by the periodogram method, and then taking the inverse transform than it is to estimate the function by the more conventional sum of products. The success of the FFT algorithm depends upon the fact that it is computationally more efficient to transform two data sequences of N points and then merge the resulting coefficients than it is to transform one sequence of 2N points. The algorithm recursively subdivides the data sequence into a basic unit (usually to the base 2), performs the transform, and then constructs the new sequence of discrete transform coefficients.

3.5.3.2. Periodogram Method

In the periodogram method the PSD estimates of the time sequence data are formed from the squares of the coefficients of the discrete Fourier transform of the time sequence according to the formula

$$x(j) \rightarrow X(n)$$

$$\downarrow \qquad (3.27)$$

$$\frac{N\Delta t\ |X(n)|^2}{2\pi} = P_{xx}(n) \quad .$$

The conventions suggested by Cooley et al. are adopted: arrows to the right indicate a DFT and arrows directed downwards indicate ordinary arithmetic operations. The time interval, Δt, is usually set to unity during computation and then reintroduced to scale the estimates appropriately.

A major problem arising during spectral analysis of a data sequence is the effect of the finite sample length on the estimates of the PSD coefficients. At least two methods can be used to highlight this effect. According to the first method, the finite data sample is considered to be the product of an infinite series ($x_{inf}(j)$) and a step function of unit height with length equal to sample period. That is,

$$x(j) = x_{inf}(j)\ w(j) \quad \text{where} \quad w(j) = 1 \text{ for } 0 \leq j < N \qquad (3.28)$$

$$= 0 \text{ for } j < 0$$

$$j \geq N \ .$$

This function, w(j), is often known as the periodogram window. Ideally, it would transform into a spectral window W(n) of a similar shape. The spectral analysis of w(j) will reveal the extent to which W(n) approximates the ideal shape. The DFT of the periodogram window yields a sequence of linear coefficients, W(n), given by

$$W(n) = \frac{N \sin(\omega N/2)}{\frac{\omega N}{2}} \qquad n = 0,1,2,\ldots,N-1 \tag{3.29}$$

where $\omega = \frac{2\pi n}{N}$.

Estimates of the PSD coefficients of the window, $P_{ww}(n)$, are then obtained by equation (3.27) to give

$$P_{ww}(n) = \frac{N^2 \sin^2(\omega N/2)}{2\pi(\frac{\omega N}{2})^2} \quad . \tag{3.30}$$

Ideally, the shape of the spectral window is rectangular; the distortion present in $P_{ww}(n)$ is effected by the finite length of the sample.

The second way to examine the effect of the necessary truncation of the infinite sequence is to compare a sequence of covariance coefficients of an infinite series to that calculated from the finite data sequence. (This derivation is extracted from Cooley et al.). The discrete PSD function $P_{xx}(n)$ and the covariance function $\gamma(k)$ are well known to be a Fourier pair (Blackman-Tukey) where

$$P_{xx}(n) = \frac{1}{2\pi} \sum_{k=-\infty}^{k=+\infty} \gamma(k) \cos(\omega k) \; .$$

Similarly, the periodogram estimator $\hat{P}_{xx}(n)$ and the sample covariance function $\hat{\gamma}(k)$ are also a Fourier pair where

$$\hat{P}_{xx}(n) = \frac{1}{2\pi} \sum_{k=-N-1}^{k=N-1} \hat{\gamma}(k) \cos(\omega k) \quad .$$

The sample covariance function which is defined by the relation

$$\hat{\gamma}(k) = \frac{1}{N} \sum_{j=0}^{N-k-1} x(j)x(j+k)$$

is a triangular function of the true covariance function, viz.,

$$\hat{\gamma}(k) = (1 - \frac{k}{N})\gamma(k) \quad .$$

Thus the periodogram can be seen to be the convolution of the triangular function and the true covariance function:

$$\hat{P}_{xx}(n) = \frac{1}{2\pi} \sum_{k=-N-1}^{N-1} (1 - \frac{k}{N})\gamma(k) \cos(\omega k) \quad .$$

Hence, the periodogram coefficients are the product of the PSD estimates of the infinite series and the transform of a triangular function. This triangular function may be considered as a data window; its transform is given by

$$P_{ww}(n) = \frac{N \sin^2(\omega N/2)}{2\pi(\frac{N\omega}{2})^2} \qquad (3.31)$$

for large values of N (Cooley et al.). Equation (3.31) which is identical to (3.30) describes the PSD distribution of the basic periodogram window.

The basic periodogram window, shown in Figure C.1 as a part of the presentation in Appendix C, cannot be used to generate accurate PSD estimates. Although the statistical bandwidth* of $P_{ww}(n)$, given by

$$B = 1.5/N\Delta t \quad ,$$

is comparable to the ideal bandwidth

$$B_{ideal} = 1/N\Delta t \quad ,$$

the total area of the window which represents the true PSD is not concentrated in the primary lobe. Large side lobes constitute a considerable leakage of power. Moreover, it is not possible to increase the accuracy of the estimates (which may be measured by the variance of the

---

*Equivalent statistical bandwidth is that bandwidth of a hypothetical rectangular window that would give the similar statistical characteristics as the actual window when the input is white noise (Bendat and Piersal (1966)).

distribution of the spectral window) by increasing the length of the sample. In fact, the estimates converge in distribution to a chi-square random variable on two degrees of freedom and therefore are not suited to the production of reliable estimates of the PSD coefficients.

In order to generate accurate PSD estimates, the variance of the spectral distribution must be decreased. This result can be achieved in two ways. The data window can be modified in order to limit power leakage in the side lobes or else several adjacent estimates can be averaged to obtain an increased convergence of the PSD estimates.

All data windows suitable for power spectral analysis suffer from side lobe leakage; however, by selecting an appropriately shaped data window, this leakage can be limited. Instead of using a rectangular data window, a parabolic or triangular window or some other function can be used to modify the data sequence. Although the side lobes of the power spectral window are attenuated, the shape of the data window is distorted (see appendix C). Thus, the selection of an appropriate data window is clearly a compromise between one, such as the periodogram, that has good temporal, but poor spectral characteristics, and one that has reasonable characteristics in both domains.

Correcting for the large variance of the periodogram estimates involves yet another compromise. Any improvement in the accuracy of the estimates diminishes the spectral resolution of the estimator. Two forms of ensemble averaging are used to improve the reliability. In one method several adjacent estimates are averaged. This averaging technique is known as rectangular smoothing because the unit weighting factor is employed. The secondary (smoothed) spectral estimator is given by

$$P_{xx}'(m) = \frac{1}{q} \sum_{k=m}^{k=m+q} P_{xx}(k) \qquad m = 0,1,2,\ldots,N-1 \quad . \tag{3.32}$$

If the frequency spacing ($\Delta f = 1/N$) of the primary estimates is less than that of the half power width of the primary window, then the secondary window will be almost flat over the central region, with side lobe characteristics of the primary window as shown in Figure 3.6.

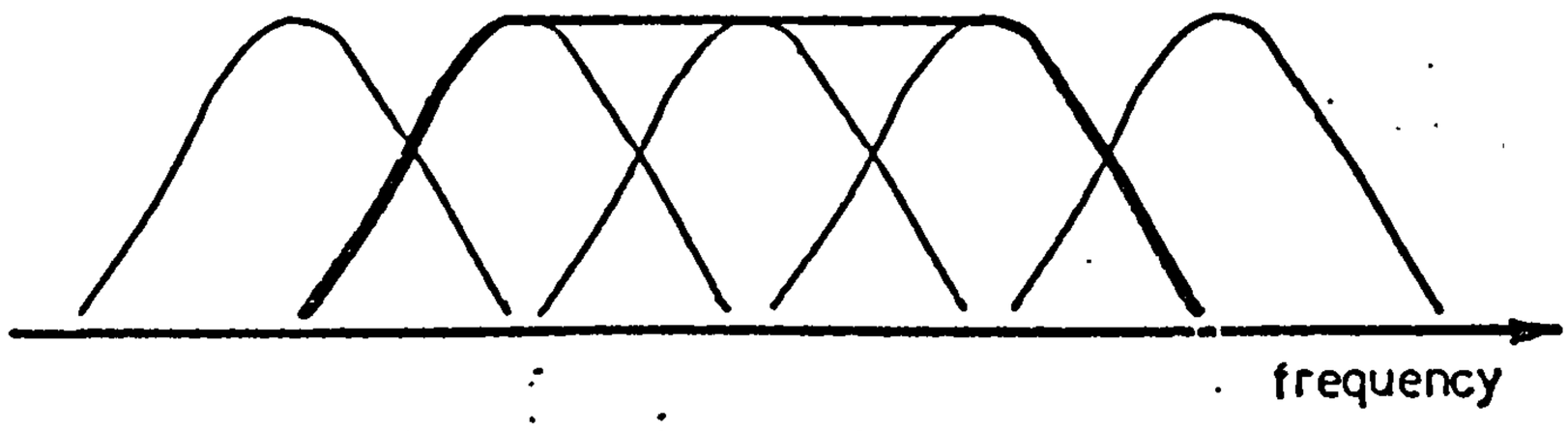

Rectangular smoothing

Figure 3.6

The bandwidth of the secondary window is given by

$$B' = q\Delta f + B \quad .$$

The secondary PSD estimator converges in distribution to chi-square random variable on K' degrees of freedom where K' is proportional to the number of intervals averaged and is given by $K' = 2q$.

As an alternative to rectangular smoothing, time averaging over short data segments is sometimes used to improve the accuracy of the PSD estimates (Welch (1967), Kinns (1971)). This method involves sub-dividing the time sequence into a number of smaller segments and ensemble-averaging the periodograms of the segments. The number of segments (R), the length of the segment (L), and the length of the data record N are related by the inequality

$$RL \leq N \quad .$$

Periodogram estimates are calculated for each segment

$$P_{xx_r}(n) = L\, x_r(n) + X_r(n) \quad \text{where} \quad 0 < n < L-1$$

$$0 < r < R-1$$

and then averaged

$$P_{xx}''(n) = \frac{1}{R} \sum_{r=0}^{R-1} P_{xx_r}(n) \quad . \tag{3.33}$$

The final estimates will have a bandwidth B'' which is proportional to the number of data segments

$$B'' = \frac{1.5}{L} = B\, R \quad ,$$

and the increased precision for these estimates will converge in distribution to a chi-square random variable on K'' degrees of freedom where K'' = 2R.

One advantageous feature associated with the short data segment technique is the capability of transforming long data sequences on a small computer. Also, as Welch pointed out, fewer computations may be required to obtain the final results than would be needed with a single periodogram of an equivalent length.

In practice, a modified data window, ensemble averaging over short segments, and rectangular smoothing are all used. The final data window has a bandwidth B* given by

$$B^* = 9RB+$$

where B+, the bandwidth of the modified window, is a function of B and has an estimate with a distribution which converges to that of a chi-square random variable on K* degrees of freedom where

$$K^* = 9RK+ \quad .$$

K+ is the degree of freedom of the modified data window.

3.5.3.3. Joint Power Density Distributions

Estimates of joint power spectral density functions can be generated by the periodogram method in a manner similar to that followed by the calculation for a single time sequence x(j). Two simultaneous data sequences, x(j) and y(j), are transformed and the raw joint PSD estimates are formed from taking their product as shown by

$$x(j) \rightarrow X(n)$$

$$y(j) \rightarrow Y(n)$$

$$\downarrow$$

$$\frac{N\Delta t}{2\pi} X(n)Y(n) = P_{xy}(n) \quad .$$

As in the case of a single data sequence, modified data windows and ensemble averaging can also be used to improve the reliability of these estimates.

3.5.3.4. Programming Details

Certain details concerned with the programming of an FFT package for a periodogram analysis may be helpful*. In most cases the FFT package is programmed to accommodate a complex data sequence. Since many data records are strictly real, it is a distinct advantage to compute the discrete Fourier transforms of two temporal records simultaneously. It can be shown that if x(j) and y(j) are regarded as the real and imaginary parts, respectively, of z(j), i.e.,

$$z(j) = x(j) + iy(j) \quad , \tag{3.34}$$

then the transform Z(n) is a linear sum of the two transforms X(n) and Y(n), i.e.,

$$Z(n) = X(n) + iY(n) \quad . \tag{3.35}$$

---

*Cooley, Lewis and Welch (1967) give a comprehensive summary of general uses of the FFT routine.

The complex transform Z(n) must be unscrambled in order to obtain the two transforms of the individual data records (which are complex in themselves). The equations (3.34) and (3.35) outline the calculations which are necessary in order to unscramble Z(n).

$$X(n) = \tfrac{1}{2}\{Z(n) + Z(N-n)\}$$

$$= \tfrac{1}{2}\{[Re(Z(n)) + Re(Z(N-n))]^2 + [I_m(Z(n)) + I_m(Z(N-n))]^2\}^{0.5} \qquad (3.36)$$

Similarly

$$Y(n) = \tfrac{1}{2}\{Z(n) - Z(N-n)\} \quad .$$

Since the DFT has a period of N, the unscrambling routine need be applied only for n = 0,1,2,...,N/2 and this operation may be performed in the same core store.

If PSD estimates are desired at finer intervals than the frequency spacing, $\Delta f = 1/N\Delta t$, the periodogram window can be effectively applied more often. The data series is augmented by zeros so that $N+N_z$ equals 2^p for some integer p where N_z is the number of zeros.

The DFT of the extended series generates a finer grid of primary estimates with a spacing f(n) given by the relation

$$f(n) = \frac{n}{(N+N_z)\Delta t} \qquad \text{for} \qquad n = 0,1,2,\ldots,(N+N_z)/2 \quad .$$

The bandwidth of the spectral window has not been altered; however, the estimates must be properly scaled (Figure 3.7).

3.6. Conclusions

In this chapter, the consideration of a thermocouple and a hot-wire anemometer as suitable sensors for the measurement of free convection flow led to the examination of the merits of signal data processing methods.

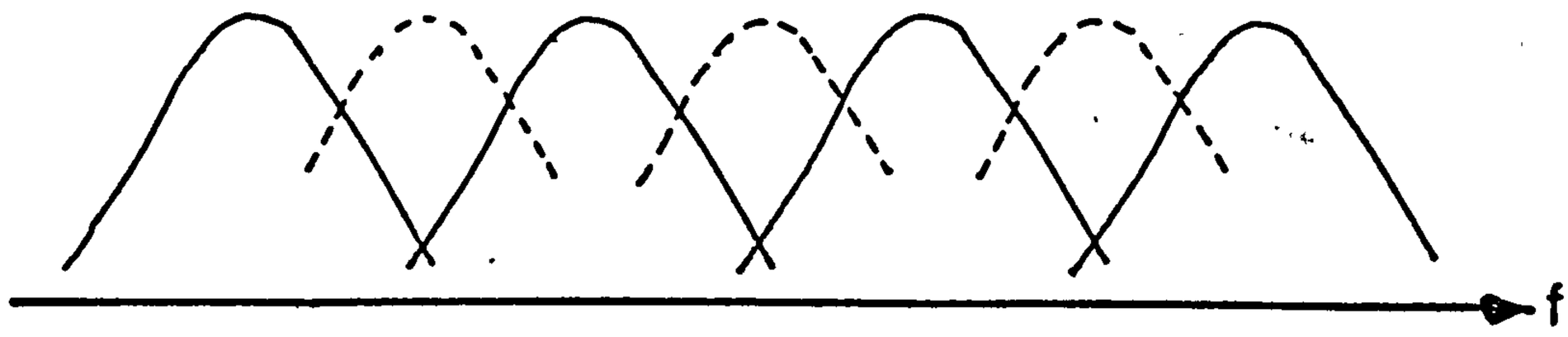

Figure 3.7

Low frequencies and variable temperature of the flow complicate the use of the analogue methods with these two sensors. The employment of digital data processing techniques, on the other hand, was very attractive: each set of data could be transformed into velocity and temperature. In conjunction with digital data processing, the hot-wire anemometer + thermocouple arrangement was selected as the means of flow measurement.

Although alternative methods of employing digital data processing with the hot-wire anemometer were explored, the use of empirical functions for the representation of the normal and yaw cooling was adequate for this study. In reviewing current practices, alternative formulations of these functions were suggested and many of them are adopted in the digital data processing programs found in Appendices F, G and H. These programs were designed to employ either of the two algorithms considered for the data transformation.

In the examination of principles of digital data acquisition, it was reported that the use of equispaced sampling techniques facilitated the analysis of the data but that it also gave rise to a problem known as aliasing. The applications of many of the principles discussed here are presented in Chapters 5 and 7.

Following the discussion about the generation of digital data sequences, analysis methods were considered for the amplitude and time dependency characteristics of the data. Whereas data processing for the amplitude analyses was straightforward, spectral analyses processes were more complicated. Details of these methods, particularly the application of the FFT routines to power spectral analyses, are considered further in Chapter 5 and Appendices F, G and H.

CHAPTER 4

THE VERTICAL PLATE AND TRAVERSING GEAR

4.1. The Vertical Plate

One distinction of an investigation into the development of a free convection boundary layer along a vertical plate is that only a heated (or cooled) plate is needed to generate the flow. The plate may be either cylindrical, as in the case of Fujii et al., or plane, as used by most investigators. Regardless of the form of the plate, it is enveloped by the fluid. In this research programme, a plane plate situated in a small room was used. Air was the ambient fluid.

The vertical plate, 0.6 m wide × 2.75 m high, was constructed for the investigation of Cheesewright (1966). It consisted of several electrical heating elements sandwiched between two sheets of 12 mm duralumin and thus had two working surfaces. The plate was manufactured in three sections: the bottom section was 1.55 m high, the middle and top sections were each 0.6 m high. Only one of the surfaces was used in this research project.

The electrical elements were arranged so that the bottom section had five small heaters whereas the middle and top sections each had one large element. Additional heaters along the leading and trailing edges permitted control over the heat transfer in these regions. Each of the nine elements was regulated by a variable voltage transformer which in turn was supplied from a stabilised power transformer.

A turbulent framework supported the plate 0.25 m from the floor leaving a space of 0.5 m between the trailing edge and the ceiling.

Side walls of Perspex 0.26 m wide extended, normal to the plate surface, from the edges of the plate over its full length.

The temperature of the laboratory could be controlled thermostatically from ambient temperature up to 40 C, by electrical heaters round the perimeter of the room. Heaters between the double glazing of the windows could be used to maintain a constant temperature in the window cavity.

4.2. The Traversing Gear

The traversing gear consisted of a main carriage (Plate 4.1), which moved parallel to the plate, and a cross slide (Plate 4.2), which moved perpendicular to the plate. No lateral movement was possible.

In order to provide adequate space for the developing boundary layer, the cross slide mechanism was fastened to the main carriage with a clearance of 0.36 m between it and the plate and was electrically insulated from the carriage in order to isolate probes from interference. The cross slide was positioned by a lead screw which could be driven manually or by a small electric motor under remote control.

The vertical position of the carriage could be determined to the nearest 0.1 mm over a range of 2.80 m. In the horizontal direction, a dial test indicator attached to the cross slide permitted a resolution of 0.002 mm over the first 10 mm of movement. A vernier scale gave a resolution of 0.1 mm over 300 mm. Remote positioning of the cross slide was only accurate to 1 mm as the rule was viewed through a small convex mirror.

CHAPTER 5

INSTRUMENTATION

5.1. Introduction

The instrumentation required for this experimental investigation comprised analogue instruments, a digital datalogger and programs which controlled the data processing*.

Analogue instrumentation was required to raise the signal (micro-volts) from the thermocouple sensor to the order of volts so that it was compatible with the input requirements of the analogue-to-digital converter (ADC) (0 to 10V+ve). Similarly, an analogue signal conditioner was employed to amplify the anemometer signal so that the maximum possible resolution of the dynamic signal on the ADC scale could be obtained.

The datalogger was capable of digitizing up to four channels of analogue signal and of recording the binary data on magnetic tape. (A 7-track NRZ1 industry compatible tape system was used so that the data tapes were potentially acceptable at most computing centres.) Since it was intended to process the data on an ICL 1900 series computer, the data were written on the tape in a standard ICL format. With this arrangement, the special routines, written for use with the data tapes on the ICL machine, had only to recast the binary data into a format compatible with the software of the Fortran IV language.

The datalogging system was also used in other modes. In one, the data was processed in real time ('on-line'). In another it was used in place of the large computer to process the data stored on magnetic tape ('off-line').

---

*Program software is not usually considered as instrumentation. In this case, it does replace analogue data processing instruments.

A brief description of the analogue instrumentation is given in section 5.2. Because the concept of digital data processing systems is relatively new and because much of this research programme was concerned with the development of different methods of digital data processing, a fuller description of these aspects of the instrumentation is given. In section 5.3 the organisation of the datalogger is presented, and in section 5.4 various methods of data processing are discussed: the 'on-line' mode (5.4.1), the 'off-line' mode with the small computer as the data processor (5.4.2) and lastly, the 'off-line' mode with the use of a large computer (5.4.3).

5.2. Analogue Instruments

Each of the two strings of analogue instruments used in the experiments consisted of a primary instrument (P) (a high gain d.c. amplifier for a thermo-couple system and an anemometer unit for the hot-wire anemometer system) and a secondary signal processing unit (S) (see Figure 5.1). The latter unit was used to suppress the zero level, to filter out high frequency noise, and to provide low gain (3x) amplification. To ensure that any phase shift resulting from signal conditioning was common to all signals, the same model of signal processor was used*.

In addition to the signal processing instruments, several instruments were used to monitor the signals. The specifications of the processing instruments are listed in Table 5.1 and those of the monitoring instruments in Table 5.2. The arrangement of the instrumentation is shown in Plate 5.1.

---

*There was no detectable phase shift in the range of frequencies (0-50Hz) between the output of the instrument string of the thermocouple and that of the signal processor of the anemometer when the inputs to these units were stimulated by a common input. The anemometer unit could not be included in this test.

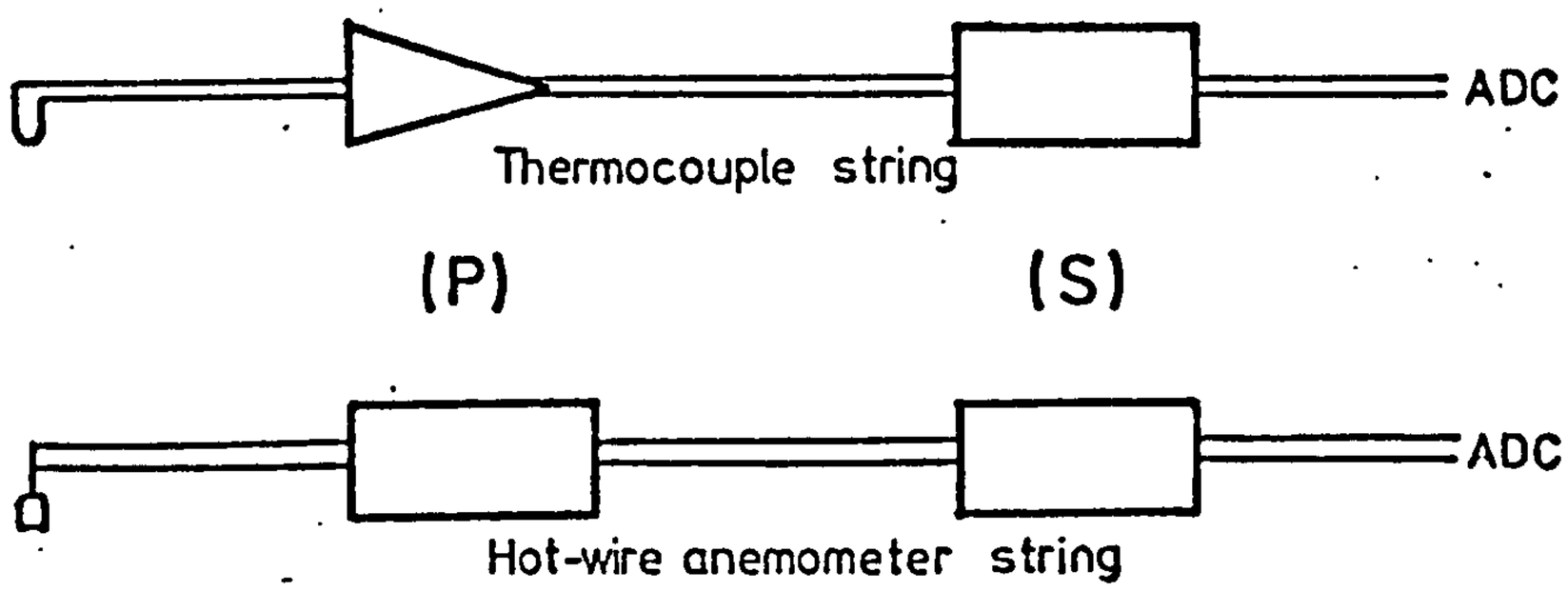

Figure 5.1

In the thermocouple system, the signal from the sensor was strengthened to the order of one to two volts by the high gain d.c. amplifier. Then, with the analogue signal processor, the signal was manipulated so that a voltage equivalent of 25 to 75 C covered the full range (0 to 10V) of the ADC. In this way an overall amplification of 5000 was achieved.

Initially, several difficulties were encountered from electrical interference. To overcome some of these, a special thermocouple lead cable was designed. It consisted of an outer screen enclosing chromel and alumel wires from the thermocouple to the cold junction and a co-axial copper cable from the cold junction to the amplifier. The cold junction was sealed with araldite and immersed in an ice water bath. This configuration also permitted a robust use of the thermocouple system and with the careful elimination of ground loops, the peak to peak noise level at output was less than seven mV. (This was less than one division of the ADC.)

With the hot-wire anemometer system, it was possible to use only a dynamic range of one-tenth of the ADC scale due to a lack of suitable

amplifiers. However, this still enabled a signal resolution of 1:100 which was comparable to the error of the calibration of the hot-wire anemometer (cf. 6.5.1). The noise level of the signal on the output was also less than one scale division of the ADC.

5.3. The Digital Datalogger

The heart of the datalogger was a small computer (4K of store) which was used for control, intermediate data storage, and simple data processing. In order to obtain the datalogger configuration, several peripherals were interfaced to this basic unit.

1. A combination of a multiplexor and an analogue-to-digital converter (ADC) permitted the sampling of four analogue inputs.
2. A digital clock provided for an adjustable sampling rate between 33 and 4000 Hz.
3. A magnetic tape deck provided a high-speed input/output channel.
4. An ASR 33 teletype provided slow input/output facilities via its keyboard and paper tape reader/punch.

The arrangement of these peripherals is presented in Plate 5.1 and in a schematic form in Figure 5.2 while their specifications are given in Table 5.3.

The datalogger could have been used in several modes. This is easily illustrated by following the acquisition of a data element. The analogue signal from a selected channel is directed by the multiplexor to the ADC where a binary representation of the signal is produced by a successive approximation procedure. The binary information is then transferred to the accumulator of the small computer.

The subsequent manipulation of the data element depends largely upon the method of data processing employed. If the data sequence is processed

'on-line', then the data element is immediately analysed by a simple program and is then overwritten by the next data element. Thus the detail of an 'on-line' analysis is restricted by the number of calculations which can be performed between successive samplings.

However, if the data processing is 'off-line', then a more detailed data analysis becomes possible. Here the binary data element is recorded on magnetic tape. This process is not, however, straightforward. It requires the coordination of the digitizing of the analogue signals at regular intervals with the grouping of the data into large blocks and the writing of these data blocks onto magnetic deck. The program to perform this coordination was developed by Miss G.Hall and for further details on this subject the reader is referred to her reports.

5.4. Data Processing Software

5.4.1. 'On-line' Data Processing

The decision to process data 'on-line' was prompted by the delay in acquiring the magnetic tape deck and digital clock which were required to complete the datalogger mode of the system. In place of the digital clock, the internal timing cycle of the computer was used to regulate the sampling rate. The ADC service routines were included in a long sequence of operations through which the program control cycled recursively. Delay routines within this loop were used to adjust the sampling frequency.

Two 'on-line' processing programs were written. The first was designed to determine the amplitude density distribution of a linear scalar function, such as the signal from the thermocouple. (This estimator completely described the amplitude characteristics of the signal.) The second was designed to process the signals from a combination of a single hot-wire anemometer and a thermocouple.

Unfortumately, the interpretation of signals from the anemometer-thermocouple arrangement was complicated because each set of data had to be transformed before an analysis could be performed. Further, in order to accommodate involved calculations and the wide range of magnitudes of parameters in this transformation, floating point arithmetic was needed. The resulting program, which determined the expected value and the variance of the effective cooling velocity, the temperature and the joint covariance, had a sampling rate of thirty Hz. This acquisition rate was inadequate and the approach was abandoned.

The 'on-line' data processing of the signal from the single thermocouple was more successful. Because the sensor had a linear response, the transformation of the data could be postponed until the statistical measurements were obtained. This meant that all the data calculations could be worked in integer form. In this program one analogue channel was sampled at approximately 100 Hz and the amplitude density distribution was constructed from the binary data sequence. After the data acquisition was completed, the first four moments of the distribution were calculated and printed out on the teletype. The values of the distribution could also be printed if required. (For further details the reader is referred to Appendix E.)

The advantage of the 'on-line' data processing was that with immediate analysis of the data sample, the quality of the sample and the relationship between successive data sequences could be assessed during the experiment. On the other hand, its disadvantages were that another sequence of data was required for each data analysis and that the scope of the analysis was restricted. It was only with the storage of the data that several analyses could be made using the same data. The use of the small

computer to process data was very attractive as there was little delay in obtaining the results, and direct control of the operation was possible.

5.4.2. 'Off-line' data processing with the Small Computer

In the initial development of this project, it was planned to perform all calculations in floating point arithmetic because a large variation in values of parameters was expected. Since the machine did not have a hard wired arithmetic unit, a floating point package (DEC-08-YQ3A-PB) was used. However, a program which calculated the amplitude moments of several analogue signals proved to be too complicated and too large to be modified for different applications. The scheme was abandoned. Greater success was achieved with a more modest form of the program which used integer arithmetic. This reduced the demand on core storage, but the need to program in a low-level language still made alterations to the program inconvenient. All the preliminary analyses of the intermittency in the outer edge of the boundary layer were performed with this program.

One point in favour of using the small computer as an 'off-line' data processor was the low overhead cost. Nevertheless, the scope of the processing was restricted by the lack of machine software facilities and by the limited size of core store. It was necessary to use a larger digital computer to overcome these restrictions.

5.4.3. 'Off-Line' Data Processing with a Large Computer*

'Off-line' data processing with a large digital computer offered several advantages. The availability of a versatile high-level language such as Fortran IV brought access to standard software (such as the Fast Fourier Transform package) and the large core storage permitted the use of extensive data processing routines. Also the use of standard peripherals,

---

*ICL 1905E at Queen Mary College Computer Centre.

such as a line printer and graph plotter, aided the presentation of the results of the analyses.

There were two major considerations in the development of the data processing routines on the ICL 1900 series computer. The first was the organization of the statistical analyses and the second was the efficiency of the data transfer routines. We will consider the efficiency of the data transfers first.

As the 'off-line' method of data processing required large quantities of data to be transferred into computer core storage for each analysis of the data, it was desirable to have the most efficient transfer process possible. In processing the 'raw' data from the datalogger tape, special routines were used to transfer the data into core and to restructure the internal coding so that they were compatible with the Fortran IV software before they were transformed into sequences of velocities and temperatures. These special routines transferred the data much more efficiently than the general purpose magnetic tape routines (see Appendix D). The special routines were, however, restricted to use only with the densely-written datalogger tapes and were not suitable for use with magnetic tapes written by standard ICL software.

Because of this limitation, two possible data sources for subsequent analyses were feasible*. Either the use of the 'raw' data could be continued or newly created files of transformed data sequences could be used. The generation of new files was attractive because there would be a saving on the time consumed in the transformation of the data. Also

---

*Of course, the initial data processing was performed from the 'raw' data tapes.

if only a part of the data was to be examined further, then the data file could be reorganized to delete the superfluous data.

The creation of these files and the use of them, however, would have had to be performed through standard operations available in the Fortran IV language. Thus, with the use only of magnetic tape storage facilities, the advantages of recording the transformed data were not distinct*. Indeed, the cost of generating the files of transformed data and the subsequent use of them could have exceeded the cost of using the relatively fast special routines on the 'raw' data files. In view of the costing scheme on the QMC computer which charged for the use of peripheral time as well as for processing time, it was decided to use the 'raw' data files as the data source for all calculations.

So that there could be an economy in the number of data transfers, the greatest possible number of calculations was performed after each data transfer. On the other hand, an exhaustive analysis of each sequence was not always required. Moreover, many statistical analyses required data sequences having an expected value of zero. For these reasons, the data processing was divided into primary and secondary parts:

In the primary data processing, estimates of the expected values and of the variances of the transformed data sequences were evaluated. Each file on the datalogger tape was considered sequentially. An example of the program used for the primary processing of crossed-wire data is presented in Appendix F.

On the basis of the information obtained from the primary processing, certain files were selected for more extensive analysis of the

---

*If there had been access to a fast storage peripheral such as disk, this method may have been feasible.

statistical properties of the data. In these secondary data processings, the transformed data sequences were further modified by the removal of the expected values (obtained from the primary data processing) before any calculations were made.

The software of the secondary processing was subdivided into analyses of amplitude and of power spectral density. The former program had a very loose structure so that a variety of quantities, such as probability density distributions and conditional averages, could be determined. In contrast, and possibly reflecting the more difficult task of examining the time dependent characteristics of a signal, the spectral analysis program was specialized and was designed to examine the auto- and co-power spectral density distributions of two simultaneous data sequences. The details of typical examples of these programs are presented in Appendices G and H.

TABLE 5.1

ANALOGUE INSTRUMENTS

Instrument	Manufacturer and Model	Use	Mode of Operation/ Characteristics
d.c.amplifier	DANA model 2615 option VI	primary amplification of signal from thermo-couple	gain 20-2500x
bandpass filter zero suppressor	DANA model 2612	conditions signal from amplifier (2615)	low pass filter at 100 Hz variable <|10V|
d.c.amplifier and low pass filter	DANA model 2850	primary amplification of signal from thermo-couple	gain 0.1-2500x low pass filter at 100 Hz
hot-wire anemometer	DISA 55D01	operation of hot-wire sensor	20:1 bridge (high mode)
low gain amplifier zero suppressor low pass filter	DISA 55D25	secondary signal conditioning for all channels	variable gain <3x, zero suppression ⁎-30V, low pass filter at 200 Hz (-6db/octave)

TABLE 5.2

ANALOGUE MONITORING INSTRUMENTS

Instrument	Manufacturer and Model	Use	Mode of Operation/ Characteristics
digital voltmeter	Solatron LM 1420	calibration, monitor	Range 2.5µv - 1000V
digital voltmeter	DISA 55D39	monitor	Range 1 mV to 1000V
oscillo-scope	Tektronic 561B	monitor (also monitor of noise level)	Range 0.01V - 20V/cm

TABLE 5.3

DIGITAL INSTRUMENTS

Instrument	Manufacturer and Model	Specifications
Digital computer	Digital Equipment Company (DEC) PDP-8L	12 bit words, 4096 words. 1.2 µsec cycle.
Teletype	Westron	ASR 33 10 characters per second, Keyboard, slow paper punch and reader.
Analogue to digital converter	DEC AD08B	10 bit accuracy 10 µs aperture time multiplexor for 4 channels input.
Digital Impulse Clock		33-3300 Hz (set at 100 Hz).
Magnetic Tape Deck	Racial Thermionic T5000	7 track NRZ1, industrial compatible, data break mode.

CHAPTER 6

THE CALIBRATION OF A HOT-WIRE ANEMOMETER

6.1. Introduction

In this chapter an investigation designed to calibrate a hot-wire anemometer from flow velocities between 0.05 m/s and 1.00 m/s in a vertical direction and for a temperature range of 40 K is presented.

The determination of the response of the anemometer for these very low flow velocities is beset by two major problems. Firstly, the generation of a steady flow with a uniform velocity is difficult because of the possibility that the buoyancy forces in a heated flow may exceed its dynamic pressure. Secondly, because few anemometers are sensitive to the range of velocities of interest, there are difficulties in the evaluation of these velocities. As a consequence, a variety of techniques suitable for low velocity calibration have been considered.

The common practice is to calibrate the hot-wire anemometer against another standard; it can be either a reference probe in the flow (e.g. a pitot tube) or a gauge of the volume flow rate. The latter technique has been preferred in low velocity calibration even though it does require a uniform flow. In an extensive study of low-speed calibration, Kung and Binder (1967) employed a venturi tube to gauge the flow through a special micro-tube tunnel. Hatton, James and Swire used a gasometer and an orifice plate to measure the flow through the potential core of a longitudinal jet.

In another variation, Cheesewright (1966) calibrated a hot-wire anemometer in the laminar free convection boundary layer assuming that the

boundary layer conformed to the theoretical solution. Although the sensor can be exposed only to a limited number of conditions of velocity and temperature, with this method there is the marked advantage that the probe is calibrated in a flow field similar to that in which it is to be used.

Distinct from the extension of conventional techniques are the uses of ingenious mechanisms to produce and measure a relative velocity between the fluid and the hot wire. Baille used a method in which the hot wire was moved, on a trolley, through a stationary fluid. Dring and Gebhart (1969) developed this method further: both the fluid and the probe were stationary and the relative motion was produced by moving the container of the fluid past the probe mount. Although the successful use of both these mechanically assisted techniques has been reported, the adaptation to include a calibration for temperature is hampered by the need to have a stationary isothermal fluid.

One aspect which encouraged serious consideration of the calibration against another standard in the flow was the realisation of a technique that is particularly suited to low velocity calibration. This technique, which will be referred to as a wake vortex anemometer, is based on the fact that the periodicity of the vortex street in the wake of a cylinder, placed transverse to a steady flow, is a function of the Reynolds number of the flow. Over the temperature range of the present calibration, the response function of the wake vortex anemometer can be considered independent of variations of physical properties of the fluid. Because an uncalibrated hot-wire anemometer can be used to detect the vortex street, the wake vortex anemometer is suitable for use in the calibration of a hot-wire anemometer.

The method used for the very low velocity calibration of a hot wire is presented in four parts. Section 6.2 gives a description of the wind tunnel used to generate the flow and an assessment of its performance. Section 6.3 contains a discussion of various aspects of the wake vortex anemometer: previous studies on the regular vortex streets pattern behind a cylinder are examined (6.3.1); the components that constitute a wake vortex anemometer are listed (6.3.2), and the results of a brief investigation on the Strouhal number-Reynolds number relationship are presented (6.3.3). The method of calibration is described in section 6.4, before the calibration data from both a single hot-wire and a crossed-wire anemometer are reported in section 6.5.

6.2. The Calibration Wind Tunnel

6.2.1. Introduction

A special wind tunnel, in which the wake vortex anemometer could be used, was designed to simulate the velocity temperature and direction of the free convection flow. The need to place large aspect ratio cylinders across the flow determined the size of the calibration section. This, in turn, established the scale of the rest of the tunnel. The diameters of the cylinders were set by the required range of flow velocities because the regular vortex structure can only be observed at Reynolds numbers between 50 and 150.

Other design features were derived from characteristics of the required air flow. Special attention was given to the stability of the flow because small transient changes in ambient pressure could have been comparable to the low dynamic pressures of the flow. The minimum sensitivity to these changes was gained by placing the blower at the

entrance to the tunnel. It was anticipated that any turbulence created by the blower could have been easily dissipated.

6.2.2. Air Flow

The calibration tunnel is shown in Plates 6.1 and 6.2. It consisted of the following:

(a) Air Blower

The blower (Watkin and Watson type 8.25 UA) was fitted with a special impellor (6.3 mm) which had steep pressure-volume flow characteristics in order to reduce the volume flow sensitivity to small changes at inlet pressure. The flow velocity was varied by changing the speed of the blower. An overall variation of 20:1 was achieved in two stages. A ten-to-one change was obtained by driving the fan impellor by a counter-shaft through a variable speed belt drive (Sextet by Industrial Drive Ltd.). A further two-to-one variation was added by driving the counter-shaft from a constant speed 3 hp motor through one of two pulley ratios. The impellor was driven at twice the rated speed (5500 rev/min) to deliver the maximum volume flow required (15 m^3/min). The variable belt drive could be operated manually or by an electrical motor remotely controlled from the working platform.

(b) Primary Air Heater

The primary heater was a 64 mm diameter × 0.9 m long steel pipe wrapped with three heating elements, each rated at 1.5 kW. Each heater was operated by off-on switches. The unit was manufactured by Eltron Ltd. (Croydon).

(c) Diffuser

The diffuser was rectangular in cross-section and was built of wood in two layers. The outer shell, of 12 mm plywood, was built for support,

and the smooth-faced inner lining, of 12 mm Waydec, was sectioned in order to secure the screens. The screens (20 mesh, 50% blockage) were initially placed according to a formula: a screen at every position where the cross-section area was double that of the previous screen. The end walls had an expansion half-angle of 30^{o} and the side walls had a half-angle of 22^{o} to give an expansion ratio of 50 in a height of 1 m.

(d) Secondary Heaters

Bare nichrome wire, 0.46 mm in diameter, was strung over the exit of the diffuser on a 12 mm grid. To position the wires, asbestos string was woven across on an 80 mm grid. The wires were divided into three sections. Each section was supplied from the mains through a variable transformer. The maximum dissipation was limited to 1.2 kW.

(e) Settling Chamber

The settling chamber was 1.20 × 0.84 × 0.76 m high with a construction similar to that of the diffuser. Over the entire length of this duct screens were sandwiched between 6.3 mm wide, hexagonal honeycomb in layers of 0.10 m.

(f) Contraction Section

The section was 1.20 × 0.84 m at the entrance and 0.43 × 0.30 m at the exit to give an overall contraction ratio of 7.8. The section was 2.45 m high. Each pair of sides was a symmetrical contraction designed by a method developed by Whitehead (1951). It was built of 3 mm birch plywood supported by mahogany stringers (A.B.Fuller, Croydon).

(g) Calibration Section

The calibration section was 1 m high with walls slightly tapered outwards to compensate for the boundary layer growth. The side walls were

Perspex and the end walls were of Waydec. One of the Perspex walls was fitted with a panel to give access into this section. At the entrance to the section, two screens 80 mm apart were placed across the flow.

(h) Exit Duct

A 0.9 m high duct was attached to the calibration section with a 0.1 m layer of honeycomb at its entrance.

(i) The Support Structure

The tunnel was mounted inside a scaffolding tower (S.G.B.sureframe) using rubber pads to reduce vibration transmission. A wooden platform provided access to the calibration section.

6.2.3. Development

The initial trials of the tunnel were quite unsatisfactory because the air stream separated from the walls very early in the diffuser. Detection of this separation, indeed of any air flow in the wider sections of the tunnel, was difficult since the velocities were less than 0.20 m/s.

Various attempts were made to introduce a favourable pressure gradient into the diffuser. The use of cotton cloth, of glass fibre and, later, of layers of expanded polystyrene balls (3.2 mm diameter) was not successful because the dense blockage of these screens generated further turbulence downstream. Finally, with twelve wire gauze screens placed at 80 to 100 mm intervals through the diffuser and two more at the entrance to the calibration section, a sufficiently negative pressure gradient was achieved to give stable flow in the calibration section at ambient temperature.

When the air was heated with the primary heater, the problem of separation in the diffuser was again encountered. In order to eliminate

the buoyancy forces that were caused by any non-uniformities in the lateral temperature distribution, the entire duct was lined with polystyrene insulation to a thickness of 8 mm. Unfortunately, little improvement was effected in the flow by this change. In the final modification, a set of secondary heaters was placed across the exit of the diffuser so that the flow could be allowed to expand through the diffuser before it was heated. (With this arrangement, the primary heater was not used.) There was now no longer any separation in the diffuser but the flow downstream from the secondary heaters was disturbed by the free convection plumes rising from the hot elements. Hence, little overall improvement in the flow through the calibration section was achieved.

6.2.4. Performance

With the above modifications, the 'cold' flow through the calibration section was steady at velocities between 0.05 and 0.95 m/s. (These velocities were measured with the wake vortex anemometer.) In heated flow, the range was from approximately 1.00 m/s down to a lower limit which was dependent upon the temperature difference between the flow and the ambience. At a temperature difference of 20 K, this limit was 0.40 m/s and at 40 K, the velocity was 0.50 m/s. The velocity distribution across the calibration section was affected by the shape of the screens at the entrance to the calibration section but it was fairly uniform over the centre of the section.

6.2.5. Discussion

Even though the performance of the calibration tunnel was eventually satisfactory, much effort was expended in obtaining the result. Some of the difficulties were presented by the scale of this prototype tunnel: in

view of the size of the structure, alterations were very costly in materials, in labour and especially in time.

Other problems were caused by the nature of the flow. The rapid growth of boundary layers at very low velocities along the comparatively long tunnel walls hindered attempts to obtain uniform distributions of velocity . Also, because the drag coefficient was linearly dependent on velocity in this range, wire gauze was not very effective in the dispersion of non-uniformities in the flow.

The author believes that his disregard (or ignorance) of many of the conventional practices in design of diffusers created several problems. For example, so that separation in a diffuser may be avoided, a half-angle of about 11° is generally recommended (Kline, 1959). In the present design, the compromise between a long, narrow diffuser which would encourage boundary layer growth and a short, wide diffuser strongly favoured the latter. The use of a narrow angle diffuser for the high velocities in the inlet region in conjunction with a wider angle diffuser in the low velocity region might have reduced the problems of separation.

In addition, a square duct should have been used in the diffuser in order to obtain a symmetrical expansion of the flow. (In that case, the transformation from square to rectangular would have occurred in the contraction section.) Finally, in view of the problems in obtaining a satisfactory expansion of the flow, it is probable that a smaller contraction ratio could have been used. (Collis and Williams conducted an investigation of hot-wire calibration in a tunnel with a contraction ratio of 4:1.) This, in turn, would have reduced the requirements of the diffuser section.

Despite these possible faults, the present tunnel is satisfactory for calibration purposes over the required range of velocities at ambient temperature and for the upper part of this range in a heated flow.

If a more complete calibration is required in future work, it may be possible to adopt a novel calibration technique proposed by Hollasch and Gebhart (1972). They suggested that the wire temperature and not the fluid temperature could be adjusted in order to effect variations in the temperature difference. This approach is very attractive as not only would it reduce the time required for a calibration, but it would also eliminate the problems caused by buoyancy forces. However, this technique may not prove suitable. It is the author's present belief that the calibration of hot wires for low velocity flow is most economically performed in an apparatus of a small scale that generates a steady flow with a region of uniform velocity. The evaluation of the velocity in this region would have to be obtained from a probe (e.g. a hot-wire anemometer) that is, in turn, calibrated in a laminar flow of known properties.

6.3. The Wake Vortex Anemometer

6.3.1. Vortices in the wake of a cylinder

Although vortices in the wake of a circular cylinder promised to be a suitable anemometer sensor, the exact form of the dependency of the Strouhal number ($St \equiv fd/u$) on the Reynolds number ($Re \equiv ud/\nu$) was uncertain. The regular pattern of the vortex street is not particularly well understood even though it was examined as early as 1912 by von Karman. (Hence, the vortex streets are known as von Karman vortices.) Kovasznay (1949) concluded that the sudden appearance of a periodic wake downstream of a cylinder, at a definite Reynolds number, was the result of laminar

instabilities in the wake. He reported that the instantaneous flow pattern was stable from the transition at Re equal to 40 up to Re equal to 160 and was sinusoidal in nature.

The measurements of Roshko (1954) agreed with those of Kovasznay; Roshko observed further that the vortex streets in the range 40 < Re < 150 were regular and decayed gradually by viscous action. The following relationship for the dependency of St on Re was proposed:

$$St = 0.212\ (1.0 - 0.212/Re) \quad . \tag{6.1}$$

Whereas Kovasznay measured the velocity of the free stream by a heat pulse detector and by a pitot tube in conjunction with a micromanometer, Roshko based his measurements of flow velocities less than four m/s on the principle that the St-Re relationship was independent of velocity, i.e., the principle of self-consistency. the

Tritton (1959, 1971) discovered a discrete displacement in the St-Re function between 85 < Re < 105. This discrete step was noted over a wide range of velocities in both a wind tunnel and a water tunnel. An irregular pattern in the vortex street was observed when the flow conditions were set close to this transition point. However, the variations in the value of Re at which this phenomenon occurred could not be explained by a systematic investigation.

Tritton concluded that the phenomenon corresponded to the transfer of the generation mode of the vortex street from one of laminar instability to one of detachment of vortices from the cylinder and, further, that the variation of the Reynolds number of the transition could be caused by changes in the intensity of free stream turbulence. He suggested that the St-Re relationship could be described by two overlapping functions.

These were given as

$$St\ Re = (-2.1 \pm 0.3) + (0.144 \pm 0.010)Re + (4.0E\text{-}4 \pm 0.0E\text{-}4)Re^2 \qquad (6.2)$$

for $50 < Re < 105$, and

$$St\ Re = (-6.7 \pm 0.2) + (0.224 \pm 0.006)Re \qquad (6.3)$$

for $80 < Re < 150$.

The discrete step in the St-Re function was also observed by Berger (1964a, b); however, he reported the occurrence at different values of Re to those observed by Tritton.

In his studies of the shedding of vortices from tapered and parallel cylinders, Gaster (1969, 1971) has shown that the vortex wake structure may exist in a number of discrete cells, each having a different shedding frequency. The intensity of the free stream turbulence and the non-uniformity of the mean flow appeared to influence the mode of shedding. Gaster also confirmed Roshko's observation that there was a span-wise variation in the shedding mode and further reported that the shedding mode could be stabilized by the addition of end plates. In an attempt to explain the diversity of observations, Gaster concluded that at low Reynolds numbers the number of frequency shedding cells in the vortex sheets was a minimum. At very low Reynolds numbers, the wake probably comprised only one cell.

6.3.2. Components of the Wake Vortex Anemometer

Apart from a graduated set of cylinders (aspect ratio 30-250) the wake vortex anemometer used in this study comprised an uncalibrated hot-wire anemometer, an analogue signal processor, a d.c. amplifier and a frequency counter. In addition, an oscilloscope was used to identify

the wave pattern of the vortex street. These instruments are shown in Plate 5.1 and their specifications are given in Table 6.1. The arrangement of the wake vortex anemometer is shown in Plate 6.2.

6.3.3. Experimental Investigation of the St-Re Relationship

In view of the disagreement among the proposed relationships for the dependency of St on Re, particularly between those of Roshko and Tritton (Figure 6.1), a brief study was conducted in order to select the most suitable relationship for this calibration programme.

The basis of the investigation was similar to that used by Roshko; that is, the vortex phenomena was assumed to be self-consistent (6.3.1). The flow velocity was determined from measurements of the frequency of the vortex street behind a cylinder chosen to give a value of Re between 50 and 75*. This flow velocity was then used for the determination of the St-Re relationship at larger values of Re.

The correlated data are presented in Figure 6.2 along with the relationships of Roshko and Tritton. Despite the scatter, a definite agreement between the data and the relationship of Tritton, at Re less than 90, can be seen. At higher Reynolds numbers the data mainly resides below Tritton's relationship. The investigation was not intensive enough to verify this trend.

On the evidence of this study, the quadratic relationship proposed by Tritton (eq.6.2) was used as the response function of the wake vortex anemometer.

6.4. Method of Calibration

For each calibration point, estimates of the velocity and temperature

---

*Tritton's formula (eq.6.2) was used for this estimate. However, at these values of Re, there was little difference between the formulae of Roshko and Tritton.

of the flow and of the response of the anemometer to be calibrated were required. The velocity and temperature were measured by the use of the wake vortex anemometer and a thermocouple respectively.

The measurement of the velocity in the calibration section was executed in three stages. First the blower was set to give approximately the desired flow rate. Secondly, a cylinder was placed across the flow and its wake structure was searched for the signature of the vortex street. If the quest proved negative, the cylinder was replaced by others until the characteristic pattern was detected. The frequency of the vortex street was measured and a preliminary estimate of the velocity was made. Lastly, on the basis of this estimate of the velocity, a cylinder that would give a value of Re between 50 and 75 was placed across the flow. The frequency of its vortex street (usually between 1 and 100 Hz) was measured for a period of at least 100 seconds to complete the required measurements.*

The uncalibrated hot-wire probe and the cylinder were then removed from the calibration section, and the anemometer probe to be calibrated, together with a thermocouple probe, was positioned in the same region of the flow. Measurements of the bridge voltage (or a corresponding voltage from the signal processor unit) and the e.m.f. from the thermocouple completed the acquisition of the required information. These data were then formulated into non-dimensional parameters based on the diameter of the wire.

The heat transfer from the hot wire was correlated in the form proposed by Collis and Williams, $Nu(T_f/T_g)^{-0.17}$. (This parameter was selected on the basis of its wide usage.) In accordance with these investigators, the properties of the fluid were evaluated at the film

---

*For purposes of cross references, however, measurements on another cylinder in the same range of Re were often taken.

temperature T_f, given by

$$T_f = 0.5(T_w + T_g) \tag{6.4}$$

where T_g is the local air (gas) temperature

and T_w is the mean temperature of the wire.

The mean temperature of the wire, T_w, was determined from the linear relationship between the resistance of the wire and its temperature. Hence, T_w was obtained from the formula

$$T_w = T_1 + \frac{R_w - R_1}{\alpha R_1} \tag{6.5}$$

where R_w is the resistance of the wire at operating conditions,

α is the thermal coefficient of resistivity

and R_1 is the 'cold' resistance of the wire evaluated at a temperature T_1.

The heat-transfer rate, $\dot{Q}_w$, from the wire was calculated from the measurement of the anemometer bridge voltage. In the Disa 55D01 anemometer system, the hot-wire sensor forms one arm of a wheatstone bridge (DISA), a schematic drawing of which is shown in Figure 6.3, where C, L, R_L are the capacitance, inductance and resistance of the lead cable, e_b is the anemometer bridge voltage, e_w is the voltage across the wire and R_w is the resistance of the wire.

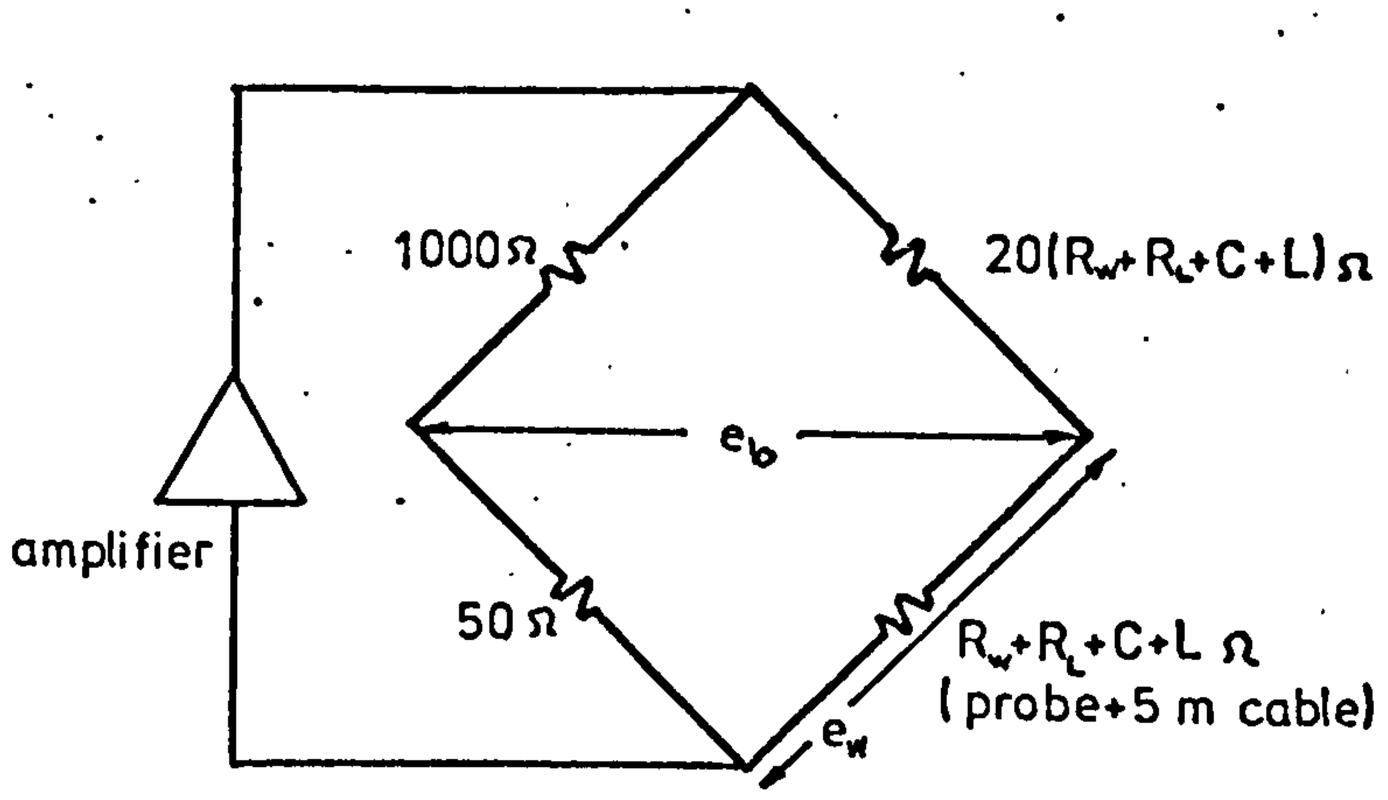

Figure 6.3

From Figure 6.3 it can be shown that the energy dissipated in the wire is given by the relationship

$$\dot{Q}_w = \frac{e_w^2}{R_w} = \frac{e_b^2 R_w}{(50 + R_L + R_w)^2} \qquad (6.6)$$

With this estimate of heat transfer, the Nusselt number (Nu) was calculated by the formula

$$Nu = \frac{\dot{Q}_w}{k_f \pi \ell (T_w - T_g)} = \frac{e_b^2}{k_f (T_w - T_g)} \frac{R_w}{\pi \ell (50 + R_L + R_w)^2} \qquad (6.7)$$

where k_f is the thermal conductivity of air evaluated at T_f.

The calculation of the weighted Nusselt number and the Reynolds number completed the acquisition of one calibration point.

6.5. Presentation of Calibration Data

The calibration of the hot wire was not designed to study the characteristics of the hot-wire response but, instead, it was intended simply as a means to relate the response of the anemometer to the flow. Consequently, the parameters of the heat-transfer correlation, $Nu(T_f/T_g)^{-0.17}$, were manipulated until the agreement among the data was obtained: the best data correlation was achieved with the adjustment of the specific thermal resistivity, α, by up to $\pm$ 10% of its measured value (α = 0.0029). The absolute value of the heat-transfer correlation was altered appreciably by this practice.

6.5.1. The Single Hot-Wire Anemometer

Figure 6.4 shows the data from the calibration of the single wire used for the final studies in this programme. The anemometer was calibrated over a range of U between 0.10 m/s and 0.95 m/s for ambient

temperature and between 0.4 m/s and 1.00 m/s over a temperature range up to 40 Kabove ambience (c.f. 6.2.4). The wire was aligned normal to the flow by means of its yaw sensitivity.

The calibration data are expressed as a dependency of Re on $Nu(T_f/T_g)^{-0.17}$ in contrast to the widespread preference for the inverse function (see section 3.3.4). The relationship is expressed by means of a polynomial since the evaluation of this function is slightly more efficient than alternate forms. A least squares fit was used to determine the coefficients of a third order polynomial, which gave a variance of 2% compared to the maximum velocity (U = 1.0 m/s), marginally better than a quadratic function. The deviation of the fit most probably reflects upon the scatter of the data rather than on any discrepancies in the shape of the polynomial expression. In view of some comparisons that will be made, it is important to note that the stagnation velocity data were used in these regressions.

In Figure 6.5 the present relationship is compared to those proposed by Collis and Williams and by Hatton, James and Swire. The values given by the present relationship are much larger than those of the other two. However, the shape of all three expressions is similar. It is most probable that whereas in the effort to optimize the agreement among the heat-transfer data, the absolute values of $Nu(T_f/T_g)^{-0.17}$ were distorted but the shape of the $Nu(T_f/T_g)^{-0.17}$ vs. Re relationship was only slightly altered.

In order both to verify the accuracy of the wake vortex anemometer and to confirm the present methods of data interpretation, two lateral profiles of velocity and temperature in the laminar free convection

boundary layer were measured with the single hot-wire anemometer+ thermocouple arrangement. A dimensionless form of these measurements is compared with the theoretical solution of the governing equations (Ostrach, Pr = 0.707) in Figure 6.6. (A more detailed presentation of these data is given in Chapter 8.) The data show a very good agreement with the theory for the region of higher temperatures and velocities although the effect of the plate on the anemometer's response is evident for $\eta < 0.2$ ($y < \approx 1.5$ mm). A definite discrepancy, however, is evident in measurements of the cooler, low velocity region of the outer boundary layer. This discrepancy increases to a value of approximately 7% of the maximum velocity (40% of the local velocity) at u = 0.10 m/s which represents the lowest limit of calibration.

Several sources of error can account for the discrepancy. The first of these stems from the calibration procedure. Since the flow in the calibration tunnel was unsteady at the lowest flow rates, the wake vortex anemometer may have been inaccurate. (The frequency of the vortex structure was 0.5 - 2.0 Hz at these velocities.) A more probable source of error is that the Nu-Re relationship was not specified correctly. Collis and Williams pointed out that the practice of using the stagnation velocity data to determine this relationship is at fault when considering the characteristics of the heat transfer at low velocities. If the stagnation velocity data had not been included, the relationship would have yielded slightly higher velocities.

The most probable source of error is the form of the relationship that was used. It is surprising that while there was a lack of agreement in the temperature range in which a detailed calibration was performed, agreement was obtained between measurements and theory at the higher

temperatures where fewer calibration points were taken. This might have been caused by the need to manipulate the heat-transfer parameters in order that a unique functional representation could be secured. Collis and Williams suggested that the relationship used above was not adequate at very low Reynolds numbers and that a further variable temperature factor, in addition to $(T_f/T_g)^{-0.17}$, might be required.

In conclusion, the calibration appears to be satisfactory for an investigation of the free convection boundary layer flow near the plate but absolute values of velocity below 0.15 m/s must be treated with some reservation.

6.5.2. The Crossed-Wire Anemometer

In order that the data from a crossed-wire sensor could be interpreted, both the yaw response and the velocity response of each wire had to be known. It was decided to measure the yaw response of a single wire instead of assuming a correlation function because of the uncertainty of low Reynolds' effects on this response. A single normal wire (the probe discussed in the previous subsection) was positioned on a protractor mechanism (see Plate 6.2) which allowed the wire to be rotated about its centre. With the wire exposed to the known flow conditions, the yaw response was measured from β equal to $\pi/2$ to $-\pi/2$ in both unheated and heated flows. The effective cooling velocities were determined from the normal cooling relationship of the single wire.

The data, non-dimensionalized by the normal cooling velocity (U_n), are presented in Figure 6.7. The only function that successfully described the distribution of data was of a trigonometric form proposed by Hinze:

$$\frac{U_\beta}{U_n} = \cos^2(\beta) + k^2\sin^2(\beta) \quad . \qquad (6.8)$$

It can be seen in Figure 6.7 that this relationship with k equal to 0.27 gave a good description of the data for U_n > 0.20 m/s for $|\beta| < \pi/3$. For values of U_n < 0.20 m/s, the yaw response of the wire was less sensitive to orientation although there remained a characteristic response at stagnation conditions. The interpretation of the data for U_n less than 0.15 m/s must be treated as qualitative in view of the inaccuracies in the normal cooling calibration of the single wire (section 6.5.1). Although digital data processing methods permit the parameter, k, to be a variable (Baille) and this might have improved the interpretation of U < 0.20 m/s, the above description of the yaw characteristics with k equal to 0.27 was adopted.

The calibration of the crossed-wire sensor required the determination of the responses of two anemometers as well as the measurement of the flow properties in the wind tunnel. In order that the tedious use of the wake vortex anemometer could be avoided, the crossed-wire anemometers were calibrated against the single wire anemometer (6.5.1). (As great care was taken to obtain the single wire calibration, it is improbable that a more accurate calibration would have been obtained with the vortex wake anemometer.) The crossed wires were calibrated in a position inclined to the flow. Their effective normal cooling correlations were derived with the use of the yaw cooling function.

The calibration data for this probe are not presented; they exhibit the same general shape as the curve of the single wire calibration. The values given by the Nu-Re relationships for the two wires were not in agreement with each other. This fact was not important considering the flexibility available with digital data processing. (Since the anemometers were accidentally set to slightly different overheat

ratios, this may have been the cause of the disagreement. Moreover, the same optimization procedure as used with the single wire was employed.)

Further details on the calibration methods may be extracted from the data processing programs in Appendices F, G, H.

TABLE 6.1

INSTRUMENTS OF WAKE-VORTEX ANEMOMETER

Instrument	Manufacturer and Model	Use	Mode of Operation/ Characteristics
hot-wire amemometer	DISA 55D01	operation of hot-wire sensor	20:1 bridge (high mode)
analogue signal conditioner	DISA 55D25	zero suppressor, amplification, filter	neg ✗-30✗ gain <3x low pass filter 200Hz
d.c.amplifier	DANA model 2615 option VI	amplification, low pass filter	gain 20x
oscilloscope	Tektronic 561B	pattern recognition	range 10 mV/cm - 20V/cm
zero crossing Frequency counter	Solatron EM 1616	measurement of frequency	d.c. and a.c.coupled, signal >100 mV/r.m.s., max resolution 0.01 Hz.

CHAPTER 7

EXPERIMENTAL PROCEDURE

A series of experiments, which lasted five or six days, was commenced by calibrating the anemometers against the vortex anemometer in the wind tunnel (a procedure that required two or three days). The entire analogue instrument string was calibrated as one unit in order to avoid cumulative errors which could have resulted from the calibration of separate units. When this preparation was completed, the instruments were moved into the laboratory which was then prepared for the test series. During the experiments, the response of the anemometer was occasionally verified by comparing measurements of the velocities in the laminar boundary layer against the theoretical solution. Upon the completion of the tests, the instruments were taken back to the wind tunnel for a further calibration.

7.1. Preparation of the Laboratory and its Equipment

A full experiment on the free convection boundary layer required eight to ten hours. In order to maintain stable conditions for this length of time, an equilibrium between the energy input (from the instruments, the plate and the author) and the natural energy losses was established by a careful preparation of the laboratory.

In the early stages of the research, the equipment was switched on twelve to fifteen hours before an experiment so that this balance could be obtained; but with the installation of a thermostat to control the electrical heaters on the perimeter of the room, it was no longer necessary to subject the instruments to this wasteful usage. Instead, the heaters were used to maintain the laboratory at approximately equilibrium

temperature (8-10 K above the normal temperature) for at least twelve hours; then two or three hours before the experiment these heaters were switched off and the electrical instrumentation (including a heat lamp to simulate the body heat of the author when he was absent) was turned on. The plate heaters were on continuously. The conditions in the laboratory were not altered again although the heaters between the double glazed windows were occasionally used to compensate for changes in the heat losses to the exterior. With this technique the drift in the fluid temperature at any point was restricted to less than 2 K in ten hours.

One penalty that had to be paid in order to obtain a stable ambient fluid was the loss of homogeneity in the ambient fluid temperature. Fortunately, the thermal stratification was not severe (Fig.7.1): there was a 4 to 5 K temperature difference between the floor and ceiling and only 1.5 K change over the height in which the turbulent boundary layer developed. Nonetheless, the local ambient temperature was used in all the thermal boundary layer correlations instead of a mean laboratory temperature.

Although it was desirable to create a constant temperature difference between the plate and the local ambient temperature, the concept would have involved an intensive control of the plate heaters. Instead the heaters were adjusted to produce a uniform temperature.* The mean temperature of each of the three sections of the plate was adjusted to within 0.5 K of the overall average although, because there was only one large heater in each of the top sections (see section 4.1),

---

*The plate temperature was measured by an insulated thermocouple placed in contact with the surface.

the local temperatures in these regions deviated by $\pm$ 1 K. Only one plate setting, which produced a boundary layer temperature difference of 42 K, was used in this research programme.

During the main part of this research, three probe systems were used:

1. a single thermocouple probe (used in the early research);
2. a single hot wire normal to the flow and parallel to the plate in conjunction with a single thermocouple probe; and
3. a specially designed array of crossed hot wires and a thermocouple.

Often a second thermocouple was used either to monitor the local ambient temperature or, in close proximity to the first, tc verify its response.

Great care was taken in positioning the single thermocouple probe with respect to the plate. The thermocouple junction was moved very near the plate; then, with the junction and its reflection in the plate being observed through a 20x stereo microscope (Prior) (Plate 4.2), it was moved into contact with the plate. The dial gauge was used to locate this position with respect to the traversing gear. To establish the zero position, at least ten independent measurements were taken. The standard deviation of the observations was less than 0.002 mm and often less than 0.001 mm.

In spite of the accuracy of the positioning method, it was important to expose the quartz tube of the probe support to the steep temperature gradients near the plate for at least ten minutes. There was a significant discrepancy between the zero position of a probe conditioned to ambient temperature and that of the same probe when it had been in contact with the plate for some time.

Less stringent procedures were adopted for positioning the hot-wire probes since these elements were very fragile. For the single wire+ thermocouple arrangement, the thermocouple was first located with respect to the plate and then moved away from it. The hot wire was aligned with the thermocouple by eye and the composite probe was brought very near the plate to verify the alignment.

It was not possible to bring the cross-wire probe near the plate because of its construction. A 4.70 mm gauge block was therefore temporarily fastened to the plate, and one of the wire-support needles was brought into contact with it. Both this practice and the positioning of the single wire were estimated to be accurate to $\mp$ 0.1 mm.

7.2. Execution of an Experiment

During a typical experiment at a selected streamwise station, data observations were commenced very near the plate and were terminated in the outer regions of the boundary layer. Over the 10 mm next to the plate, the probes were positioned manually; beyond this distance they were placed by remote control. For the observations of boundary layer flow conditions with $Gr > 2 \times 10^{10}$ the sample period was five minutes; for measurements at lower Grashof numbers, the period was seven to eight minutes (except in the laminar observations where it was about two and a half minutes).

In view of the long periods, the data signals were sampled at the lowest possible rate that would permit an analysis of both their amplitude and the spectral characteristics. This minimised the number of data points. A preliminary spectral analysis of the thermal fluctuations suggested that the power contributions of fluctuation at frequencies above

50 Hz were negligible and consequently a sampling rate of 100 Hz was used throughout the tests. However, low pass analogue filters at 50 Hz were not available, and since the low pass filter on the anemometer system was 200 Hz and on the thermocouple system was 100 Hz, aliasing of any power above 50 Hz was possible.

CHAPTER 8

PRESENTATION AND DISCUSSION OF EXPERIMENTAL RESULTS

A free convection boundary layer in air along a vertical flat plate with a constant temperature surface was observed through various stages of its development. Only one temperature difference across the boundary layer (42 K) was used.

The results of this experimental investigation are presented in three sections. Section 8.1 is concerned with the development of the flow. Data are presented on the heat transfer from the plate (8.1.1), on the laminar flow (8.1.2), on the 'transitional' flow (8.1.3) and on the streamwise development of the amplitude characteristics of the flow (8.1.4). The transverse structure of the 'fully developed' boundary layer is discussed in section 8.2: attention is given to the flow adjacent to the plate (8.2.1), in the mid-region of the boundary layer (8.2.2) and in the outer region (8.2.3). All experimental data generated in this research programme are summarized in section 8.3.

8.1. Flow Development along the Plate

8.1.1. Heat Transfer from the Plate

Data on the local rate of heat transfer from the plate were obtained as a consequence of the study of the mean temperature profiles very near the plate. With the mean temperature gradient at the plate estimated from a linear fit of three or four points (located within 1.2 mm of the plate), the Nusselt number was calculated* from the formula

$$Nu = \left.\frac{\partial T}{\partial y}\right|_{y=0} \left(\frac{x}{T_w - T_\infty} \frac{k_w}{k_f}\right) \qquad (8.1)$$

*This practice follows the approach of Cheesewright (1966).

where k_w, k_f are values of the thermal conductivity of air evaluated at the plate temperature and the boundary layer film temperature respectively. (T_w-T_∞) is the local temperature difference across the boundary layer.

Figure 8.1 shows Nu plotted against Gr, the local Grashof number. The measurements at the lower values of Gr agree with the theoretical solution given by

$$Nu = 0.354\ Gr^{0.25} \quad . \tag{8.2}$$

Both the abrupt change at Gr approximately equal to 5.0E+9 and the trend of the present data above Gr equal to 1.0E+10 are in reasonable agreement with the results of Cheesewright. The values of the heat-transfer coefficient, h, and of the heat-transfer distance, y_N*, calculated from the same flow measurements, are plotted against Gr in Figure 8.2. The exact trend of the heat-transfer data at higher Gr is difficult to discern. The more thorough investigations of Cheesewright (1968) and of Pirvano et al. suggested that a definite trend only emerges at Gr greater than 5.0E+10, near the upper limit of the present study.

8.1.2. Laminar Flow

Laminar flow was observed at two streamwise stations (Gr = 2.81E+8 and 7.47E+8). Figure 8.3 compares the non-dimensionalized mean velocity γ and mean temperature β with the theoretical solution of the governing equations. The temperature data agree well with theory. The velocity estimates in the near-plate region, particularly the maximum velocities (0.398 m/s and 0.462 m/s), are also in good accord with theory. In the outer region, however, there is a lack of agreement between theoretical and

---

*$y_N \equiv (T_w-T_\infty)/\left.\frac{\partial T}{\partial y}\right|_{y=0}$.

observed velocities. These discrepancies may be caused by inaccuracies in the calibration of the hot-wire anemometer (see section 6.5.1).

Small disturbances in the laminar flow, particularly over the outer regions, were observed at Gr equal to 7.47E+8. (The upstream profile was not examined for such disturbances.) Figure 8.4 provides values of the non-dimensional power spectra* of T'^2, u'^2 and $\overline{u'T'}$ for one representative lateral position (y = 1.45 mm). The power is concentrated at several peaks with dominant ones at 3.1 and 9.5 Hz**. These spectral data must be regarded as qualitative, however, since the sample period was only two and a half minutes and the signal level of the fluctuations was only just above the discretization level.

The measurements of the deviation of these disturbances are shown in Figures 8.11 and 8.12 as a part of subsection 8.1.4.

8.1.3. 'Transitional' Flow

The development of an "organized' boundary layer structure of random motion' (Townsend (1959)) from laminar flow involves several mechanisms. My appreciation for the nature of these mechanisms was greatly assisted by a report by Colak-Antic and Gortler (1971). A summary of their report is given here as an introduction to 'transitional' flow and as an aid to the discussion of overall flow development in subsection 8.1.4. In their visual observations of aluminium particles in a flow in water, Colak-Antic

---

*The non-dimensionalized spectral density $\phi_{x'y'}(f)$ is defined as $\phi_{x'y'}(f) \equiv P_{x'y'}(f)/\overline{x'y'}$, where $P_{x'y'}(f)$ is the PSD distribution of $x'y'$ (thus $\int P_{x'y'}(f)df = \overline{x'y'}$) and $x'y'$ represents a covariance such as $\overline{u'u'}$, $\overline{T'T'}$ or $\overline{u'T'}$.

**All the PSD distributions are presented with estimates at 0.2 Hz. Although a finer grid could be used, the confidence level of the estimates would decrease correspondingly.

and Gortler saw that two-dimensional Tollmien-Schlictning waves developed from the laminar flow and that, as these disturbances grew, three-dimensional effects were introduced. These effects warped the wave fronts and caused the growth of spanwise shear concentrations that later developed into longitudinal vortex streets.

The vortex action intensified and then decayed. The development of the longitudinal mechanisms was observed in both the outer region and the near-plate region of the flow. The development of Tollmien-Schlictning waves from laminar flow has also been studied by Gebhart and his colleagues and a survey of their work is given in the paper by Gebhart.

In the present investigation, estimates of the velocity and temperature were taken at streamwise stations giving Gr equal to 4.79E+9 and 8.92E+9. In addition, several other profiles of temperature were observed but the data are not presented as they simply confirm the trends of the main data and do not provide any further understanding of the flow structure.

The power spectra of the velocity and temperature data at the downstream station (Gr = 8.92E+9) were devoid of harmonic characteristics and were approximately similar to the spectra which characterized the random motion still further downstream. The data are not presented. The analyses of the samples obtained from the upstream station (Gr = 4.79E+9) revealed strong periodicity in the flow structure. Figures 8.9 to 8.12 show non-dimensionalized PSD distributions of temperature, $\phi_{T'T'}(f)$, velocity, $\phi_{u'u'}(f)$, and their covariance, $\phi_{u'T'}(f)$ for positions on the inner side of the velocity maximum (y = 3.25 mm), near U_m (y = 8.25 mm) and in the outer region (y = 18.25 mm).

In the sample obtained at y equal to 3.25 mm, the first peak appeared at 2.0 ($\pm$ 0.2) Hz although the dominant lobe was situated at 3.6 Hz. The higher harmonics could be seen at intervals of approximately 2.8 Hz (and sometimes 1.4 Hz) in the PSD distributions of temperature and velocity. The data of the samples from y = 8 mm and 20 mm revealed much the same trends as data from y = 3.25 mm.

At y equal to 2.25 mm, the spectra (not shown) of temperature and velocity had a primary frequency of 1.7 Hz which agreed remarkably well with observations of Colak-Antic who noted that when the flow was artificially disturbed, the frequency of 1.65 Hz was selectively amplified.

The phase angle* of $\phi_{u'T'}(f)$ for two samples of the data (y = 3.25 mm and 18.25 mm) is shown in Figure 8.8. A definite relationship exists between the phase angles (θ) and the frequency (f) at the lower values of f (where most of the power resides) but at higher frequencies, the data scatter appears to be random. (The data of the higher frequencies are omitted for the sample obtained at y = 18.25 mm.) In the data from the innermost sample (y = 3.25 mm) the phase angles of the two principal modes differ in sign. At the first peak (f = 2.0 Hz), θ is equal to 28°, whereas at the second (f = 2.6 Hz), θ is equal to -18°. The opposite dependency of θ on f can be detected in the data at the outermost position. This difference accords with the detailed investigations of Knowles and Gehbart (1968) who noted that the phase relationships between temperature and velocity on the inner side of the peak were of opposite sign to those on the outer side. The amplitude analyses of these data are presented in the next subsection.

---

*The phase angle θ is defined as $\theta \equiv \tan^{-1} \frac{Im[\phi_{u'T'}(f)]}{Re[\phi_{u'T'}(f)]}$

8.1.4. Development of the Flow

Measurements of the amplitude distributions of T and U at several streamwise stations are plotted against natural y in Figures 8.9 to 8.12. These data describe the development of the flow near the plate, from the laminar state (Gr = 2.81E+8) into turbulent flow (Gr = 6.81E+10).

Figure 8.9 presents the non-dimensional mean temperature β. A slight lateral redistribution and an increase in the temperature gradient at the plate can be detected as the flow develops, although there are no major changes in the profiles. The streamwise development of U (Fig.8.10) is in contrast to that of β (Fig.8.9). The lateral extent of the velocity profiles is greatly increased with the transition of the flow. In the earlier stages of this change, the maximum velocity decreases as the momentum of the flow is rapidly diffused outward. Further downstream the maximum velocity begins to increase with Gr as it did in the laminar flow.

Figure 8.11 contains a description of the downstream development of the non-dimensionalized temperature deviation β'. As the flow develops along the plate, a definite movement in the position of the peak intensity, β_m', towards the plate can be detected. The magnitude of β_m' increases to a maximum in the transition region (1.0E+9 < Gr < ≈2.0E+10) and diminishes as the flow develops downstream. The lateral profiles of $\sqrt{u'^2}$ (Figure 8.12) have a similar streamwise development in that they grow to a maximum in the transition region. The characteristic broad shape of $\sqrt{u'^2}$ is evolved (Gr < 5.0E+9) before a similar development in the β' profiles occurs.

The streamwise development of the peak intensity β_m', the non-dimensional mean peak velocity γ_m and the maximum deviation γ_m'* are plotted

*γ_m and γ_m' are obtained from the comparison of the maximum velocities of the v and $\sqrt{u'^2}$ profiles with the buoyancy velocity, U_B.

against Gr in Figure 8.13.

The maximum mean velocity, γ_m, has a constant value of 0.57 for Gr < ≈ 1.0E+9 and then gradually decays to a value of ≈ 0.29 at Gr equal to 1.0E+10 and is constant at this value for larger Gr. This behaviour is in good agreement with the data of other investigatcrs reviewed in section 2.2.2. In the range of Gr above 1.0E+9, the values of β_m' grow to a maximum of 0.22 at Gr = 8.0E+9 before they decrease to a constant value of 0.175 above Gr = 2.0E+10. In a similar range of Gr, the value of γ_m' increases to a value of at least 0.14 before it decreases to a constant value of 0.08.

The last Figure (8.14a) in this section contains estimates of the wall shear stress non-dimensionalized with U_m^2, plotted against Gr. These data were determined from the extrapolation of the mean velocity profiles near the plate. (The method is discussed in the following section.) Inaccuracies in the near-plate velocity data probably account for the scatter. Nevertheless, the data show distinct differences from the theoretical solution for the wall shear stress in the laminar flow.

Several characteristics of the present observations accord with other investigations. The growth of the temperature fluctuations to a maximum in the transition region and the decrease to a constant level for higher values of Gr correspond to the fluctuations of the plate temperature observed by Fujii et al. (c.f. 2.2.1). Several aspects of the data also agree with the observations of Colak-Antic and Gortler (c.f. 8.2.3). Whereas a definite harmonic structure could be detected in the measurements at Gr = 7.47E+8 and 4.79E+9, no such structure was observed when the flow had progressed to Gr = 8.92E+9. This would correspond to the development

and decay of Tollmien-Schlictning waves reported by these authors. Further the growth of γ_m' and β_m' to a maximum (Gr ≈ 8.0E+9) and the subsequent decay agrees with their observations of the intensification and decay of longitudinal vortex streets.

The lateral position at which β_m' occurs (y ≈ 6.3 mm) is nearly coincident with that of γ_m', being just outside that of γ_m(≈ 4.8 mm) at Gr equal to 4.79E+9. This observation agrees with the suggestion of Colak-Antic and Gortler and of Knowles and Gebhart that laminar instabilities erupt in the region of the outer inflection point of the mean velocity profile. As the flow evolves downstream, however, the position of β' shifts towards the plate, moving to the inner side of the mean velocity peak, whereas the position of γ_m' becomes almost ccincident with that of γ_m.

It can be seen from a comparison of the data for the heat transfer, the mean velocity, the deviation of temperature and velocity, and the wall shear stress that the transition from laminar to turbulent flow is fairly well defined. For Gr > 2.0E+10 the constancy of the values of γ_m, γ_m' and β_m' suggests that in this range the flow has established itself in a 'self-preserving' structure. It appears that the temperature distributions, of which β_m' is a representative measure, are independent of the flow station* and that the velocity field gradually evolves in strength. In the next section some of the features of the lateral profiles of the 'fully developed' turbulent flow will be examined.

8.2. 'Fully Developed' Turbulence

Above Gr equal to 2.0E+10, the free convection boundary layer developed into a structure that appears to have 'self-preserving' characteristics. In this region, amplitude and power spectrum measurements were taken over a range of Gr extending up to 6.8E+10.

---

*$(T_w - T_\infty)$ was almost constant in this study.

8.2.1. Flow Region very near the Plate

Accurate measurement in the flow adjacent to the plate ($y < 2.0$ mm) was only possible with the thermocouple. Great care was taken to position the sensor with respect to the plate and in the final tests of this series it is estimated that the positional error was less than 0.02 mm (see section 7.1). (One of the sets of data presented, at Gr equal to 6.90E+10, was taken before the final refinements in the positioning technique were developed.) The error in the relative position between two successive observation stations during any one test was much less than the uncertainty in the plate position, being < 0.002 mm (section 4.2).

A linear dependence of β and β' on y (for $y < 1.8$ mm) can be seen in the data provided in Figure 8.14b. The linear dependence of β on y over a relatively wide region suggests that the near-plate region is dominated by molecular exchanges even though β' grows rapidly with y to over one half its maximum value ($\beta_m' = 0.175$) within this region. The growth of the non-linear turbulence transfer mechanisms can be detected for $y > 2.0$ mm.

Although measurements made with a hot-wire anemometer very near the plate ($y < 1.5$ mm) were highly distorted (probably due to the steep thermal gradients), the observations of $\sqrt{\overline{u'^2}}$ in this region nevertheless displayed a linear dependency on y.

Finally, the results of the power spectral analyses suggest that the energy of the flow adjacent to the plate does not have a regular wave pattern. Neither the detailed data from the velocity measurements nor those of the PSD distributions is presented.

Accurate determination of the wall shear stress could not be made from the near-plate velocity data. It was, however, estimated by two methods. In the first, the measurements of the velocities in this region were

'corrected' with a function that was derived from a comparison of the response of a hot wire in laminar flow with the theoretical solution (section 6.5.1). With the best linear fit of the corrected data and the assumption that the viscous shear forces were dominate in this region, an estimate of the wall shear stress was calculated. Unfortunately, the error in the velocity data was not substantially reduced by the correction factor. This may have been caused by the differences between the mean temperature gradient at the plate in the laminar flow ($\approx$ 4500 K/m) and in the turbulent flow (7000 K/m). Consequently, error in the estimates of the wall shear stress may be fairly large (+-50%).

The above evidence that the near-plate flow is controlled by molecular transfer gave rise to a second estimate of the wall shear stress. With the assumptions that there were no streamwise variations of flow properties, and that V was equal to 0, the flow could be approximated by a Couette flow. The conservation of the momentum of such a flow is described (section 9.2) by the equation

$$\frac{\partial}{\partial y}(\mu\frac{\partial U}{\partial y}) + \rho g \frac{(T(y)-T_\infty)}{T_\infty} = 0 \quad . \qquad (8.2)$$

Using the evidence that the temperature is linear over the near-plate region, this equation may be integrated with respect to y. The introduction of the appropriate boundary conditions ($\mu\frac{\partial U}{\partial y} = \tau_w$ and U = 0 at y = 0) provides an equation that describes the behaviour of the streamwise velocity near the plate:

$$u(y) = \frac{1}{\mu}[\tau_w y - \rho_\infty g \frac{(T-T_\infty)}{T_\infty}\frac{y^2}{2} + \frac{\rho_\infty g}{T_\infty}\left.\frac{\partial T}{\partial y}\right|_{y=0}\frac{y^3}{6}] \quad . \qquad (8.3)$$

This expression agrees with that of Yang and Nee who also considered the possible influences of turbulence in this region before concluding that they were negligible (c.f. section 2.2.2). The second estimate of the wall shear stress was calculated from equation 8.3 and velocity data near the plate. (These data were presented in section 8.1.4.) In view of the errors involved in both methods of calculation, the values can only represent 'ball park' estimates of the true wall shear stress.

Evidence which points to the importance of the thin viscous layer in the control of the lateral extent of the boundary layer was given by Fujii et al. They demonstrated that a non-dimensional lateral distance, ζ, obtained from the gradient of mean temperature at the plate, successfully correlated temperature data over a wide range of Pr. This parameter also appeared to correlate the velocity data of Cheesewright (Fujii (1971)). The non-dimensional distance ζ is defined as y/y_N where the heat-transfer distance, y_N, is defined by

$$y_N \equiv (T_w - T_\infty) / \left.\frac{\partial T}{\partial y}\right|_{y=0} .$$

The variation of y_N against Gr is shown in Figure 8.2.

If ζ does correlate the lateral growth of the boundary layer considered in this study, y_N must gradually increase with increasing x. This implies that $\left.\frac{\partial T}{\partial y}\right|_{y=0}$ decreases with increasing x which would, in turn, suggest that the heat-transfer coefficient, h, may have a very slight negative dependency on x. This dependency was, in fact, reported by Fujii et al.

8.2.2. Overall Structure of the Boundary Layer

The viscous sublayer constitutes a very thin portion (1 - 2 mm) of the lateral extent of the flow. Outside this layer, the flow is

characterized by random motion with high local intensities of turbulence and it extends beyond 200 mm albeit that the turbulence is intermittent there. Some of the characteristics of this region of the turbulent boundary layer are examined in the following subsections.

The flow was observed with the use of a single thermocouple, an arrangement of a single hot-wire + thermocouple and crossed-wires + thermocouple. The data from the different probe configurations had varying degrees of accuracy and are presented separately. The discussion is divided into four subsections: amplitude analyses of the temperature data from the thermocouple (8.2.2.1) and of velocity data from the single wire + thermocouple arrangement (8.2.2.2), amplitude analyses of data from the crossed-wire arrangement (8.2.2.3) and spectral analyses of the data from the single wire + thermocouple (8.2.2.4).

8.2.2.1. Distributions of Temperature

In Figures 8.15 to 8.19 the most accurate measurements of probability density distributions of temperature are presented. In Figure 8.15 three probability distributions of temperature at Gr = 3.8E+10 are presented. These representative samples were selected because the values of their third moments were at a minimum (y = 2.00 mm), at zero (y = 6.0 mm) and at a maximum (y = 25.0 mm). (The third moment is a measure of the asymmetry of a distribution.)

The distributions of the innermost (y = 2.0 mm) and outermost (y = 25.0 mm) samples were skewed strongly toward the higher and lower temperatures, respectively, whereas the distribution at y = 6.0 mm was symmetrical. These distributions also showed the probability that the local temperature would assume the value of the ambience (c.f. section 2.2.3).

This measure was still finite very near the plate. For example, local temperatures equal to that of the ambience have been detected 4 mm from the plate.

In Figures 8.16 to 8.19, non-dimensional functions of the probability density distributions are presented against the non-dimensional distance ζ. Good agreement of the data for the expected value β (Fig.8.16) may be expected over the inner region of the flow since ζ is determined from the mean temperature gradient at the plate. The significant aspect, however, is the good correlation in the outer regions. This is analogous to the case in forced convection flow where lateral profiles of the boundary layer are correlated with a function of the non-dimensional wall shear stress.

Figure 8.17 shows the profiles of the deviation β'. The value of β' grows linearly with ζ through the near-plate region (see section 8.2.1) to a maximum ($\beta' = 0.175$) at $\zeta = 0.95$ ($y \approx 5$ to 6 mm) and then gradually decays over the outer region. The maximum values, β_m', are significantly greater than those reported by Cheesewright (1966) and Hall and Price (c.f. section 2.2.3). Cheesewright performed his survey investigation with the use of a resistance wire that was over 10 mm in length whereas Hall and Price employed a similar resistance wire. It is probable that in both cases the resistance wires were not sensitive (spatially or timewise) to the higher frequency components and/or that the analogue instrumentation used to process the signals did not respond to the lowest frequencies of the signals.

In the next Figure (8.18), the skewness factor (S) is plotted against ζ. These data provide a measure of the asymmetry that was detected in the representative samples of probability distributions shown in Figure 8.15.

Except for a very small region, just outside the position of maximum intensity (ζ = 0.95), all the distributions of temperature are skewed either towards the plate temperature or towards the ambient temperature. The scatter in the data for the near-plate region and for the outermost region is probably due to the highly peaked nature (small variance) of the distributions. Either the probability cell width (0.4 K) was not fine enough or else the sample times were not long enough (five and ten minutes) to resolve these moments.

The flatness factors (F) are plotted on a logarithmic scale against ζ in Figure 8.19. The data indicate that the distributions within the near-plate region and in the outer extents of the flow are very 'peaked' but that over the region where β' is at a maximum, the distributions are uniformly dispersed.

The characteristics of the instantaneous temperature may be broadly interpreted from these measures of the probability density distributions. Within the near-plate region, the distributions are skewed toward the plate and highly peaked. Although some convective transport from the cooler regions occurs, any mixing is mainly of a local nature. Further out (ζ = 1.0), the distributions are much wider, more symmetrical and uniformly dispersed. This is a region of intense mixing of fluid elements of different thermal energies. The local temperatures have an equal probability of assuming the value of the ambient temperature or the plate temperature. Beyond this region, the distributions are very biased toward the lower temperatures; also, the deviation, β', of the distribution decays with an increase in y.

8.2.2.2. Distributions of Velocity

In this section, an analysis of probability density distributions of the streamwise velocity, similar to that of the temperature in the previous section, is presented. Figure 8.20 presents only one representative of the probability density distributions because the shapes of the distributions across the boundary layer were fairly similar.

In Figure 8.21 the non-dimensional mean velocity γ is plotted against ζ. (The near-plate data for Gr = 6.81E+10 are not presented because of an experimental error.) The agreement between the data taken at different Gr is good. The ratio between the maximum value of γ (0.285) and that of the maximum valocity γ_L (which a laminar boundary layer would attain in similar conditions) is

$$\kappa = \frac{\gamma}{\gamma_L} = 0.52 \ .$$

This is in good agreement with the results of a similar analysis presented in section 2.2.2.

The values of $\sqrt{\overline{u'^2}}$ are compared with the local mean values U in Figure 8.22 and with the maximum velocity U_m in Figure 8.23. Although Figure 8.22 shows more scatter among the data from different values of Gr than can be seen in the data for γ (Figure 8.21), there is still a fair degree of correlation. From the plate the local intensity increases with y, rising to a value of nearly 0.3 just outside the viscous sublayer. This value corresponds with that of Vliet and Lui (c.f. section 2.2.4). The local intensity remains constant at this value over much of the inner layer ($y < 25$ mm) but increases to a maximum of between 0.70 and 0.90 near y equal to 150 mm.

A close examination of the non-dimensional $\sqrt{\overline{u'^2}}$ profiles in Figure 8.23 and the β' profiles in Figure 8.17 reveals that β_m' occurs at $\zeta \approx 0.95$ whereas the position of maximum $\sqrt{\overline{u'^2}}$ coincides with that of U_m (at $\zeta \approx 1.5$); hence, a separation of the positions of maximum intensity of velocity and temperature exists. The position of β_m' may be explained as the optimum point of interaction between the intensity of quantities such as $\sqrt{\overline{u'^2}}$ which increase with distance from the plate and the mean temperature gradient which decreases with increasing ζ. Figure 8.23 also shows that the profile of $\sqrt{\overline{u'^2}}$ appears to have two peaks: one that is coincident with U_m and one further out at $\zeta \approx 5 - 6$. The position of this second maximum roughly coincides with those of the maximum third moment of the temperature distribution and the outer inflection point of the mean velocity profiles.

The analysis of the higher moments of selected data samples taken from several positions across the boundary layer revealed that all the velocity distributions are nearly symmetrical ($|S| < 0.1$). The measurements of the flatness (F) are shown in Figure 8.24. Although the values are slightly higher in the near-plate and outer-most regions than the value for a Gaussian distribution ($F = 3.0$), the measurements agree with the Gaussian value over the mid region.

Thus, in contrast to the temperature distributions which are not similar for different positions across the flow, the distributions of velocity appear to be similar over the mid region of the boundary layer. Their agreement with Gaussian distribution suggests that motion over this region ($1 < \zeta < 10$) is completely random. The higher values of the flatness factor for the velocity distributions near the edges of the flow possibly reflect the influence of the boundary conditions.

The mean velocity data are presented in two further forms. First, non-dimensionalized by the shear stress velocity U_*, they are shown in Figure 8.26 plotted against the shear stress distance y_*. This analysis was performed at only one station (Gr = 6.81E+10) because of the uncertainty in the estimation of the shear stress (see subsection 8.2.1). Secondly, the mean velocity measurements (observed at Gr = 4.84, 6.81E+10) are compared with those of Cheesewright (3.04, 5.72E+10) in Figure 8.25. The comparison shows that Cheesewright's data, though slightly higher, are in general agreement with the present results. The minor difference represents a velocity of 0.01 - 0.02 m/s which is well within experimental error.

The data presented in Figure 8.27 do not strictly belong in a discussion of the characteristics of velocity but measurements of the correlation coefficient between temperature and streamwise velocity ($R_{u'T'}$) are derived from the same observations of the flow. The values of $R_{u'T'}$ are close to zero in the near-plate region; they rise to 0.6 over the middle portions and then fall back to zero in the extreme outer region. These characteristics indicate that the temperature and velocity fluctuations are nearly independent of each other close to the plate and in the outermost region, but over the major part of the layer there is a fair degree of correlation. In one of the data series analysed (Gr = 3.51E+10), $R_{u'T'}$ becomes negative in the outer region. Since most of the observations in this part of the flow must be treated as qualitative (see Section 6.5.1), no attempt was made to verify this measurement.

8.2.2.3. Measurement of Covariances

Two survey experiments were performed (at Gr = 4.84E+10) with a crossed-wire+thermocouple probe aligned perpendicular to the plate. A second

thermocouple was situated near the main probe to serve as a monitor on the response of the first. Although full profile studies were performed, the measurements for distances less than 10 mm were highly distorted, probably because of the large temperature gradients along the wire. The observations in the outer region (y > 80 mm) showed that the response of the thermocouple was affected by the wakes of the hot-wire elements. Earlier velocity measurements with the single wire+thermocouple probe over the intervening region (section 8.2.2.2) indicated that the local intensities were about 0.30, too high for reliable measurements to be made with a crossed-wire probe having wires inclined to the flow at about 40°. Nevertheless, the data present some interesting results.

In Figure 8.28 the expected values of U are compared with measurements made with a single wire+thermocouple arrangement. The values of the data from the crossed-wire probe are considerably higher than those from the single wire arrangement. There is also a lack of repeatability between the measurements from the crossed-wires themselves. Fortunately there is an overall agreement in the shape of the profiles which leads to the hope that the measurements presented in the following discussion may at least portray the correct trends.

Figure 8.29 provides the measurements of V. Only one of the tests shows the expected increase of V with distance from the plate.

The values of β' obtained from the crossed-wire+thermocouple probe are compared with those taken from the single thermocouple (section 8.3.1) in Figure 8.30. Agreement between the data is good over most of the layer but the effect of the wakes of the hot wires may be seen in the data for y > 80 mm. The same Figure shows the values of ratio $\overline{u'^2}/\overline{v'^2}$ which are in general agreement with the data of Klebanoff.

In the following Figure (8.31) measurements of the correlation coefficients $R_{u'v'}$, $R_{u'T'}$, $R_{v'T'}$ are given. The values of $R_{u'T'}$ are slightly higher than those reported in Figure 8.27 (section 8.2.2.2). The shear stress coefficient $R_{u'v'}$ and the lateral heat-transfer coefficient $R_{v'T'}$ are fairly constant over the layer with values between 0.4 and 0.5.

The observed values of $\overline{u'v'}$ and $\overline{v'T'}$ are given in Figure 8.32 while in Figure 8.33 the estimates of the turbulent Prandtl number are presented. This correlation was determined from the formula

$$Pr_t = \frac{\overline{u'v'}(\frac{\partial T}{\partial y})}{\overline{v'T'}(\frac{\partial U}{\partial u})} \quad . \tag{8.4}$$

The values of Pr_t are dominated by the characteristics of $\frac{\partial T}{\partial y}$ and $\frac{\partial U}{\partial y}$: the estimates of Pr_t become increasingly large in the region of the maximum mean velocity (where $\partial U/\partial y$ approaches zero) and they tend towards zero in the outer regions (where $\partial T/\partial y$ approaches zero). The dependency of Pr_t on y is singularly distinct from other reports (see Kestin and Richardson (1963)).

8.2.2.4. Power Spectra Distributions

Of particular interest in this study of the spectra of temperature and velocity in the 'self-preserving' region of free convection turbulence is the possibility that the dissipation of turbulence kinetic energy may be isotropic. Kolmogorov (1941) suggested that in an extensive spectral range containing no production or dissipation of energy and in which only inertial transfers to smaller and smaller eddies were occurring, the power spectrum should be independent of viscosity. Such a range is called the inertial subrange and in it, $P_{u'u'}(f)$ is proportional to $f^{-5/3}$. At

frequencies above this range, the spectrum should be a function only of the rate at which energy is dissipated by viscous forces (Lumley and Panofsky).

Similar arguments can be applied to the annihilation of the temperature fluctuations, yet with the difference that the temperature field is transported by the velocity field. Corrsin (1951) showed that, where the inertial ranges of temperature and velocity overlap, $P_{T'T'}(f)$ is proportional to $f^{-5/3}$ as well. It is the identification of the inertial sub-range that forms the particular interest of this study.

The non-dimensional spectra* of $\overline{u'^2}$, $\overline{T'^2}$ and $\overline{u'T'}$ taken at three y stations for Gr equal to 6.81E+10 (near the maximum velocity, $\bar{y}$ = 10.55 mm, at y = 55.6 mm and in the outer region y = 90.6 mm) are shown in Figures 8.34 to 8.36. These data were obtained with the use of the single wire+thermocouple arrangement.

In the spectra from the innermost position, the PSD distribution of $\overline{T'^2}$ is fairly constant for frequencies less than 1 Hz and decays at a rate proportional to $f^{-5/3}$ in the range between 4 and 15 Hz. Above this upper limit, the spectrum decays at a higher rate. The PSD distributions of $\overline{u'^2}$ is different in that it decays at a rate proportional to f^{-1} for f > 0.5 Hz. It also falls off more quickly at frequencies above 15 Hz.

The characteristics of the $\overline{T'^2}$ spectra at y equal to 55.6 and 90.6 mm are very similar to those at the innermost position. The spectral distributions of the velocity have altered, however. In the frequency range between 0.5 Hz and $\approx$10 Hz, the decay rate is proportional to $f^{-5/3}$.

---

*The PSD data are compared with a frequency parameter rather than a wave number value for uniformity in presentation with section 8.1. The information necessary to derive the wave numbers is given.

Above this frequency the spectra of temperature and velocity fall at rates of $f^{-1/5}$ and $f^{-1/3}$ respectively.

The decay rates at the higher frequencies may have been influenced by aliasing since data signals were not properly filtered before digitizing (see section 7.2). As a consequence, no analysis of this range of the spectra was performed.

It appears that on the outer side of the velocity peak, in accordance with Kolmogorov's hypothesis, the spectra contains an inertial subrange in which neither the production nor the dissipation of turbulence kinetic energy takes place. Nearer the plate (in the region of the maximum mean velocity) the structure of the temperature field possesses similar characteristics to those further from the plate, but the velocity field does not. It is probable that this region is still influenced by the plate.

8.2.3. Flow in the Outermost Regions

A study of intermittency in the temperature and velocity structure, near the free boundary, was undertaken in this programme, the single wire + thermocouple arrangement being used to obtain the data. It became clear during the early studies of the temperature that measurements of intermittency were very sensitive to the threshold levels of the criteria employed to distinguish between turbulent and ambient fluid. Several methods of determining intermittency were developed in order to reduce this sensitivity. A summary of these methods is presented in Table 8.1.

The major problem in the study was the lack of a criterion by which the results of the analyses could be assessed. Earlier investigators (e.g., Fielder and Head (1966)) suggested that the intermittency function across the layer may be described by a Gaussian probability curve. In the

present case, acceptable fits to such a function were obtained with reasonable values of threshold levels which positioned the midpoint of the intermittency (I = 0.5)* anywhere within the middle half of the boundary layer.

Two criteria were used for most models. The first was usually a measure of an amplitude characteristic and the second was a measure of the temporal characteristic (Table 8.1). Only two or three data samples of the immediate past history were considered in the determination of intermittency in order to minimize computing costs. (Each data point of the time history was examined sequentially.) One of the more promising developments is the use of a histogram of 'ambient intervals' in conjunction with a primary amplitude criterion (Model F, Table 8.1).

This model was developed in the later stages of the study and final details of such an analysis have not been formulated. With a histogram of time intervals where an ambient condition occurs, there should be a characteristic that will provide a foundation on which the intermittency measure may be based.

In the analysis, the shape of the intermittency measure of the temperature field rarely agreed with that of the velocity although the parameters of each model could be adjusted to produce a reasonable profile of intermittency. Furthermore, a 'cross intermittency' measure (that is, a measure of the interval where both temperature and velocity were ambient) never yielded realistic estimates. This may indicate that turbulence is isothermal in the outer regions for relatively long time intervals - if all

---

*I is the conventional definition of intermittency.

$I \equiv \frac{N_t}{N}$ where N, N_t are the number of total points and turbulence points respectively.

other factors are reliable. However, the inaccuracy of the hot-wire anemometer must also be considered. Moreover, the measurement of the intermittency of the turbulence may not be possible with a single hot-wire. It may be that the examination of an appropriate covariance term (Antonio (1972)) or a spatial derivative (Kovasznay et al.(1970)) would provide a better measure of the intermittency.

8.3. Résumé

Quantitative measurements of the streamwise development, the lateral profiles of amplitude and the spectral characteristics of temperature and velocity of a free convection boundary layer have been provided in this chapter. Considerable evidence has been also presented on the transition of the free convection boundary layer from the laminar state to a 'fully turbulent' flow. Further evidence of the evolution of the turbulent boundary layer has been given up to the limit imposed by the experimental apparatus. Below is a collation of many of the features that were observed in this experimental programme.

Measurements of the heat transfer from the plate and the mean velocity profiles revealed that a definite transition occurs between 5.0E+9 and 1.0E+10, whereas data for the non-dimensional deviations β' and γ' suggest the same lower limit but do not attain a constant value until Gr equal to 2.0E+10. In the lower part of the transition region, the disturbances in the flow have a periodic structure with a dominant frequency of 3 Hz although other frequencies, particularly 9 Hz, are evident. The phase angles of the covariance $\overline{u'T'}$ of these dominant frequencies are often different in sign. Furthermore, the periodic motion on the inner side of the peak of the mean velocity is out of phase with the motion well outside the peak region.

As the flow develops up the plate, evidence of the periodic structure disappears but the temperature and velocity intensities continue to increase. This behaviour corresponds to the visual observations of Colak-Antic and Gortler who noted that the development of Tollmien-Schlictning waves spawned the growth of longitudinal vortices which intensified and then dissipated. Above Gr equal to 2.0E+10, the flow reached a 'self-preserving' state in which the rate of development of the temperature field becomes static whereas the growth of the velocity field is proportional to $x^{0.5}$.

A detailed examination of the lateral structure of the 'fully developed' flow revealed that the temperature field adjacent to the plate is linearly dependent on x which suggests that the heat-transfer interaction between the flow and the plate is governed by molecular action.

Just outside this layer, the intensity of the temperature fluctuation reaches a maximum. This maximum is nearer to the plate than the peak of the mean velocity profiles, whereas the position of the maximum intensity of the velocity fluctuations coincides with that of the peak mean velocity. Analyses of the spectra of $\overline{T'^2}$ and $\overline{u'^2}$ in the region of the peak mean velocity revealed the existence of an inertial subrange in the spectrum of temperature fluctuations in which energy is neither produced nor dissipated, whereas the spectrum of $\overline{u'^2}$ does not have this characteristic. However, beyond this region of peak velocity ($y > 25$ mm), the spectrum of $\overline{u'^2}$ also possesses a sub-inertial range. Over the mid-region ($20 < y < 90$ mm) the value of $\overline{u'^2}$ was fairly constant, although there was evidence of a second maximum at a value of y between 50 and 75 mm.

Qualitative measurements of the cross-correlations revealed that the turbulent shear stress and lateral heat transfer were constant in this

region whereas the values of the streamwise heat transfer gradually decreased as y increased. The values of the turbulent Prandtl number determined from the estimates of the covariances were very surprising.

In the outer region (y > 60 mm), the local intensity attains a value above 0.7. It is most probable that instantaneous negative velocities are present in this region. No detailed analyses of the data were made.

In general, the measurements were self-consistent (possibly as a result of the long sample periods) and compared favourably with many other works. Many of the qualitative observations and exploratory measurements of the behaviour of free convection flow past a vertical plate reviewed in Chapter 2 were also confirmed by these measurements.

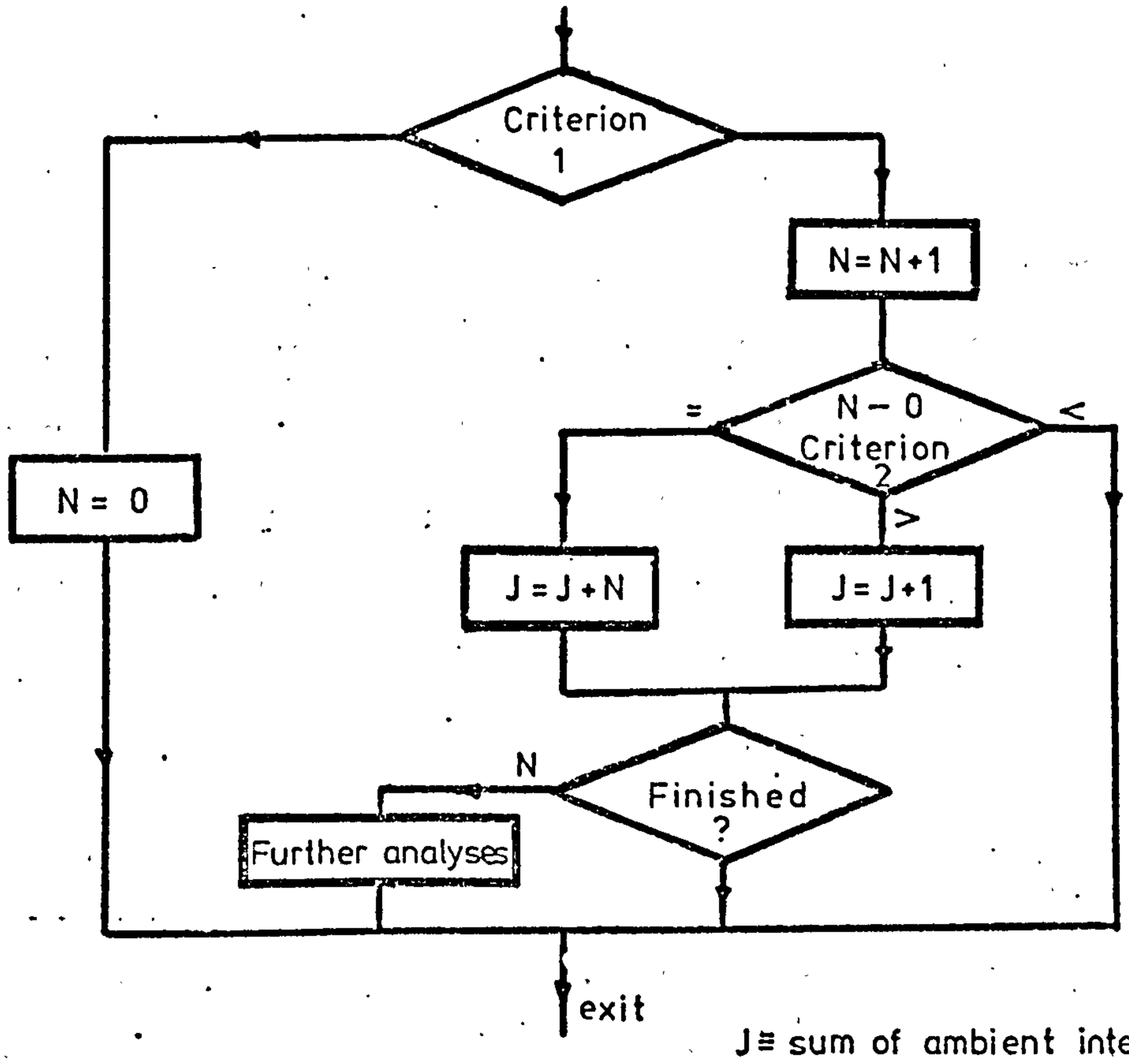

TABLE 8.1 METHODS OF DETERMINING INTERMITTENCY

Model	Data	Criterion 1	Criterion 2
A	u, T	Amplitude	Time, t
B	u, T	Amplitude	$\frac{dU}{dt}, \frac{dT}{dt}$
C	u, T	$\frac{dU}{dt}, \frac{dT}{dt}$	Time
D	$\frac{dU}{dt}, \frac{dT}{dt}$	$(\overline{\frac{d^4x}{dt^4}})/(\overline{\frac{d^2x}{dt^2}})^2$,	Townsend's flatness proposal
E	$\overline{u'^2}, \overline{T'^2}$	Amplitude	Time
F	$\overline{u'^2}, \overline{T'^2}$	Amplitude	Histogram of Time intervals

CHAPTER 9

THEORETICAL DESCRIPTION OF THE TURBULENT FREE CONVECTION BOUNDARY LAYER

The free convection boundary layer has several features in common with other flows. For example, it is similar to a wall jet issuing into stagnant surroundings in that both are strongly asymmetric boundary layer flows along a wall. But whereas the flow in the wall jet decelerates, the free convection boundary layer flow along the plate is accelerated by the buoyancy forces. In this sense it is similar to a flow along a flat plate in a favourable pressure gradient, but in the free convection flow, the 'pressure gradient' is a function of the distance from the plate. This 'internal source of momentum' is one of the most distinguishing features of the free convection flow. However, the application to free convection of turbulence models designed for the prediction of forced flows is justified by the features which the flows have in common. Furthermore, in recent years the advancement of computational techniques has encouraged the formulation of models of turbulence which incorporate more physics than did earlier hypotheses. The good agreement found between the experimentally measured characteristics of a diverse range of forced convection flows and the solutions of the transport equations employing these models leads to the hope that the turbulence characteristics embodied by the models can be used to advance the understanding of the structure of turbulent free convection flow.

Previous theoretical analyses of the turbulent free convection boundary layer are reviewed in the first section of this chapter. The second section, 9.2, contains a résumé of the derivation of the boundary layer equations and a description of the transport equations for the mean kinetic energy, turbulence kinetic energy and the variance of the

temperature fluctuations. The last section, 9.3, examines some of the hypotheses of turbulence which are applicable to this flow, summarizes the modelled transport equations which are used in Chapter 10 and describes the method used to solve the set of transport equations.

9.1. Review of Previous Theoretical Analyses

The turbulent free convection boundary layer is governed by conservation equations for momentum, energy and mass (see equations (9.1) to (9.4), section 9.2). Before the system of coupled differential equations could be solved, investigators have had to approximate the lateral turbulent transport terms, in particular, the Reynolds shear stress $\overline{u_1'u_2'}$. Everyone except Yang and Nee has relied upon relationships derived from the study of forced convection flow in order to accomplish this approximation. Eckert and Jackson (1953) employed an integral solution based on a power law description of the velocity and temperature profiles of Griffith and Davis and forced flow relationships such as that of the Blaius[4] for the wall shear stress. Bayley (1955), Fujii (1959b) and Larson (1966) adopted similar integral techniques. These solutions provided satisfactory correlations of the heat transfer but the predicted velocities were not in good agreement with the experimental data.

Kato et al. also treated the free convection boundary layer as a special case of forced convection. By adopting a lateral distribution of the effective viscosity from a forced boundary layer flow, they solved the momentum and energy transport equations by a trial and error method. The non-dimensional profiles of mean velocity and temperature thus obtained agreed with existing data and, in particular, their predictions of the heat-transfer rates correlated well with experimental evidence over a wide range of Prandtl numbers.

More recently, the development of numerical methods to solve differential equations has led Lockwood and Ong (1968) and Oosthuizen (1970) to use the Prandtl mixing length hypothesis in the solution of the equation set. The results of both analyses show good agreement in a non-dimensional comparison with the velocity data of Cheesewright (1968). The heat-transfer data exhibit a reasonable agreement as well.

In the first analysis to model the lateral turbulent shear stress by a single differential transport equation, Yang and Nee had to alter the optimized empirical constants of the total viscosity transport hypothesis (Nee and Kovasznay*) in order to fit the solution to Cheesewright's data. Possibly due to the lack of further experimental data, no attempt was made to assess the accuracy of their solution. Nonetheless, their analysis, which suggests that the inner region of the flow is dominated by mechanisms of generation and dissipation and that the outer region (well outside the peak) is controlled by convective and diffusive processes, has aided the understanding of the flow structure.

From the analyses of Kato and of those using the mixing length hypothesis, it appears that the mechanisms of turbulence governing the gross features of the boundary layer are similar in forced and free convection flow. This implies that the lateral turbulent convection processes are independent (to the first order at least) of whether the source of momentum is external or internal to the flow.

The disparity in the empirical constants of the total viscosity models used in forced and free convection flows suggests a lack of similarity between the mechanisms of turbulence in these flows, but this

---

*These constants were optimized using forced flow data on a flat plate.

difference may equally indicate the limited application of the hypothesis. It is unlikely that the proposed rate equation would successfully predict other types of turbulent flows, such as jet flow, without further alterations. (This model of turbulence is reconsidered in section 9.3.)

It is possible that few qualitative comparisons have been made in these investigations because of the lack of sufficient experimental evidence of the streamwise development of the turbulent boundary layer. Yet it is in this direction that the buoyancy forces are orientated. One of the aims of this analysis was to study the streamwise growth of the boundary layer with the use of several models of turbulence designed for the prediction of forced convection flow. But before these models are presented, the governing equations of motion must be considered.

9.2. Governing Equations

In the following analysis of a two-dimensional free convection boundary layer, the cartesian coordinate system is orientated with the x_1 axis in the vertical direction (along the plate), the x_2 axis extending out from the plate and the x_3 axis defined by the right hand rule. The analysis is restricted to boundary conditions of uniform plate temperature, T_w, and uniform ambient fluid temperature, T_∞, where $T_w > T_\infty$. It is assumed that body forces are derived from small changes in the local fluid density and that all physical properties are functions of the local mean temperature only (except in the buoyancy term). (The specific heat of constant pressure, c_p, is treated as a constant.)

The equations which govern the motion of a viscous incompressible fluid in a uniform gravitational field may be written in a form similar to that used by Townsend (1956). Given below are the equations for the conservation of momentum, energy and mass respectively*.

---

*Wherever the tensor notation is used, the summing convention over repeated indices is adopted.

$$\rho \frac{D}{Dt}(U+u')_i = \frac{\partial}{\partial x_k}(\mu \frac{\partial (U+u')_i}{\partial x_k}) - \frac{\partial (P+p')}{\partial x_i} - \rho g \delta_{1i} \tag{9.1}$$

$$\rho \frac{D}{Dt}(T+T') = \frac{\partial}{\partial x_k} \frac{\mu}{\sigma} \frac{\partial (T+T')}{\partial x_k} \tag{9.2}$$

$$\rho \frac{\partial (U+u')_i}{\partial x_i} = 0 \tag{9.3}$$

where U, u' are the mean and fluctuating components of instantaneous velocity; T, T' temperature and P, p' static pressure. σ is the Prandtl number. For pure free convection flow ($U_\infty = 0$) the mean static pressure gradient may be eliminated (Cheesewright (1966)).

With this modification the equation for the momentum in the streamwise direction reads

$$\rho \frac{D}{Dt}(U+u')_1 = \frac{\partial}{\partial x_k}(\mu \frac{\partial}{\partial x_k}(U+u')_1) - \frac{dp'}{dx_i} - g(\rho-\rho_\infty) \quad . \tag{9.4}$$

If a gaseous fluid (strictly only a 'perfect' gas) is considered, a version of this equation given by

$$\rho \frac{D}{Dt}(U+u')_1 = \frac{\partial}{\partial x_k}(\mu \frac{\partial}{\partial x_k}(U+u')_1) - \frac{dp'}{dx_i} + \frac{g\rho_\infty}{T_\infty}(T-T_\infty) \tag{9.5}$$

can be applied. It is convenient to use both forms in the following discussion.

For a two-dimensional boundary layer flow, the motion is considered statistically independent of the flow property variations in the x_3 direction (i.e., $U_3 = 0$, $\frac{\partial \phi}{\partial x_3} = 0$ where ϕ represents any flow property). With this restriction, equations (9.1) to (9.5) form the fundamental set which describes instantaneous motion in a two-dimensional turbulent free convection flow.

With the use of the boundary layer assumption (i.e., derivatives with respect to the lateral distance tend to be one order of magnitude larger than streamwise derivations; see Rotta (1962), Hinze, Bradshaw (1971b) for discussion), several terms in the fundamental set of equations may be judiciously neglected. Further simplifications with the use of the continuity equation to regroup various terms lead to steady time-averaged equations of the conservation of streamwise momentum energy and mass which may be written as

$$\underbrace{\rho\frac{DU_1}{Dt}}_{\text{convection}} = \underbrace{\frac{\partial}{\partial x_2}\left(\mu\frac{\partial U_1}{\partial x_2} - \rho\,\overline{u_1'u_2'}\right)}_{\text{diffusion}} - \underbrace{g(\rho-\rho_\infty)}_{\text{generation}} \tag{9.6}$$

$$\rho\,\frac{DT}{Dt} = \frac{\partial}{\partial x_2}\left(\frac{\mu}{\sigma}\,\frac{\partial T}{\partial x_2} - \rho\overline{u_2'T'}\right) \tag{9.7}$$

$$\frac{\partial U_i}{\partial x_i} = 0 \tag{9.8}$$

where the x_1 derivatives of the momentum and energy diffusion are neglected.

In addition to this set of equations, the transport equations expressing conservation of other flow properties may be obtained from the fundamental equations (9.1) to (9.5). Examples of different methods of derivation are given by Bradshaw (1971b), Rotta (1962) and Hinze. Details of these will not be presented here; rather, attention is directed to the study of the resulting equations and their significance.

For steady free convection flow, the mean kinetic energy or the mechanical flow energy, K*, is governed by the equation

---

*defined as $K \equiv \frac{U_i U_i}{2}$ but since U_1 is usually >> U_2, in this study K is considered as given by $U_1U_1/2$.

$$\underbrace{\rho \frac{DK}{Dt}}_{\text{convection}} = \underbrace{\frac{\partial}{\partial x_2}(\mu\frac{\partial K}{\partial x_2} - U_i\overline{u_1'u_2'}) - \frac{\partial}{\partial x_1}(U_i(\overline{u_1'^2}-\overline{u_2'^2}))}_{\text{diffusion}} - \underbrace{U_i g(\rho-\rho_\infty)}_{\text{generation}}$$

$$\underbrace{-\mu(\frac{\partial U_1}{\partial x_2})^2 + (\overline{u_1'^2}-\overline{u_2'^2})\frac{\partial U_i}{\partial x_1} + \overline{u_1'u_2'}\frac{\partial U_i}{\partial x_2}}_{\text{decay}} \qquad (9.11)$$

This transport equation* describes the first stages of the extraction of kinetic energy from the mean flow and its subsequent dissipation. The term $Ug(\rho-\rho_\infty)$ which represents the work of the buoyancy force against the velocity U_1 generates the mean kinetic energy which is then distributed by convective and diffusive processes to regions where it is dissipated**. The term which describes a direct dissipation into heat $(\mu(\frac{\partial U_i}{\partial x_2})^2)$ is negligible over most of the layer.

The other dissipation processes represent an interaction between a turbulent stress and the mean gradient and are highly important in the energy transfer processes. To appreciate their significance, the transport equation for turbulence kinetic energy must first be considered.

The transport equation for turbulence kinetic energy (defined as $k \equiv \frac{\overline{u_i'u_i'}}{2}$) may be thought of as controlling the last stages of the dissipation of mechanical energy. It is obtained by summing over the transport equations for the normal Reynolds stresses, each derived from the fundamental set. Hence,

---

*The streamwise derivatives, normally negligible compared to the lateral derivatives, are included because some of these terms may be important in the region where the lateral shear stress changes sign. Their importance is assessed more closely in the discussion of the transport equation of turbulence kinetic energy.

**Although in this discussion of some of the transport equations each term is categorized as serving only one function, this analysis is not strictly true since every interaction of motion results in redistribution and viscous dissipation of energy (Rotta).

$$\rho \frac{Dk}{Dt} = \underbrace{\frac{\partial}{\partial x_2}\left(\mu \frac{\partial}{\partial x_2}(k+\overline{u_2'^2}) - \overline{u_2'(k+p')}\right)}_{\text{diffusion}}$$

$$\underbrace{\text{convection}}$$

$$\underbrace{- (\overline{u_1'^2}-\overline{u_2'^2})\frac{\partial U_1}{\partial x_1} - \overline{u_1'u_2'}\frac{\partial U}{\partial x_2} + \frac{g\rho_\infty}{T_\infty}\overline{u_1'T'}}_{\text{generation}} - \underbrace{\varepsilon}_{\text{dissipation}} \tag{9.10}$$

The examination of the generation processes will be deferred until the function of some of the other terms has been considered. There are several terms representing the diffusion of k which are difficult to evaluate. The term $\overline{u_2'p'}$ can be interpreted as the redistribution of k by the pressure fluctuations and is usually ignored (Hanjalic and Launder (1972)). This is not the case with another unknown term, $\overline{u_2'k}$, a third order term which must be accounted for with the other diffusion and convection terms in the solution of this equation.

The dissipation of turbulence kinetic energy is embodied in the quantity ε which comprises a number of terms. Although the signs of the individual terms may not always be the same, their sum is always positive (Lumley and Panofsky (1964)); hence,

$$\varepsilon \equiv \tfrac{1}{2}\mu\overline{\left(\frac{\partial u_i}{\partial x_j} + \frac{\partial u_j}{\partial u_i}\right)\left(\frac{\partial u_i}{\partial x_j} + \frac{\partial u_j}{\partial x_i}\right)} \geq 0 \quad .$$

Daly and Harlow reported that the dissipation rates of k are unlikely to be affected by buoyancy forces; consequently the dissipation rates in free convection flows should be governed by mechanisms similar to those present in forced flows.

Two of the source terms in equation (9.9) may be recognized as the terms which represent the dissipation of the mean kinetic energy, (equation (9.10)). A lucid interpretation given by Rotta (1962) may provide a deeper understanding of the function of these terms. He suggested that the streamwise velocity component $(U+u')_{1,A}$ shown in Figure 9.1 will be laterally convected through a distance $u_2'\Delta t$ in the time Δt. The kinetic energy of the fluctuating component with respect to the local mean $U_{1,B}$ is given by

$$u_{1,B}'^2 = (u_{1,A}' - (u_2'\Delta t \frac{\partial U_1}{\partial x_2})^2 = (u_{1,A}' - u_1' u_2' \frac{\partial U_1}{\partial x_2}\Delta t + \ldots) \quad (9.11)$$

It can be seen that the rate at which the longitudinal component $\overline{u_1'^2}$ gains energy is determined by the work of $\overline{u_1'u_2'}$ against $\frac{\partial U}{\partial x_2}$ when all other effects are ignored.

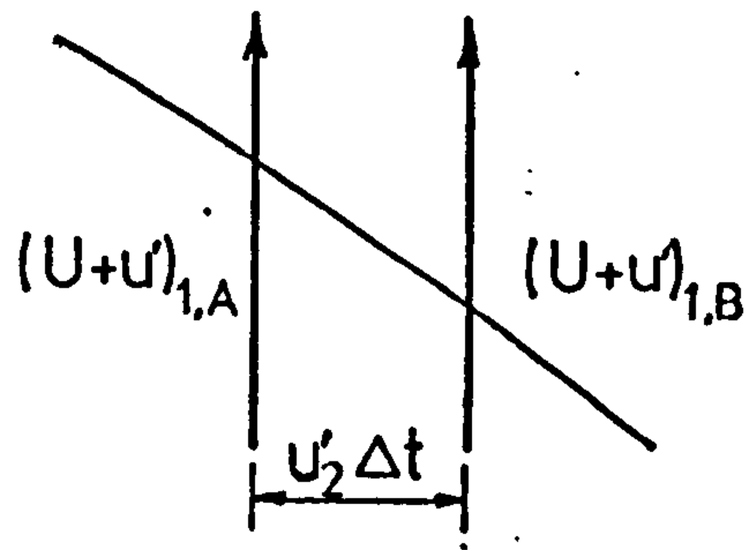

Figure 9.1

Over most of the free convection boundary layer, these generation processes transfer energy from the mean motion into turbulence. However, in the region of maximum velocity, their function is less well defined. Experimental evidence indicates that in flows characterized by asymmetrical velocity profiles, the zero crossings of $\frac{\partial U_1}{\partial x_2}$ and $\overline{u_1'u_2'}$ are not coincident; consequently, the sign changes from negative to

positive. Because of possible implications of this unusual sign change, all the other interactions between Reynolds stresses and mean gradients (given as $\rho\overline{u_i'u_j'}\,\partial U_i/\partial x_j$) should be considered. In two-dimensional flows, the only other contribution is from the normal stress terms given by $(\overline{u_1'^2} - \overline{u_2'^2})\frac{\partial U_1}{\partial x_2}$. Experimental evidence (Klebanoff, section 8.2.2.3) indicates that $\overline{u_1'^2} > \overline{u_2'^2}$ and that in accelerating flows, such as the free convection boundary layer, $\frac{\partial U_1}{\partial x_2} > 0$. Thus the energy transfer to the turbulence by these functions appears to be either negligible or positive in the region near the peak velocity. If this is true and a separation of the zero crossings of $\overline{u_1'u_2'}$ and $\frac{\partial U_1}{\partial x_2}$ does exist, then a phenomenon known as reversal energy feeding (Eskinazi and Erian (1969), Palmer and Keffer (1972), Lumley and Panofsky) may serve to reorder the random turbulent motion. In the light of Rotta's interpretation (Figure 9.1) this means that whenever the term $\overline{u_1'u_2'}\,\frac{\partial U_1}{\partial x_2}$ is positive, it convects momentum in a direction that increases the disparity between the instantaneous momentum vector and the local mean, and that whenever this term is negative the action serves to decrease the difference. Consequently, in a region where the term is positive, the effect is to suppress the intensity of the time averaged turbulence quantities (Eskinazi and Erian). The characteristic dip in the measured values of the $\overline{u'^2}$ just outside its maximum shown in Figure 10.6 may be caused by this phenomenon.

This analysis, however, ignores the contribution of the third generation term in equation (9.12), $g\rho_\infty\,\overline{u'T'}/T_\infty$, which represents an energy flux between k and the potential energy and is significant only in flows dominated by thermal effects. For example, if the flow is convected through a temperature field where $\frac{\partial T}{\partial x_1} > 0$, k would be transferred into potential energy. The function of the term in a free convection boundary

layer has not been determined; the studies in Chapter 10 suggest that it serves to increase the intensity of k. If this is true, then its greatest effect would be nearest to the plate, in the region on the inner side of the peak of mean velocity profiles and this contributes to the peak of $\overline{u'^2}$ shown in Figure 10.6.

From this brief examination of the transport equation for k, it can be seen from the indeterminacy of the terms in the diffusion and the dissipation and the uncertainty of the function of the source terms that little is known about the mechanisms governing turbulence kinetic energy.

A property of the free convection flow that is conveniently measured is the variance of the temperature fluctuations defined as $J \equiv \overline{T'^2}/2$. The transport equation for this quantity can be derived from the equation of conservation of energy and is given, as in boundary layer form, as

$$\rho \frac{DJ}{Dt} = \frac{\partial}{\partial x_2}\left(\frac{\mu}{\sigma}\frac{\partial J}{\partial x_2} - \overline{u_2'J}\right) + \overline{u_2'T'}\frac{\partial T}{\partial x_2} - \frac{\mu}{\sigma}\overline{\left(\frac{\partial T'}{\partial x_2}\right)^2} \qquad (9.12)$$

convection | diffusion | generation | decay

The decay term does not represent energy conversion but can be interpreted as the annihilation of temperature fluctuations by molecular action. The other terms are easily identified as convection, diffusion and generation of the 'temperature energy', J. Since the gradient of mean temperature is monotonic, the uncertainty in the interpretation of the nature of the source term which arose in equation (9.11) does not exist here.

Although transport equations can be derived for many of the significant measures of turbulence, each equation involves even more unknowns. At some point the unknowns must be approximated. These approximations are considered in the next section.

9.3. Turbulence Hypotheses

In recent years the interest in extending the prediction of the turbulent shear stress $\overline{u_1'u_2'}$ has stimulated many proposals. (The reader is referred to Spalding and Launder (1971), Rotta (1971) and Bradshaw (1971a, 1972) for an introduction to this art!) The special requirement of the present work which requires the approximation of the turbulent processes over the region next to the plate severely limits the choice of applicable models*. Nevertheless, there are several hypotheses that are applicable to this study. All but one (an adapted version of Hanjalic and Launders' hypothesis which will be considered later) employ the Boussinesq 'effective-viscosity' concept (1877) to model $\overline{u_1'u_2'}$. This concept, in turn, is generalized to approximate other required turbulent transport terms by means of a gradient diffusion model. In these models a turbulent exchange coefficient is given by

$$\frac{\mu_t}{\sigma_\phi} = \frac{\overline{u_2'\phi'}}{\frac{\partial \Phi}{\partial x_2}}$$

where ϕ' represents any turbulent component, Φ a mean property, μ_t the effective turbulent viscosity, and σ_ϕ the appropriate turbulent 'Prandtl-Schmidt' number. All models of μ_t are founded on a function of a velocity and a length scale. Some hypotheses, such as the Prandtl mixing length, use algebraic expressions; others use one or two differential equations to specify these parameters. A summary of the equations for the models of turbulence used in the study in Chapter 10 follows a résumé of hypotheses which are applicable to such a study.

---

*The significant features of the free convection boundary layer, e.g., the region of the maximum velocity, are affected by the presence of the plate (c.f. 8.2.2.4).

In perhaps the best known model of this type, namely the Prandtl mixing length model, μ_t is a function of $\frac{\partial U_1}{\partial x_2}$ and an algebraic expression for the length scale. The specification of this length scale is not invariant for jets, plane mixing layers, and wall boundary layers; nevertheless, the hypothesis can be employed to provide a reasonable prediction of these flows*. However, there is a more serious disadvantage with regard to the use of this model in a study of the free convection flow. With μ_t expressed as a function of the mean velocity gradient and a finite length scale, the model of $\overline{u_1' u_2'}$ is a quadratic function of $\frac{\partial U_1}{\partial x_2}$ and cannot be expected to correctly predict the turbulence transport processes across a boundary layer with a strongly asymmetric velocity profile.

In the total viscosity hypothesis ($n \equiv \mu + \mu_t$) employed by Yang and Nee, n is obtained from a transport equation instead of from an algebraic function. This specification permits the distribution of n through convective and dissipative processes whereas the algebraic expressions of this hypothetical quantity (μ_t) only represent local generation and dissipation processes. However, the turbulence length scale still appears as an algebraic function in Yang and Nee's rate equation** which may account for the different sets of empirical constants noted in computations based on section 9.1. This hypothesis was made in the present study of turbulence approximations, but the results of these studies are not presented in Chapter 10 because no additional contribution to Yang and Nee's work was made.

---

*For wall boundary layers, a Van Driest modification is often used to account for low Reynolds effects near the wall.

**It is interesting that whereas the other models account for the low Reynolds effects by using an explicit function (e.g. Van Driest formula), in this model these allowances appear to be implicit in the formulation.

Several investigators have proposed more complex models which provide a transport equation for the turbulence kinetic energy and function of a length scale, but only the model proposed by Jones and Launder (1972) has made provision for regions where the Reynolds number of turbulence is low. In their hypothesis, the formula for μ_t is founded on the Prandtl-Kolmogorov proposal

$$\mu_t \propto \rho k^{\frac{1}{2}} \ell \quad .$$

Since ε^* may be assumed to be proportional to $\rho k^{3/2}/\ell$ at high Reynolds numbers, Jones and Launder have suggested that μ_t may be estimated from $\mu_t = \rho c_\mu f_\mu k^2/\varepsilon$ where c_μ is a constant and f_μ is a function of the turbulence Reynolds number ($R \equiv \rho k^2/\mu\varepsilon$). Thus they propose that μ_t may be determined from the solution of a modelled transport equation for k and ε. This model has been applied to the prediction of a forced flow over a flat plate as well as boundary layers with severe accelerations in the streamwise direction and in both cases good agreement was obtained between the predicted development and the measured behaviour of the flow.

Certain features of the boundary layer demanded that alterations or extensions of existing models be made. An adapted version of the k-ε model which involved the solution of a modelled transport equation for J was employed to investigate the influence of the generation term $\frac{g\rho_\infty \overline{u_1'T'}}{T_\infty}$, on the modelled equation for k. The transport equation for $\overline{u_1'T'}$ contained too many terms for a realistic approximation (see Bradshaw (1971b)); instead, the estimates of $\overline{u_1'T'}$ were obtained with the

---

*In this model ε is interpreted as the isotropic part of the total energy dissipation rate.

values of J, k and the correlation coefficient $R_{u_1'T'}$*. The only optimization that this model of turbulence received (the version will be referred to as the k-ε-b model) was the adjustment of the coefficients of the transport equation for J to bring the maximum values of the prediction and the experimental data into agreement.

In another stage of this study, it was desired to determine the influence of a possible non-coincidence of the zero crossings of $\overline{u_1'u_2'}$ and $\frac{\partial U_1}{\partial x_2}$ in this strongly asymmetric flow. A model provided by Hanjalic and Launder for use in the prediction of such flows effects the closure to the conservation equations (9.6) - (9.8) through the solution of a transport equation for $\overline{u_1'u_2'}$ as well as for k and ε. (The adapted version of their hypothesis will be referred to as the k-ε-s model.) The prediction resulting from the use of this model accords well with experimental data for a diverse range of flows and so its use in this study was quite attractive; however, no provision was made for low Reynolds number effects. Nevertheless, since this model and the k-e model are founded on similar concepts, the inclusion of the proposals of Jones and Launder for the prediction of low Reynolds turbulence into the k-ε-s model is facilitated. The only alterations that were required were

(a) the substitution of the expression $\rho f_\mu \overline{u_1'u_2'}$ for $f_\mu c_\mu \frac{\rho k^2}{\varepsilon} \frac{\partial U_1}{\partial x_2}$ in the appropriate terms of low Reynolds number versions of the k and ε equations,

(b) the introduction of a low Reynolds number factor into the modelled transport equation for $\overline{u_1'u_2'}$, and

(c) the adjustment of one empirical coefficient in the ε equation proposed by Jones and Launder.

---

*It was assumed that $k \approx \overline{u'^2}$; hence $R_{u'T'} \propto \overline{u_1'T'}/\sqrt{J}\sqrt{k}$. A constant value of $R_{u_1'T'} = 0.6$ was used (see section 8.2.2.2.).

The adapted version of the k-ε-s model has not been optimized with respect to any flow; the first reasonable prediction of behaviour near the plate was sufficient for the purposes of this study.

Each analysis of the turbulent free convection boundary layer comprised the solution for the mean momentum and the energy equation together with any transport equations required by the model of turbulence. The complete form of the equations used in this study are listed below.

I. Basic Conservation Equations for the Effective Viscosity Models

Mean Momentum

$$\rho\frac{DU_1}{Dt} = \frac{\partial}{\partial x_2}((\mu+\mu_t)\frac{\partial U_1}{\partial x_2}) - g(\rho-\rho_\infty) \qquad (9.13)$$

Energy

$$\rho\frac{DT}{Dt} = \frac{\partial}{\partial x_2}((\frac{\mu}{\sigma} + \frac{\mu_t}{\sigma_T})\frac{\partial T}{\partial x_2}) \quad \text{where } \sigma_T = 0.8 \qquad (9.14)$$

Effective Viscosity Models of Turbulence:

(a) Prandtl's mixing length hypothesis (P)

$$\mu_t = p\ell^2\left|\frac{\partial U_i}{\partial x_2}\right|; \quad \ell = \kappa x_2(1 - e^{x_2/26}) \text{ for } x_2 < \frac{\lambda\delta}{\kappa}$$
$$\ell = \lambda\delta \text{ for } x_2 \geq \lambda\delta \qquad (9.15)$$

where $\kappa = 0.435$, $\lambda = 0.089$ (Patankar and Spalding (1971)) and δ is the momentum boundary layer width (0.99).

(b) Turbulence kinetic energy-dissipation model (k-ε)

$$\mu_t = c_\mu f_\mu \rho k^2/\varepsilon \quad .$$

Turbulence Kinetic Energy

$$\rho\frac{Dk}{Dt} = \frac{\partial}{\partial x_2}((\mu + \frac{\mu_t}{\sigma_k})\frac{\partial k}{\partial x_2}) + \mu_t(\frac{\partial U_1}{\partial x_2})^2 - \rho\varepsilon - 2\mu(\frac{\partial k^{\frac{1}{2}}}{\partial x_2})^2 \qquad (9.16)$$

Dissipation

$$\rho\frac{D\varepsilon}{Dt} = \frac{\partial}{\partial x_2}((\mu + \frac{\mu_t}{\sigma_\varepsilon})\frac{\partial\varepsilon}{\partial x_2}) + c_1 f_1 \frac{\varepsilon}{k}\mu_t(\frac{\partial U_1}{\partial x_2})^2 - c_2 f_2 \frac{\rho\varepsilon^2}{k} + c_4\mu\mu_t(\frac{\partial^2 u}{\partial x_2^2})^2 \quad (9.17)$$

The functions f_1, f_2, f_μ are given by

$$f_1 = 1.0$$

$$f_2 = 1.0 - 0.3\exp(-R)$$

$$f_\mu = \exp(-2.5/(1+R/50))$$

where $R \equiv \frac{\rho k^2}{\mu\varepsilon}$ is the turbulence Reynolds number.

The constants are assigned values which are recommended by Jones and Launder and are listed in Table 9.1.

(c) Turbulence kinetic energy-dissipation-buoyancy model (k-ε-b)

'Temperature Energy'

$$\rho\frac{DJ}{Dt} = \frac{\partial}{\partial x_2}((\frac{\mu}{\sigma} + \frac{\mu_t}{\sigma_J})\frac{\partial J}{\partial x_2}) + c_3\frac{\mu_t}{\sigma_T}(\frac{\partial T}{\partial x_2})^2 - 2.0\frac{\mu}{\sigma}(\frac{\partial J^{0.5}}{\partial x_2})^2 \quad (9.18)$$

Turbulence Kinetic Energy

$$\rho\frac{Dk}{Dt} = \frac{\partial}{\partial x_2}((\mu + \frac{\mu_t}{\sigma_k})\frac{\partial k}{\partial x_2}) + \mu_t(\frac{\partial U_1}{\partial x_2})^2 + \frac{0.6g(kJ)^{\frac{1}{2}}}{T} - 2.0\mu(\frac{\partial k^{0.5}}{\partial x_2})^2 \quad (9.19)$$

Dissipation

Identical to the k-ε model.

The constants are assigned the values listed in Table 9.1.

Table 9.1

c_μ	c_1	c_2	c_4	σ_k	σ_ε	σ_J
0.09	1.55	2.0	2.0	1.0	1.3	1.3

II. Equations for the Turbulence kinetic energy-dissipation-shear stress model of Turbulence (k-ε-s)

Mean Momentum

$$\rho \frac{DU_1}{Dt} = \frac{\partial}{\partial x_2}((\mu + \mu_t)\frac{\partial U_1}{\partial x_2}) - \rho \overline{u_1'u_2'} - g(\rho-\rho_\infty) \qquad (9.20)$$

Energy

$$\rho \frac{DT}{Dt} = \frac{\partial}{\partial x_2}((\frac{\mu}{\sigma} + \frac{f_\mu c_\mu \mu R}{\sigma_T})\frac{\partial T}{\partial x_2}) \qquad (9.21)$$

Lateral Shear Stress

$$\rho \frac{D\overline{u_1'u_2'}}{Dt} = \frac{\partial}{\partial x_2}((\mu+f_\mu c_\mu \mu R)\frac{\partial \overline{u_1'u_2'}}{\partial x_2}) - 2.8c_\mu f_\mu \rho k \frac{\partial U_1}{\partial x_2} - 2.8f_S \frac{\rho\varepsilon}{k}\overline{u_1'u_2'} \qquad (9.22)$$

Turbulence Kinetic Energy

$$\rho \frac{Dk}{Dt} = \frac{\partial}{\partial x_2}((\mu+0.8f_\mu c_\mu \mu R)\frac{\partial k}{\partial x_2}) + f_\mu \rho\overline{u_1'u_2'}\frac{\partial U_1}{\partial x_2} - \varepsilon - 2\mu(\frac{\partial k^{0.5}}{\partial x_2})^2 \qquad (9.23)$$

Dissipation

$$\rho \frac{D\varepsilon}{Dt} = \frac{\partial}{\partial x_2}((\mu+0.5f_\mu c_\mu \mu R)\frac{\partial \varepsilon}{\partial x_2}) + c_1 f_1 \overline{u_1'u_2'}\frac{\rho\varepsilon}{k}\frac{\partial U_1}{\partial x_2} - c_2 f_2 \frac{\rho\varepsilon^2}{k} + c_4 \mu\mu_t(\frac{\partial^2 U_1}{\partial x_2^2})^2 \qquad (9.24)$$

The functions f_1 and f_2 are identical to those specified in the k-ε model; f_s is given as

$$f_s = \exp(-1/(1 + R)) .$$

The values which are assigned to the constants are similar to those in the k-ε model (except for c_4). For completeness they are given in Table 9.2.

Table 9.2

c_μ	c_1	c_2	c_4
0.09	1.55	2.0	0.1

Boundary Conditions

Boundary values selected to simulate the experimental conditions used in this study were imposed on the transport equations. These are given in Table 9.3.

Table 9.3

x_2	u	T	k	ε	J	$\overline{u_1'u_2'}$
0	0	60C	0	0	0	0
δ	∿0	20C	∿0	∿0	0	0

Method of Solution

The set of parabolic partial differential equations was solved by a modified version of the finite difference procedure of Patankar and Spalding (1970). Sixty cross-stream intervals were used with the mixing length model of turbulence and ninety points were used with the other models. The forward step length was set at 0.1 - 0.2 times the boundary layer thickness to ensure good computational accuracy.

CHAPTER 10

PRESENTATION AND DISCUSSION OF RESULTS OF PREDICTIONS

The turbulence models considered in Chapter 9 have been applied to the prediction of free convection flow. In the first section of this chapter, predictions are compared to data observed in the experimental part of the programme. In general, only the predictions made with the use of the mixing length model and the model comprising transport equations for the turbulence kinetic energy (k) and its rate of dissipation (ε) (i.e., the k-ε model) are compared with experiments since the constants in these models have been optimized for use with forced flows. The other two models of turbulence (k-ε-s, k-ε-b; see section 9.3) have not received much optimization although the results from the use of these models are in general agreement with those from the employment of the k-ε model. For the sake of clarity in presentation, results arising from the use of the k-ε-s and k-ε-b models are given only for those specific features which they were developed to investigate.

The second section comprises a prediction of the mean and turbulence kinetic-energy balances obtained with the use of the k-ε model. These balances contain information about the flow that was too difficult to obtain experimentally.

10.1. Comparison of Prediction and Experiment

One of the main objectives of this theoretical study was the comparison of the prediction of the streamwise development with the data obtained from experiment. In order to accomplish this comparison, a suitable starting procedure for the integration of the equations had to be determined. Some investigators, such as Kato et al. and Oosthuizen, assumed that the turbulent boundary layer commenced at the leading edge but

Lockwood and Ong initiated their solution of the turbulent flow from the solution of the laminar flow mid-way through the transition region. These practices are possible with turbulence models that do not incorporate a dependency on the past history of the flow, but the multi-equation turbulence models require initial specifications that approximate the characteristics of the turbulent flow. In an attempt to resolve this problem, computations employing the mixing length model were begun both near the leading edge and from the solution of the laminar flow at Gr equal to 4.77E+9 (x = 1 m). The solutions were almost identical for Gr > 6.0E+10, but the predicted values of the maximum of the mean velocity profiles (U_m) were considerably higher than those observed in experiment. Better agreement between these values of U_m could have been obtained if the value of x at which the solution had been started had been increased; that is, if the turbulent flow had been analysed as if it had a virtual origin. Such practices, however, would not have altered any of the details of the predictions because the solutions were independent of the value of x. In the case of the solution using the mixing length model, it was decided not to present the data in any optimized form but to use the solution initiated from the laminar profiles (Gr = 4.77E+9).

With regard to the multi-equation models of turbulence, it was not possible to start the solutions with mean velocity profiles small enough to obtain predicted values of U_m that agreed with observation at the Gr of experiments*. In view of this failure it was decided to study the characteristics of the theoretical solutions in a range of higher Gr where

---

*The difficulty that the solution would predict 'relaminarization' (see Jones and Launder) unless a sufficiently high level of k was specified was one of the problems encountered.

agreement could be obtained*. In this approach the solution was started well upstream of the station where the maximum velocity of the converged solution approximately agreed with that obtained from the experimentally derived relationship $\gamma = 0.29$. This station marked the beginning of the 'region of interest' ($Gr \approx 3.0E+11$). The upper limit was simply determined by a convenient station at which the predicted lateral profiles could be obtained; thus, the region of interest was defined as $3.0E+11 < Gr < 1.0E+12$.

Figure 10.1 shows the values of U_m and $y_{0.5}$ from predictions employing the mixing length and k-ε models. These values are plotted against x to illustrate the predicted linear growth of $y_{0.5}$. Also shown are both the values of U_m derived from the experimental relationship $\gamma = 0.29$ and $y_{0.5}$ obtained from the experimental observations at $Gr = 4.84E+10$ and $6.81E+10$.

The predicted and experimental rates of growth of U_m are in reasonable accord although the values of U_m are not. However, this may only reflect on the lack of attention given to an optimum starting position. Some disagreement regarding the predicted rate of growth of $y_{0.5}$ can be noted but the experimental evidence is not sufficient to determine whether the relationship $y_{0.5} \propto 0.088x$, suggested by the solution using the k-ε model, is more accurate than the expression $y_{0.5} \propto 0.063x$, obtained from using the mixing length model. Since the experimental data on $y_{0.5}$ were inadequate to assess the accuracy of the predicted growth rates, further evidence of the boundary layer expansion

---

*This only involved a change of x at which the solution was commenced, and did not affect the characteristics in any way.

was sought. A suggestion that the rate of expansion was dependent on the heat-transfer coefficient was contained in the experimental data of Fujii et al. and also in the data of Chapter 8. It was also noted (section 8.2.1) that if ζ^* was a similarity parameter of the expanding boundary layer, then the heat-transfer rate $h \propto x^{-n}$ $(n > 0)$. However, every theoretical solution that was employed in this study predicted dependencies of the type $h \propto x^{n}$, which agreed with an earlier investigation of Eckert and Jackson. The solutions using the mixing length and k-ε models suggested that $h \propto x^{0.15}$ whereas the use of the k-ε-b model predicted that $h \propto x^{0.13}$. Unfortunately these predictions could neither be verified nor refuted because of general uncertainty in the experimental evidence about the dependency of h on x. Therefore, this disagreement meant that the available evidence of correlation between the lateral growth rate and the heat-transfer rate could not be used to assess the accuracy of the predicted rate of lateral expansion. Moreover, without additional evidence from which the accuracy of the predicted trends of boundary layer expansion could be determined, very few conclusions can be drawn from this part of the present study.

Even though the accuracy of the predictions could not be adequately measured, two other comparisons of streamwise development were possible. Over the range of interest, the predicted values of the non-dimensional maximum of the variance of temperature fluctuations $\overline{T'^2}$ (obtained with the k-ε-b model) were constant, a trend which agreed with that of the experimental evidence (see section 8.1.4). The second comparison was between the predicted values of $\sqrt{k}$ and the observed values of $\sqrt{\overline{u'^2}}$ †.

---

*$\zeta \equiv \dfrac{y}{(T_w - T_G)} \left.\dfrac{\partial T}{\partial y}\right|_{y=0} = f(h, x)$

†Measurement of k was not possible. However, experimental evidence (section 8.2.2.3) indicated that $u'^2 \approx 2v'^2$. Assuming that $v'^2 \approx w'^2$, then $k \approx u'^2$.

Experimental evidence suggested that the maximum value of $\sqrt{\overline{u'^2}}/U_m$ ($\approx .30$) was independent of x in the fully developed region. The use of the k-ε model predicted that the maximum value on the lateral profile of $\sqrt{k}/U_m$ decreases from 0.23 to 0.22 over the region of interest. The discrepancy between the predicted growth rate of $\sqrt{k}$ and the observed measurements of $\sqrt{\overline{u'^2}}$ is well within the error contained in the experimental data (determined over a range of 2.0E+10 < Gr < 6.0E+10). However, the disagreement between the predicted values of $\sqrt{k}$ and measured values of $\sqrt{\overline{u'^2}}$ represents an important discrepancy which will be discussed below. It is concluded that the growth rates of $\overline{T'^2}$, $\overline{u'^2}$ and U_m with Gr, predicted with the mixing length and k-ε models of turbulence, are all in reasonable agreement with those obtained from experiment.

The disagreement regarding the streamwise variation of h reflects on the accuracy of prediction of the flow structure near the plate. It is possible that the provisions in these models for low turbulence Reynolds number effects (see section 9.3) are not adequate for the prediction of many of the significant flow processes which occur in this region. On the other hand, characteristics of the flow which are not accounted for by either the mixing length or k-ε models (such as the possible non-coincidence of the zero crossing of $\overline{u'v'}$ and $\partial U/\partial y$) may significantly affect the turbulent transfer mechanisms near the plate. In the following discussion, the accuracy of the prediction of the flow structure near the plate is assessed by comparing the predicted non-dimensional distribution of various quantities (obtained at Gr = 1.03E+12, x = 6.0 m) with similar non-dimensional profiles across the boundary layer obtained from experiment at Gr = 4.84E+10 and 6.81E+10.

Although ζ did not correlate the predicted development of the lateral profiles, this parameter is nonetheless used in Figure 10.2 to compare the predictions of non-dimensional mean temperature β with experimental data because it illustrates a feature that is not obvious with other forms of presentation*. The solution employing the mixing length model predicted higher values of β over the region of maximum velocity ($1.0 < \zeta < 2.0$) than those suggested by the measurements, but the use of the k-ε model predicted lower values. Beyond the region of the maximum velocity, the solution using the k-ε model yielded higher values of β than that employing the mixing length and both yielded higher values than those obtained from experiments.

The remaining comparisons of predicted characteristics with experimental data are presented on the basis of a lateral distance non-dimensionalized by comparison with the half-width $y_{0.5}$ because this parameter correlated the streamwise development of the lateral profiles of any one solution over the region of interest ($3.0E+11 < Gr < 1.03E+12$). The velocities are non-dimensionalized by comparison with the maximum mean velocity instead of with the buoyancy velocity U_B /.

The predicted distributions of $\overline{u'v'}$ obtained by using the k-ε, k-ε-s and mixing length models are presented in Figure 10.3. The measurements of $\overline{u'v'}$ obtained in the experimental programme (see section 8.2.2.3) are also presented in this Figure. The predicted and experimental values are

---

*The values of $\left.\frac{\partial T}{\partial y}\right|_{y=0}$ predicted with the use of the k-ε and the mixing length models ($\approx$ 6200) compared favourably with experimental measurements ($\approx$ 7000), so that the values of y_N are similar.

/Although this form of data presentation gave a good comparison of the shapes of the profiles, it did change the relative proportion of them. See Figure 10.1 for the differences in the predictions of $y_{0.5}$ and U_m.

similar in view of the limited confidence associated with the experimental observations. However, the most interesting data in this Figure are those obtained from the solution using the k-ε-s model which predicted a separation of the zero crossing of $\overline{u'v'}$ and $\partial U/\partial y$. The concept of an eddy viscosity, on which the other models used in this study were founded, does not allow for such a characteristic, and yet this phenomenon may be fairly important in the prediction of the turbulent boundary layer which has a highly asymmetric velocity profile.

Furthermore, such a characteristic may be expected to alter the distribution of the mean velocity across the boundary layer. Figure 10.4 provides a comparison of the values of U/U_m obtained from experiment and the solutions using the k-ε, k-ε-s and mixing length models. The predicted values grow much more rapidly on the inner side of the peak than the experimental data suggests. It can be seen that the solution which predicts the non-coincidence of zero crossings of $\overline{u'v'}$ and $\partial U/\partial y$ also provides a mean velocity profile that shows marginally better agreement with experimental data than the other solutions. In the region beyond the peak, the solutions using the multi-equation turbulence models are in good agreement with experimental evidence; however, the prediction arising from the use of the mixing length model yields values of U/U_m which are much lower than those of the observations.

The disagreement between the solutions arising from the mixing length and the k-ε models may be accounted for by the fact that in the former model the turbulent viscosity, μ_t, is linearly dependent on $\partial U/\partial y$ whereas in the k-ε model there is no direct relationship between μ_t and $\partial U/\partial y$. However, more relevant to this study of characteristics of turbulent

free convection flow is the lack of agreement between the predictions and the experimental results. This lack of agreement, particular in the near-plate region, suggests that the free convection flow is affected by processes that are not accounted for by the turbulence models used. The slightly improved prediction of the mean velocity distributions obtained with the k-ε-s model suggests that a lack of coincidence of the zero crossings of $\overline{u'v'}$ and $\partial U/\partial y$ does in fact exist. If this is the case, an accurate prediction of the flow structure near the plate may require the inclusion of turbulence convection processes which are usually negligible (e.g., the normal stresses; also see section 9.3). Nonetheless, the effects of the inadequate prediction of the mean temperature profiles (Figure 10.2) must also be considered* in the assessment of the failings in the predictions. Furthermore, reliable measurements of $\overline{u'v'}$ and $\overline{v'T'}$ are not available for comparison with the predictions.

The remaining comparisons are derived from the solutions employing the multi-equation turbulence models. Figure 10.5 compares experimental estimates of $\sqrt{\overline{u'^2}}/U_m$ with predicted values of $\sqrt{k}/U_m$ obtained with the use of the k-ε and k-ε-s models. Although agreement is found in the outer region between the prediction of k with the use of the k-ε model and experimental observation, the predicted values of k are smaller than those of the observed data in the near-plate region. Better overall agreement is obtained between the values of the solution using the k-ε-b model and measurement but there is still not much agreement in the distribution of the turbulence energy across the boundary layer.

The k-ε-b model, which introduced a buoyancy effect into the transport equation of k, to explain the lack of agreement between the shape

---

*One of the big problems in diagnosing inadequate predictions is that up to five coupled differential equations must be considered!

of the profiles of $\sqrt{\overline{u'^2}}$ and that predicted for $\sqrt{k}$. The use of this model was expected to preferentially increase the values of k near the plate because the added generation term in the transport equation for k is based on the covariance $\overline{u'T'}$ which has its maximum value in the near-plate region. However, $\overline{u'T'}$ proved to be too complicated to model so a function of $\overline{T'^2}$ and k was used instead (see section 9.3). The failure of this model to significantly shift the maximum of the predicted profiles of k towards the plate may be partly accounted for by the inadequate prediction of the $\overline{T'^2}$ profiles. Figure 10.6 compares the experimental values of the deviation of temperature $\overline{T'^2}$ with those from the prediction. Although the agreement in the near-plate region is reasonable, a lack of agreement is evident over the middle part of the boundary layer. This may have been caused by coupling between the transport equation for $\overline{T'^2}$ and k (see section 9.3). Nevertheless, the prediction of $\overline{T'^2}$ displays a reasonable overall agreement with experimental observation.

In summary, the favourable overall comparison between the predicted and the observed structure across the boundary layer is somewhat surprising because many of the detailed predictions do not agree with experiment, particularly in the near-plate region. In this region, the fact that predicted values of k are smaller than those from the observed data suggests that additional sources of k may be present in the flow. This observation is supported by the fact that the application of the k-ε model to the prediction of k in a forced flow over a flat plate was in excellent agreement with the data of Klebanoff. Buoyancy effects may give rise to one of these additional sources of generation of k. The flow structure may also be affected by a possible separation of the zero crossings of $\overline{u'v'}$ and $\partial U/\partial y$. These inadequacies in the predictions of the flow

structure near the plate may also explain the failure to predict the streamwise dependency of the heat-transfer coefficient on x.

The above disagreements do not necessarily reflect on omissions in the models so much as on the lack of understanding of the processes which significantly affect the turbulent free convection boundary layer. On several occasions during this study, assessment of the predictions was hindered by the lack of experimental data. One example was the lack of measurements from which the processes that govern the distribution of k could be estimated. The predictions of the kinetic energy of both the mean flow and the turbulence are presented in the next section.

10.2. Kinetic Energy Balances

It was much too difficult to observe the data required to formulate a kinetic-energy balance of the turbulence or indeed, even of the mean flow, but the application of the k-ε turbulence model did provide an estimate of these balances. In view of the lack of agreement in detail between the distribution of k and $\overline{u'^2}$ in the near-plate region discussed above, the predictions of the balances can serve only as an indication of the energy 'flows' within the boundary layer.

Figure 10.7 shows the balance of the mean kinetic energy K. The maximum rates of both generation and dissipation are very close to the plate. The generation of K appears to be significant over most of the layer although in view of the prediction of β, discussed in the preceding section, these values are probably too high. Over the inner layer, the diffusive processes represent a loss to the local strength of K, but in the outer region they are the main source of the local values of K. The role of the convective processes appears to be opposite that of diffusion.

Over most of the layer, the strength of the dissipation processes is fairly uniform. It can be seen that over the inner region, the generation and diffusion processes appear to be dominant while in the outer part of the layer the most significant processes are diffusion and convection.

The turbulence kinetic-energy balance (Figure 10.8) reveals that the generation processes are at a maximum just outside the viscous sublayer, are negligible over the region of the maximum mean velocity, and increase to a second peak in the outer region. This distribution corresponds to that of the dissipation of K (although the latter also includes viscous dissipation, see section 9.2). In the outer region, k is diffused away from the region of the second peak of generation towards both the outer boundary and the inner region where the maximum rates of dissipation are located. Outside the very near-plate region, the dissipation processes appear to be fairly uniformly distributed except in the outermost region where they gradually diminish in strength. In this outer layer, convective processes account for the dominant loss in the local balance of k.

The proportions of these processes may be assessed in the light of the comparison of the distribution of k and $\overline{u'^2}$ already made. Although agreement was noted in the outer region, the predicted values of k are seen to decrease more rapidly than do the measurements of $\overline{u'^2}$ as the plate is approached. Consequently, though the relative proportions of the components of the energy balance may be reasonable in the outer region, the components representing losses in the inner layer may be disproportionately large. With this view, the predicted balance of k suggests that

(a) the regions of the maximum generation and dissipation are near the plate;

(b) the processes of generation and dissipation are dominant over most of the layer; and

(c) diffusive and convective processes govern the distributions of k in the outer regions.

In conclusion,it has been seen that the predictions of the streamwise flow development and the lateral structure of the boundary layer are in general agreement with the data obtained from experiment. In particular, the predicted growth rate of the maxima of the mean velocity, kinetic energy and variance of temperature are in good agreement. The predicted flow structure across the boundary layer is also in overall agreement with observations but the predictions are inadequate for many detailed comparisons, especially in the near-plate region. It has been noted that in this region the predictive processes must allow for low turbulence Reynolds number effects as well as a possible non-coincidence of the zero crossings of $\overline{u'v'}$ and $\partial U/\partial y$ and a generation of k through the buoyancy effects. However, the development of prediction methods for this boundary layer is hampered by the scarcity of good experimental data and it is believed that before any accurate predictions of the turbulent free convection boundary layer can be obtained, further experimental evidence and a deeper understanding of the physics governing the turbulence are required.

CHAPTER 11

CONCLUSIONS

The main conclusions of this investigation, which have been formulated in the preceding pages, are summarized below.

Method of Measurement

The free convection boundary layer flow was observed with a hot-wire anemometer + thermocouple arrangement in conjunction with digital data processing methods.

1. The hot-wire anemometer is suitable for measurements of the flow near the plate but is not adequate for observations of the flow very close to ($y < 1$ mm) the plate or in the outer region. The high intensities of turbulence in the flow preclude the use of conventicnal crossed-wire arrays.

2. The regular vortex wake behind a cylinder ($50 < Re < 90$) provides a suitable standard for calibration at very low velocities.

3. Digital data processing techniques are very advantageous to an extensive study of turbulent free convection flow. Apart from enabling the application of the hot-wire anemometer to the observation of the velocity, the use of digital methods provides a means to integrate the analogue signals over periods of five to ten minutes. In view of the fatigue induced by long hours (8-10) in a room at approximately 30 C, the use of a datalogger also reduces the possibility of misrecording data. Furthermore, its use provides an opportunity to perform both amplitude and spectral analyses on the same data sample which, in turn,reduces the number of tests required.

Theoretical Investigation

Characteristics of the turbulent boundary layer were investigated by a study of the boundary layer equations. Closure to the equation set was

effected by the use of several turbulence hypotheses, the most notable being the low turbulence Reynolds number version of a hypothesis which includes differential equations for the turbulence kinetic energy and the dissipation.

4. Near the regional maximum mean velocity, a flow structure may exist in which energy is fed from turbulent motion to the mean motion, contrary to the usual energy flow. (This phenomenon is often called 'energy reversal'.)

5. The prediction of the streamwise growth of the maxima of the mean velocity and of the intensity of the temperature fluctuations is in good accord with experiment. The predicted growth rate of turbulence kinetic energy showed reasonable agreement with measurements but the predicted dependence of Nu on x could not be confirmed by available experimental evidence.

6. The use of the multi-equation turbulence hypotheses provided predictions of mean velocity profiles across the boundary layer which are in good agreement with experimental data except in the region near the plate. In this region the use of a hypothesis which predicted a non-coincidence of the zero crossings of the $\overline{u_1'u_2'}$ and $\partial U/\partial x_2$ provided a slightly better prediction of the mean velocity profiles.

7. The generation and dissipation of turbulence kinetic energy are both at a maximum near the plate and are dominant over most of the flow. Diffusion of k is smaller but still significant over most of the layer whereas convection is only important in the outermost region. (The energy balance must be treated as speculative because of the disagreement between the predicted values of k and the measurements near the plate.)

In the following experimental investigations of the transitional and fully turbulent flow some of the observed characteristics may be slightly affected by the limited width of the plate and its side walls, but these effects are not considered to be important.

Transitional Flow

8. The most significant feature of the study of transition from laminar to turbulent flow was the identification of flow characteristics that agreed with visual observations of Colak-Antic and Gortler. These are:

(a) a periodicity in the flow structure which indicates the presence of Tollmien-Schlictning waves; and

(b) the growth and subsequent decay of the intensities of temperature and velocity which corresponds to the above authors' observations of the intensification and decay of longitudinal vortex streets.

9. The phase angles of the dominant peaks of a power spectrum of $\overline{u'T'}$ are often of opposite sign. Furthermore, the flow structure in the inner side of the mean velocity peak is out of phase with the structure well outside the peak.

'Fully developed' turbulent flow

10. The free convection boundary layer appears to be fully turbulent for $Gr > 3.0E+10$. This is shown by good correlation over a range of $2.0E+10 < Gr < 7.0E+10$ between the lateral profiles of the first four moments of the probability density distributions of temperature and by reasonable correlation between the velocity distributions. The lateral structure may be seen as being comprised of three regions:

(a) a viscous sublayer adjacent to the plate;

(b) a buffer layer which contains the peak of the mean velocity profile and the maximum intensities of velocity and temperature fluctuations; and

(c) a fully turbulent layer, beyond the buffer region. In this part of the flow, both velocity and temperature spectra contain inertial subranges in accordance with the hypothesis of Kol_mogorov. It was suspected that the identification of a viscous subrange was prevented by aliasing.

Considerable scope exists for future work. With simultaneous observations from hot-wire + thermocouple arrangements at two or more positions and the possible employment of selective sampling techniques, much information on the spatial structure of the turbulence could be obtained with the present apparatus. Further work in the analysis of the spectral characteristics of the flow is also possible. Nevertheless, the work should be extended to include a range of boundary layer temperature differences. Also, the effects of the relatively narrow plate and of the side walls should be examined. In order to study the trends of the streamwise development, the use of a longer plate would be desirable; barring its use, however, trip-rods may be considered to promote an earlier transition and thus enable the study of the flow at more developed states of turbulent flow. Future studies may also investigate the use of the laser-doppler technique, possibly in conjunction with digital data processing techniques, so that the difficulties encountered in observing the flow adjacent to the plate and in the outer region may be alleviated.

In contrast to the possibilities for an experimental investigation, the extension of the theoretical work should not be attempted until further understanding of the physics governing the turbulence is secured. It is towards this goal - the provision of information to formulate better predictions of the turbulent free convection flow - that further work is commended.

APPENDIX A

MANUFACTURE OF PROBES

The nature of turbulent free convection flow allowed considerable latitude in the design of probes for the thermocouple and hot-wire sensors: its low velocities permitted fine thermocouple wires to be mounted in fragile U-shaped loops and its large scale of turbulence allowed the sensing elements to be widely separated, thus easing their construction. The very large thermal gradients near the plate, however, demanded special attention: to minimize their effects on the response of the probe, the lead wires from the sensors were taken downstream, along mean isothermals, before being taken through the boundary layer (cf. section 2.2.2).

Three boundary layer probes were used in this study: a single thermocouple sensor, a single normal hot-wire sensor, and a tri-element probe comprising a thermocouple and two hot wires (Plate A.1). Another probe with three hot wires and a thermocouple was built but was not employed in the experiments.

The Chromel-Alumel thermocouples, supplied by Omega (Connecticut, U.S.A.), were of bare wire, 12.5 μm in diameter. They proved to be remarkably robust as not one was broken during the research programme. Unfortunately, the hot-wire elements were not as strong and several breakages occurred. They were made from 5 μm tungsten wire supplied by Mullards Ltd. The elements were 2 mm long with copper plated ends.

A.1. Mounting the Thermocouples

The thermocouples were mounted in two forms: the ones for the hot-wire array were fixed in a straight sheath; the single thermocouple sensor was threaded through a right-angle stem so that the first 30-40 mm of the

lead wires would be parallel to the plate. In both cases the wires were encased in a double bore quartz tubing which was drawn down to an inner diameter of 7 mm. The capillary tube was threaded by pushing the 12.5 μm wire together with the stiffer 40 gauge wire through it. The larger wire was then used as a support for the finer wire. The only successful attempt to form a rigid loop at the thermocouple junction was to wrap the fine wire round the larger wire 3 to 4 mm from the thermocouple junction and then solder the joint. A strong flux (phosphoric acid) was used to aid the operation as it was imperative that the solder flowed without persuasion. At the far end of the tubing, similar wires of 36 gauge were soldered to the 40 gauge wires and the connection was fastened to the tubing with Araldite to rigidly secure the wire assembly. The thermocouple in a straight sheath was now ready to mount in the hot-wire array head. To complete the single thermocouple probe, the right-angle capillary tubing was mounted in a stainless steel tube.

A.2. The Hot-wire Array Head

Common sewing needles were used to support the hot-wire elements. During the early development of the manufacturing technique, the needles were bent to give a parallel offset in order to reduce the diameter of the support tube. This proved to be unnecessary as the larger tube did not cause any flow obstruction and the practice was abandoned. Instead, the straight sheath thermocouple and the sewing needles were mounted together in an Araldite resin base. To do this the needle tips were placed through a lightly greased teflon matrix into a jig that held them in the desired configuration while resin, warmed so as to reduce its viscosity, was poured into the mould. As soon as the resin had set, the piece was ejected from the mould and allowed to harden. A hole was drilled in its centre and the

thermocouple was fixed into it with further resin. Copper leads were soldered to the needles and, with the aid of another jig, the completed head was set in a straight section of stainless steel tubing. To complete the probe support a right-angle bend was placed 70 to 90 mm from the head. The next stage was to prepare the hot-wire elements.

A.3. Manufacture of a Plated Hot-wire Element

Each wire element was plated for several reasons. Firstly, because the plated wire could be mounted on supports at least 1 mm from the bare wire, the flow over the active element was unlikely to be affected by disturbances caused by the supports. Secondly, a regular, defined element could thus be constructed. Thirdly, the copper plating removed the difficulties met when soldering with tungsten wire.

The basic technique of copper plating the wires was developed at the Institute of Sound and Vibrations Research, Southampton*. The wire was wound on a frame that had a copper bus bar along one of its long sides and was held in place by strips of drafting tape along the edges (see Plate A.1). The frame was placed over a bath with a copper terminal along the length of the bottom. In the centre of the bath was a bridge which was mounted slightly higher than the level of the bath and had a width slightly less than the length of the desired hot wire. With the use of a washing bottle, the bath was filled with a solution of copper sulphate to the point of overflowing in order to raise the miniscous of the liquid above the level of the bridge. A very high miniscous was desirable so that the plating could be well-defined. The terminals of the bath were than placed in series

---

*Report No.189. This report is a good introduction to the use of the constant resistance hot-wire anemometer.

with a current meter, a potentiometer and a nine-volt battery. In the early development, some trouble was experienced in obtaining a smooth plating of the wires. A successful remedy was to electroetch the wires for sixty seconds before plating (-ve to the bottom of the bath). This circuit was dismantled and a second circuit (same components, -ve to the wires) was assembled. The current was adjusted to 0.5 mAmps by means of the potentiometer. After five to ten minutes, the current was raised to 1 - 1.5 mAmp for a further twenty to twenty-five minutes. These settings were not crucial as good plating was obtained with considerable deviations from these values. The process was terminated when the plated wire diameter was about 30 μm. Drafting tape was applied to hold the wire to the frame during the next and final stage, that of mounting the wires to the probe support.

A.4. Mounting the Wires

A soft solder was used to join the plated wires to the sewing needles. The supports were held in position against the wires while the joint was first painted with phosphoric acid and then put in contact with a small amount of molten solder. In the presence of the strong flux, the solder flowed along both the needle and the copper plating to form a very smooth junction. The ends of the plating wires were twisted off and the entire array was dipped into a water bath to wash away the excess flux. It was necessary to stabilise the wire resistance by heating the completed probe in an oven for at least twelve hours at 100 C. It is suspected that the mechanical stresses resulting from the manufacture of the wires and the thermal stresses due to the mounting of the wires together caused the instability. Having completed the annealing of the wire, the probe was ready for use.

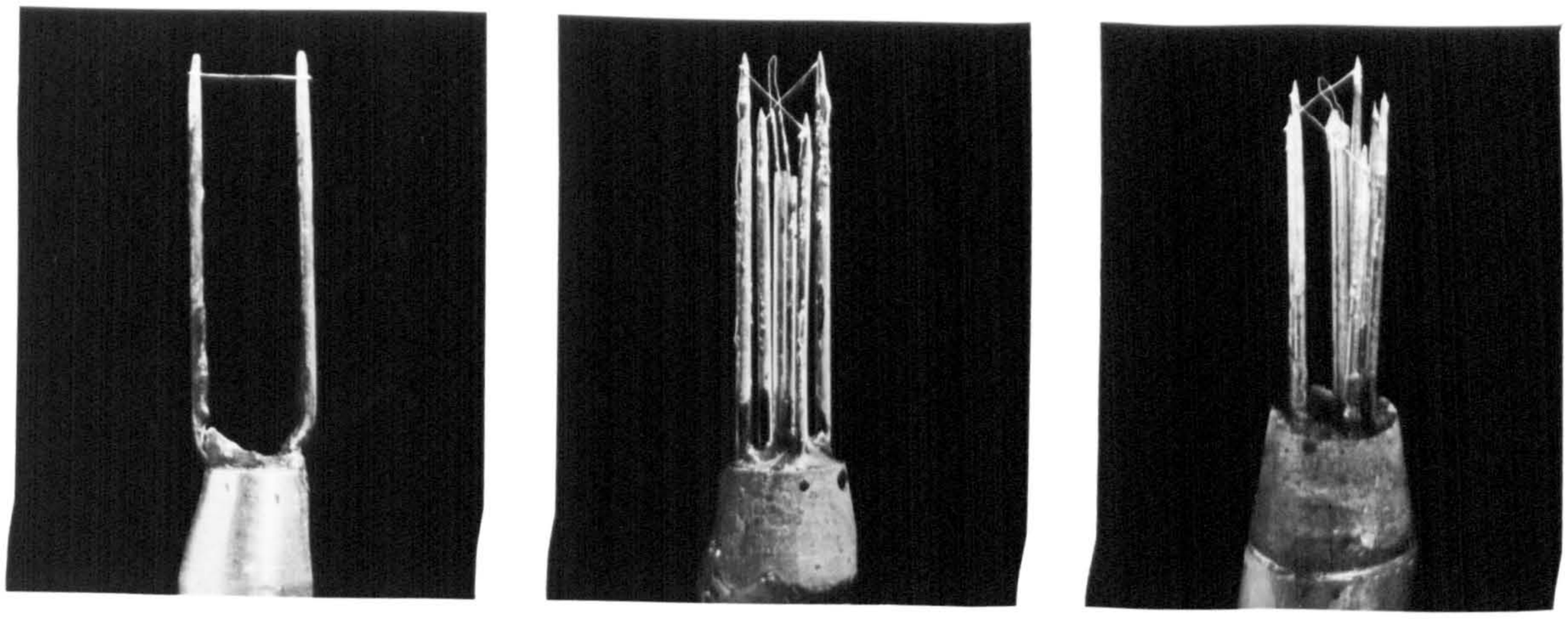

Plate A.1 Probe Manufacture

APPENDIX B

SOLUTION OF SIMULTANEOUS NON-LINEAR EQUATIONS

The solution of a set of non-linear, simultaneous equations has no recommended algorithms; however, the methods used for solving sets of linear equations may be extended to include certain well-behaved equations such as the ones considered in Chapter 3 (see section 3.2.3). Of these, Newton's iterative method is probably the most reliable technique. It is an extended version of his method that has been used in this study to solve the non-linear equation sets.

It is well known that for the solution of the roots, a root of a single equation

$$f(x) = 0$$

and the successive approximations to one of the roots are given by Newton's iterative formula

$$x_{i+1} = x_i - f(x)/f'(x_i) \quad . \tag{B.1}$$

It is necessary that the initial approximation must be sufficiently near the value of the root or else the solution may diverge or converge on another root. It should be noted that this formula may be derived from a first order Taylor's expansion of f(x) about an arbitrary value x_o.

Consider the extension of this method for two simultaneous non-linear equations given by

$$g(x, y) = 0 \qquad \text{and} \qquad h(x, y) = 0 \ .$$

The Taylor's series expansion about x_o, y_o is given as

$$\begin{aligned} g &= g_o + g'_{x,o}\ \delta x + g'_{y,o}\ \delta y + \ldots \ = 0 \\ h &= h_o + h'_{x,o}\ \delta x + h'_{y,o}\ \delta y + \ldots \ = 0 \quad . \end{aligned} \tag{B.2}$$

Similarly, as in the derivation of equation B.1, second order and higher orders are ignored. With some rearrangement, the equations are given as

$$g_x'\delta x + g_y'\delta y = -g$$
$$h_x'\delta x + h_y'\delta y = -h \qquad \text{(B.3)}$$

where it is understood that the functions are evaluated at x_o, y_o.

The set of linear equations can be solved by several methods; Cramner's rule is possibly as computationally efficient as any for cases where there are fewer than four simultaneous equations. With this method, successive approximations of the values of the root are given by

$$x_{i+1} = x_i + ((-gh_y') - (-hg_y'))/J$$
$$y_{i+1} = y_i + ((-gh_x') - (-hg_x'))/J \qquad \text{(B.4)}$$

where J represents the Jacobian given by

$$J = (g_x'h_y' - h_x'g_y') .$$

The solution of the equation set is successively approximated until the desired accuracy is obtained for both roots or until the solution diverges. Details of the application of this algorithm to the solution of two response equations of the crossed-wire anemometer may be extractedfrom subroutine CAL in the program listing in Appendix F.

APPENDIX C

DATA WINDOWS

In power spectral analyses of a time history, the ideal data window given as

(a) $w_o(j) = 1 \qquad 0 \leq j < N$

$w_o(j) = 0 \qquad 0 > j, j \leq N$

would transform into a spectral window of a similar shape. However, the transform of the box-car window, as the above window is called, is not suitable for many power spectral analyses (see section 3.3.5.2). Instead, spectral analyses often employ data windows which improve the characteristics of the spectral window but which distort the temporal window.

Several such data windows exist and their characteristics are well tabulated (Blackman-Tukey, Cooley et al., Welch). Some of these windows alter the entire shape of w(j). Three recommended data windows of this type are the following:

(b) cosine window (Hanning)

$$w_1(j) = 0.5\ (1 - \cos(2\pi j/N))$$

(c) parabolic window

$$w_2(j) = 1 - \left(\frac{j-N/2}{N/2}\right)^2$$

(d) triangular window

$$w_3(j) = 1 - \left(\frac{j-N/2}{N/2}\right) \text{ where } j = 0, 1, 2, \ldots, N-1 .$$

Another window may be used in place of the above which distorts the ends of the time series sequence. This proposal, offered by Bingham et al., is given as

$$(e)\quad w_4(j) = 0.5\,(1 - \cos(\pi j/0.1N) \qquad 0 \leq j \leq 0.1N$$

$$= 1 \qquad 0.1N < j < 0.9N$$

$$= 0.5\,(1 - \cos(\pi(N-j)/0.1N) \qquad 0.9N \leq j \leq N\ .$$

The spectral windows a, b, c, e are shown in Figures C.1 and C.2.

These windows may be applied to the data sequence before it is transformed or, alternatively, the sequence of the transformed coefficients W(j) may be applied to the sequence of linear Fourier coefficient X(j). This latter practice may be computationally efficient, especially with the use of the cosine window. However, with the use of FFT routines to calculate the power spectra of real data series, the determination of sequence X(j) may be avoided. Instead, the sequence of squared coefficients $\bar{X}^2(j)$ may be calculatcd directly. In this case the application of the sequence w(j) to time series x(j) is preferred (see Appendix H).

Presently there are few guidelines to aid the choice of a data window. The cosine window is in wide use but the triangular and parabolic windows are recommended by both Welch and Kinns.

APPENDIX D

ICL DATALOGGER SERVICE ROUTINES

The datalogging system was capable of digitizing up to four channels of analogue data and recording it in binary form on magnetic tape in a standard ICL format. With this arrangement, the special routine written for use with the datalogger tapes had only to recast the binary data into a coding compatible with the ICL version of Fortran IV.

Three considerations entered into the design of this software. First, although each twelve-bit data word was written on the magnetic tape in two bytes (a byte consists of six data bits of information and one parity bit written across the tape), the data were transferred from the magnetic tape into twenty-four-bit words of the ICL machine in groups of four bytes. (This was, in fact, a bonus because it halved the number of data transfers from a peripheral.) Secondly, the binary coding of the data had to be altered to conform to a FORTRAN format. Thirdly, since the purpose of the special software was to transform only numerical data, many standard data transfer check routines, such as an alphanumeric character recognition, were not needed. The parity error check was retained, however, to indicate when a faulty data transfer occurred.

The special software routines for the datalogger system were written at the QMC Computer Centre (J.Steele). The routine which controls the transfer and the restructure of the data was at least ten times faster than standard magnetic tape data transfer under FORTRAN program control. In addition, several other routines were written to control the tape deck.

A standard format of the ICL magnetic tape (the form in which the datalogger is written) is listed below to facilitate the description of the

routines which follow. The terminology is sometimes ambiguous; in this text we will refer to a series of data blocks that is terminated by a tape mark (T.M.) as a record. The series of data records between the header record and the trailer record is called a file. At the beginning of each data record, there is a short block called a data sentinel. It contains any pertinent information about the record.

The data structure of the datalogger tape is given in Figure D-1.

```
                    header record

                    T.M.

                   (data sentinel
                   (
          repeatable (data blocks
                   (
                   (T.M.

                    trailer record

                    T.M.
```

Figure D-1

The following coding will be used in the description of the special routines.

IUN ≡ the unit number by which an input/output peripheral is identified in a FORTRAN program

IN ≡ an integer name which contains the identifying label of the magnetic tape

IA ≡ an integer array designated to store information from the data sentinel.

IE, IF, IG, IH ≡ integer arrays designated to contain the data.

NC ≡ number of channels to be used.

1. PDPOPEN (IUN, IN)

This routine assigns the unit number to the appropriate peripheral channel of the magnetic tape deck and then opens a standard data tape with a name given by the first twelve characters of the integer array.

2. PDPSENT (IUN, IA)

This routine reads a block from the data tape and transfers the first twenty ICL words directly into the integer array, IA. It is used to read through and retrieve the information from the data sentinel at the beginning of each file.

3. PDPREAD (IUN, NC, IE, IF, IG, IH, k)

where k is an integer variable.

This routine is used to transfer one data block into integer arrays in core. Groups of two data points are transferred into core, separated and sequentially placed into the integer arrays. For example, if there are two channels, the first two arrays in the list are filled, beginning with the pointers given in the array subscript.

As the first four words of each block are required for a word count, each block of data contains 1020 points of data, i.e., there are 510 points for each of two channels.

If the data transfer was successful, k is used to distinguish a data block (k = 1) from an end of file (k = -10). If k equals 0, parity errors have occurred in the data transfer. Under the present operating system, the control attempts to read a block twelve times before a parity error is declared. Other errors indicate malfunction of the machine and are self-explanatory. If the end-of-tape reflective marker is reached, the programme is halted.

4. PDPCLOSE (IUN)

This routine rewinds the tape and releases it from program control.

5. PDPBACKSP (IUN)

This routine should skip backwards over one data block. It is intended for use when there is a parity error encountered and it is desired to attempt to read the block once again.

6. PDPSKIP (IUN)

This is a very useful routine not provided in the standard version of FORTRAN IV language. It searches down the tape for the next T.M. and stops directly after it. Thus with its use a file could be abandoned or the tape could be rapidly traversed file by file. The present practice is that if more than ten parity errors are located on a file, that file is abandoned (with the PDPSKIP routine) for reasons of misrecording or of a malfunction of the tape deck.

APPENDIX E

'ON-LINE' DATA PROCESSING FOR AN AMPLITUDE DISTRIBUTION ANALYSIS

The primary advantages of 'on-line' data processing on the PDP-8L were that the analysis was immediate and that no peripheral data storage was required. The present program controlled the digital sampling of one analogue signal and then classified the binary data in an amplitude distribution routine. The sampling rate was determined by the real time required to complete the calculations for data point.

After the programe was initialized (various counters were either cleared or set), programme control passed to a sampling routine which was executed 2^N times (where N is a selected value). Within the loop each data point was added to a running total (a four word register) and also compared to the mid-point of every cell in a histogram distribution. This form of classification was necessary to ensure a regular sampling interval and consequently made the sampling rate a function of the number of cells (e.g. for 128 cell distribution, the rate was 100 Hz).

On completion of the sampling loop, the ensemble average (the first moment) was determined by the right justification of the linear sum by N places. Then moments of the distribution about this value were calculated.

The calculation of the second moment was straightforward, using a two-word multiplication routine. The calculation of the third and fourth moments, however, involved arithmetic operations on very large integer values and so indirect methods were used. Because the averaging of the sums by a number that was not a binary power was too involved, the third moment was not entirely determined; instead, the immediate sums of the negative products and of the positive products were printed. Also, because the magnitudes of

the higher moments of some elements were very large, these products were formed by a recursive four word summing routine instead of by a multiplication routine.

All values were converted from binary code to decimal code before they were printed on the teletype.

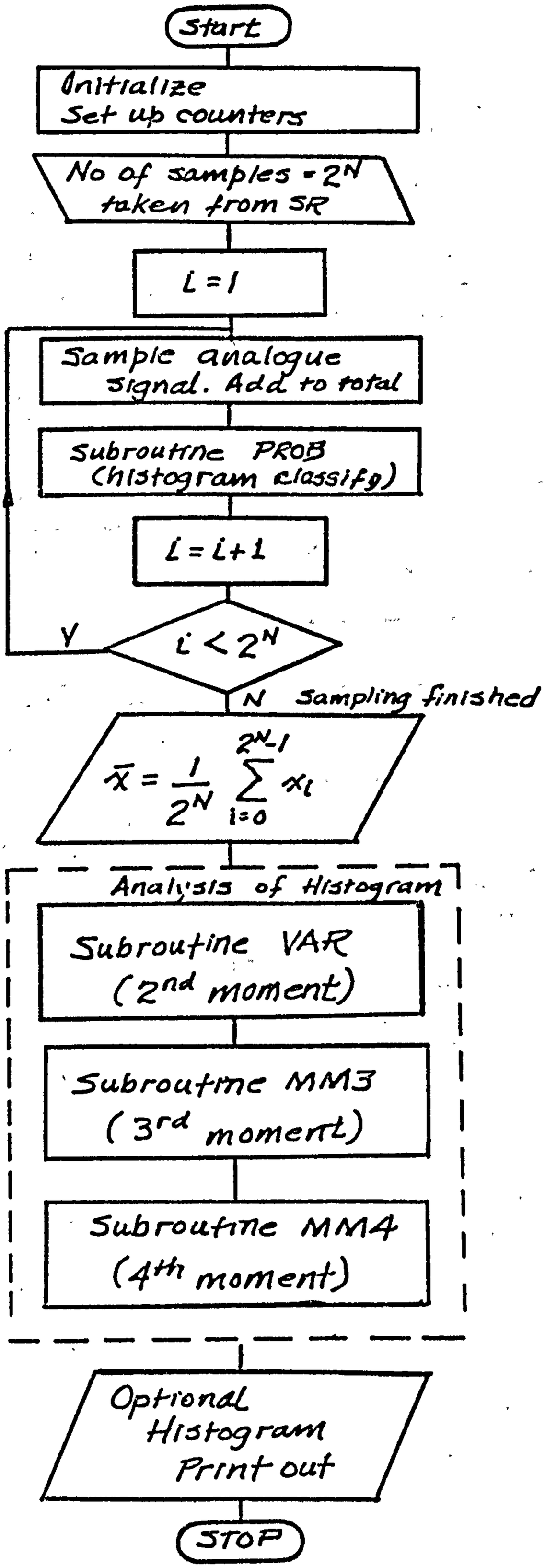

On-line data processing

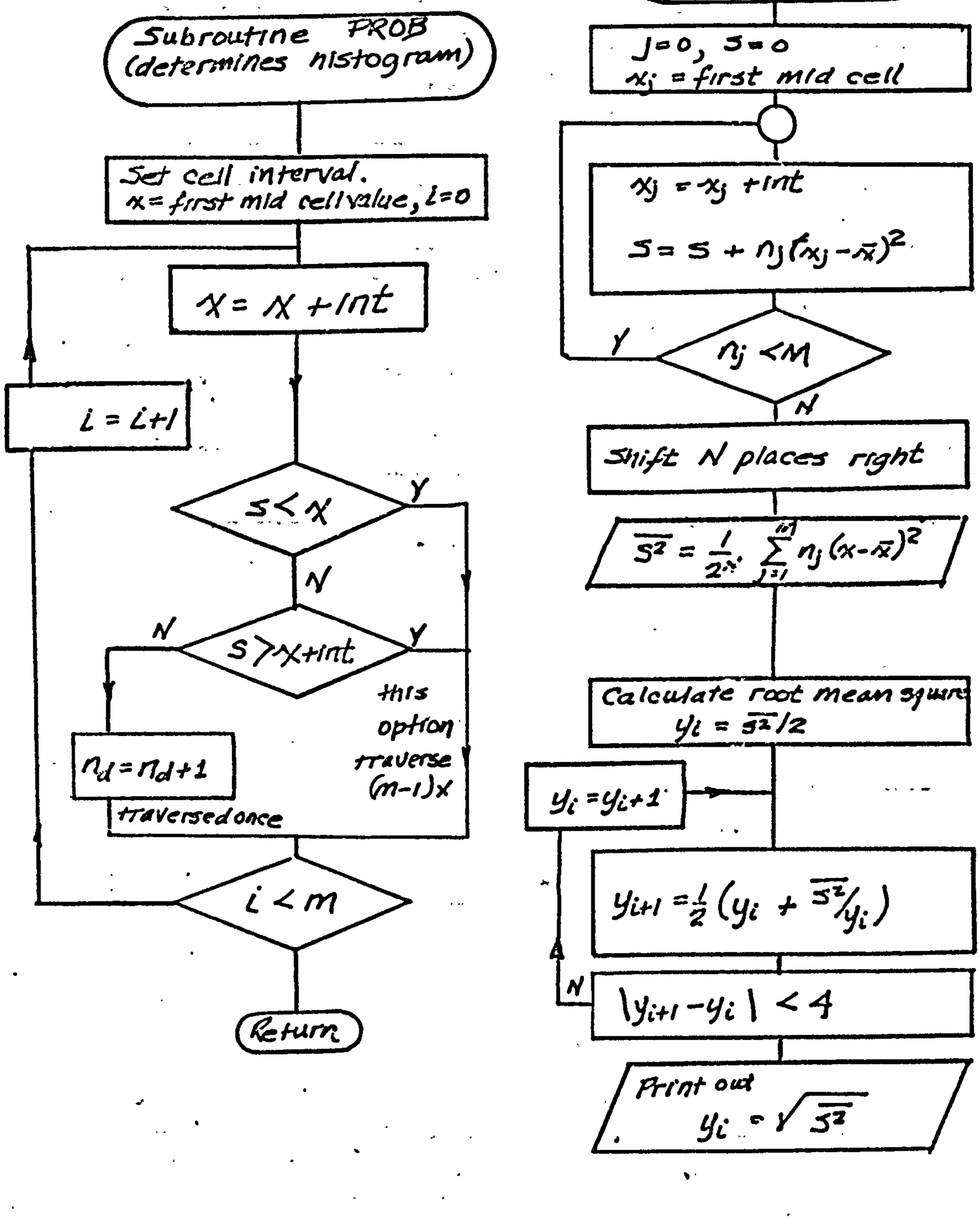

Subroutines for the on-line data processing program

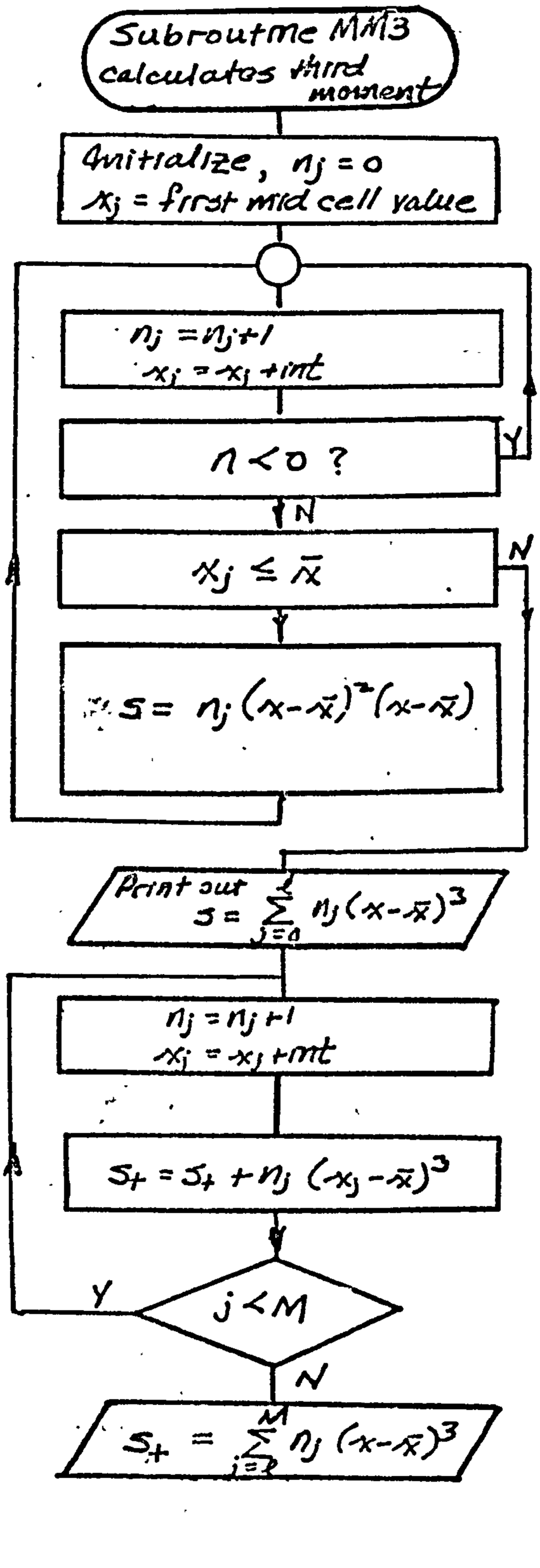

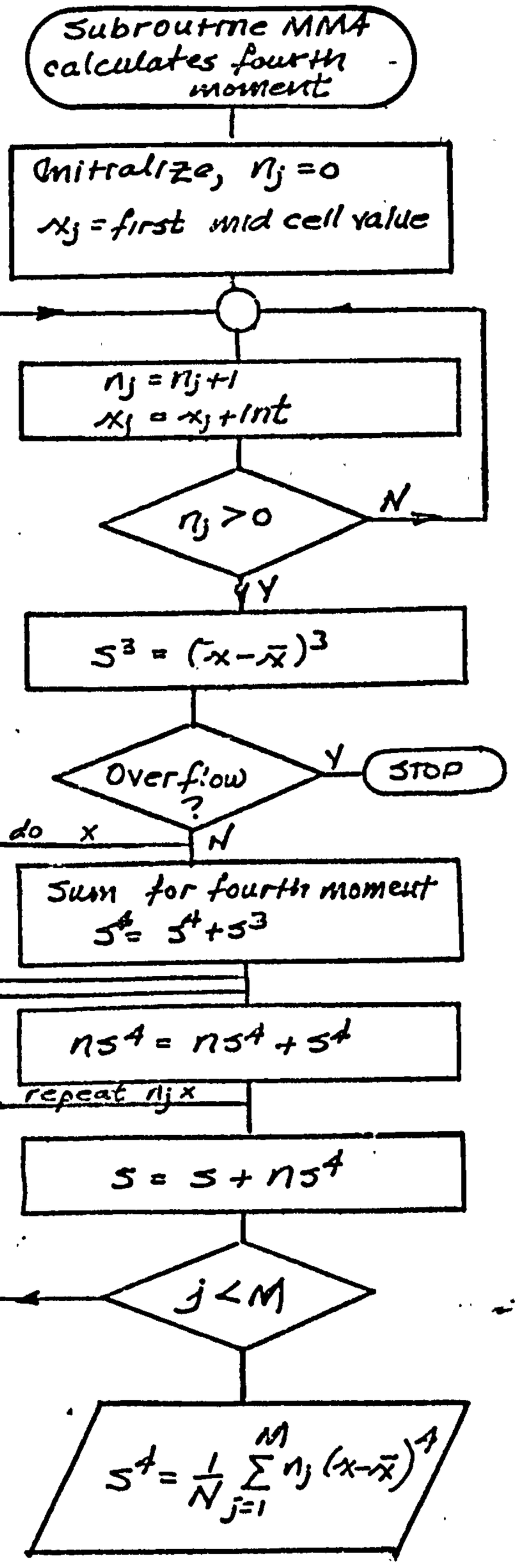

Subroutines for on-line data processing

APPENDIX F

PRIMARY DATA PROCESSING PROGRAM CROS

In Chapter 5, some of the advantages of processing data in two or more stages were discussed. The first stage was a primary data processing to obtain estimates of the expected values of the velocity and temperature data. In subsequent data processings, more extensive analyses were applied.

Program CROS was designed to transform data obtained from the crossed wire + thermocouple arrangement into sequences of temperature and coordinate velocity components, and to calculate the expected values, the variances, and the covariances of these quantities. A matrix-type algorithm was employed to perform the transformation (see section 3.3.3.3).

The structure of the program is basically divided into two parts: the creation of a transformation matrix and the processing of the data sequences. The following general aspects of the array generation routines should be noted:

1. A generalized Hinze-type cooling law is used to interpret the hot-wire signals. An extended version of Newton's iterative method (see Appendix C) is employed for the solution of two simultaneous non-linear equations.

2. For non-isothermal studies, such as the present work, a three-dimensional transformation array is required: one dimension for each hot-wire anemometer and one for the thermocouple.

3. To make the most efficient use of computer store, the values of both coordinate velocity components are stored in one word (see section 3.6).

4. The initialization of the iterative solution technique required that all roots of the solution be located using a grid search technique before the realistic root was selected. This root was selected by the application of two criteria: that $U_1 > 0$ and that the absolute value of U_2 was small.

The details of the solution may be obtained from the flow charts and listings which follow.

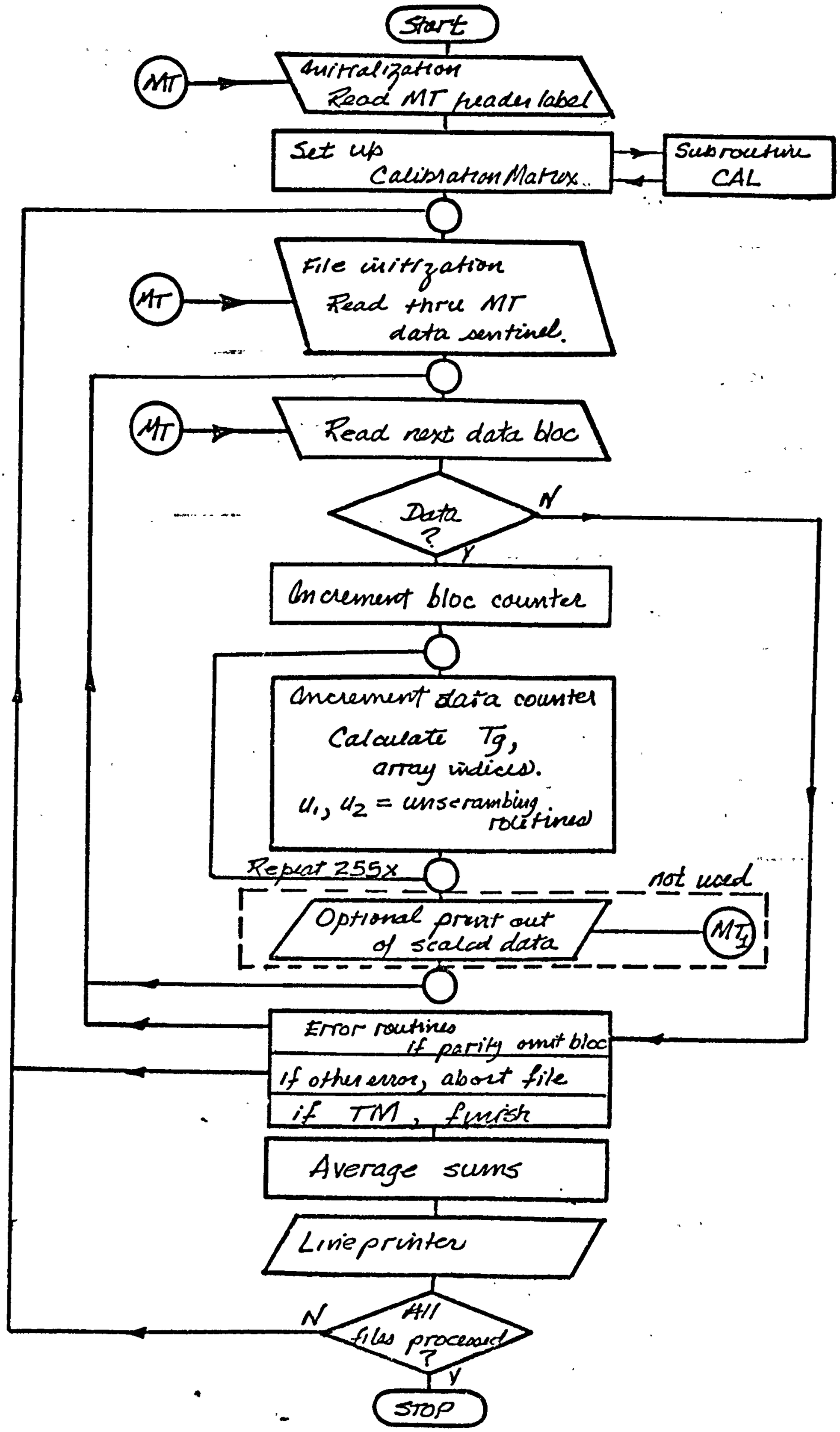

Program CROS

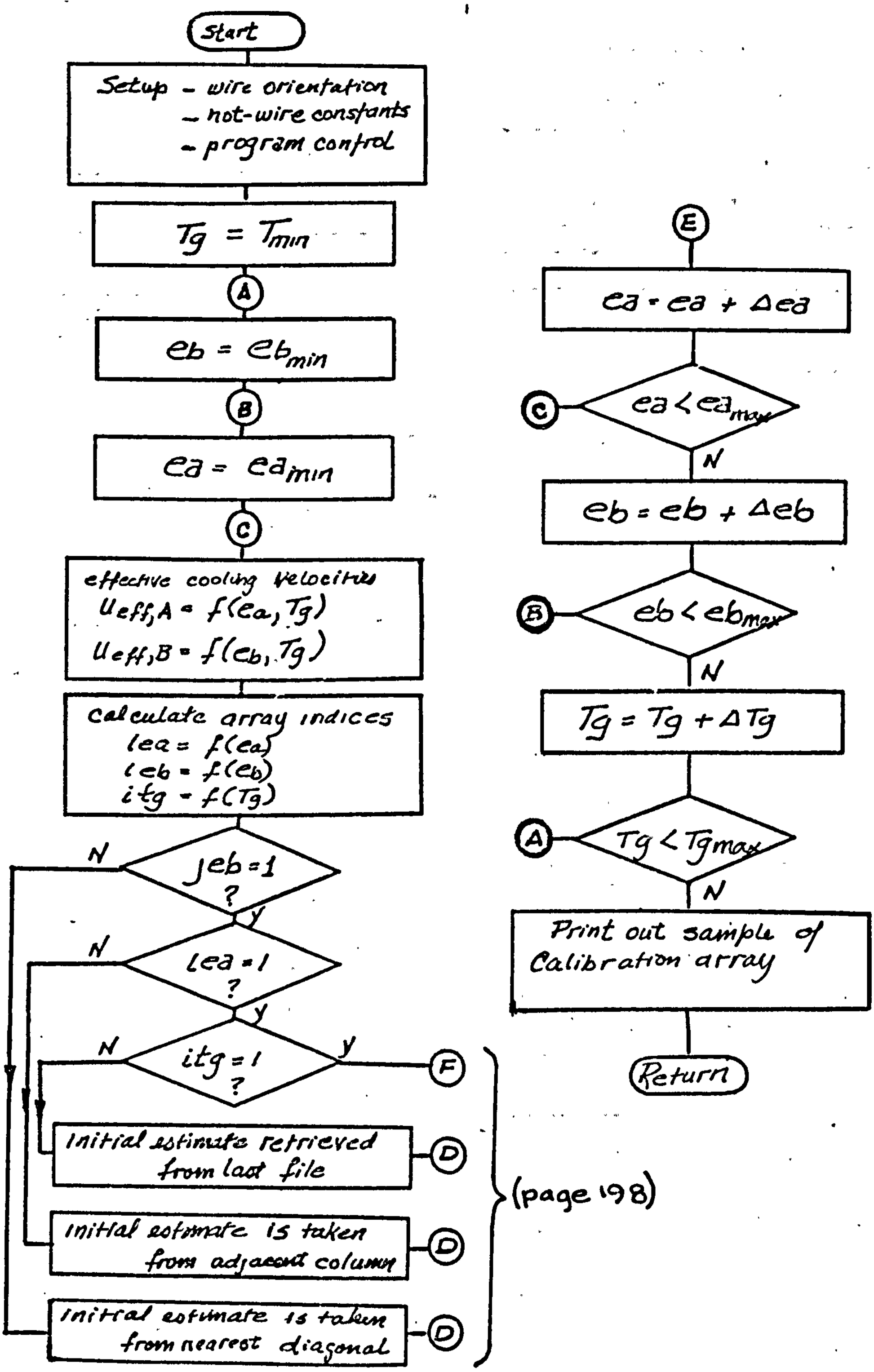

(page 198)

Subroutine CAL

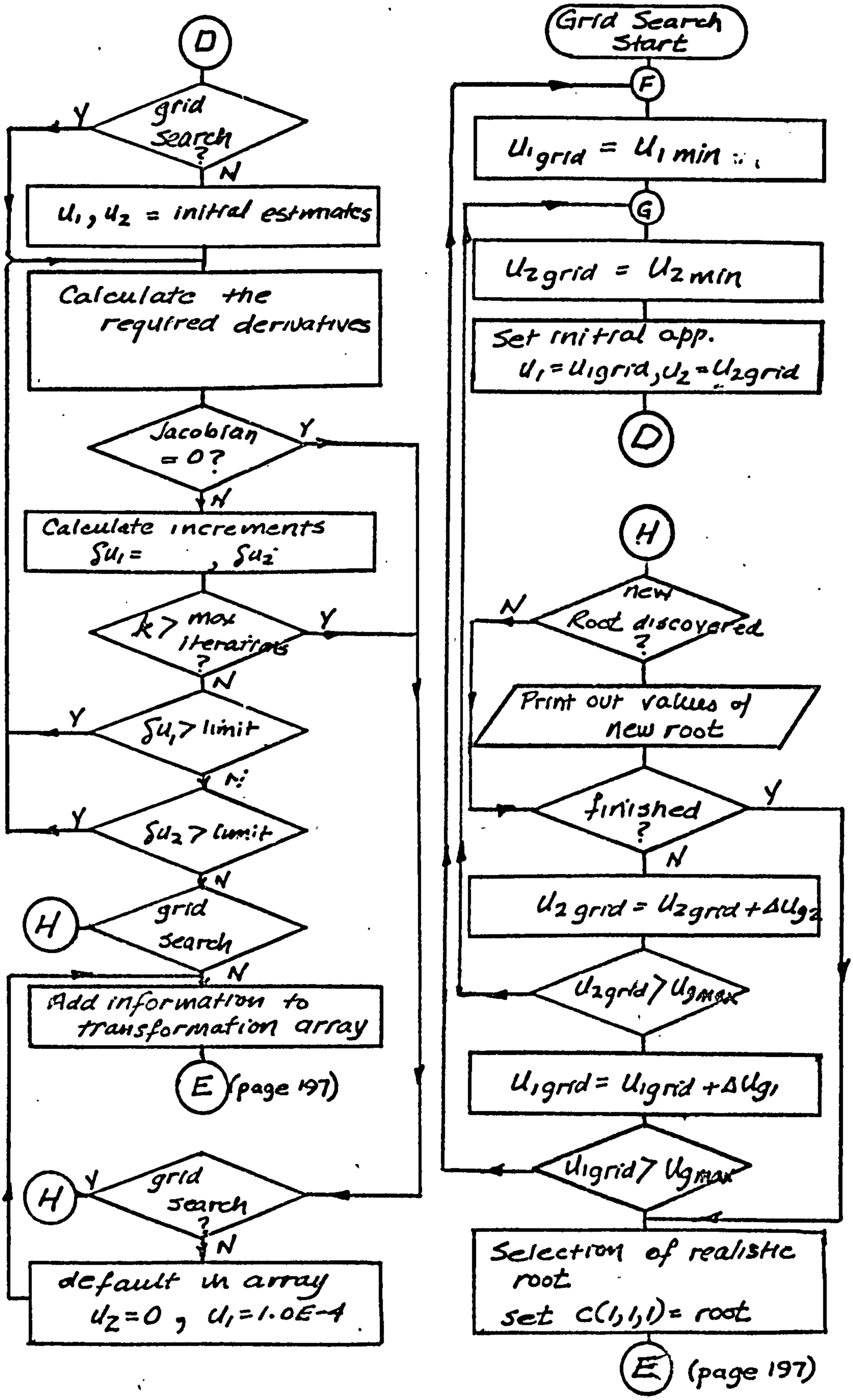

Subroutine CAL

APPENDIX F

```
      MASTER ANAL
C     PROGRAM TO PROCESS DATA FROM A CROSSED WIRE-THERMOCCOUPLE PROBE
                          AND AN ADDITIONAL THERMOCOUPLE
C     ----------------------QMC  R.R. SMITH 1972 ----------------------
      INTEGER JMX(3),JMO(3),IND(3)
      INTEGER E(256),F(256),G(256),H(256)
      INTEGER TURB,TAMB,EAA,EBB,IEA,JEB
      INTEGER IHEAD(3),ISENT(20)
      INTEGER A(1024)
      REAL SUM(9),QSUM(9),RD(9)
      INTEGER C,EABK,DEA,EAXX,EBBK,DEB,EBXX,TBCK,DTG,TMAX
      COMMON C(50,50,9),EABK(10),DEA,EAXX(10),EBBK(10),DEB,EBXX(10),TBCK
     U ,DTG,TMAX,MAX(3)
      EQUI VALENCE (U1,RD(1)),(U2,RD(2)),(TB,RD(3))
      EQUI VALENCE (IEA,IND(1)),(JEB,IND(2)),(ITG,IND(3))
CHAPTER 1  SETTING UP
      IUNIT=3
C     READ THRU MEDATA LOG HEADER
      READ(5,50) IHEAD
   50 FORMAT(3A4)
      CALL PDPOPEN(3,IHEAD(1))
      IFILE=0
C SETTING UP OF CALIBRATION ARRAY  , C(JEB,IEA,ITG)
      CALL CAL
C
C INPUT A NEW FILE
  110 CONTINUE
C NFILE IS THE NO OF FILES ON THE DATALOGGER TAPE
C NTOT IS THE NO OF POINTS EXPECTED FROM ONE CHANNEL
C NSAM IS NO OF POINTS PER SEQUENCE PER BLOCK
C NI IS A PROGRAM CHECK ON NO OF PTS FROM 1 CHANNEL
C     TEST D2     MEDATALOG005
      NFILE=29
      NFILE= 5
      NBLC=96
      NSAM=255
      NTOT=NSAM*NBLC
C INITIALIZE THE STORAGE SUMS AND COUNTERS
      IBLC=0
      NI=0
      DO 150 I=1,6
  150 SUM(I),QSUM(I)=0.
      DO 160 I=1,3
  160 JMX(I),JMO(I)=0
      IPAR=0
C     READ SENTENEL INFORMATION
      CALL PDPSENT(3,ISENT(1))
C
CHAPTER 2 INPUT DATA
  200 K=0
      CALL PDPREAD(3,4,E(1),F(1),G(1),H(1),K)
C CHECK FOR EOF
      IF(K) 290,285,210
  210 CONTINUE
C  INCREMENT BLOC COUNTER
 2000 FORMAT(///  (1H ,10I10))
      IBLC=IBLC+1
  215 FORMAT(1H ,2I10)
      DO 280 J=1,255
C SCALING.....LINEARIZING.....
      TURB=5*E(J)+TBCK
      TGAS=5*H(J)+TBCK
C     CALCULATE THE INDICES OF THE TRANSFORMATION ARRAY
      ITG=(TURB-TBCK)/DTG + 1
      IEA=(F(J)-EABK(ITG))/DEA + 1
      JEB=(G(J)-EBBK(ITG))/DEB + 1
C     OVER AND UNDER FLOW CATCHMENT
      DO 230 I=1,3
      IF(MAX(I)-IND(I)) 220,225,225
  220 JMX(I)=JMX(I)+1
```

APPENDIX F

```
      IND(I)=MAX(I)
      GOTO 230
  225 IF(IND(I)) 227,227,230
  227 IND(I)=1
      JMO(I)=JMO(I)+1
  230 CONTINUE
C     CHECK IF ARRAY ELEMENT IS VALID...IF NOT ABANDON THE DATUM
      IU21=C(JEB,IEA,ITG)
      IF(IU21-2000) 240,270,240
  240 CONTINUE
C INCREMENT THE SAMPLE COUNTER
      NI=NI+1
      U2=FLOAT(IU21/10 000)*1.0E-3
      U1=ABS(FLOAT(MOD(IU21,10 000))*1.0E-3)
      IF(ITG.GT.MAX(3)) GOTO 255
C     LINEAR INTERPOLATION BETWEEN TEMPERATURE FILES
      IU34=C(JEB,IEA,ITG+1)
      IF(IU34-2000) 250,255,250
  250 CONTINUE
      U3=ABS(FLOAT(MOD(IU34,10 000))*1.0E-3)
      U4=FLOAT(IU34/10 000)*1.0E-3
      PC=(FLOAT(TURB-TBCK)-FLOAT(ITG*DTG))/FLOAT(DTG)
      U1=U1 + (U3-U1)*PC
      U2=U2 + (U4-U2)*PC
  255 CONTINUE
C     UPDATING THE SUMS OF THE EXPECTED VALUES AND VARIANCES
      RD(3)=TURB*0.01
      RD(4)=U1*U2
      RD(5)=U2*TB
      RD(6)=U1*TB
C     RD(7)     CONTAINS TEMPERATURE FROM MONITOR PROBE
      RD(7)=TGAS*0.01
      DO 260 I=1,7
      RDI=RD(I)
      SUM(I)=SUM(I)+RDI
  260 QSUM(I)=QSUM(I) + RDI*RDI
  270 CONTINUE
  280 CONTINUE
C END OF DATA INPUT CALCULATIONS
C
C RETURN TO ACCEPT ANOTHER BLOC
      GOTO 200
C
C     DEFAULT ROUTINES
  285 CONTINUE
C     OMIT THE BACK SPACING PRESENTLY
      GOTO 287
      CALL PDPBACKSP(IUNIT)
C     TRY TO READ THE FAULTY BLOCK ONCE AGAIN   (TOTAL OF 24-X )
      CALL PDPREAD(3,4,E(1),F(1),G(1),H(1),K)
      IF(K) 290,286,210
  287 CONTINUE
  286 IPAR=IPAR+1
      IF(IPAR-10) 200,200,292
C     CHECK FOR T.M.
  290 IF(K+10) 400,400,292
  292 WRITE(6,295) K,IBLC,IPAR
  295 FORMAT(1H0,5H K = ,I6,5X,6H IBLC ,I6,5X,7H IPAR =,I6,///)
C     ABANDON THE FILE
      CALL PDPSKIP(3)
      CALL PDPREAD(3,4,E(1),F(1),G(1),H(1),K)
      GOTO 110

CHAPTER 4  WRITING EOF TO SECOND MT
  400 CONTINUE
C AVERAGING
      DO 420 I=1,7
      FNI=FLOAT(NI)
      SUM(I)=SUM(I)/FNI
  420 QSUM(I)=SQRT(QSUM(I)/FNI - SUM(I)*SUM(I))
```

APPENDIX F

```
CHAPTER 5     OUTPUT  TO LPO
      WRITE(6,504) (ISENT(I),I=1,20,1)
      WRITE(6,505) IFILE
      WRITE(6,510) NTOT,NI,IPAR
      WRITE(6,507)
      WRITE(6,506) SUM(1),QSUM(1)
      WRITE(6,508) SUM(2),QSUM(2)
      WRITE(6,511) SUM(3),QSUM(3)
      WRITE(6,512) SUM(4),QSUM(4)
      WRITE(6,514) SUM(5),QSUM(5)
      WRITE(6,516) SUM(6),QSUM(6)
      WRITE(6,518)   SUM(7),QSUM(7)
      WRITE(6,520) (I,JMO(I),I=1,3)
      WRITE(6,522) (I,JMX(I),I=1,3)
  504 FORMAT(1H1,///,20A4,///)
  505 FORMAT(      ///,7H FILE   ,I3,////)
  506 FORMAT(1HO,10X,6H U1    ,4X,1PE10.3,10X,1PE10.3)
  507 FORMAT(1HO,23X,4HMEAN,17X,3HRMS   /)
  508 FORMAT(1HO,10X,6H U2    ,4X,1PE10.3,10X,1PE10.3)
  510 FORMAT(1H ,22H NUMBER OF DATA POINTS,I8,5H NI=
     1,I6,10H      IPAR =,I3 ///)
  511 FORMAT(1HO,10X,6H TEMP  ,4X,1PE10.3,10X,1PE10.3)
  512 FORMAT(1HO,10X,6H U1U2  ,4X,1PE10.3,10X,1PE10.3)
  514 FORMAT(1HO,10X,6H TBU2  ,4X,1PE10.3,10X,1PE10.3)
  516 FORMAT(1HO,10X,6H TBU1  ,4X,1PE10.3,10X,1PE10.3)
  518 FORMAT(1HO,10X,6H TMON  ,4X,1PE10.3,10X,1PE10.3)
  520 FORMAT(///    12X,2HJO,I1,I6,6H     JO,I1,I6,6H     JO,I1,I6/)
  522 FORMAT(  1H ,11X,2HJM,I1,I6,6H     JM,I1,I6,6H     JM,I1,I6)
      IFILE=IFILE+1
      IF(IFILE.NE.NFILE) GOTO 110

CHAPTER 6   TERMINATION
      CALL PDPCLOSE(3)
      STOP
      END
```

```
      SUBROUTINE CAL
C     SUBROUTINE TO SET UP THE TRANSFORMATION ARRAY,   ITS INDICES ARE
CC          GIVEN BY   IEA=F(EA),   JEB=F(EB),   ITG=F(TG)
C     ----------------------QMC   1972   R.R. SMITH ----------------------

      REAL ALF(3),E(4),F(3,4),PHI(3),JOB,ROOT(8,4),U(3),UW2(3)
      REAL RLD(3),RWC(3),RWH(3),TWH(3),CNU(3)
      REAL KHIN,KH2,LW
      INTEGER EA,EB,TG
      INTEGER IP(3),JLIM(3),JINC(3),JLL(3)
      INTEGER C,EABK,DEA,EAXX,EBBK,DEB,EBXX,TBCK,DTG,TMAX
      DIMENSION KEA(10),KEB(10)
      COMMON C(50,50,9),EABK(10),DEA,EAXX(10),EBBK(10),DEB,EBXX(10),TBCK
     U ,DTG,TMAX,MAX(3)
      EQUIVALENCE (U1,U(1)),(U2,U(2)),(U3,U(3))
      EQUIVALENCE (UW21,UW2(1)),(UW22,UW2(2)),(UW23,UW2(3))
      EQUIVALENCE (F11,F(1,1)),(F12,F(1,2)),(F13,F(1,3)),(F14,F(1,4))
      EQUIVALENCE (F21,F(2,1)),(F22,F(2,2)),(F23,F(2,3)),(F24,F(2,4))
      EQUIVALENCE (F31,F(3,1)),(F32,F(3,2)),(F33,F(3,3)),(F34,F(3,4))
      DATA ALF,PHI /0.727,0.730,1.0,3.14,0.0,0.0  /
      DATA UG1M,DG1,UG1X / -.30,.05,.30  /
      DATA UG2M,DG2,UG2X  / -.30,.15,.30  /
      DATA KEA /236,  227,  217,  208,  199,  190,  181,  172,  0,  0 /
      DATA KEB / 168,  163,  157,  151,  145,  140,  134,  128,  0,  0 /
C
CHAPTER 1  CHAPTER 1  CHAPTER 1  CHAPTER 1  CHAPTER 1  CHAPTER 1
C     PROGRAM CONTROL
      EP=0.0005
      EP=0.001
      KMAX=25
      IWIRE=2
      IGRID=0
```

APPENDIX F

```
C
CHAPTER  2  CHAPTER  2  CHAPTER  2  CHAPTER  2  CHAPTER  2  CHAPTER  2
C       WIRE ORIENTATION
C
        CAL1=COS(ALF(1))
        CAL2=COS(ALF(2))
        CAL3=COS(ALF(3))
        SASP1=SIN(ALF(1))*SIN(PHI(1))
        SASP2=SIN(ALF(2))*SIN(PHI(2))
        SASP3=SIN(ALF(3))*SIN(PHI(3))
        SACP1=SIN(ALF(1))*COS(PHI(1))
        SACP2=SIN(ALF(2))*COS(PHI(2))
        SACP3=SIN(ALF(3))*COS(PHI(3))
C
CHAPTER  3  CHAPTER  3  CHAPTER  3  CHAPTER  3  CHAPTER  3  CHAPTER  3
CC      SETTING UP CONSTANTS
CC      WIRE  A IS ALSO DESIGNATED BY  1   AND  COLOUR RED (YELLOW)
CC      WIRE B IS DESIGNATED  BY  2  AND COLOR BLACK
CC      EABK,EBBK  ARE THE LOWEST LIMITS OF THE DYNAMIC RANGE OF THE
CC                 AUXILLARY VOLTAGES
CC      DEA,DEB  ARE THE ARRAY INCREMENTS IN THE AUXILLARY VOLTAGE ARRAYS
CC      EAXX,EBXX ARE THE TOP LIMITS OF THE DYNAMIC RANGE OF THE AUXILLARY
CC      TBCK,DTG,TMAX ARE THE RESPECTIVE PARAMETERS FOR THE TEMPERATURE
C       SET THE LIMITS OF THE CALIBRATION ARRAY
        MAX(1),MAX(2)=40
        MAX(3) = 8
        TBCK=3000
        DTG=500
        TMAX=TBCK + DTG*(MAX(3)-1)
        DEA,DEB=5
        DO 9  I=1,10
        EABK(I)=KEA(I)
        EBBK(I)=KEB(I)
        EAXX(I) = EABK(I) + DEA*(MAX(1)-1)
        EBXX(I) = EBBK(I) + DEB*(MAX(2)-1)
    9 CONTINUE
C        HOT WIRE CONSTANTS
        TC=19.8
        RWC(1)=9.12
        RWH(1)=14.59
        ALF(1)=.0032
        RWC(2)=10.29
        RWH(2)=16.46
        ALF(2)=.00275

        PI = 3.14159
        LW=0.002
        DIA=5.0E-06
        DO 10  I=1,2
        RLD(I)= .46
        TWH(I)=(RWH(I)-RWC(I))/(ALF(I)*RWC(I)) + TC
        CNU(I)=RWH(I)/((RLD(I)+50.+RWH(I))**2*PI*LW)
   10 CONTINUE
C SETTING UP OF CALIBRATION ARRAY

C       Y DESIGNATES THE GAS TEMPERATURE IN CENTIGRADE
C       X DESIGNATES THE ANEMOMETER VOLTAGE
        DO 1000 ITF= TBCK,TMAX,DTG
        IT=TMAX+TBCK-ITF
C       TEMPERATURE
        Y=FLOAT(IT)*0.01
        ITG=(IT-TBCK)/DTG+1
        DO 1000 EB=EBBK(ITG),EBXX(ITG) ,DEB
        DO 1000 EA=EABK(ITG),EAXX(ITG),DEA
C
CC      INTERPRETATION OF WIRE A
C       AUXILLARY CALIBRATION OF YELLOW   APRIL/72
        X=2.002 + .003070*FLOAT(EA)
        TFLM=(Y+TWH(1))*0.5
        FKW=0.02414*(1.+0.003124*TFLM)
        VK= 1.328E-05 + 8.244E-08*TFLM + 1.240E-10*TFLM*TFLM
        FNU=CNU(1)*X*X/(FKW*(TWH(1)-Y))*((TFLM+273.)/(Y+273.))**(-.17)
C       CALIBRATION OF WIRE A   (YELLOW)      APRIL/72
         REA = -.8144 + 3.3768*FNU - 5.1338*FNU*FNU + 2.8676*FNU*FNU*FNU
```

APPENDIX F

```
      UEFFA=VK/DIA*REA
      UW2(1)=UEFFA*UEFFA
C     INTERPRETATION OF WIRE B
C     CALIBRATION OF AUXILLARY  (BLACK)   APRIL/72
      X = 1.9925 + .00307Z*FLOAT(EB)
      TFLM=(Y+TWH(2))*0.5
      FKW=0.0241*(1.+0.003124*TFLM)
      VK= 1.328E-05 + 8.244E-08*TFLM + 1.240E-10*TFLM*TFLM
      FNU=CNU(2)*X*X/(FKW*(TWH(2)-Y))*((TFLM+273.)/(Y+273.))**(-.17)
C     CALIBRATION OF WIRE B   (BLACK)     APRIL/72
      REB = -.5260 + 2.9533*FNU - 6.2152*FNU*FNU + 4.8952 *FNU*FNU*FNU
      UEFFB = VK/DIA*REB
      UW2(2)=UEFFB*UEFFB
  100 CONTINUE
C
C     CALCULATION OF THE ACCESS PARAMETERS
      IEA=(EA-EABK(ITG))/DEA + 1
      JEB=(EB-EBBK(ITG))/DEA + 1
      IF=ITG+1
      IF(IF.EQ.MAX(3)+2) GOTO409
  430 IR=JEB
      IC=IEA
      GOTO 600
  409 CONTINUE
      IF=ITG
C     SOLUTION OF THE EQUATION FOR THE AXIAL COMPONENTS
C     IS THE EQUATION OF THE FIRST ROW OF THE MATRIX ?
      IF(JEB-1) 410,410,420
C     IS   IEA = 1?   IF NOT  INITIAL APPROXIMATION IS BY ROWS
  410 IF(IEA-1) 412,412,415
C     IS   IF = 1 ?   IF SO GOTO GRID SEARCH; IF NOT GOTO LOWER FILE
  412 IF(MAX(3)+1-IF) 440,440,413
  413 IF=IF+1
      GOTO 440
      IR=JEB
      IC=IEA
      GOTO 600
C     THE INITIAL APPROXIMATION IS BY ROWS
  415 IR=JEB
      IC=IEA-1
      GOTO 600
C     THE INITIAL APPROXIATION IS BY COLUMNS
  420 IR=JEB-1
      IC=IEA-1
      IF(IC.LT.1) IC=1
      IF(JEB.EQ.IEA) IC=IEA
      GOTO 600
C
C
  440 CONTINUE
C     GRID CONTROL FOR ROOT SEARCH

      WRITE(6,900) IEA,JEB,ITG
      IGRID=1
      IROOT=0
      UG1=UG1M-DG1
   34 UG1=UG1+DG1
      UG2=UG2M-DG2
   35 UG2=UG2+DG2
      U1=UG1
      U2=UG2
C SOLVING FOR A ROOT AND RETURN
      GOTO 600
C
C EXAMINATION FOR A REPETITIVE ROOT
   36 CONTINUE
C     GRID SEARCH TO LOCATE THE ROOTS OF EQUATION (1,1)
      IF(IROOT.EQ.0) GOTO 371
      DO 370 I=1,IROOT
      IR=0
      DO 37 J=1,2
   37 IF(ABS(U(J)-ROOT(I,J)).LT.0.0001) IR=IR+1
  370 IF(IR.EQ.2) GO TO 385
C DISCOVERY OF A NEW ROOT
```

APPENDIX F

```
  371 IROOT=IROOT+1
      ROOT(IROOT,1)=U(1)
      ROOT(IROOT,2)=U(2)
   38 WRITE(6,380) (U(I),I=1,3)
  380 FORMAT(6H ROOTS,7X,3(1PE11.3,11X))
  385 CONTINUE
C
C ARE ALL POSITIVE ROOTS LOCATED ?
   39 CONTINUE
      IF(IROOT.GE.2**IWIRE) GO TO 390
      IF(UG2.LT.UG2X) GOTO 35
      IF(UG1.LT.UG1X) GOTO 34
C     YES SELECTION OF A REALISTIC SOLUTION
  390 CONTINUE
      IALL=IROOT
C     FIRST CRITERION     U(1) >0.
      J=0
      DO 392 I=1,IALL
      IF(ROOT(I,1).LT.0.) GOTO 392
      J=J+1
      IP(J)=I
  392 CONTINUE
C     POSSIBILITY TO ASSIGN A VALUE IF J=0
C     SECOND CRITERION     SMALLEST ABS(U(2))
      IM=1
      IF(J.LT.1) GOTO 396
      IM=IP(1)
      DO 395 I=1,J
  395 IF(ABS(ROOT(IP(I),2)).LT.ABS(ROOT(IM,2))) IM=IP(J)
  396 CONTINUE
      U1=ROOT(IM,1)
      U2=ROOT(IM,2)
      WRITE(6,397) IM
  397 FORMAT(///,4HIM =,I6,///)
  398 CONTINUE
      IU1=U1*1000
      IF(ABS(U2).GT.0.80) U2=0.80*(U2/ABS(U2))
      IU2=U2*1000
      IU2=IU2*10 000
      C(1,1,ITG)=(IU1+IABS(IU2))*( U2/ ABS( U2))
      IGRID=0
      GOTO 1000
C     END OF GRID SEARCH

CHAPTER 6  SOLUTION OF RESPONSE EQUATIONS BY NEWTON'S METHOD
C
C     F(I,1) = D (UW2I) / DU1
C     F(I,2) = D (UW2I) / DU2
C     F(I,3) = D (UW2I) / DU3
C     F(I,4) = TOTAL EQUATION
C
  600 CONTINUE
      KHIN=.27
      KS=1
      KH2=KHIN*KHIN
      IF(IGRID-1)61,60,60
C     INITIAL APPROXIMATION
   61 CONTINUE
      IU21=C(IR,IC,IF)
      U2=FLOAT(IU21/10 000)*1.0E-3
      U1=FLOAT(MOD(IABS(IU21),10 000))*1.0E-3
      IF(U1.LT.0.005) U1=0.005
   60 CONTINUE
      A=U1*CAL1 + U2*SACP1
      B=-U1*SACP1 + U2*CAL1
      F11=2.*CAL1*A - 2.*KH2*SACP1*B
      F12=2.*SACP1*A + 2.*KH2*CAL1*B
      F14=A*A + KH2*B*B - UW21
      A= U1*CAL2 + U2*SACP2
      B=-U1*SACP2 + U2*CAL2
      F21=2.*CAL2*A - 2.*KH2*SACP2*B
      F22=2.*SACP2*A + 2.*KH2*CAL2*B
      F24 = A*A + KH2*B*B - UW22
      JOB=F11*F22 - F12*F21
```

APPENDIX F

```
C       IF JOB = 0  ABANDON THE POINT
  660   WRITE(6,661) (U(I),I=1,3)
        GOTO 685
  661   FORMAT(1SH J IS ZERO  UIS ,1P3E11.3)
  670   CONTINUE
        D1=(-F14*F22 + F24*F12)/JOB
        D2=(-F24*F11 + F14*F21)/JOB
        U1=U1+D1
        U2=U2+D2
        KS=KS+1
C TEST  FOR CONVERGENCE
C IF  DIVERGENT  ABANDON THE POINT
        IF(KS-KMAX) 689,689,685
  685   IF(IGRID-1) 686,39,39
  686   U2=0.
        U2=1.0E-4
        U1=2.00000
        GOTO 692
  689   IF(ABS(D1)-EP) 690,690,60
  690   IF(ABS(D2)-EP) 691,691,60
  691   IF(IGRID-1) 692,36,36
  692   CONTINUE
C
        IU1=U1*1000
        IF(ABS(U2).GT.0.80) U2=0.80*(U2/ABS(U2))
        IU2=U2*1000.
        IU2=IU2*10 000
        C(JEB,IEA,ITG)=(IU1+IABS(IU2))*(U2/ABS(U2))
 1000   CONTINUE
C       END OF SOLUTION
CC      PRINT OUT SAMPLE OF TRANSFORMATION ARRAY
C
        WRITE(6,910)
        WRITE(6,900) ((C(I,J,1),I=1,10),J=1,20)
        WRITE(6,910)
        WRITE(6,900) ((C(I,J,2),I=1,10),J=1,20)
        WRITE(6,910)
        WRITE(6,900) ((C(I,J,3),I=1,10),J=1,20)
        WRITE(6,910)
        WRITE(6,900) ((C(I,J,4),I=1,10),J=1,20)
        WRITE(6,910)
        WRITE(6,900) ((C(I,J,5),I=1,10),J=1,20)
        WRITE(6,910)
        WRITE(6,900) ((C(I,J,6),I=1,10),J=1,20)
  900   FORMAT(3X,10I10)
  910   FORMAT(///)
        RETURN
        END
```

APPENDIX G

SECONDARY DATA PROCESSING PROGRAM EXAM

Most extended statistical analyses require data sequences which have an expected value of zero. In order to obtain these data sequences, the 'raw' data had to be processed at least once in a 'primary' program to determine the expected values. In the subsequent (secondary) data processings, these expected values were often removed from the data before any analysis was performed.

Program EXAM was designed to be general purpose. It is structured so that one subroutine contains all the basic data preparation, including data transfers from magnetic tape and the transformation routines, while other subroutines include the data processing required for the statistical analysis. The main program provides the coordination of the data transfers.

The program in the following listing contains two of the conditional sampling routines which were developed for the determination of intermittency in the outer boundary layer (see section 8.2.3).

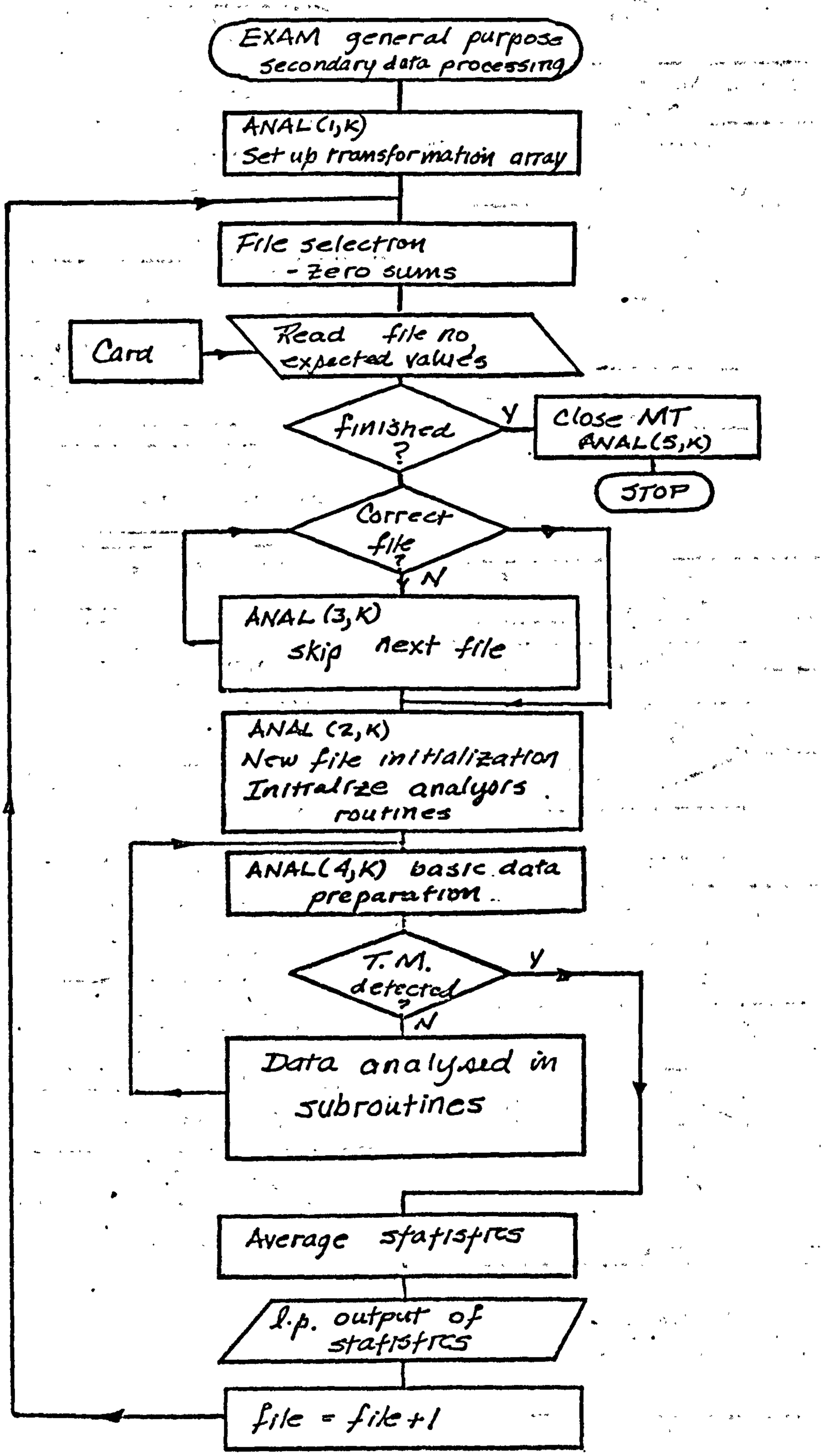

Program EXAM

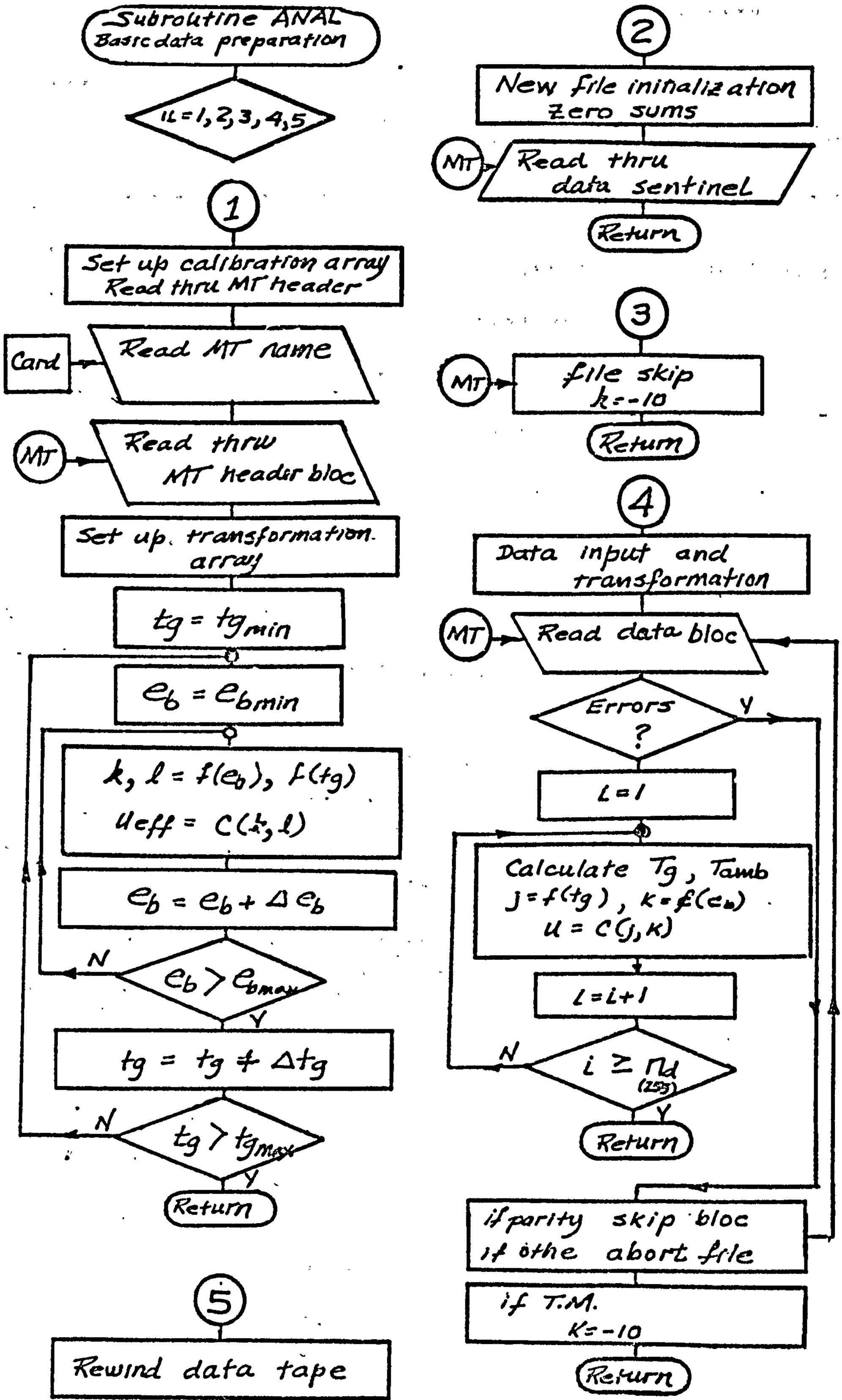

Subroutine ANAL

APPENDIX G

```
      MASTER EXAM
C     SAMPLE PROGRAM FOR THE SECONDARY AMPLITUDE DATA PROCESSING
C       CONTAINS TWO METHODS TO ANALYSE INTERMITTENCY OF TEMPERATURE
                              AND VELOCITY
C     ----------------------R.R. SMITH  QMC   1972 ----------
      INTEGER ISAM
      COMMON      A(1024),FMEAN(4),SM2(4),SM3(4),SM4(4),PRIM(4)
     1 ,IHEAD(3),ISENT(20)
CHAPTER 1       SETTING UP  PROGRAM  CONSTANTS
C  NBLC IS TOTAL NO OF BLOCS
C  NSAM IS  NO OF SAMPLES  FROM ONE CHANNEL IN ONE BLOC
C  BSAM IS  NO OF SAMPLES IN ONE BLOC
C  NTOT IS TOTAL NO OF SAMPLES FROM ONE CHANNEL
C  NFILE IS NO OF FILES TO BE ANALYSED
C  KFILE IS CURRENT FILE UNDER EXAMINATION
C  SET UP THE INTERPRETATION MATRIX
      CALL ANAL(1,K)
      NBLC=48
      NBLC=128
      NSAM=255
      BSAM= NSAM*4.
      NTOT= NSAM* NBLC
      NFILE=21
      IFILE=0
C  START OF NEW FILE
C  INITIALIZE  SUMS
  100 CONTINUE
      READ(5,120) KFILE,(FMEAN(J),J=1,4)
      IF(KFILE) 999,115,115
  115 CONTINUE
  120 FORMAT (I10,4F0.0)
CHAPTER 1   SELECTION OF FILE
  140 IF(IFILE-KFILE) 150,200,200
  150 CALL ANAL(3,K)
  155 CONTINUE
      IFILE = IFILE+1
      GOTO 140
C  END OF FILE SELECTION LOOP

CHAPTER 2   INPUT DATA AND ANALYSIS
C  SET UP PASS VARIABLES
  200 CONTINUE
C  SET UP THE FILE VARIABLE IN ANAL
      CALL ANAL(2,K)
C       SET UP THE INTERMITTENCY ROUTINES
      CALL CINTO(A(I),A(I+2),A(I+1),1)
      CALL FINTO(A(I),A(I+2),A(I+1),1)
      NI=0
      IBLC=0
CHAPTER 3     DATA ANALYSES
C  INPUT NEW RECORD
  205 CALL ANAL(4,K)
C  DETECTION OF EOF
      IF(K+1) 300,210,210
  210 CONTINUE
      IBLC=IBLC+1
      DO 260 I=1,BSAM,4
      NI=NI+1
      A(I)=A(I)-FMEAN(1)
      A(I+2) = A(I+2) - FMEAN(3)
      CALL CINTO(A(I),A(I+2),A(I+1),2)
      CALL FINTO(A(I),A(I+2),A(I+1),2)
  260 CONTINUE
  280 CONTINUE
C  RETURN TO READ NEXT BLOC
      GOTO 205
C  END OF DATA LOOP CALCULATIONS
C
```

APPENDIX G

```
CHAPTER 4          DATA ANALYSES COMPLETED   COMPUTE AVERAGES
                 AND PRINT OUT TO LP
  300 CONTINUE
C     TRIP COUNTERS IN MODEL F
      CALL FINTO(10.,10.,10.,2)
  309 CONTINUE
      IF(NI) 100,100,308
  308 NTOT=NI
      FNTOT=FLOAT(NTOT)
      X1=0.
      X2=0.
      WRITE(6,410) ISENT
  410 FORMAT (1H1,///,30A4,////)
      WRITE (6,400) KFILE,NTOT
  400 FORMAT (1H ,30H STATISTICAL ANALYSIS OF FILE ,I2,5X,8H NTOT = ,I5,
     1//)
      CALL CINTO(FNTOT,X1,X2,3)
      CALL FINTO(FNTOT,X1,X2,3)
      IFILE=IFILE+1
      GOTO 100

CHAPTER 5 TERMINATION
  999 CONTINUE
C     CLOSE DATA TAPE
      CALL ANAL(5,K)
      STOP
      END
```

```
      SUBROUTINE CINTO( T,V,TA,IS)

C     SUBROUTINE FOR INTERMITTENCY METHOD C----SLOPE + TIME CRITERIA---
C     ----------------------------R.R. SMITH   QMC  1972----------------------

      GOTO(1000,2000,3000) IS
C     SETTING UP CONSTANTS FOR FILE ANALYSIS
 1000 CONTINUE
      NCROS=0
      NTP,NTMT=0
      NVL,NVLT=0
C     INTERMITTENCY PARAMETERS
CC    TEP IS THE MAXIMUM LIMIT TO VARIATION BETWEEN CONSECUTIVE SAMPLES
CC    VEP IS A SIMILAR PARAMETER FOR THE VELOCITY
C     NTIM IS THE TIME INCREMENT BEFORE WHICH A SAMPLE IS AMBIENT
      NTIM=10
C     RUN 4
      TEP=10.
      VEP=0.05
C     RUN 5
      TEP=15.
      VEP=.03
      NTIM=60
C     RUN 6
      TEP=5
      VEP=0.005
      NTIM=30
C     RUN 7
      NTIM=20
C     RETURN TO MAIN PROGRAM
      RETURN
C
C
 2000 CONTINUE
C     INTERMITTENCY STUDY
C     CLEAR CROSS INTERMITTENCY DETECTOR
      ICROS=0
C
      IF(ABS(T-TM1)-TEP) 240,240,243
  240 NTP=NTP+1
      IF(NTP-NTIM) 245,242,241
  241 NTMT=NTMT+1
```

APPENDIX G

```
      ICROS=1
      GOTO 245
  242 NTMT=NTMT+NTP
      ICROS=1
      GOTO 245
  243 NTP=0
  245 CONTINUE
      IF(ABS(V-VM1)-VEP)250,250,253
  250 NVL=NVL+1
      IF(NVL-NTIM) 255,252,251
  251 NVLT=NVLT+1
      ICROS=ICROS+1
      GOTO 255
  252 NVLT=NVLT+NVL
      ICROS=ICROS+1
      GOTO 255
  253 NVL=0
  255 CONTINUE
      IF(ICROS-2) 270,265,265
  265 NCROS=NCROS+1
  270 CONTINUE
C     SET TM1 VL1     TO I-1 VALUES
      TM1=T
      VM1=V
C     RETURN TO MAIN PROGRAM
      RETURN
C
CC
C     OUTPUT
 3000 CONTINUE
      TMT=(T-FLOAT(NTMT))/(T+1.0E-10)
      CMT=(T-FLOAT(NCROS))/(T+1.0E-10)
      VLT=(T-FLOAT(NVLT))/(T+1.0E-10)
      T1=TEP*0.01
      T2=FLOAT(NTIM)
      V1=VEP
      V2=FLOAT(NTIM)
      WRITE(6,440) T1,T2,V1,V2
  440 FORMAT( 10H  MODEL C0, 8X,6H  T1 =,F6.3,6H  T2 =,F6.3,6H  V1 =,
     1 F6.3,6H  V2 =,F6.3,/)
      WRITE(6,450) TMT,VLT
  450 FORMAT(1H0,25H THERMAL INTERMITTENCY = ,  F6.3,5X,27H VELOCITY  I
     1TERMITTENCY =  ,  F6.3)
      WRITE(6,460) CMT
  460 FORMAT(1H0,25H  CROSS INTERMITTENCY =     ,F6.3////)
C     RETURN TO MAIN PROGRAM
      RETURN
      END



      SUBROUTINE EINTO( T,V,TA,IS)
C     SUBROUTINE FOR INTERMITTENCY METHOD F---TIME INTERVAL HISTOGRAM--
C     ----------------------R,R, SMITH   QMC  1972----------------------

      DIMENSION XAB(100),PITP(100),PIVL(100)
      GOTO(1000,2000,3000) IS
C     SETTING UP CONSTANTS FOR FILE ANALYSIS
 1000 CONTINUE
      NCROS=0
      NTP,NTMT=0
      NVL,NVLT=0
      DO 90 I=1,100
      PITP(I) = 0.0
      PIVL(I) = 0.0
   90 XAB(I) = FLOAT(I)
C     INTERMITTENCY PARAMETERS
CC    TMAR, VMAR  ARE THE LEVEL THESHOLDS
C     NTIM IS THE TIME INCREMENT BEFORE WHICH A SAMPLE IS AMBIENT
      VMAR = 0.0125*0.0125
```

APPENDIX G

```
      TMAR = 0.25*0.25
C     RETURN TO MAIN PROGRAM
      RETURN
C
C
 2000 CONTINUE
C     INTERMITTENCY STUDY
C     CLEAR CROSS INTERMITTENCY DETECTOR
      ICROS=0
C
C     CALCULATE THE SQUARE
      V=V*V
      T=T*T

      IF(T  - TMAR ) 240,240,241
240   NTP=NTP+1
      ICROS=1
      GOTO 245
241   IF(NTP) 245,245,242
242   NTMT=NTMT+NTP
      IF(NTP-100) 244,244,243
243   NTP=100
244   PITP(NTP)=PITP(NTP)+1
      NTP=0
245   CONTINUE
      IF( V-VMAR) 250,250,251
250   NVL=NVL+1
      ICROS=ICROS+1
      GOTO 255
251   IF(NVL) 255,255,252
252   NVLT=NVLT+NVL
      IF(NVL-100) 254,254,253
253   NVL=100
254   PIVL(NVL)=PIVL(NVL)+1
      NVL=0
255   CONTINUE
      IF(ICROS-2) 270,265,265
265   NCROS=NCROS+1
270   CONTINUE
C     RETURN TO MAIN PROGRAM
      RETURN
C
CC
C     OUTPUT
 3000 CONTINUE
      TMT=(T-FLOAT(NTMT))/(T+1.0E-10)
      CMT=(T-FLOAT(NCROS))/(T+1.0E-10)
      VLT=(T-FLOAT(NVLT))/(T+1.0E-10)
      T1 = SQRT(TMAR)
      T2=FLOAT(NTIM)
      V1 = SQRT(VMAR)
      V2=FLOAT(NTIM)
      WRITE(6,440) T1,T2,V1,V2
440   FORMAT( 10H  MODEL E0, 8X,6H  T1 =,F6.3,6H  T2 =,F6.3,6H  V1 =,
     1 F6.3,6H  V2 =,F6.3,/)
      WRITE(6,450) TMT,VLT
450   FORMAT(1H0,25H THERMAL INTERMITTENCY = ,  F6.3,5X,27H VELOCITY  I
     1TERMITTENCY = ,  F6.3)
      WRITE(6,460) CMT
460   FORMAT(1H0,25H  CROSS INTERMITTENCY =     ,F6.3////)
      WRITE(6,470)
470   FORMAT(1H0,45H DISTRIBUTION OF THERMAL INTERMITTENCY       ,/)
      DO 471 I=1,100,10
      K=I-1
471   WRITE(6,480) K,(PITP(J),J=I,I+9)
      WRITE(6,475)
475   FORMAT(//  ,45H DISTRIBUTION OF VELOCITY INTERMITTENCY       ,/)
      DO 476 I=1,100,10
      K=I-1
476   WRITE(6,480) K,(PIVL(J),J=I,I+9)
      CALL VLOT(100,XAB,PIVL,-1)
      CALL TLOT(100,XAB,PITP,-1)
480   FORMAT(1H0,I10,10F10.0)
C     RETURN TO MAIN PROGRAM
      RETURN
```

```
      END


      SUBROUTINE TLOT(NB,XP,YP,K)
C     SUBROUTINE CALLED BY METHOD F FOR GRAPHICAL PRESENTATION
C     ------------------------R.R. SMITH   QMC  1972----------
      REAL XMAX,YMAX
      INTEGER NB,GRAPH(100,50),L,M,P(9),BLK,DOT,DASH,PARA,MM
      DIMENSION XP(100),YP(100),SCALE(11),LSYMB(11)
      DATA BLK/1H /,DOT/1H./
      DATA P/1H1,1H2,1H3,1H4,1H5,1H6,1H7,1H8,1H9 /
      DATA SCALE / 1.,10.,20.,30.,40.,50.,60.,70.,80.,90.,100. /
      DATA LSYMB/1H0,1H1,1H2,1H3,1H4,1H5,1H6,1H7,1H8,1H9,1H0 /
      YMAX,XMAX=1.0
      AB=FLOAT(NB)
      DO 24 I=1,NB
      XMAX=AMAX1(XMAX,XP(I))
      YMAX=AMAX1(YMAX,YP(I))
24    CONTINUE
25    CONTINUE
      XZZ=1.0/XMAX*100.
      YZZ=1.0/YMAX*50.
      DO 26 I=1,NB
      XP(I)=XP(I)*XZZ
26    YP(I)=YP(I)*YZZ
27    CONTINUE
      IF(IABS(K)-1) 32,30,32
30    DO 32 J=1,50
      DO 32 I=1,100
      GRAPH(I,J)=BLK
      GRAPH(I,1)=DOT
      GRAPH(100,J)=DOT
      GRAPH(I,50)=DOT
31    GRAPH(1,J)=DOT
32    CONTINUE
      DO 34 I=1,NB
      L=MAX1(XP(I),1.)
      M=MAX1(YP(I),1.)
      L=MINO(L,100)
      M=MINO(M,50)
34    GRAPH(L,M)=P(IABS(K))
35    CONTINUE
      IF(K) 669,37,37
37    CONTINUE
      DO 38 K=1,11
      IF(SCALE(K).GT.XMAX) GOTO 39
      X=SCALE(K)*XZZ
      LS=NINT(X)
38    GRAPH(LS,1)=LSYMB(K)
39    CONTINUE
      WRITE(6,91)
      DO 36 J=1,50
      JJ=51-J
36    WRITE(6,92) (GRAPH(I,JJ),I=1,100)
669   RETURN
91    FORMAT( ///////)
92    FORMAT(1H ,100A1)
99    WRITE(6,93) XP(I),YP(I)
93    FORMAT(1H1,43HGRAPH SCALE EXCEEDED - FIRST ILLEGAL VALUES,//,2HX=,
     1X,F8.3,/,2HY=,5X,F8.3)
      STOP
      END
      SUBROUTINE VLOT(NB,XP,YP,K)
C     SUBROUTINE CALLED BY METHOD F FOR GRAPHICAL PRESENTATION
C     ------------------------R.R. SMITH   QMC  1972----------
      REAL XMAX,YMAX
      INTEGER NB,GRAPH(100,50),L,M,P(9),BLK,DOT,DASH,PARA,MM
      DIMENSION XP(100),YP(100),SCALE(11),LSYMB(11)
      DATA BLK/1H /,DOT/1H./
      DATA P/1H1,1H2,1H3,1H4,1H5,1H6,1H7,1H8,1H9 /
      DATA SCALE / 1.,10.,20.,30.,40.,50.,60.,70.,80.,90.,100. /
```

APPENDIX G

```
      DATA LSYMB/1H0,1H1,1H2,1H3,1H4,1H5,1H6,1H7,1H8,1H9,1H0 /
      YMAX,XMAX=1.0
      AB=FLOAT(NB)
      DO 24 I=1,NB
      XMAX=AMAX1(XMAX,XP(I))
      YMAX=AMAX1(YMAX,YP(I))
24    CONTINUE
25    CONTINUE
      XZZ=1.0/XMAX*100.
      YZZ=1.0/YMAX*50.
      DO 26 I=1,NB
      XP(I)=XP(I)*XZZ
26    YP(I)=YP(I)*YZZ
27    CONTINUE
      IF(IABS(K)-1) 32,30,32
30    DO 32 J=1,50
      DO 32 I=1,100
      GRAPH(I,J)=BLK
      GRAPH(I,1)=DOT
      GRAPH(100,J)=DOT
      GRAPH(I,50)=DOT
31    GRAPH(1,J)=DOT
32    CONTINUE
      DO 34 I=1,NB
      L=MAX1(XP(I),1.)
      M=MAX1(YP(I),1.)
      L=MINO(L,100)
      M=MINO(M,50)
34    GRAPH(L,M)=P(IABS(K))
35    CONTINUE
      IF(K) 669,37,37
37    CONTINUE
      DO 38 K=1,11
      IF(SCALE(K).GT.XMAX) GOTO 39
      X=SCALE(K)*XZZ
      LS=NINT(X)
38    GRAPH(LS,1)=LSYMB(K)
39    CONTINUE
      WRITE(6,91)
      DO 36 J=1,50
      JJ=51-J
36    WRITE(6,92) (GRAPH(I,JJ),I=1,100)
669   RETURN
91    FORMAT( ///////)
92    FORMAT(1H ,100A1)
99    WRITE(6,93) XP(I),YP(I)
93    FORMAT(1H1,43HGRAPH SCALE EXCEEDED - FIRST ILLEGAL VALUES,//,2HX=
     1X,F8.3,/,2HY=,5X,F8.3)
      STOP
      END
```

```
C     SUBROUTINE ANAL    SERVICE ROUTINE FOR DATA INPUT
C     ------------------------------------------------------------
      SUBROUTINE ANAL(IL,K)
      INTEGER E,F,G,H
      INTEGER TMIN,EMIN,EMM1,TBM1,TBCK,DEB,DTG
      REAL LW
      DIMENSION C(50,80),E(260),F(260),G(260),H(260)
      COMMON      A(1024),FMEAN(4),SM2(4),SM3(4),SM4(4),PRIM(4)
     1 ,IHEAD(3),ISENT(20)
      GOTO (1010,2000,3000,4000,5000) IL
CHAPTER 1   SETTING UP
 1010 CONTINUE
      IUNIT=3
C     READ THRU MEDATA LOG HEADER
      READ(5,50) IHEAD
   50 FORMAT(3A4)
      CALL PDPOPEN(3,IHEAD(1))
      IFILE=0
C     SETTING UP CONSTANTS FOR TEST C16
```

APPENDIX G

```
      PI = 3.14159
      ALF=.00265
      TC=21.5
      RWC=10.63
      RWH=16.63
      TWH=(RWH-RWC)/(ALF*RWC)+TC
      RLD=0.46
      LW=0.002
      CNU=RWH/((RLD+50.+RWH)**2*PI*LW)
      DIA=5.0E-06
C
C  SETTING UP OF CALIBRATION ARRAY
C  NOTE ORDER OF THE PARAMETERS OF ARRAY C(TEMPERATURE,BRIDGE VOLTAGE)
C  NOTE  TBCK, EB, TG,  AND ASSOCIATED VARIABLES ARE INTEGERS AND ARE
C  SCALED BY A FACTOR OF 100
C
      TBCK=2500
      TMIN=TBCK
      EMIN=225
      DEB=1
      DTG=100
C
      EMM1=EMIN-DEB
      TBM1=TMIN-DTG
      Y=FLOAT(TMIN-DTG)/100.
      XMIN,X=FLOAT(EMIN-DEB)/100.
      DY=FLOAT(DTG)/100.
      DX=FLOAT(DEB)/100.
      DO 80 I=1,50
      Y=Y+DY
      X=XMIN
      DO 80 J=1,80
      X=X+DX
      TFLM=(Y+TWH)*0.5
      FKW=0.02414*(1.+0.003124*TFLM)
      VK= 1.328E-05 + 8.244E-08*TFLM + 1.240E-10*TFLM*TFLM
C     NUSSULT NO IS WEIGHTED
      FNU=CNU*X*X/(FKW*(TWH-Y))*((TFLM+273.)/(Y+273.))**(-0.17)
C     CALIBRATION      MARCH 72
      RE=-.9672 + 4.9757*FNU - 9.1570*FNU*FNU + 6.2127*FNU*FNU*FNU
      C(I,J)=VK/DIA*RE
   80 CONTINUE
 1000 FORMAT(1H0,10I8)
 1001 FORMAT(1H0)
      WRITE(6,1001)
      WRITE(6,1002) TWH
 1002 FORMAT(22H0 WIRE TEMPERATURE  =     ,F10.2)
C END OF SET UP ROUTINE
      RETURN
C
C INPUT A NEW FILE
C
 2000 CONTINUE
  110 CONTINUE
C NTOT IS THE NO OF POINTS FROM ONE CHANNEL
C NSAM IS THE NO OF POINTS SAMPLED BY ONE CHANNEL
C NI IS A PROGRAM CHECK ON NO OF PTS FROM 1 CHANNEL
      NSAM=255
C INITIALIZE THE STORAGE SUMS AND COUNTERS
      NI=0
      K50,J70=0
      J0,K0=0
      IPAR=0
      IBLC=0
C
C     READ SENTENEL INFORMATION
      CALL PDPSENT(3,ISENT(1))
      RETURN
C
 3000 CONTINUE
  150 CALL PDPSKIP(3)
      K=-10
```

```
  160 RETURN
C
CHAPTER 2 INPUT DATA
 4000 CONTINUE
  200 K=0
  204 FORMAT(1H1)
  208 FORMAT(1H ,4H K =,I4)
      CALL PDPREAD(3,4,E(1),F(1),G(1),H(1),K)
C CHECK FOR EOF
      IF(K) 290,285,210
  210 CONTINUE
C  INCREMENT BLOC COUNTER
      IBLC=IBLC+1
      DO 280 I=1,255
      IMT=I*4-3
C INCREMENT THE SAMPLE COUNTER
      NI=NI+1
C SCALING....LINEARIZING....
      TURB = 5*FLOAT(E(I)) + TBCK
      TAMB = 5*FLOAT(F(I)) + TBCK
      EBRD= 199. + .3265*FLOAT(G(I))
C     OVER AND UNDER FLOW CATCHMENT
      L=(TURB-TBCK)/100
      J=EBRD-EMM1
      L=MAX0(1,L)
      L=MIN0(50,L)
      J=MAX0(1,J)
      J=MIN0(70,J)
      A(IMT+2)=C(L,J)

      GOTO 270

C     AUXILLARY CALIBRATION MARCH 72
      X=199. + .3265*FLOAT(G(I))
      X=X*0.01
      Y=TURB*0.01
      TFLM=(Y+TWH)*0.5
      FKW=0.02414*(1.+0.003124*TFLM)
      VK= 1.328E-05 + 8.244E-08*TFLM + 1.240E-10*TFLM*TFLM
C     NUSSULT NO IS WEIGHTED
      FNU=CNU*X*X/(FKW*(TWH-Y))*((TFLM+273.)/(Y+273.))**(-0.17)
C     CALIBRATION      MARCH 72
      RE=-.9672 + 4.9757*FNU - 9.1570*FNU*FNU + 6.2127*FNU*FNU*FNU
      A(IMT+2)=VK/DIA*RE

  270 CONTINUE
      A(IMT) = TURB * 0.01
      A(IMT+1)=TAMB
  280 CONTINUE
C END OF DATA INPUT CALCULATIONS
C
  310 CONTIN UE
C RETURN TO MAIN PROGRAM
  300 RETURN
C     DEFAULT ROUTINES
  285 CONTINUE
C     OMIT THE BACK SPACING PRESENTLY
      GOTO 287
      CALL PDPBACKSP(IUNIT)
C     TRY TO READ THE FAULTY BLOCK ONCE AGAIN   (TOTAL OF 24 X )
      CALL PDPREAD(3,4,E(1),F(1),G(1),H(1),K)
      IF(K) 290,286,210
  287 CONTINUE
  286 IPAR=IPAR+1
      WRITE(6,288) IBLC
  288 FORMAT(22H PARITY ERROR  BLOCK    ,I4,7HOMITTED )
      IF(IPAR-10) 200,200,292
C     CHECK FOR T.M.
  290 IF(K+10) 400,400,292
  292 WRITE(6,295) K,IBLC,IPAR
  295 FORMAT(1H0,5H K = ,I6,5X,6H IBLC ,I6,5X,7H IPAR =,I6,///)
      STOP
  400 CONTINUE
      RETURN
 5000 CONTINUE
```

```
CALL PDPCLOSE(3)
RETURN
END
```

APPENDIX H

SECONDARY DATA PROCESSING PROGRAM FREQ

Program FREQ was designed to calculate the spectral and co-spectral distributions of time data sequences. The following general aspects of this program should be noted:

1. A short segment, modified periodogram method was employed (see section 3.5.3.2).
2. Two real data sequences were transformed simultaneously to yield both the spectral and co-spectral density distributions with one data processing. Using two real time series also provided for an efficient use of the Fast Fourier Transform package.
3. A parabolic data window was applied to the time series (see Appendix C).
4. Rectangular smoothing was also employed (see section 3.5.3.2).
5. The data were printed in numerical and in graphic form on a line printer.

The structure of the program is similar to that of program EXAM (Appendix G) in that all the basic data preparations are contained in one subroutine but a majority of the calculations are performed in the main program. A standard IBM library routine for the Fast Fourier Transform was incorporated into this program. Further details of the method may be obtained from the following flow charts and program listings.

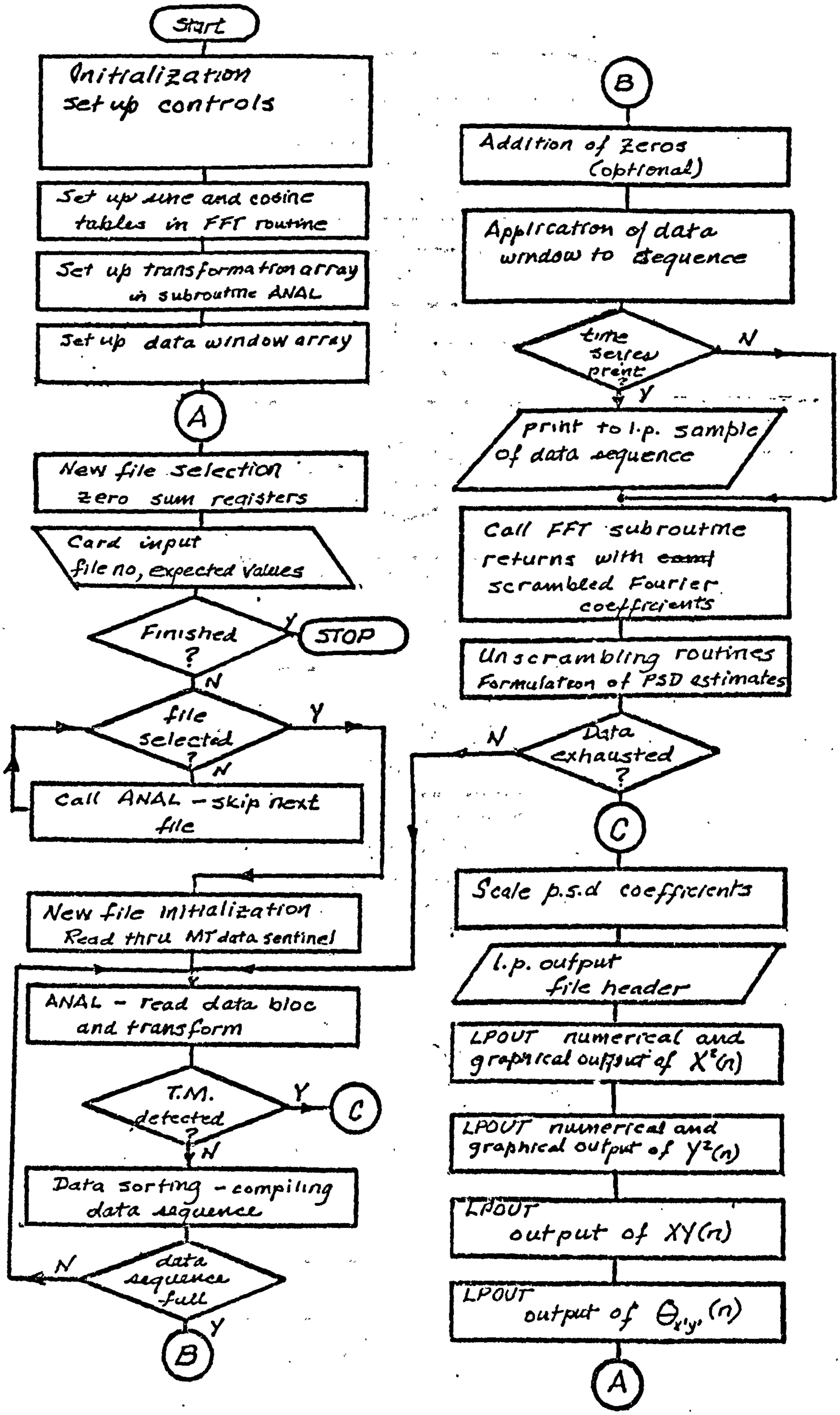

Program FREQ

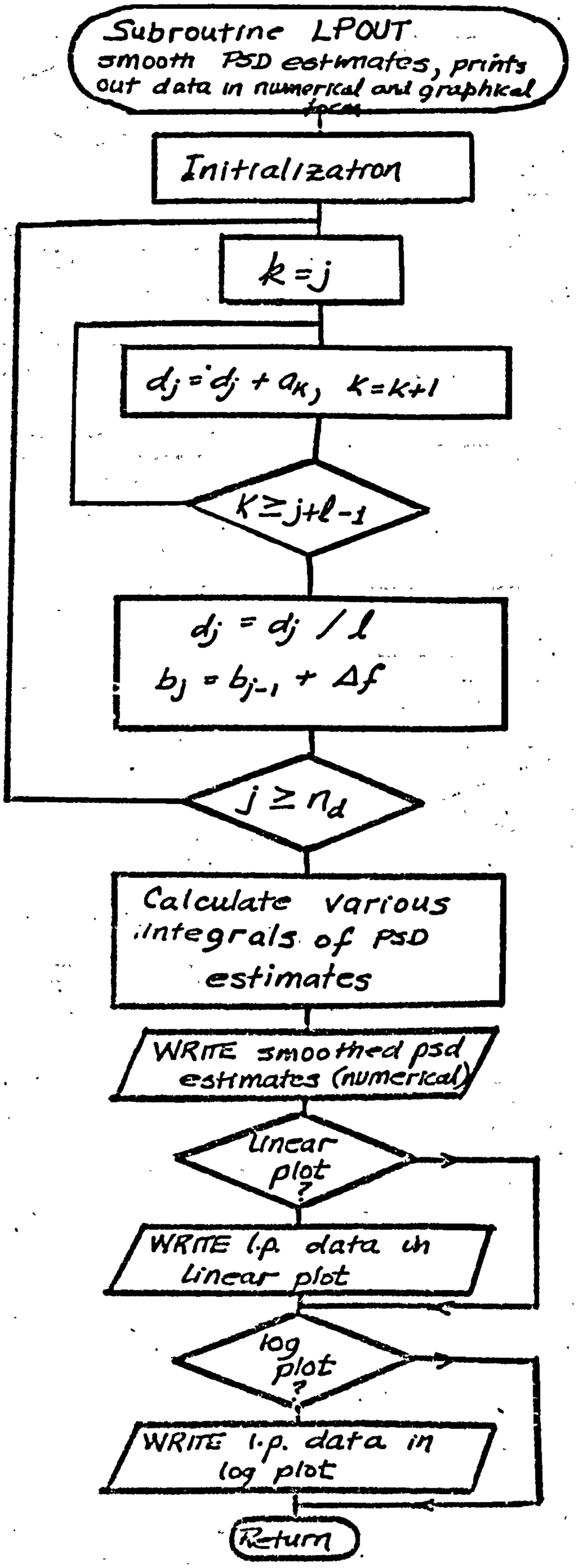

Subroutine LPOUT

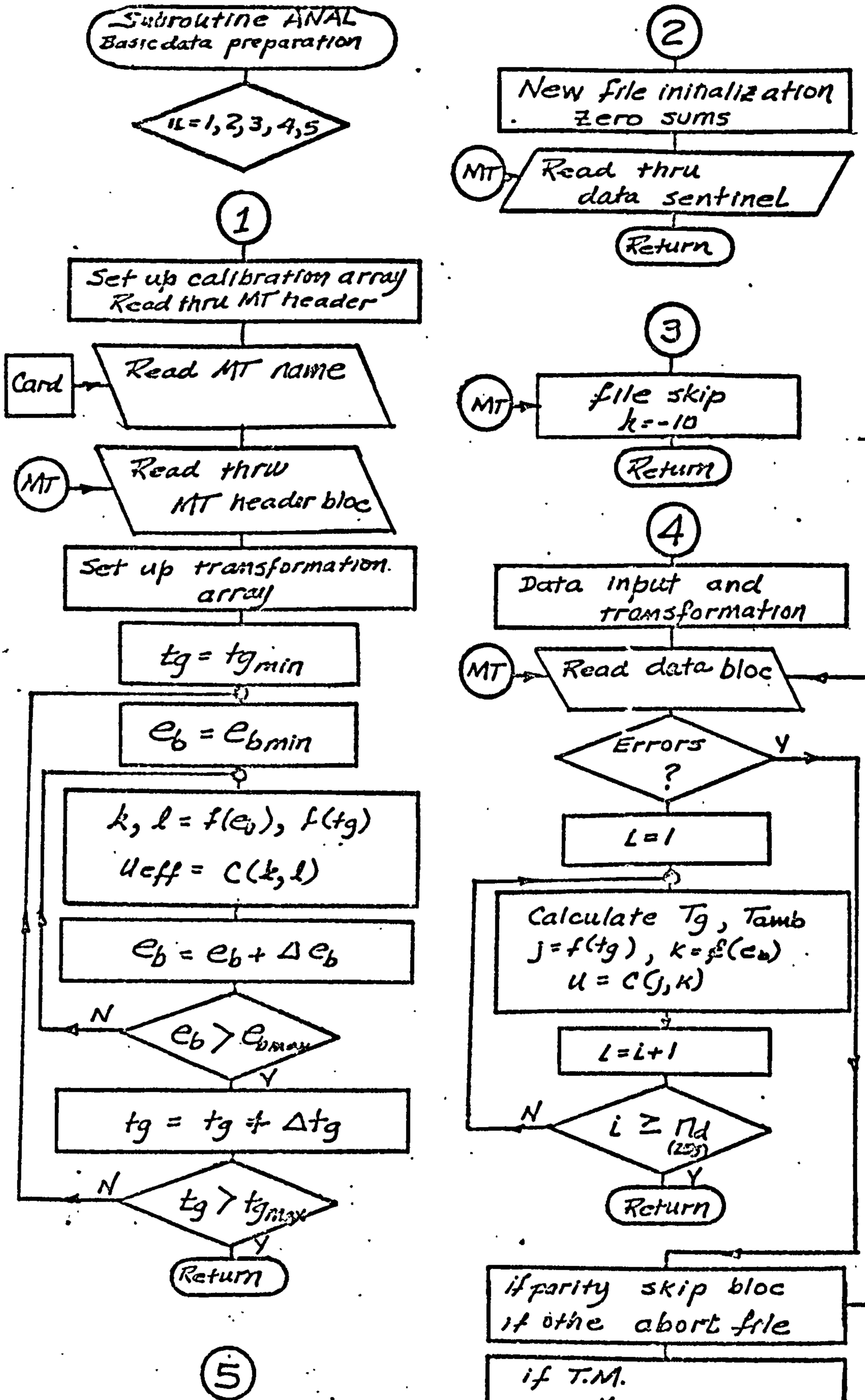

Subroutine ANAL

APPENDIX H

```
      MASTER FOUR
C     PROGRAM TO COMPUTE THE AUTO AND CO-POWER SPECTRAL DISTRIBUTIONS
C          STREAMWISE VELOCITY AND TEMPERATURE DATA
C     ----------FFT SPECTRAL ANALYSES  R.R. SMITH QMC 1972----------

      INTEGER BSAM,CHNA,CHNB
      REAL MEANA,MEANB
      DIMENSION W(1024)
      DIMENSION XP(512),YP(512),XYP(512),XYQ(512)
      COMMON /HRM/A(2510),INV(256),S(256),M(3)
      COMMON /PLT/B(1025),D(1025),MEANA,MEANB
      COMMON /ANL/IHEAD(3),ISENT(20)
C CHNA SELECTS A CHANNEL FOR FREQUENCY ANALYSIS   MEANA IS MEAN OF CHANN
C CHNB SELECTS A SECOND CHANNEL FOR FREQUENCY ANALYSIS
C SRATE IS RATE OF SAMPLING  (SAMPLES/SEC)
C SPRD IS THE SAMPLE PERIOD  (SEC)
C NSAM IS NO OF DATA SAMPLES OF ONE CHANNEL IN ONE BLOC
C BSAM IS NO OF DATA SAMPLES IN ONE BLOC
C NTOT IS NO OF DATA POINTS OF ONE CHANNEL IN FOURIER ANALYSIS
C NFOUR IS TOTAL NO OF POINTS USED BY THE COMPLEX FOURIER ANALYSIS
C 2**M(1) IS TOTAL NO OF POINTS IN ONE SERIES
      CHNA=0
      CHNB=2
      MEANA=0.
      MEANB=0.
      NSAM=255
      BSAM=NSAM*4
      NR=128
      M(1)=10
      M(2)=0
      M(3)=0
      NFOUR=2**(M(1)+1)
      NF21=NFOUR/2-1
      NFD2=NFOUR/2
      NFD4=NFOUR/4
      NTOT=NSAM*(NFD2/NSAM)
      NT2=NTOT*2-2
      SRATE=100.
      SPRD=NTOT/SRATE
      DT=1./SRATE
      DF=1./(DT*FLOAT(NFD2))
CCCCC
CCCCC
      SET UP ROUTINES
      SET UP SINE AND COSINE ARRAYS IN HARM
      CALL HARM(0.,IFERR)
CC
CC     SET UP CALIBRATION MATRIX  IN  SUBROUTINE ANAL
C     CALLS FOR MT NAME FROM CARD INPUT
      CALL ANAL(1,K)
C
CCC   SET UP WINDOW (TEMPORAL)  COEFFICIENTS
C     PARABULIC WINDOW IS USED
      FNTD2=FLOAT(NTOT/2)
      DO 65 J=1,NTOT
      FWX=ABS(FLOAT(J)-FNTD2)/FNTD2
      W(J)=1.-FWX*FWX
   65 CONTINUE
      UWD2=0.53333
C     OUTPUT TO LP   SAMPLE OF WINDOW ARRAY
      WRITE(6,60) (W(I),I=1,512,4)
   60 FORMAT(1H ,1P8E10.1)
C     SET UP FINISHED
CCC
CCC
CCC
C SELECTION OF NEW FILE TO BE EXAMINED
      IFILE=0
  100 CONTINUE
      IR=0
C     ZERO POWER COEFFICINET STORE BEFORE ENTERING DATA LOOP
      DO 105 I=1,NFD4
```

APPENDIX H

```
  105 XP(I),YP(I),XYP(I),XYQ(I)=0.
      IBLC=0
C     CALLS FOR IFILE NO AND MEANS  FROM CARD INPUT
      READ(5,110) KFILE,(D(I),I=1,4)
  110 FORMAT(I10,4F0.0)
C
C     CHECK FOR PROGRAM TERMINATOR     -   NEGATIVE KFILE
      IF(KFILE) 999,115,115
C
  115 MEANA=D(CHNA+1)
      MEANB=D(CHNB+1)
  140 IF(IFILE-KFILE) 150,200,200
C     SEARCHES DATA MT FOR TM
  150 CALL ANAL(3,K)
  155 IFILE=IFILE+1
      GOTO 140
C END OF FILE SELECTION LOOP
CCC
CCC
C     BEGINNING OF FILE ANALYSIS
  200 CONTINUE
      IBLC=0
C WRITE NEW PAGE
      WRITE(6,502)
C     READ THROUGH SENTENIEL HEADER
      CALL ANAL(2,K)
      WRITE(6,2010) ISENT
 2010 FORMAT(20A4,///)
C J1 IS A POINTER TO THE LAST FILLED ARRAY POSITION
CC LOAD CHANNEL A INTO THE REAL PART OF ARRAY A
C LOAD CHANNEL B INTO THE IMAGINARY PART OF ARRAY A
      TIME=0.
C
C     BEGINNING OF NEW RECORD INPUT
  201 CONTINUE
      J1=0
C     BEGINNING OF DATA INPUT FROM MT
C     INPUT ONE DATA BLOC FROM MT  INTO ARRAY D
  203 CONTINUE
      CALL ANAL(4,K)
C     DETECTION OF TAPE MARK (END OF FILE)
      IF(K+10) 202,204,202
C     DATA SORTING ROUTINE
  202 DO 21 I=1,BSAM,4
      J=(I+1)/2+J1
      A(J)=D(I+CHNA)-MEANA
      A(J+1)=D(I+CHNB)-MEANB
   21 CONTINUE
      IBLC=IBLC+1
      J1=J+1
      IF(J-NT2) 203,203,208
C     END OF DATA SORTING
CC
CCC
C     TAPE MARK HAS BEEN DETECTED     TERMINATE DATA INPUT
  204 WRITE(6,205) J,NTOT,NBLC,IBLC,IR
  205 FORMAT(1H0,20H DATA OVERFLOW    J =,  16,7H NTOT =,16,7H NBLC =,16
     1  7H IBLC =,16  ,7H  IR = ,14 ///)
      NR=IR
      GOTO 241
C
C     END OF DATA INPUT TO RECORD
  208 CONTINUE
      IR=IR+1
C     ADD ZEROES TO PREVENT WRAP AROUND
      DO 210 I=J1+1,NFOUR
  210 A(I)=0.
C     WEIGHT WITH A TEMPORAL WINDOW
      DO 310 I=1,NTOT
      J=2*I-1
      A(J)=A(J)*W(I)
  310 A(J+1)=A(J+1)*W(I)
C
CC
```

APPENDIX H

```
      IF(IR.GT.1) GOTO 214
C     SAMPLE OF DATA TIMES SERIES TO LP
      WRITE(6,2000) (A(I),I=1,200 ,2)
      WRITE(6,2001)
      WRITE(6,2000) (A(I),I=2,200 ,2)
 2000 FORMAT(1P10E12.3)
 2001 FORMAT(//////)
  214 CONTINUE
C     TRANSFORM ONE DATA RECORD      HARM RETURNS COMPLEX FOUR COEFF IN
      CALL MTIME(ITIME)
      CALL HARM(-2,IFERR)
      CALL MTIME(I)
      TIME=FLOAT(I-ITIME)*1.0E-3+TIME
C UNSCRAMBLING ARRAY A INTO TWO SERIES
CC C NOTE THAT ONLY ONE HALF OF THE ARRAY IS UNSCRAMBLED     THE HIGHER
C FREQUENCIES ARE FOLDED BACK AROUND THE NYQUIST FREQUENCY
      XP(1)=A(1)*A(1)+XP(1)
      YP(1)=A(2)*A(2)+YP(1)
      XYP(1)=A(1)*A(2)+XYP(1)
      DO 230 J=3,NFD2,2
      J2=(J+1)/2
      NJ=NFOUR-J+2
      AJ=A(J)
      XR=A(J)+A(NJ)
      XI=A(J+1)-A(NJ+1)
      YR=A(J)  -  A(NJ)
      YI=A(J+1)  +  A(NJ+1)
      XP(J2)=XR*XR  +  XI*XI  +  XP(J2)
      YP(J2)=YR*YR  +  YI*YI  +  YP(J2)
      XYP(J2)=XR*YR  +  XI*YI  +  XYP(J2)
      XYQ(J2)=XR*YI  -  XI*YR  +  XYQ(J2)
  230 CONTINUE
      IF(IR-NR) 201,240,240
C     END OF DATA INPUT FOR ONE FILE ANALYSIS
CC
CC
CC
C     THE SPECTRAL POWER COEFF ARE SCALED
  240 CONTINUE
C     POSITION TAPE HEAD TO THE NEXT DATA SENTIEL
      CALL ANAL(3,K)
  241 CONTINUE
      FIR=FLOAT(IR)
      FND2=FLOAT(NFD2)
      FNTOT=FLOAT(NTOT)
C     X  IS FFT SCALING FACTOR AND UNSCRAMBLING FACTOR 0.25
      X=(FND2*FND2)/(FNTOT*UUD2 *4.) *DT
C     ADDITIONAL SCALING FACTOR
      X = X*2.
C
      FXR=X/FIR
      DO 250  I=1,NFD4
      XP(I)=XP(I)*FXR
      YP(I)=YP(I)*FXR
      XYP(I)=XYP(I)*FXR
      XYQ(I)=XYQ(I)*FXR
  250 CONTINUE
C     CORRECT FOR UNSCRAMBLING FACTOR OF 0.25 ON FIRST ELEMENTS
      XP(1)=XP(1)*4.
      YP(1)=YP(1)*4.
      XYP(1)=XYP(1)*4.
      XYQ(1)=XYQ(1)*4.
CCCCCCCC
CCCCC OUTPUT TO LP
CCCCC     NO IS THE NUMBER OF TIME DATA POINTS CONSIDERED
CCCCC      PERD IS THE TIME OF DATA SAMPLE
      NO=IBLC*NSAM
      PERD=FLOAT(NO)/SRATE
      WRITE(6,215) IFILE
      WRITE(6,220) CHNA,CHNB
```

APPENDIX H

```
      WRITE(6,222) SRATE
      WRITE(6,224) NO
      WRITE(6,226) PERD
      WRITE (6,23) TIME,IFERR
      WRITE(6,228) MEANA,MEANB
  215 FORMAT(1H1,//7H FILE  ,I3)
  220 FORMAT(1H ,  /36H FAST FOURIER ANALYSIS OF CHANNEL   ,I1,
     1 14H AND CHANNEL  ,I1 //)
  222 FORMAT(1H0,30H SAMPLING RATE  (SAM/SEC)  =      ,F7.2)
  224 FORMAT(1H0,30H NO OF SAMPLES/CHANNEL  =        ,I6)
  226 FORMAT(1H0,30H SAMPLE PERIOD (SEC)  =          ,F8.2)
   23 FORMAT (  ///,41H TIME FOR FOURIER TRANSFORM CALCULATION =  ,F8.2,5
     1H SEC.//,7H IFERR=  ,I2)
  228 FORMAT(1H ,///,21H MEAN OF CHANNEL A =  ,F8.3,21H MEAN OF CHANNEL B
     1=          ,F8.3,///)
 2050 FORMAT(1H0,1016)
   50 FORMAT(  1P5E14.3)
  500 FORMAT(1H  ,F7.2,2X,1P10E11.3)
  501 FORMAT(1H0,9X,10F11.3)
  502 FORMAT(1H1)
  351 FORMAT(1H  ,1P10E12.3,/)
C     KSF IS NO OF SMOOTHED SPECTRAL ESTIMATORS
C     LREC IS NO OF RAW ESTIMATORS TO ONE SMOOTHED ESTIMATOR
      KSF=NFD4/128
      KSF=NFD4/256
C     LREC = 1    MEANS NO LINEAR   SMOOTHING
      LREC=1
      LREC=3
      DFLP=DF*FLOAT(KSF)
C
C     WRITE POWER SPECTRUM OF CHANNEL A    (REFERRED TO AS X ALSO )
      WRITE(6,560)
  560 FORMAT(1H1,///,40H  POWER SPECTRUM OF CHANNEL A          ///)
      WRITE(6,565) XP(1)
C
CC
C     WRITE POWER SPECTRUM OF CHANNEL B    ( REFERRED TO AS Y   )
      WRITE(6,570)
  570 FORMAT(1H1,//40H  POWER SPECTRUM OF CHANNEL B          ///)
      WRITE(6,565) YP(1)
      CALL LPOUT(YP,KSF,LREC,DFLP,NFD4,3)
C
CCC
C     WRITE CROSS SPECTRM OF CHANNEL A AND CHANNEL B
C     USE ARRAYS XP,YP FOR TEMPORARY STORAGE
      DO 575 I=1,NFD4
      XP(I)=XYP(I)*XYP(I) + XYQ(I)*XYQ(I)
      YP(I)=ATAN(XYQ(I)/(XYP(I)+1.0E-10))*57.1 + 90.
  575 CONTINUE
      WRITE(6,590)
  590 FORMAT(1H1,//40H  CROSS SPECTRUM OF CHANNELS A AND B     ///)
      WRITE(6,595) XYP(1)
  595 FORMAT(1H0,10H  MEAN SQ     ,1F7.4,///)
      CALL LPOUT(XP,KSF,LREC,DFLP,NFD4,3)
      WRITE(6,502)
      WRITE(6,2001)
      CALL LPOUT(YP,KSF,LREC,DFLP,NFD4,-1)
  597 FORMAT(1H  ,10F11.3)
C
C     RETURN TO ANALYSE A NEW DATA RECORD
      IFILE=IFILE+1
      GOTO 100
C
  999 STOP
      END



      SUBROUTINE LPOUT(G,K,L,DF,ND,NP)
C     SUBROUTINE LPOUT  - GENERAL PURPOSE LP OUTPUT ROUTINE
C                   FOR   PSD DISTRIBUTIONS
C     ----------------------R.R. SMITH QMC  1972----------------------
```

APPENDIX H

```
      DIMENSION G(1)
      COMMON /PLT/B(1025),D(1025),EXA,EXB
      COMMON /HRM/A(2510),INV(256),S(256),M(3)
      CALL FMOVE(G(1),A(1),512)
      LD2=L/2
      JSTAR=LD2+2
      BM1=DF*(FLOAT(JSTAR)/FLOAT(K)-1.)
      FL=FLOAT(L)
      NLP=0
      DN0=0.
      DN2=0.
C     RECTANGULAR SMOOTHING  AND CALCULATION OF FREQUENCY INCREMENTS
      DO 100   J=JSTAR,ND,K
      NLP=NLP+1
      D(NLP)=0.
      DO 125   JI=J-LD2,J-LD2+L-1
  125 D(NLP)=D(NLP)+A(JI)
      D(NLP)=D(NLP)/FL
      B(NLP)=BM1*DF
      BM1=B(NLP)
      DN0=DN0 + D(NLP) + D(NLP)
      X=B(NLP)*B(NLP)*D(NLP)
      DN2=DN2 + X + X
  100 CONTINUE
      DN0=(DN0 - D(1) -D(NLP))*0.5*DF
      DN2=(DN2-D(1)*B(1)*B(1)-D(NLP)*B(NLP)*B(NLP))*0.5*DF
      WRITE(6,250) DN0,DN2
  250 FORMAT(22HD SUM VALUE   E(N) =          ,1PE7.3   //
     1   21H SUM VALUE N*N*E(N) =    1PE7.3   //)
      IF(NP.EQ.-1) GOTO 290
      DO 280 I=1,NLP
  280 D(I)=D(I)/(DN0+1.0E-30)
  290 CONTINUE
      NP=IABS(NP)
      DO 200 J=1,NLP,10
      WRITE(6,300) (B(I),I=J,J+9)
      WRITE(6,310) (D(I),I=J,J+9)
  200 CONTINUE
  300 FORMAT(1HO,5X,10F11.3)
  310 FORMAT(1H ,5X,10E11.3)
C     OUTPUT TO LINEPRINTER GRAPH PLOTTER
C     IF NP = 1 PLOT GIVES LINEAR ORDINATE    NP = 2  LOG ORDINATE
      IF(NP.EQ.1.OR.NP.EQ.3) CALL PLOT(NLP,1)
      IF(NP.EQ.2.OR.NP.EQ.3) CALL PLOT(NLP,2)
      RETURN
      END



      SUBROUTINE PLOT(NB,IP)
C     SUBROUTINE USED FROM LPOUT FOR LP GRAPHICAL OUTPUT
C     ------------------------R.R. SMITH QMC  1972----------------------

      REAL XMAX,YMAX
      REAL SCALE(12)
      INTEGER LSYMB(12)
      INTEGER NB,GRAPH(100,50),L,   P,BLK,DOT,MM
      COMMON /PLT/B(1025),D(1025)
      COMMON /HRM/A(2510),INV(256),S(256),M(3)
      EQUIVALENCE (GRAPH(1,1),A(1))
      DATA BLK/1H /,DOT/1H./,P/1H*/
      DATA SCALE / 1.,2.,3.,4.,6.,8.,10.,20.,30.,40.,50.,60.,  /
      DATA LSYMB /1H1,1H2,1H3,1H4,1H6,1H8,1H1,1H2,1H3,1H4,1H5,1H6  /
      AB=FLOAT(NB)
      YSPA = 100.
      IYSPA = 100
      XSPA = 50.
      IXSPA = 50
   20 XMAX,YMAX=0.0
      DO 24 I=1,NB
      IF(XMAX-B(I)) 21,22,22
   21 XMAX=B(I)
   22 IF(YMAX-D(I)) 23,23,24
```

APPENDIX H

```
   23 YMAX=D(I)
24    CONTINUE
      IF(XMAX.LT.50.) XMAX=50.
      XMIN=0.1
      XMIN=0.3
       XMIN=0.2
      ALMN=ALOG10(XMIN)
      XZZ=100./(ALOG10(XMAX)-ALMN)
      YZZ=50./YMAX
      IF(IP-1) 30,30,205
  205 CONTINUE
      IRPT=0
      IEXP=0
      YM=YMAX
      IF(YM-1.0) 210,230,220
C     YM IS LESS THAN ONE
  210 IF(YM-0.1) 211,230,230
  211 IEXP=IEXP-1
      IRPT=IRPT+1
      YM=YM*10.
      IF(IRPT-10)210,230,230
C     YM IS GREATER THAN ONE
  220 IEXP=IEXP+1
      YM=YM*0.1
      IF(IRPT-10) 225,230,230
  225 IF(YM-1.) 230,230,220
  230 CONTINUE
      ORDER=5.
      ALYN=FLOAT(IEXP)-ORDER
      YZZ=50./ORDER

      YZZ = YSPA/ORDER
      XZZ=XSPA/(ALOG10(XMAX)-ALMN)

   30 DO 32 I=1,100
      DO 31 J=1,50
      GRAPH(I,J)=BLK
      GRAPH(1,J),GRAPH(100,J)=DOT
      GRAPH(I,1),GRAPH(I,50)=DOT
   31 CONTINUE
32    CONTINUE
      DO 34 I=1,NB
      IF(B(I)-XMIN) 26,27,27
   26 B(I)=XMIN
   27 CONTINUE
      AL=(ALOG10(B(I))-ALMN)*XZZ
      IF(IP-1) 260,260,270
  260 AM=D(I)*YZZ
       L=NINT(AL)
      MM=NINT(AM)
      GOTO 280
  270 IF(D(I)-1.0E-10) 274,274,276
  274 D(I)=1.0E-10
  276 AM=(ALOG10(D(I))-ALYN)*YZZ

      MM=NINT(AL)
      L=NINT(AM)
      L=MAX0(L,1)
      L=MIN0(100,L)
      L=101-L

  280 CONTINUE
      IF(L)61,61,62
61    L=1
   62 CONTINUE
      IF(MM) 63,63,64
   63 MM=1
64    CONTINUE
      IF(MM.GT.50) MM=50
      IF(L-100) 33,33,99
   33 IF(MM-50) 34,34,99
   34 GRAPH(L,MM)=P
35    CONTINUE
      DO 38 K=1,12
      IF(SCALE(K).GT.XMAX) GOTO 39
```

APPENDIX H

```
      X=(ALOG10(SCALE(K))-ALMN)*XZZ
      LS=NINT(X)
      IF(IP.EQ.1) GRAPH(LS,1)=LSYMB(K)
      IF(IP.EQ.2) GRAPH(100,LS) = LSYMB(K)
   38 CONTINUE
   39 CONTINUE
      WRITE(6,91)XMAX,YMAX
      DO 36 J=1,50
      JJ=51-J
   36 WRITE(6,92) (GRAPH(I,JJ),I=1,100)
  669 RETURN
   91 FORMAT(1H1,22H GRAPH PLOTTED BETWEEN,//8H XMAX = ,F7.3/8H YMAX =
     1F7.3,/)
   92 FORMAT(1H ,100A1)
   99 WRITE(6,93) D(1),D(1+500)
   93 FORMAT(1H1,43HGRAPH SCALE EXCEEDED - FIRST ILLEGAL VALUES,//2HX=,
     1X,F8.3,/,2HY=,5X,F8.3)
      RETURN
      END



      SUBROUTINE HARM(IFSET,IFERR)
C     ..................................................................
C
C        SUBROUTINE HARM
C
C        PURPOSE
C           PERFORMS DISCRETE COMPLEX FOURIER TRANSFORMS ON A COMPLEX
C           THREE DIMENSIONAL ARRAY
C
C        USAGE
C           CALL HARM (A,M,INV,S,IFSET,IFERR)
C
C        DESCRIPTION OF PARAMETERS
C           A     - AS INPUT, A CONTAINS THE COMPLEX, 3-DIMENSIONAL
C                   ARRAY TO BE TRANSFORMED.  THE REAL PART OF
C                   A(I1,I2,I3) IS STORED IN VECTOR FASHION IN A CELL
C                   WITH INDEX 2*(I3*N1*N2 + I2*N1 + I1) + 1 WHERE
C                   NI = 2**M(I), I=1,2,3 AND I1 = 0,1,...,N1-1 ETC.
C                   THE IMAGINARY PART IS IN THE CELL IMMEDIATELY
C                   FOLLOWING.  NOTE THAT THE SUBSCRIPT I1 INCREASES
C                   MOST RAPIDLY AND I3 INCREASES LEAST RAPIDLY.
C                   AS OUTPUT, A CONTAINS THE COMPLEX FOURIER
C                   TRANSFORM.  THE NUMBER OF CORE LOCATIONS OF
C                   ARRAY A IS 2*(N1*N2*N3)
C           M     - A THREE CELL VECTOR WHICH DETERMINES THE SIZES
C                   OF THE 3 DIMENSIONS OF THE ARRAY A.  THE SIZE,
C                   NI, OF THE I DIMENSION OF A IS 2**M(I), I = 1,2,3
C           INV   - A VECTOR WORK AREA FOR BIT AND INDEX MANIPULATION
C                   OF DIMENSION ONE EIGHTH THE NUMBER OF CORE
C                   LOCATIONS OF A, VIZ., (1/8)*2*N1*N2*N3
C           S     - A VECTOR WORK AREA FOR SINE TABLES WITH DIMENSION
C                   THE SAME AS INV
C           IFSET - AN OPTION PARAMETER WITH THE FOLLOWING SETTINGS
C                     0     SET UP SINE AND INV TABLES ONLY
C                     1     SET UP SINE AND INV TABLES ONLY AND
C                           CALCULATE FOURIER TRANSFORM
C                    -1     SET UP SINE AND INV TABLES ONLY AND
C                           CALCULATE INVERSE FOURIER TRANSFORM (FOR
C                           THE MEANING OF INVERSE SEE THE EQUATIONS
C                           UNDER METHOD BELOW)
C                     2     CALCULATE FOURIER TRANSFORM ONLY (ASSUME
C                           SINE AND INV TABLES EXIST)
C                    -2     CALCULATE INVERSE FOURIER TRANSFORM ONLY
C                           (ASSUME SINE AND INV TABLES EXIST)
C           IFERR - ERROR INDICATOR.  WHEN IFSET IS 0,+1,-1,
C                   IFERR = 1 MEANS THE MAXIMUM M(I) IS LESS THAN 3
C                   OR GREATER THAN 20, I=1,2,3  WHEN IFSET IS
C                   +2,-2, IFERR = 1 MEANS THAT THE SINE AND INV
C                   TABLES ARE NOT LARGE ENOUGH OR HAVE NOT BEEN
C                   COMPUTED.  IF ON RETURN IFERR =0 THEN NONE OF
```

```
C
C                    THE ABOVE CONDITIONS ARE PRESENT
C
C  REMARKS
C     THIS SUBROUTINE IS TO BE USED FOR COMPLEX, 3-DIMENSIONAL
C     ARRAYS IN WHICH EACH DIMENSION IS A POWER OF 2.  THE
C     MAXIMUM M(I) MUST NOT BE LESS THAN 3 OR GREATER THAN 20,
C     I = 1,2,3
C
C  SUBROUTINES AND FUNCTION SUBPROGRAMS REQUIRED
C     NONE
C
C  METHOD
C     FOR IFSET = +1, OR +2, THE FOURIER TRANSFORM OF COMPLEX
C     ARRAY A IS OBTAINED,
C
C                  N1-1   N2-1   N3-1                          L1    L2    L3
C  X(J1,J2,J3)=SUM      SUM     SUM     A(K1,K2,K3)*W1   *W2   *W3
C                  K1=0   K2=0   K3=0
C
C            WHERE WI IS THE N(I) ROOT OF UNITY AND L1=K1*J1,
C                  L2=K2*J2, L3=K3*J3
C
C     FOR IFSET = -1, OR -2, THE INVERSE FOURIER TRANSFORM A OF
C     COMPLEX ARRAY X IS OBTAINED,
C
C  A(K1,K2,K3)=
C           1        N1-1   N2-1   N3-1                          -L1   -L2   -L3
C     -------- *SUM      SUM     SUM     X(K1,K2,K3)*W1   *W2   *W3
C     N1*N2*N3   J1=0   J2=0   J3=0
C
C     SEE J.W. COOLEY AND J.W. TUKEY, AN ALGORITHM FOR THE
C     MACHINE CALCULATION OF COMPLEX FOURIER SERIES,
C     MATHEMATICS OF COMPUTATIONS, VOL. 19 (APR. 1965), P. 297.
C
C.....................................................................
C
      SUBROUTINE HARM(IFSET,IFERR)
      DIMENSION N(3),NP(3),W(2),W2(2),W3(2)
      COMMON /HRM/A(2510),INV(256),S(256),M(3)
      EQUIVALENCE (N1,N(1)),(N2,N(2)),(N3,N(3))
   10 IF( IABS(IFSET) - 1) 900,900,12
   12 MTT=MAX0(M(1),M(2),M(3)) -2
      ROOT2 = SQRT(2.)
      IF (MTT-MT ) 14,14,13
   13 IFERR=1
      RETURN
   14 IFERR=0
      M1=M(1)
      M2=M(2)
      M3=M(3)
      N1=2**M1
      N2=2**M2
      N3=2**M3
   16 IF(IFSET) 18,18,20
   18 NX= N1*N2*N3
      FN = NX
      DO 19 I = 1,NX
      A(2*I-1) = A(2*I-1)/FN
   19 A(2*I) = -A(2*I)/FN
   20 NP(1)=N1*2
      NP(2)= NP(1)*N2
      NP(3)=NP(2)*N3
      DO 250 ID=1,3
      IL1 = IL+1
      IL = NP(3)-NP(ID)
      MI = M(ID)
      IF (MI)250,250,30
   30 IDIF=NP(ID)
      KBIT=NP(ID)
      MEV = 2*(MI/2)
      IF (MI - MEV )60,60,40
C
C     M IS ODD, DO L=1 CASE
```

```
   40 KBIT=KBIT/2
      KL=KBIT-2
      DO 50 I=1,IL1,IDIF
      KLAST=KL+I
      DO 50 K=I,KLAST,2
      KD=K+KBIT
C
CC    DO ONE STEP WITH L=1,J=0
CC    A(K)=A(K)+A(KD)
CC    A(KD)=A(K)-A(KD)
C
      T=A(KD)
      A(KD)=A(K)-T
      A(K)=A(K)+T
      T=A(KD+1)
      A(KD+1)=A(K+1)-T
   50 A(K+1)=A(K+1)+T
      IF (MI - 1)250,250,52
   52 LFIRST =3
C
CC    DEF - JLAST = 2**(L-2) -1
      JLAST=1
      GO TO 70
C
CC    M IS EVEN
   60 LFIRST = 2
      JLAST=0
   70 DO 240 L=LFIRST,MI,2
      JJDIF=KBIT
      KBIT=KBIT/4
      KL=KBIT-2
C
CC    DO FOR J=0
      DO 80 I=1,IL1,IDIF
      KLAST=I+KL
      DO 80 K=I,KLAST,2
      K1=K+KBIT
      K2=K1+KBIT
      K3=K2+KBIT
C
CCC   DO TWO STEPS WITH J=0
CCC   A(K)=A(K)+A(K2)
CCC   A(K2)=A(K)-A(K2)
CCC   A(K1)=A(K1)+A(K3)
CCC   A(K3)=A(K1)-A(K3)
CCC
CCC   A(K)=A(K)+A(K1)
CCC   A(K1)=A(K)-A(K1)
CCC   A(K2)=A(K2)+A(K3)*I
CCC   A(K3)=A(K2)-A(K3)*I
C
      T=A(K2)
      A(K2)=A(K)-T
      A(K)=A(K)+T
      T=A(K2+1)
      A(K2+1)=A(K+1)-T
      A(K+1)=A(K+1)+T
C
      T=A(K3)
      A(K3)=A(K1)-T
      A(K1)=A(K1)+T
      T=A(K3+1)
      A(K3+1)=A(K1+1)-T
      A(K1+1)=A(K1+1)+T
C
      T=A(K1)
      A(K1)=A(K)-T
      A(K)=A(K)+T
      T=A(K1+1)
      A(K1+1)=A(K+1)-T
      A(K+1)=A(K+1)+T
C
      R=-A(K3+1)
      T = A(K3)
      A(K3)=A(K2)-R
```

APPENDIX H

```
      A(K2)=A(K2)+R
      A(K3+1)=A(K2+1)-T
   80 A(K2+1)=A(K2+1)+T
      IF (JLAST) 235,235,82
   82 JJ=JJDIF   +1
C
C     DO FOR J=1
      ILAST= IL +JJ
      DO 85 I = JJ,ILAST,IDIF
      KLAST = KL+I
      DO 85 K=I,KLAST,2
      K1 = K+KBIT
      K2 = K1+KBIT
      K3 = K2+KBIT
C
CCCCC LETTING W=(1+I)/ROOT2,W3=(-1+I)/ROOT2,W2=I,
CCCCC A(K)=A(K)+A(K2)*I
CCCCC A(K2)=A(K)-A(K2)*I
CCCCC A(K1)=A(K1)*W+A(K3)*W3
CCCCC A(K3)=A(K1)*W-A(K3)*W3
CCCCC
CCCCC A(K)=A(K)+A(K1)
CCCCC A(K1)=A(K)-A(K1)
CCCCC A(K2)=A(K2)+A(K3)*I
CCCCC A(K3)=A(K2)-A(K3)*I
CCCCC
      R  =-A(K2+1)
      T  =  A(K2)
      A(K2)  =  A(K)-R
      A(K)   =  A(K)+R
      A(K2+1)=A(K+1)-T
      A(K+1)=A(K+1)+T
C
      AWR=A(K1)-A(K1+1)
      AWI  =  A(K1+1)+A(K1)
      R=-A(K3)-A(K3+1)
      T=A(K3)-A(K3+1)
      A(K3)=(AWR-R)/ROOT2
      A(K3+1)=(AWI-T)/ROOT2
      A(K1)=(AWR+R)/ROOT2
      A(K1+1)=(AWI+T)/ROOT2
      T=  A(K1)
      A(K1)=A(K)-T
      A(K)=A(K)+T
      T=A(K1+1)
      A(K1+1)=A(K+1)-T
      A(K+1)=A(K+1)+T
      T=A(K3)
      R=-A(K3+1)
      A(K3)=A(K2)-R
      A(K2)=A(K2)+R
      A(K3+1)=A(K2+1)-T
   85 A(K2+1)=A(K2+1)+T
      IF(JLAST-1)  235,235,90
   90 JJ=  JJ  +  JJDIF
C
C     NOW DO THE REMAINING JaS
      DO 230 J=2,JLAST
C
C     FETCH WAS
C     DEF- W=W**INV(J), W2=W**2, W3=W**3
   96 I=INV(J+1)
   98 IC=NT-I
      W(1)=S(IC)
      W(2)=S(I)
      I2=2*I
      I2C=NT-I2
      IF(I2C)120,110,100
C
C     2*I  IS  IN  FIRST  QUADRANT
  100 W2(1)=S(I2C)
      W2(2)=S(I2)
      GO  TO  130
  110 W2(1)=0.
      W2(2)=1.
```

```
      GO TO 130
C
CC    2*I  IS  IN  SECOND  QUADRANT
  120 I2CC = I2C+NT
      I2C=-I2C
      W2(1)=-S(I2C)
      W2(2)=S(I2CC)
  130 I3=I+I2
      I3C=NT-I3
      IF(I3C)160,150,140
C
CC    I3  IN  FIRST  QUADRANT
  140 W3(1)=S(I3C)
      W3(2)=S(I3)
      GO TO 200
  150 W3(1)=0.
      W3(2)=1.
      GO TO 200
C
  160 I3CC=I3C+NT
      IF(I3CC)190,180,170
C
CC    I3  IN  SECOND  QUADRANT
  170 I3C=-I3C
      W3(1)=-S(I3C)
      W3(2)=S(I3CC)
      GO TO 200
  180 W3(1)=-1.
      W3(2)=0.
      GO TO 200
C
CC    3*I  IN  THIRD  QUADRANT
  190 I3CCC=NT+I3CC
      I3CC=  -I3CC
      W3(1)=-S(I3CCC)
      W3(2)=-S(I3CC)
  200 ILAST=IL+JJ
      DO  220  I=JJ,ILAST,IDIF
      KLAST=KL+I
      DO  220  K=I,KLAST,2
      K1=K+KBIT
      K2=K1+KBIT
      K3=K2+KBIT
C
CCC   DO  TWO  STEPS  WITH  J  NOT  0
CCC   A(K)=A(K)+A(K2)*W2
CCC   A(K2)=A(K)-A(K2)*W2
CCC   A(K1)=A(K1)*W+A(K3)*W3
CCC   A(K3)=A(K1)*W-A(K3)*W3
CCC
CCC   A(K)=A(K)+A(K1)
CCC   A(K1)=A(K)-A(K1)
CCC   A(K2)=A(K2)+A(K3)*I
CCC   A(K3)=A(K2)-A(K3)*I
C
      R=A(K2)*W2(1)-A(K2+1)*W2(2)
      T=A(K2)*W2(2)+A(K2+1)*W2(1)
      A(K2)=A(K)-R
      A(K)=A(K)+R
      A(K2+1)=A(K+1)-T
      A(K+1)=A(K+1)+T
C
      R=A(K3)*W3(1)-A(K3+1)*W3(2)
      T=A(K3)*W3(2)+A(K3+1)*W3(1)
      AWR=A(K1)*W(1)-A(K1+1)*W(2)
      AWI=A(K1)*W(2)+A(K1+1)*W(1)
      A(K3)=AWR-R
      A(K3+1)=AWI-T
      A(K1)=AWR+R
      A(K1+1)=AWI+T
      T=A(K1)
      A(K1)=A(K)-T
      A(K)=A(K)+T
      T=A(K1+1)
      A(K1+1)=A(K+1)-T
```

APPENDIX H

```
      A(K+1)=A(k+1)+T
      R=-A(K3+1)
      T=A(K3)
      A(K3)=A(K2)-R
      A(K2)=A(K2)+R
      A(K3+1)=A(K2+1)-T
  220 A(K2+1)=A(K2+1)+T
C     END OF I AND K LOOPS
C
  230 JJ=JJDIF+JJ
C     END OF J-LOOP
C
  235 JLAST=4*JLAST+3
  240 CONTINUE
C     END OF  L  LOOP
C
  250 CONTINUE
C     END OF  ID  LOOP
CC
C     WE NOW HAVE THE COMPLEX FOURIER SUMS BUT THEIR ADDRESSES ARE
      NTSQ=NT*NT
C     BIT-REVERSED.  THE FOLLOWING ROUTINE PUTS THEM IN ORDER
      M3MT=M3-MT
  350 IF(M3MT) 370,360,360
C
C     M3 GR. OR EQ. MT
  360 IGO3=1
      N3VNT=N3/NT
      MINN3=NT
      GO TO 380
C     M3 LESS THAN MT
  370 IGO3=2
      N3VNT=1
      NTVN3=NT/N3
      MINN3=N3
  380 JJD3 = NTSQ/N3
      M2MT=M2-MT
  450 IF (M2MT)470,460,460
C
C     M2 GR. OR EQ. MT
  460 IGO2=1
      N2VNT=N2/NT
      MINN2=NT
      GO TO 480
C
C     M2 LESS THAN MT
  470 IGO2 = 2
      N2VNT=1
      NTVN2=NT/N2
      MINN2=N2
  480 JJD2=NTSQ/N2
      M1MT=M1-MT
  550 IF(M1MT)570,560,560
C
C     M1 GR. OR EQ. MT
  560 IGO1=1
      N1VNT=N1/NT
      MINN1=NT
      GO TO 580
C     M1 LESS THAN MT
  570 IGO1=2
      N1VNT=1
      NTVN1=NT/N1
      MINN1=N1
  580 JJD1=NTSQ/N1
  600 JJ3=1
      J=1
      DO 880 JPP3=1,N3VNT
      IPP3=INV(JJ3)
      DO 870 JP3=1,MINN3
      GO TO (610,620),IGO3
  610 IP3=INV(JP3)*N3VNT
      GO TO 630
```

APPENDIX H

```
  620  IP3=INV(JP3)/NTVN3
  630  I3=(IPP3+IP3)*N2
  700  JJ2=1
       DO 870 JPP2=1,N2VNT
       IPP2=INV(JJ2)+I3
       DO 860 JP2=1,MINN2
       GO TO (710,720),IGO2
  710  IP2=INV(JP2)*N2VNT
       GO TO 730
  720  IP2=INV(JP2)/NTVN2
  730  I2=(IPP2+IP2)*N1
  800  JJ1=1
       DO 860 JPP1=1,N1VNT
       IPP1=INV(JJ1)+I2
       DO 850 JP1=1,MINN1
       GO TO (810,820),IGO1
  810  IP1=INV(JP1)*N1VNT
       GO TO 830
  820  IP1=INV(JP1)/NTVN1
  830  I=2*(IPP1+IP1)+1
       IF (J-I) 840,845,845
  840  T=A(I)
       A(I)=A(J)
       A(J)=T
       T=A(I+1)
       A(I+1)=A(J+1)
       A(J+1)=T
  845  CONTINUE
  850  J=J+2
  860  JJ1=JJ1+JJD1
C      END OF JPP1 AND JP2
C
  870  JJ2=JJ2+JJD2
C      END OF JPP2 AND JP3 LOOPS
C
  880  JJ3 = JJ3+JJD3
C      END OF JPP3 LOOP
C
  890  IF(IFSET)891,895,895
  891  DO 892 I = 1,NX
  892  A(2*I) = -A(2*I)
  895  RETURN
C
CC     THE FOLLOWING PROGRAM COMPUTES THE SIN AND INV TABLES.
C
  900  MT=MAXO(M(1),M(2),M(3)) -2
       MT = MAXO(2,MT)
  904  IF (MT-20)906,906,905
  905  IFERR = 1
       GO TO 895
  906  IFERR=0
       NT=2**MT
       NTV2=NT/2
C
CC     SET UP SIN TABLE
C      THETA=PIE/2**(L+1) FOR L=1
  910  THETA=.7853981634
C
CC     JSTEP=2**(MT-L+1) FOR L=1
       JSTEP=NT
C
CC     JDIF=2**(MT-L) FOR L=1
C      JDIF=2**(MT-L) FOR L=1
       JDIF=NTV2
       S(JDIF)=SIN(THETA)
       DO 950 L=2,MT
       THETA=THETA/2.
       JSTEP2=JSTEP
       JSTEP=JDIF
       JDIF=JSTEP/2
       S(JDIF)=SIN(THETA)
       JC1=NT-JDIF
       S(JC1)=COS(THETA)
       JLAST=NT-JSTEP2
       IF(JLAST - JSTEP) 950,920,920
```

APPENDIX H

```
  920 DO 940 J=JSTEP,JLAST,JSTEP
      JC=NT-J
      JD=J+JDIF
  940 S(JD)=S(J)*S(JC1)+S(JDIF)*S(JC)
  950 CONTINUE
C
C     SET UP INV(J) TABLE
C
  960 MTLEXP=NTV2
C
C     MTLEXP=2**(MT-L), FOR L=1
      LM1EXP=1
C
C     LM1EXP=2**(L-1), FOR L=1
      INV(1)=0
      DO 980 L=1,MT
      INV(LM1EXP+1) = MTLEXP
      DO 970 J=2,LM1EXP
      JJ=J+LM1EXP
  970 INV(JJ)=INV(J)+MTLEXP
      MTLEXP=MTLEXP/2
  980 LM1EXP=LM1EXP*2
  982 IF(IFSET)12,895,12
      END



      SUBROUTINE ANAL(IL,K)
C     SUBROUTINE ANAL   SERVICE ROUTINES FOR THE DATA INPUT
C     ----------R.R. SMITH QMC  1972----------
      INTEGER C
      INTEGER F,F,G,H
      INTEGER TMIN,EMIN,EMM1,TBM1,TBCK,DEB,DTG
      REAL LW
      DIMENSION C(50,80),E(260),F(260),G(260),H(260)
      COMMON / ANL/IHEAD(3),ISSNT(20)
      COMMON /PLT/R(1025),A(1025),EXA,EXB
      GOTO (1010,2000,3000,4000,5000) IL
CHAPTER 1  SETTING UP
 1010 CONTINUE
      IUNIT=3
C     READ THRU MEDATA LOG HEADER
      READ(5,50) IHEAD
   50 FORMAT(3A4)
      CALL PDPOPEN(3,IHEAD(1))
      IFILE=0
C SETTING UP CONSTANTS
      PI = 3.14159
      ALF=.0265
      TC=21.5
      RWC=10.63
      RWH=16.63
      TWH=(RWH-RWC)/(ALF*RWC)+TC
      RLD=0.46
      LW=0.002
      CNU=RWH/((RLD+50.+RWH)**2*PI*LW)
      DIA=5.0E-06
C
C SETTING UP OF CALIBRATION ARRAY
C NOTE ORDER OF THE PARAMETERS OF ARRAY C(TEMPERATURE,BRIDGE VOLTAGE)
C NOTE  TBCK, EB, TG,  AND ASSOCIATED VARIABLES ARE INTEGERS AND ARE
C SCALED BY A FACTOR OF 100
C
      TBCK=2500
      TMIN=TBCK
      EMIN=225


      DEB=1
      DTG=100
C
      EMM1=EMIN-DEB
```

APPENDIX H

```
      TEM1=TMIN-DTG
      Y=FLOAT(TMIN-DTG)/100.
      XMIN,X=FLOAT(EMIN-DEB)/100.
      DY=FLOAT(DTG)/100.
      DX=FLOAT(DEB)/100.
      DO 80 I=1,50
      Y=Y+DY
      X=XMIN
      DO 80 J=1,80
      X=X+DX
      TFLM=(Y+TWH)*0.5
      FKW=0.0241*(1.+0.003124*TFLM)
      VK= 1.328E-05 + 8.244E-08*TFLM + 1.240E-10*TFLM*TFLM
      FNU=CNU*X*X/(FKW*(TWH-Y))*((TFLM+273.)/(Y+273.))**(-0.17)
C     CALIBRATION MARCH 72
      RE = -.9672 + 4.9757*FNU - 9.1570*FNU*FNU + 6.2127*FNU*FNU*FNU
      C(I,J)=VK/DIA*RE*10 000.
   80 CONTINUE
      GOTO 90
   90 CONTINUE
 1000 FORMAT(1H0,10I8)
      WRITE(6,1001)
 1001 FORMAT(1H0)
      WRITE(6,1001)
 1002 FORMAT(1H0,1P10E10.3)
      WRITE(6,1002) TWH
C
C END OF SET UP ROUTINE
      RETURN
C
C INPUT A NEW FILE
C
 2000 CONTINUE
  110 CONTINUE
C NTOT IS THE NO OF POINTS FROM ONE CHANNEL
C NSAM IS THE NO OF POINTS SAMPLED BY ONE CHANNEL
C NI IS A PROGRAM CHECK ON NO OF PTS FROM 1 CHANNEL
      NSAM=255
C INITIALIZE THE STORAGE SUMS AND COUNTERS
      NI=0
      K50,J70=0
      J0,K0=0
      IPAR=0
      IBLC=0
C
C     READ SENTENEL INFORMATION
      CALL PDPSENT(3,ISENT(1))
      RETURN
C
 3000 CONTINUE
  150 CALL PDPSKIP(3)
      K=-10
  160 RETURN
C
CHAPTER-2-INPUT-DATA
 4000 CONTINUE
  200 K=0
  204 FORMAT(1H1)
  208 FORMAT(1H ,4H K =,I4)
      CALL PDPREAD(3,4,E(1),F(1),G(1),H(1),K)
C CHECK FOR EOF
      IF(K) 290,285,210
  210 CONTINUE
C   INCREMENT BLOC COUNTER
      IBLC=IBLC+1
      DO 280 I=1,255
      IMT=I*4-3
C INCREMENT THE SAMPLE COUNTER
      NI=NI+1
C SCALING.....LINEARIZING.....
      TURB=5*E(I)+TBCK
      Y=TURB*0.01
      TAMB=5*F(I)+TBCK
      EBRD= 199. * .3265*FLOAT(G(I))
```

APPENDIX H

```
C       OVER AND UNDER FLOW CATCHMENT
        L=(TURR-TBCK)/100
        J=FBRD-EMM1
        L=MAXO(1,L)
        L=MINO(50,L)
        J=MAXO(1,J)
        J=MINO(70,J)
        A(IMT+2)=FLOAT(C(L,J))*1.E-4
        GOTO 270
C       AUXILLARY CALIBRATION MARCH 72
        X=199. + .3265*FLOAT(G(I))
        X=X*0.01
        TFLM=(Y+TWH)*0.5
        FKW=0.02414*(1.+0.003124*TFLM)
        VK= 1.328E-05 + 8.244E-08*TFLM + 1.240E-10*TFLM*TFLM
C       NUSSULT NO IS WEIGHTED
        FNU=CNU*X*X/(FKW*(TWH-Y))*((TFLM+273.)/(Y+273.))**(-0.17)
C       CALIBRATION      MARCH 72
        RE=-.9672 + 4.9757*FNU - 9.1570*FNU*FNU + 6.2127*FNU*FNU*FNU

        A(IMT+2)=VK/DIA*RE

  270   CONTINUE
        A(IMT)=Y
        A(IMT+1)=TAMB
        A(IMT+3)=0.

  280   CONTINUE
C  END OF DATA INPUT CALCULATIONS
C
C  RETURN TO MAIN PROGRAM
  300   RETURN
C       DEFAULT ROUTINES
  285   CONTINUE
C       OMIT THE BACK SPACING PRESENTLY
        GOTO 287
        CALL PDPBACKSP(IUNIT)
C       TRY TO READ THE FAULTY BLOCK ONCE AGAIN   (TOTAL OF 24 X )
        CALL PDPREAD(3,4,E(1),F(1),G(1),H(1),K)
        IF(K) 290,286,210
  287   CONTINUE
  286   IPAR=IPAR+1
        WRITE(6,288) IBLC
  288   FORMAT(22H PARITY ERROR  BLOCK   ,I4,7HOMITTED )
        IF(IPAR-10) 200,200,292
C       CHECK FOR T.M.
  290   IF(K+10) 400,400,292
C       ABANDON FILE
        CALL PDPSKIP(3)
        WRITE(6,296)
  296   FORMAT (///,40H  PARITY ERRORS    FILE ABANDONNED        //  )
  292   WRITE(6,295) K,IBLC,IPAR
  295   FORMAT(1H0,5H K = ,I6,5X,6H IBLC ,I6,5X,7H IPAR =,I6,///)
  400     GOTO 420
  420   CONTINUE
        RETURN
C
 5000   CONTINUE
        CALL PDPCLOSE(3)
        RETURN
        END
```

APPENDIX I

TEST CONDITIONS

The following table gives the conditions under which some of the experiments were performed.

$Gr \times 10^{-10}$	x	$T_w - T_\infty$	T_∞
0.0281	0.40	41.4	27.5
0.0747	0.55	42.5	27.5
0.479	1.04	41.0	29.1
0.892	1.26	42.6	27.9
2.24	1.75	42.7	31.3
2.84	1.88	42.5	30.5
3.45	2.01	42.0	30.5
3.51	2.01	41.8	29.0
4.84	2.26	41.2	30.5
6.81	2.53	41.8	31.0

REFERENCES

ADRIKO E.T.S., 1970, 'Flow in a plane turbulent jet of heated air', Ph.D.Thesis, University of London.

ANTONIO R.A., 1972, 'Conditionally sampled measurements near the outer edge of a turbulent boundary layer', J.Fluid Mech., 56, pp.1-18.

BAILLE A., 1971, 'Lois de refroidissement des fils chauds aux faibles vitesses', Thesis (Dr.Ing.) de l'universite de Provence, Marseille.

BAYLEY F.J., 1955, 'An analysis of turbulent free-convection heat-transfer', Proc.of the Inst.of Mech.Eng., 169, No.20, p.361.

BEARMAN P.W., 1968, 'Digital analysis of hot-wire data', Paper 15, Proc. Symp.on Instrumentation and Data Processing for Industrial Aerodynamics, NPL.

BENDAT J.S. and PIERSOL A.G., 1966, Measurement and Analysis of Random Data J.Wiley and Sons, New York.

BERGER E., 1964a, Z.Furgwiss, 12, 41.

BERGER E., 1964b, Jahrbuch 1964 der WGLR, p.164.

BINGHAM C., GODFREY M.D. and TUKEY J.W., 1967, 'Modern techniques of Power Spectrum Estimation', IEEE Trans.on Audio and Electro-acoustics, Vol.AU-15, No.2.

BLACKMAN R.B. and TUKEY J.W., 1959, The Measurement of Power Spectra, Dover Publications Inc., New York.

BOUSINESQ J. , 1877, Mem.pres.par div.savants a l'acad.sci., Paris, 23, 46.

BRADSHAW P., 1971a, 'Variations of a theme of Prandtl', AGARD-CPP-93-71.

BRADSHAW P., 1971b, An Introduction to Turbulence and its Measurement, Pergamon.

BRADSHAW P., 1972, 'The understanding and prediction of turbulent flow', Aeronautical Journal.

BRUN H.H., 1970, 'Interpretation of a hot-wire signal using a universal calibration law', Inst.of Sound and Vibration Research, University of Southampton, Southampton SO9 5NH.

CHEESEWRIGHT R., 1966, 'Natural convection from a vertical plane surface', Ph.D.Thesis, University of London.

CHEESEWRIGHT R., 1968, 'Turbulent natural convection from a vertical plane surface', J.of Heat Transfer, Trans.ASME, Series C, Vol.90, No.1.

CHEESEWRIGHT R., 1972, 'The application of digital techniques to hot-wire anemometry in highly turbulent flows', DISA Conference (1972), University of Leicester.

COLAK-ANTIC P., January 1964 der WGLR, 'Hitzdrahtmessungen des Laminar-Turbulenten Umschlags Bei Freier Konvektion'.

COLAK-ANTIC P. and GORTLER H., 1971, 'Flow visualization studies of free convection laminar-to-turbulent transition along a heated vertical plate in water induced by two-dimensional forced disturbances', Warme- und Stoffubertragung, Bd.4, S.25-31.

COLLIS D.C. and WILLIAMS M.J., 1959, 'Two-dimensional convection from heated wires at low Reynolds numbers', J.Fluid Mech., 6, p.357.

COOLEY J.W., LEWIS P.A.W. and WELCH P.D., 1970, 'The fast Fourier transform algorithm: Programming considerations in the calculations of Sine, Cosine and Laplace Transforms', J.of Sound and Vibration, 12, No.3, pp.315-337.

COOLEY J.W., LEWIS P.A.W. and WELCH P.D., 1970, 'The application of the fast Fourier transform algorithm to estimation of spectra and cross spectra', J.of Sound and Vibration, 12, No.3, pp.339-352.

CORRSIN S., 1951, 'On the spectrum of isotropic temperature fluctuations in an isotropic turbulence', J.of Applied Physics, 22, No.4.

COUTANCEAU J., 1969, 'Convection naturelle turbulente sur une plaque verticale isotherme, transition, échange de chaleur et frottement parietal, lois de repartition de vitesse et de temperature', Int.J. Heat Mass Transfer, 12, pp.753-761.

DALY B.J. and HARLOW F.H., 1970, 'Transport equations in turbulence', Physics of Fluids, 13, No.11, pp.2635-2649.

DAVIES P.O.A.L. and BRUN H.H., 1968, 'The performance of a yawed hot wire', Paper 10, Proc.Symp.on Instrumentation and Data Processing for Industrial Aerodynamics, NPL.

DAVIES P.O.A.L., DAVIS M.R. and WOLD I., 'Operation of the constant resistance hot-wire anemometer', ISAV Report No.189.

DISA, Instruction and Service Manual for Type 55001 Anemometer Unit.

DRING R.P. and GEBHART B., 1969, 'Hot-wire anemometer calibration for measurements at very low velocity', J.of Heat Transfer, ASME Series C, 91, pp.241-4.

ECKERT E.R.G. and JACKSON T.W., 1953, 'Analysis of turbulent free-convection boundary layer on flat plate', NACA Tech.Note 2207.

EDE A.J., June 1956, 'Natural convection on free vertical surfaces', Mech.Eng.Research Lab.Report, Heat 141, Glasgow.

ESKINAZI S. and ERIAN F.F., 1969, 'Energy reversal in turbulent flows', Physics of Fluids, 12, No.10, pp.1989-1998.

FIELDER H. and HEAD M.R., 1966, 'Intermittency measurements in the turbulent boundary layer', J.Fluid Mech., 25, part 4, pp.719-735.

FRENKIEL F.N. and KLEBANOFF P.S., 1967, 'Higher-order correlations in a turbulent field', Physics of Fluids, 10, No.3, p.507.

FUJII T., 1959a, 'Experimental studies of free convection heat transfer', Bull.of JSME, 2, No.8.

FUJII T., 1959b, 'An analysis of turbulent free convection heat transfer from a vertical surface', Bul.of JSME, 3, No.8.

FUJII T.et al., 1970, 'Experiments on natural-convection heat transfer from the outer surface of a vertical cylinder to liquids', Int.J.Heat Mass Transfer, 13, pp.753-787.

GASTER M., 1969, 'Vortex shedding from slender cones at low Reynolds numbers', J.Fluid Mech., 38, part 3, pp.565-576.

GASTER M., 1971, 'Vortex shedding from circular cylinders at low Reynolds numbers', J.Fluid Mech., 46, part 4, pp.749-756.

GEBHART B., 1969, 'Natural Convection flow, instability and transition', J.of Heat Transfer, Series C, 91, No.3, pp.293-309.

GRIFFITH E. and DAVIS A.H., 1922, 1931, 'The transmission of heat by radiation and convection', DSIR - Br.Food Invest.Board, Special Report 9.

HALL G., 1972, The PDP-8/T5ØØ On-line Data Logging System', Research Paper EP 5ØØ1, Queen Mary College, London.

HALL W.B. and PRICE P.H., 1969, 'Mixed forced and free convection from a vertical heated plate to air', Paris Heat Transfer Conference.

HANJALIC, K. and LAUNDER B.E., 1972, 'A Reynolds stress model of turbulence and its application to shear flows', J.Fluid Mech., 52, part 4, pp.609-638.

HATTON A.P., JAMES D.D. and SWIRE H.W., 1970, 'Combined forced and natural convection with low-speed air flow over horizontal cylinders', J.Fluid Mech., 42, part 1, pp.17-31.

HINZE J.O., 1959, Turbulence, McGraw-Hill.

HOLLASCH K. and GEBHART B., 1972, 'Calibration of constant-temperature hot-wire anemometers at low velocities in water with variable fluid temperature', J.of Heat Transfer, ASME, Series C, p.172.

JONES W.P. and LAUNDER B.E., 1972, 'The prediction of laminarization with a two-equation model of turbulence', Int.J.Heat Mass Transfer, 15, pp.301-314.

von KARMAN T., 1921, 'On laminar and turbulent friction', Z.angew.Math. Mech.1, 233.

KATO H. et al., 1968, 'On the turbulent heat transfer by free convection from a vertical plate', Int.J.Heat Mass Transfer, 11, pp.1117-1125.

KAWALL J.G. and KEFFER J.F., 1971, 'Digital analysis of turbulent signals', UTME-TP 7104, University of Toronto, Canada.

KENDAL M.G. and STEWART A., 1963, The Advanced Theory of Statistics, Griffin, 1, 2nd ed.

KESTIN J. and RICHARDSON P.D., 1963, 'Heat transfer across turbulent incompressible boundary layers', Int.J.Heat Mass Transfer, 6, pp.147-189.

KINNS R., 1971, 'Computation of power spectra, cross-spectra and related functions in the Cambridge computer in the Cambridge University Engineering Laboratory', CUED/A-Aerodynamics/TRI.

KINNS R., 1972, 'Spectral analysis on a small computer', Cambridge University Engineering Department.

KLATT F., 1969, 'The X hot-wire probe in a plane flow field', DISA Information No.8.

KLEBANOFF P.S., 1954, 'Characteristics of turbulence in a boundary layer with zero pressure gradient', NACA TN-3178.

KLINE S.J., 1959, 'On the Nature of stall', J.Basic Eng., ASME Series D, 81, No.3, p.305.

KNOWLES C.P. and GEBHART B., 1968, 'The stability of the laminar natural convection boundary layer', J.Fluid Mech., 34, part 4, pp.657-686.

KOVASZNAY L.S.G., 1949, Hot-wire investigation of the Wake behind cylinders at low Reynolds numbers', Proc.Roy.Soc.A198, 174.

KOVASZNAY L.S.G. et al., 1970, 'Large scale motion in the intermittent region of a turbulent boundary layer', J.Fluid Mech., 41, part 2, pp.283-325.

KUNG R.J. and BINDER G.J., 1967, 'Ultra-low speed anemometry', Fluid Dynamics and Diffusion Lab., Colorado State University, Fort Collins, Colorado.

KUTATELADZE S.S. et al., 1972, 'Turbulent natural convection on a vertical plate and in a vertical layer', Int.J.Heat Mass Transfer, 15, pp.193-202.

LARSON J.R. and SCHOENHALS R.J., 1966, 'Turbulent free convection in near-critical water', J.of Heat Transfer, ASME Series C, 88, No.4, 407-414.

LAUNDER B.E., November 1968, 'The Prandtl-Kolmogorov model of turbulence with the inclusion of second-order terms', Imperial College, Dept.of Mech.Eng., London.

LOCK C.S. and TROTTER F.J., 1968, 'Observations on the structure of a turbulent free-convection boundary layer', Int.J.Heat Mass Transfer, 11, pp.1225-1232.

LOCKWOOD F.C. and ONG P.H., September 1968, 'Study of combined free and forced convection turbulent boundary layer with variable fluid properties and chemical reaction', Communication, International Summer School, Herceg-Novi, Yugoslavia.

LUMLEY J.L. and PANOFSKY H.A., 1964, The Structure of Atmospheric Turbulence, Interscience Publishers, John Wiley and Sons, New York.

LUXTON C.G., SWENSON B.S. and CHADWICK, 1966, 'A Data System for Turbulence Studies', reprinted from the Collection and Processing of Field Data Symp., Canberra, Australia.

MILLER E.B., 1966, 'Program to measure the macroscale turbulence of subsonic jets', NASA CR-84423.

NEE V.W. and KOVASZNAY L.S.G., 1969, 'Simple phenomenological theory of turbulent shear flows', Physics of Fluids, 12, No.3, pp.473-484.

OOSTHUIZEN P.H., 1970, 'A numerical study of turbulent free convection from an isothermal vertical plate', Report No.1/70, Thermal and Fluid Sciences Group, Queen's University, Kingston, Canada.

OSTRACH S., 1952, 'An analysis of laminar free-convection flow and heat transfer about a flat plate parallel to the direction of the generating body force', NACA Tech.Note 2635.

PALMER M.D. and KEFFER J.F., 1972, 'An experimental investigation of an assymetrical turbulent wake', J.Fluid Mech., 53, part 4, pp.593-610.

PATANKAR S.V. and SPALDING D.B., 1970, Heat and Mass Transfer in Boundary Layers, 2nd ed., Intertext Books.

PIRVANO A. et al., 1969, 'Convection naturelle en regime turbulent le long d'une plaque plane verticale', Paris Heat Transfer Conference.

ROBERTS J.B. and SURREY D., 1971, 'Some experiences with 'on-line' spectral analysis using a small digital computer', NPL Aero Report 1328.

ROSHKO A., 1954, 'On the development of turbulent wakes from vortex streets', Report 1191 NACA.

ROTTA J.C., 1962, 'Turbulent Boundary layers in incompressible flow', Aero.Versuchsanstalt, Gottingen. From Progress in Aeronautical Sciences, Vol.2, Pergamon Press.

ROTTA J.C., 1971, 'Recent attempts to develop a generally applicable method for turbulent shear flow layers', AGARD-CPP-93-71.

SAUNDERS O.A., 1936, 'The effect of pressure upon natural convection in air', Proc.Roy.Soc.A 157, 278.

SCHMIDT E. and BECKMANN W., 1930, 'Temperature and velocity distribution around a heated vertical plate by natural convection', Tech.Mech. Therm 1, 341, 291.

SIDDAL R.G. and DAVIES T.W., 1972, 'An improved response equation for hot-wire anemometry', Int.J.Heat Mass Transfer, 15, pp.367-368.

SINGH G. and RAILLEY J.W., 1971, 'Determination of the instantaneous velocity vector in two-dimensional flow by the use of a hot wire anemometer and an on-line digital computer', Paper 26, Salford Conference on internal flows.

SPALDING D.B. and LAUNDER B.E., 1971, 'Turbulence models and their application to the prediction of internal flows', Paper I, Salford Conference on internal flows.

TOWNSEND A.A., 1956, The Structure of Turbulent Shear Flow, Cambridge Press.

TRITTON D.J., 1959, 'Experiments on the flow past a circular cylinder at 10 Reynolds numbers', J.Fluid Mech., 6, part 4, pp.547-567.

TRITTON D.J., 1971, 'A note on vortex streets behind circular cylinders at low Reynolds numbers', J.Fluid Mech., 45, part 1, pp.203-208.

VAN ATTA C.W. and CHEN W.Y., 1969a, 'Correlation measurements in turbulence using digital fourier analysis', Physics of Fluids Supp.II.

VAN ATTA C.W. and CHEN W.Y., 1969b, 'Measurements of spectral energy transfer in grid turbulence', J.Fluid Mech., 38, part 4, pp.743-763.

VLIET G.C. and LUI C.K., 1969, 'An experimental study of turbulent natural convection boundary layers', J.of Heat Transfer, Series C, 4, pp.517-531.

WARNER C.Y., 1966, 'Turbulent natural convection in air along a vertical flat plate', Ph.D.Thesis, University of Michigan.

WARNER C.Y. and ARPACI V.S., 1968, 'An experimental investigation of turbulent natural convection in air along a vertical heated flat plate', Int.J.Heat Mass Transfer, 11, pp.397-406.

WELCH P.D., 1967, 'The use of fast Fourier transform for the estimation of power spectra: a method based on time averaging over short modified periodograms', IEEE Trans. on Audio and Electro-acoustics, Vol.AU-15, No.2.

WHITEHEAD L.G., WU L.Y. and WATERS M.H.L., 1957, 'Contracting ducts of finite length', Aero.Quarterly, Vol.II.

YANG K.T. and NEE V.W., 1969, 'Structure of turbulent free-convection boundary layers along a vertical plate', Paris Heat Transfer Conference.

FIGURES AND PLATES

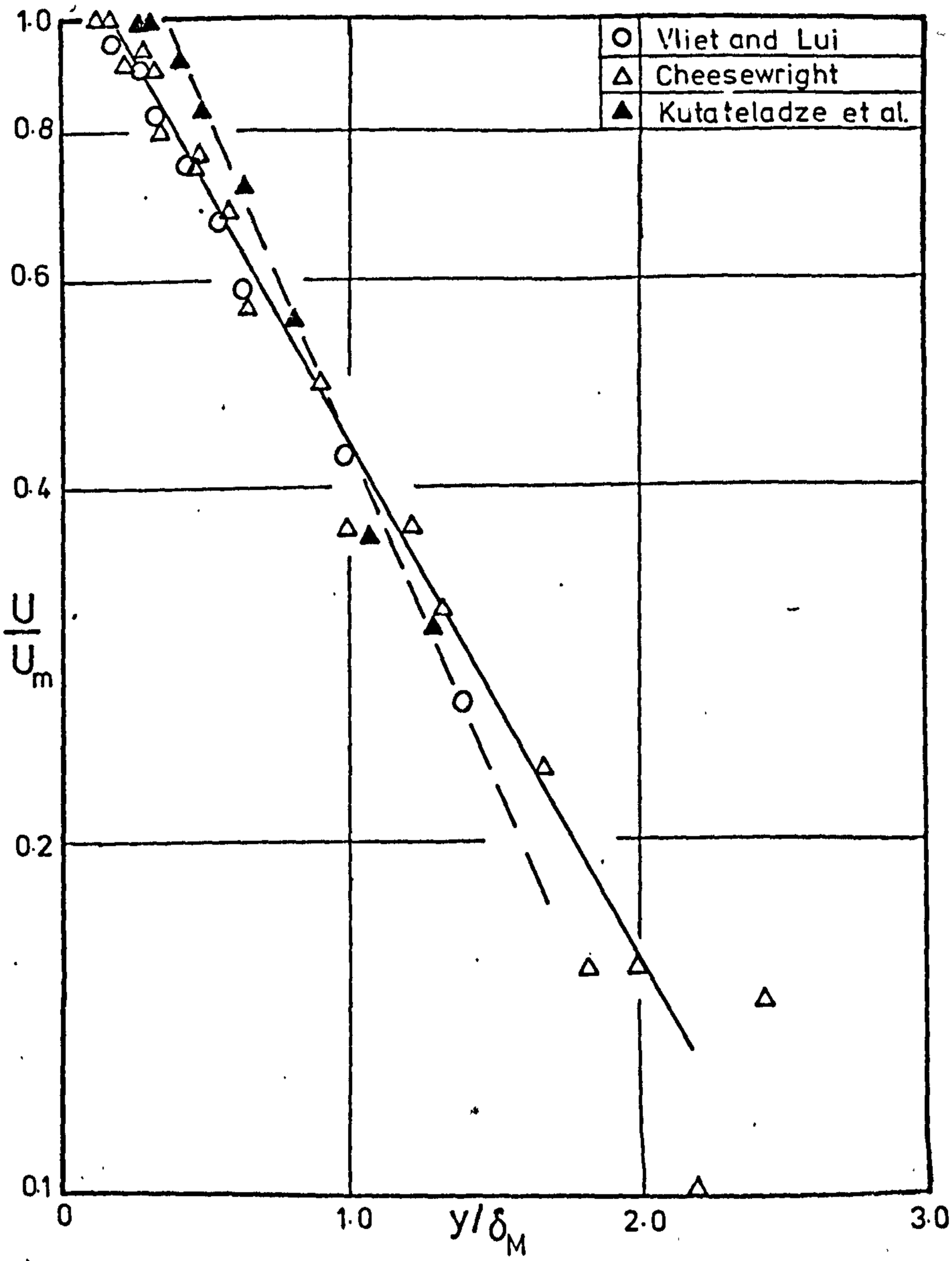

Fig. 2.1 Comparison of mean velocity data

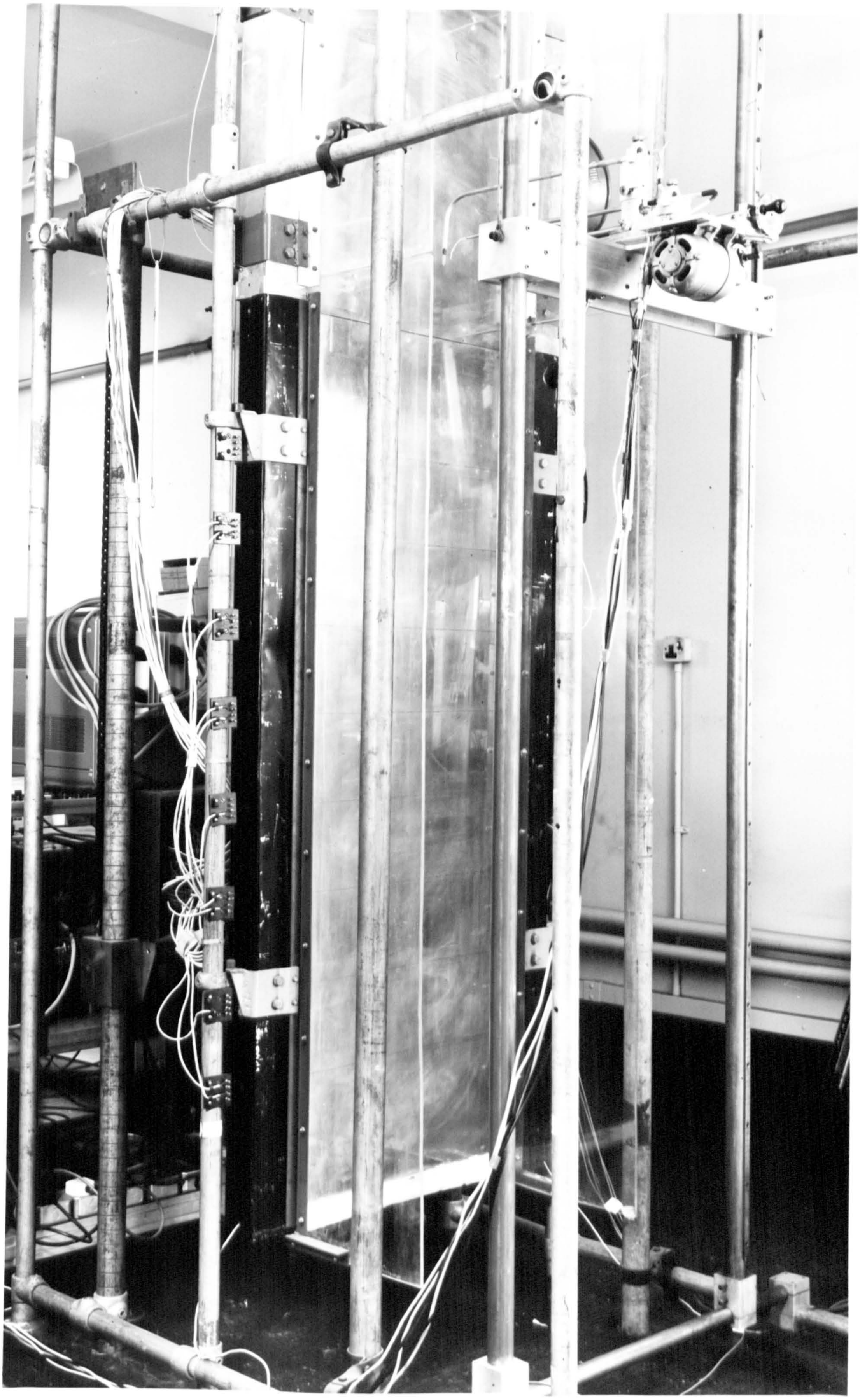

Plate 4.1 Vertical plate and traversing gear

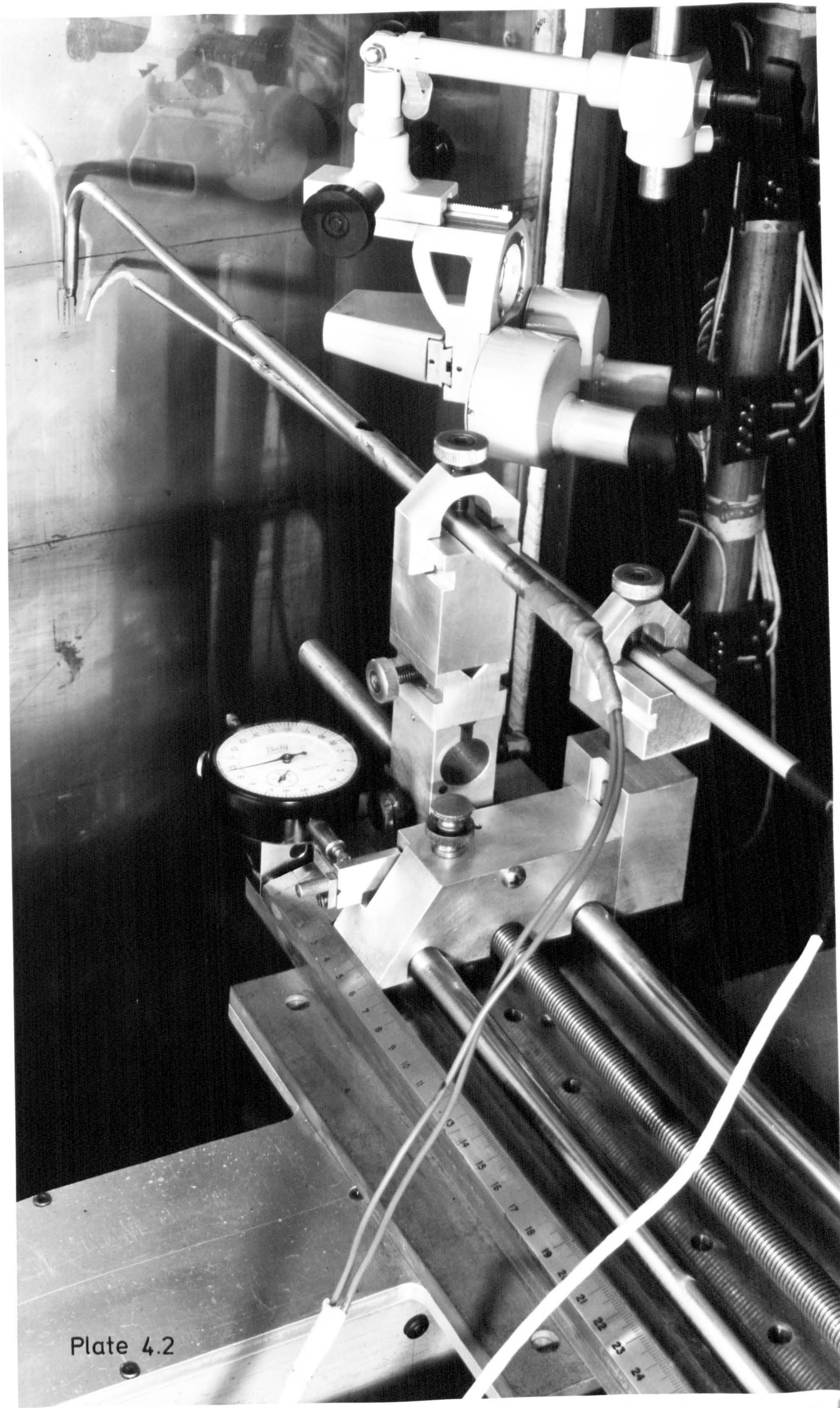

Plate 4.2

Legend

1 Digital voltmeter

2 Frequency counter

3 Oscilloscope

4 d.c. amplifier

5 Hot-wire anemomemeter

6 Signal conditioner

7 Teletype

8 Computer

9 Magnetic tape recorder

Plate 5.1 Instrumentation

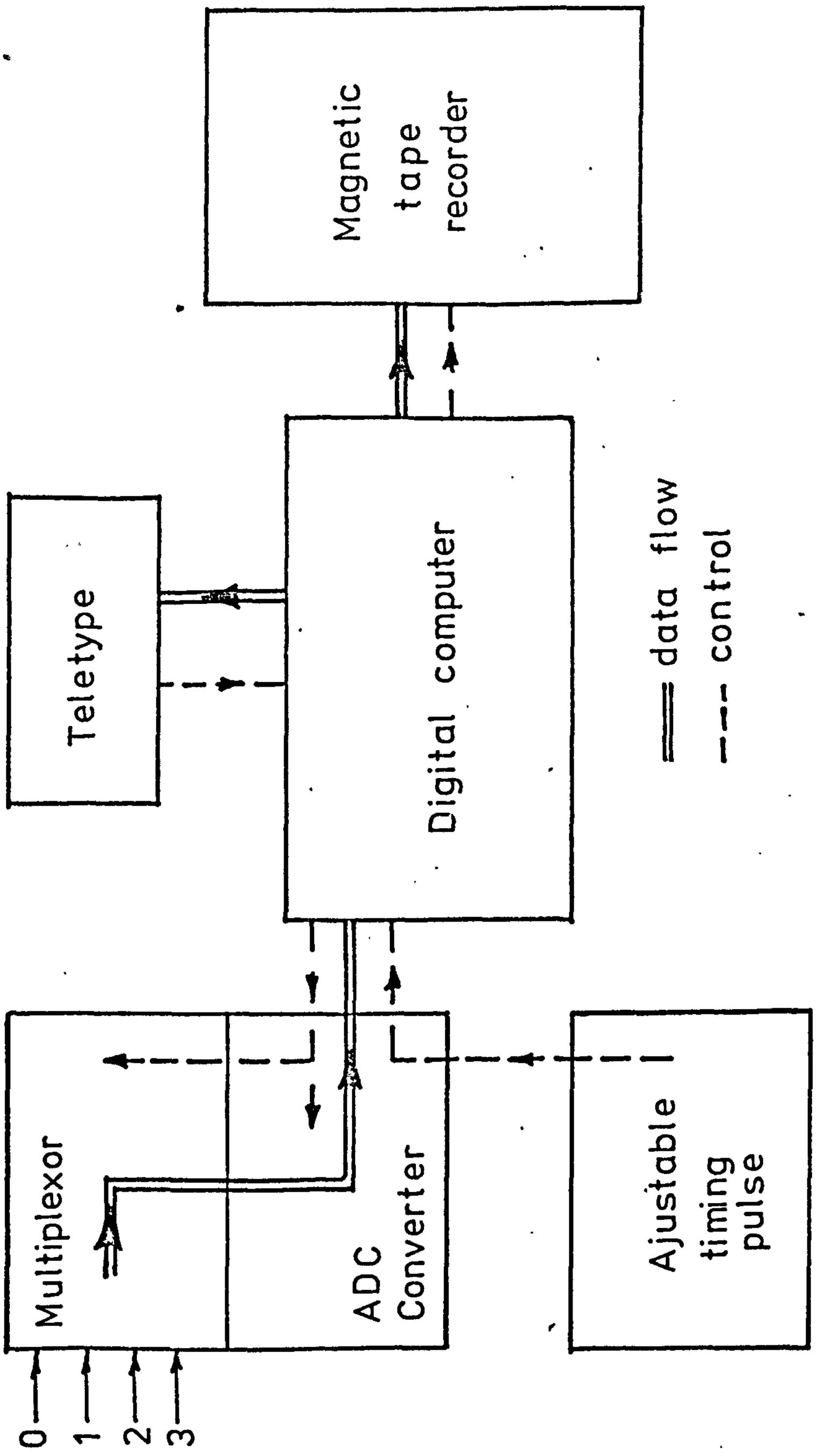
Magnetic tape recorder
Teletype
Digital computer
data flow
control
Digital instrumentation
Multiplexor
ADC Converter
Ajustable timing pulse
0
1
2
3

Fig. 5.2

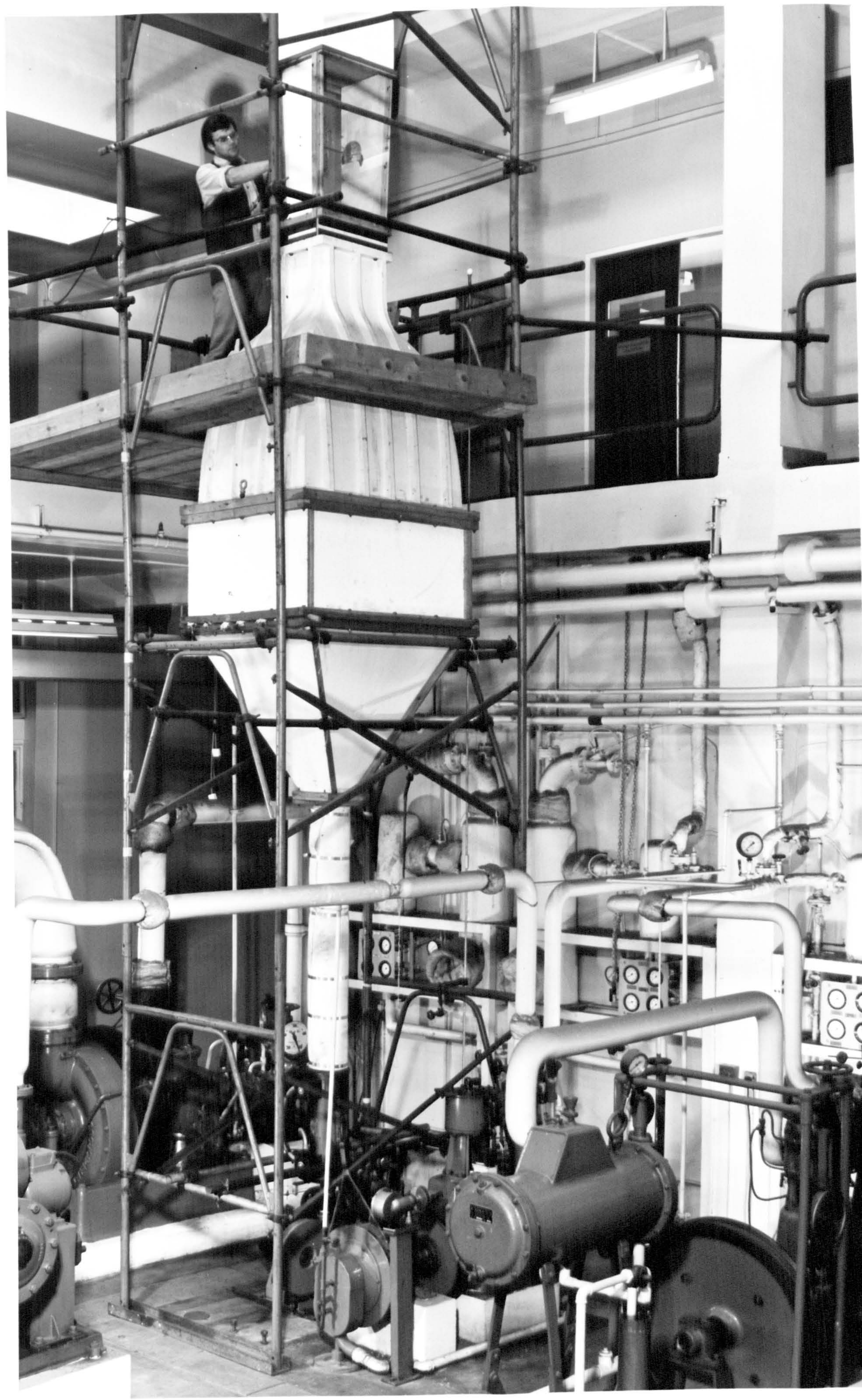

Plate 6.1 Calibration Wind Tunnel

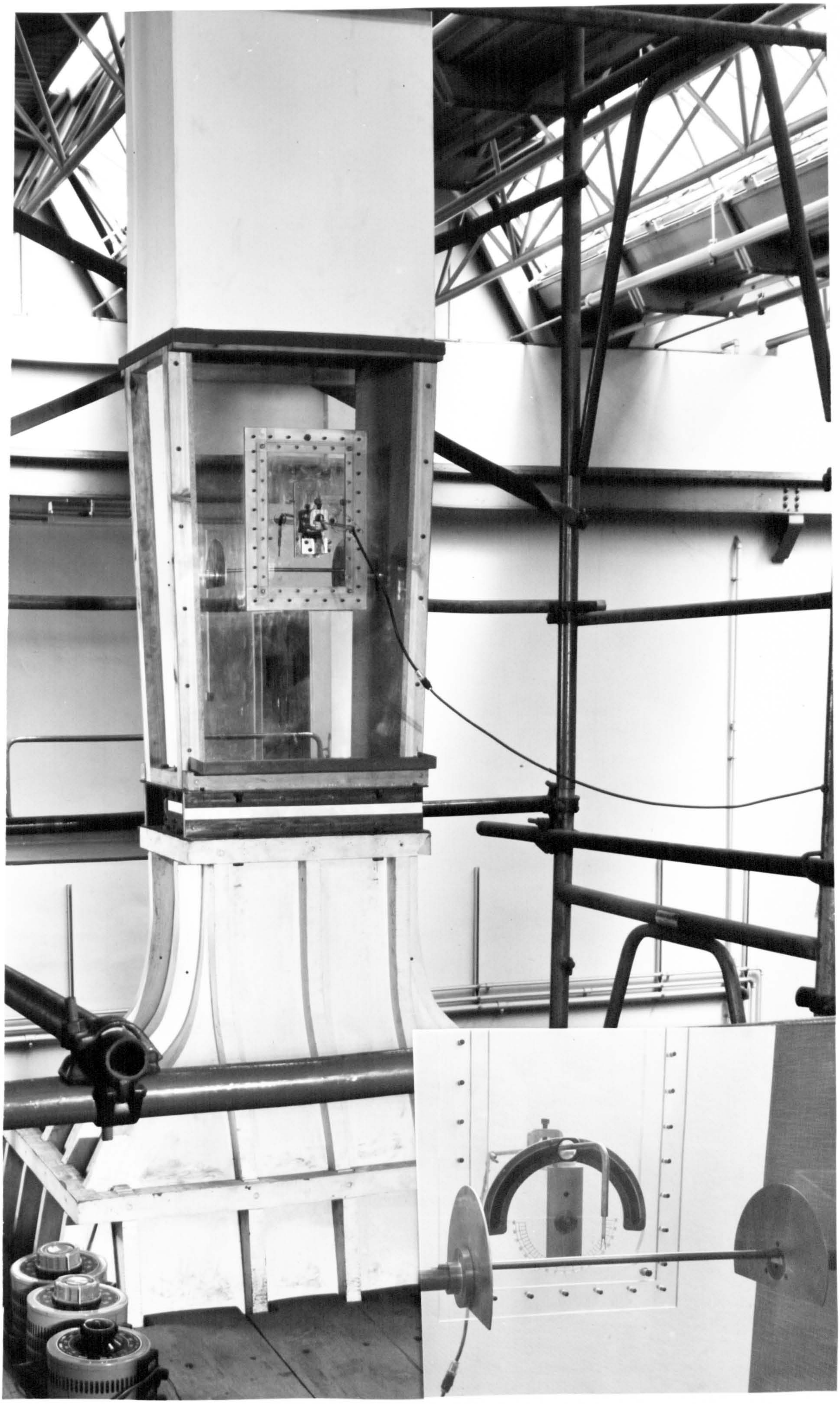

Plate 6.2 Calibration Tunnel Test Section

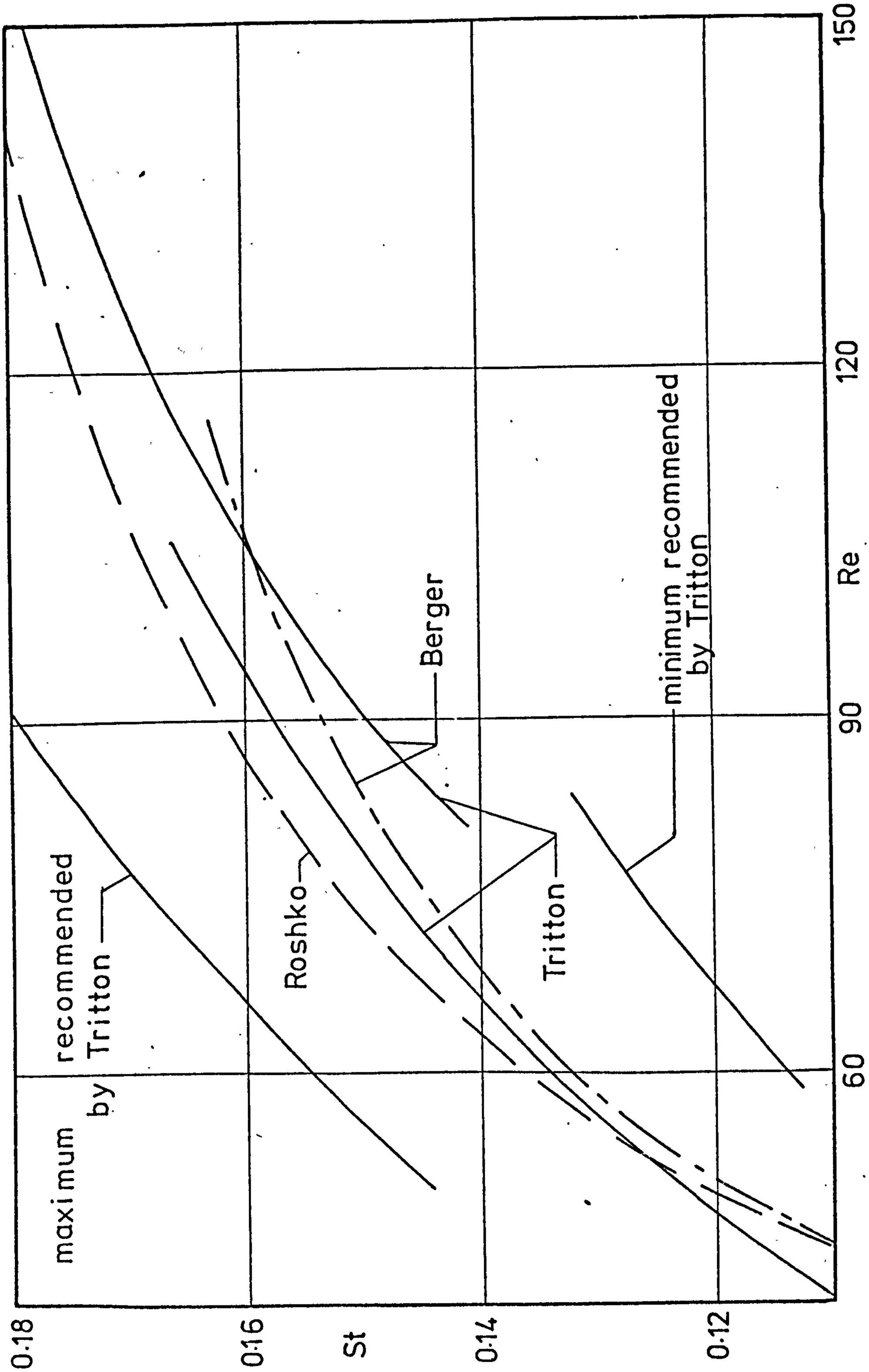

Fig 6.1 Proposed Strouhal - Reynolds relationships

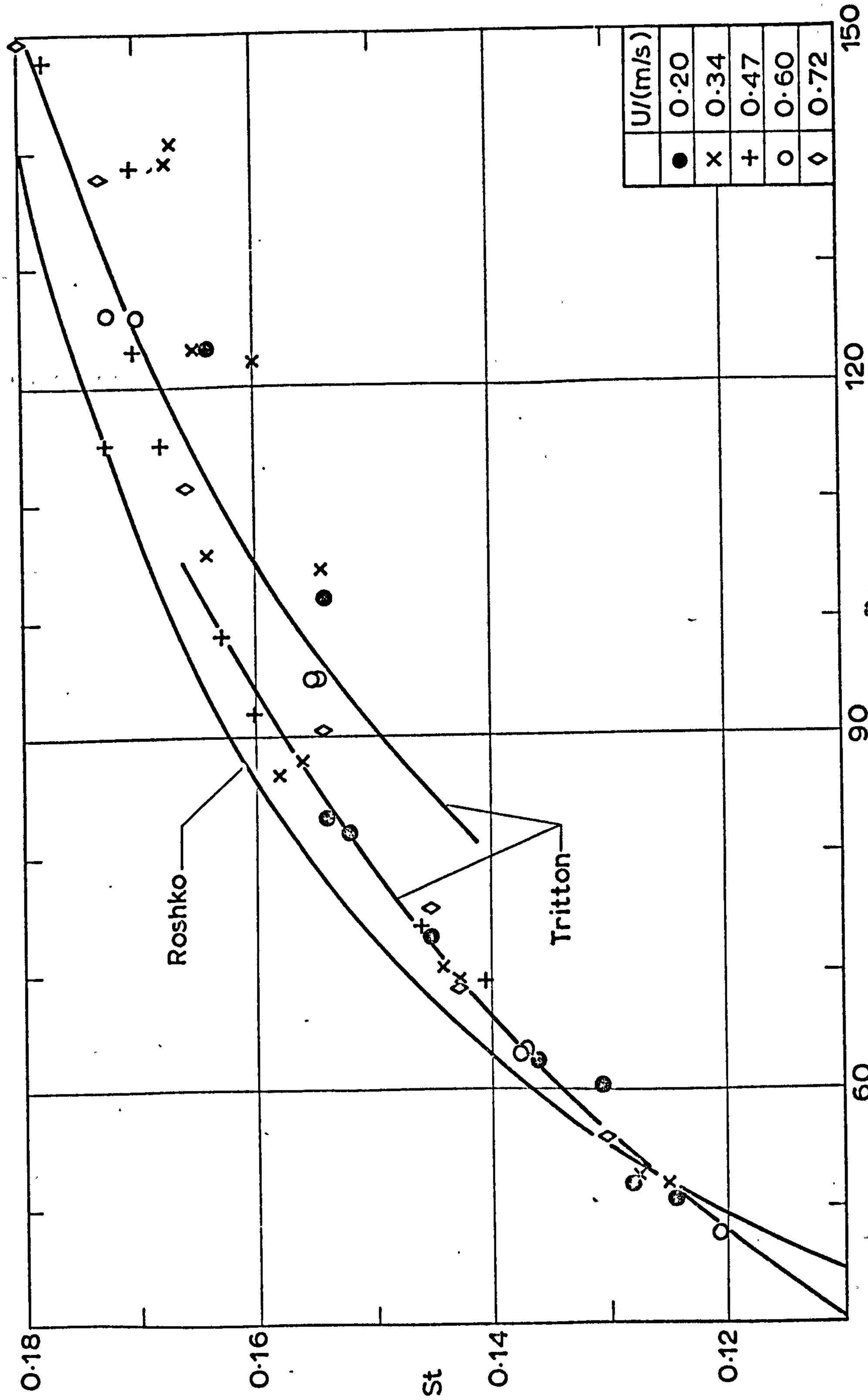

Fig. 6.2 Strouhal number vs Reynolds number

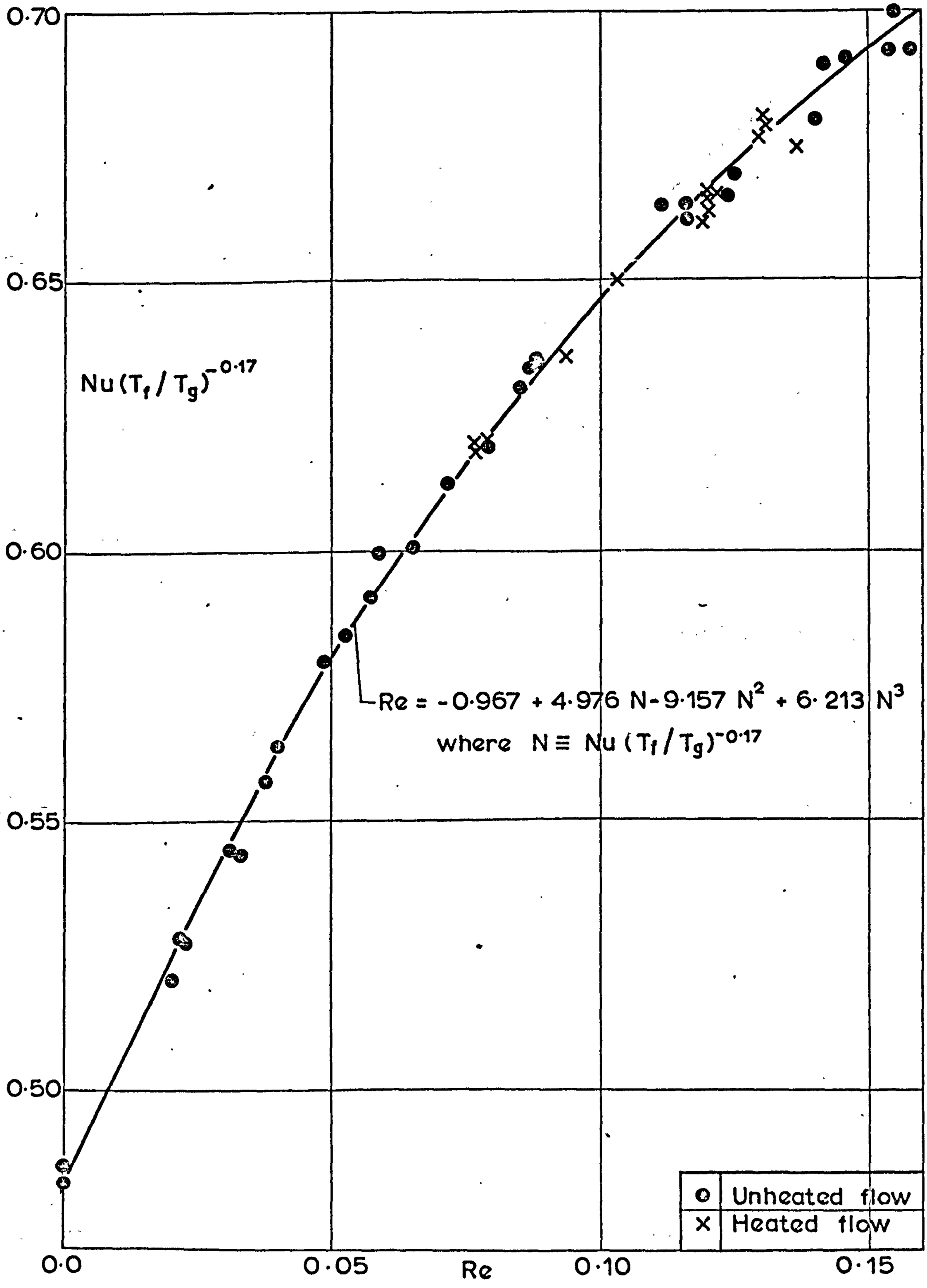

Fig. 6·4 Calibration of a hot wire for very small Re

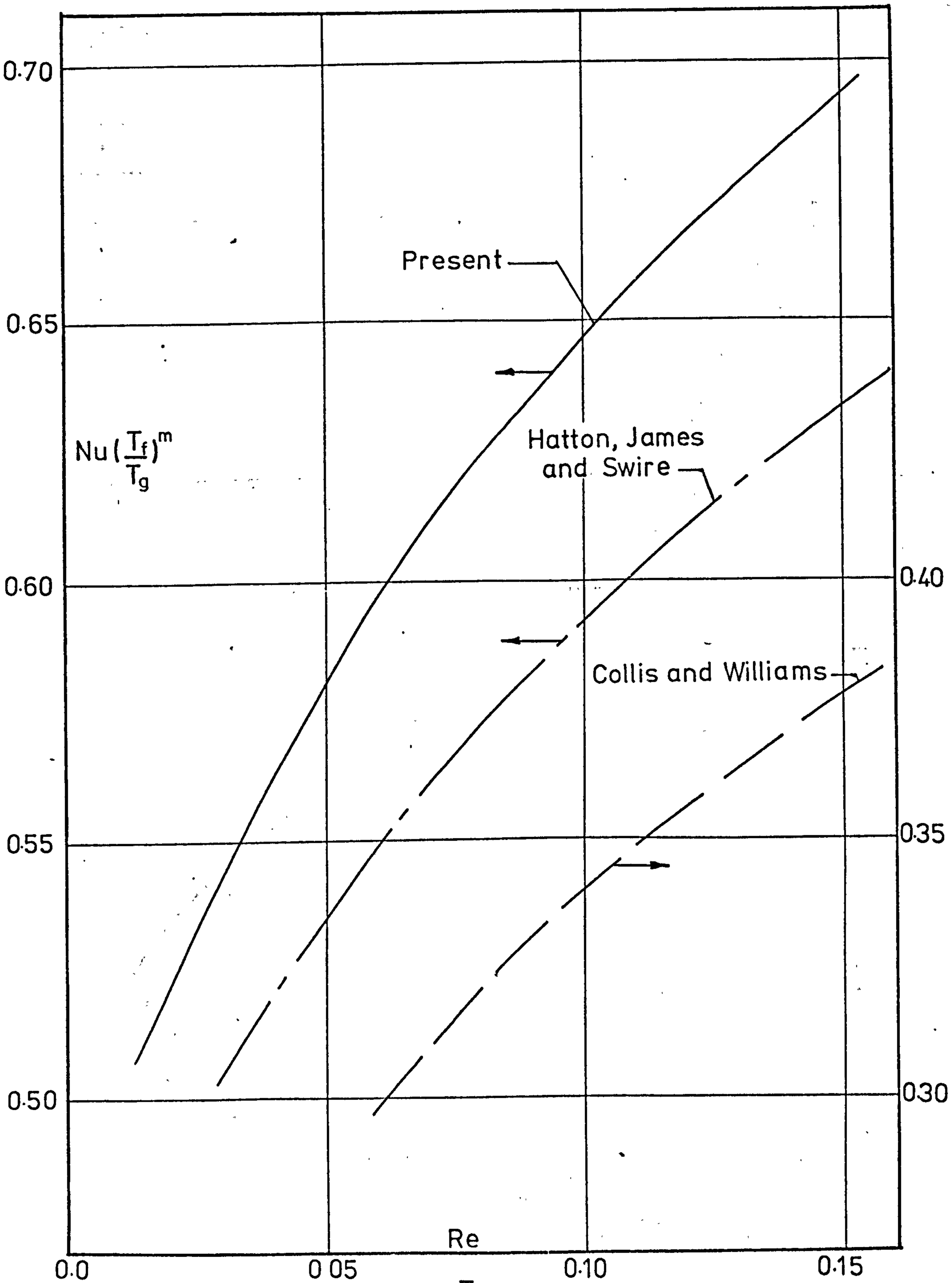

Fig. 6.5 Comparison of $Nu(\frac{T_f}{T_g})^m$ – Re relationships

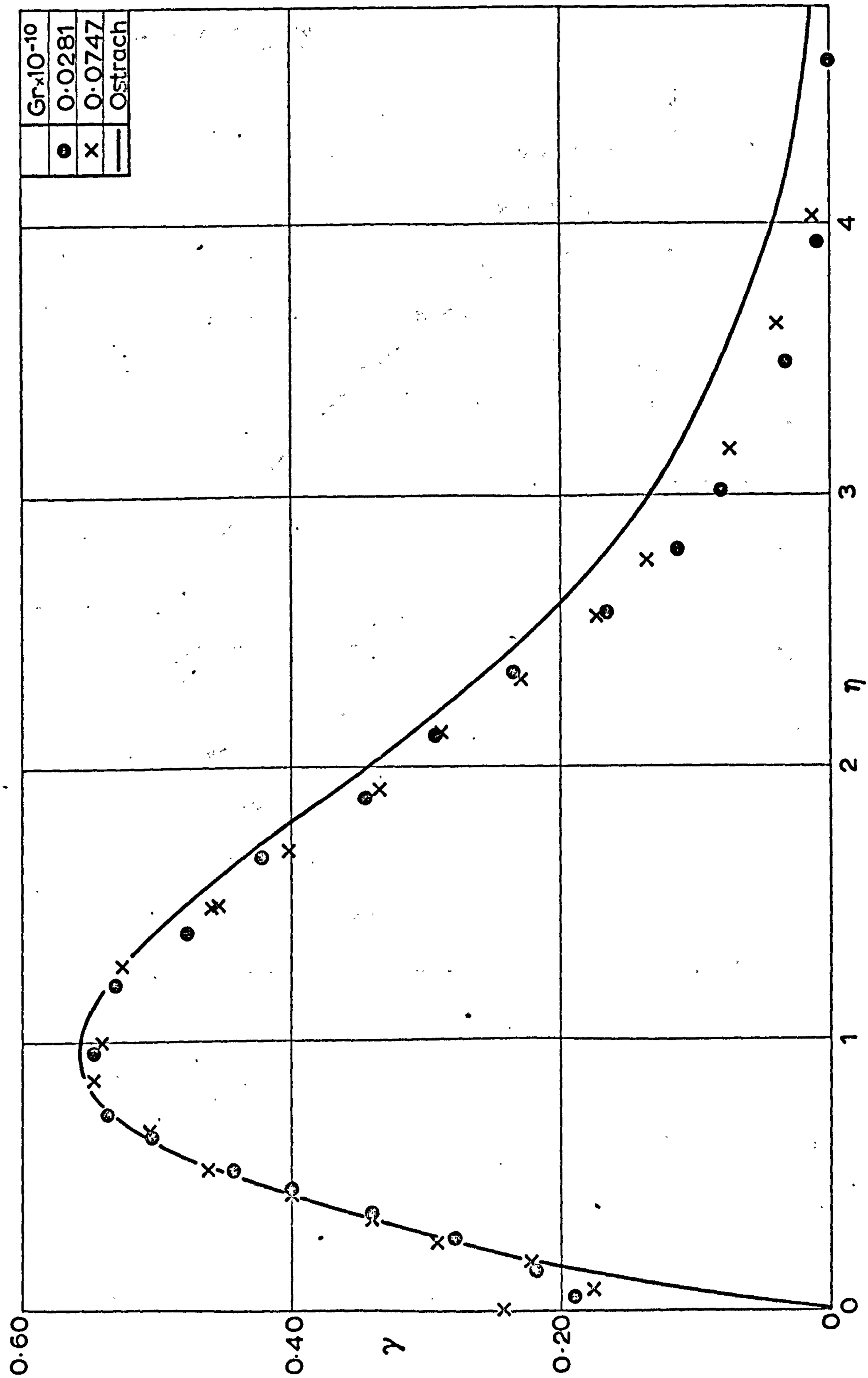

Fig. 6.6 Mean velocity profiles across a laminar boundary layer

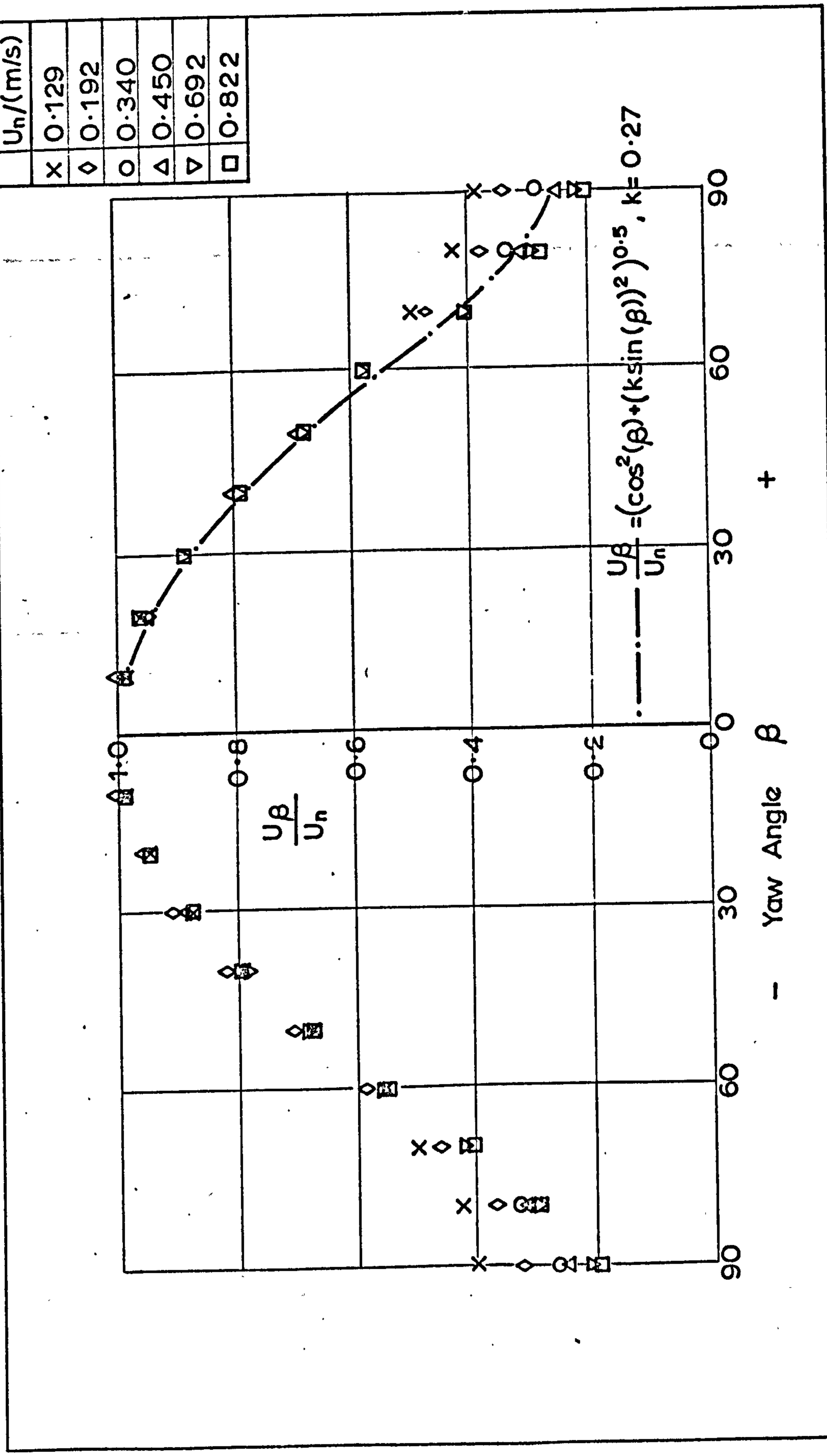

Fig. 6.7 Yaw Calibration at very low velocities

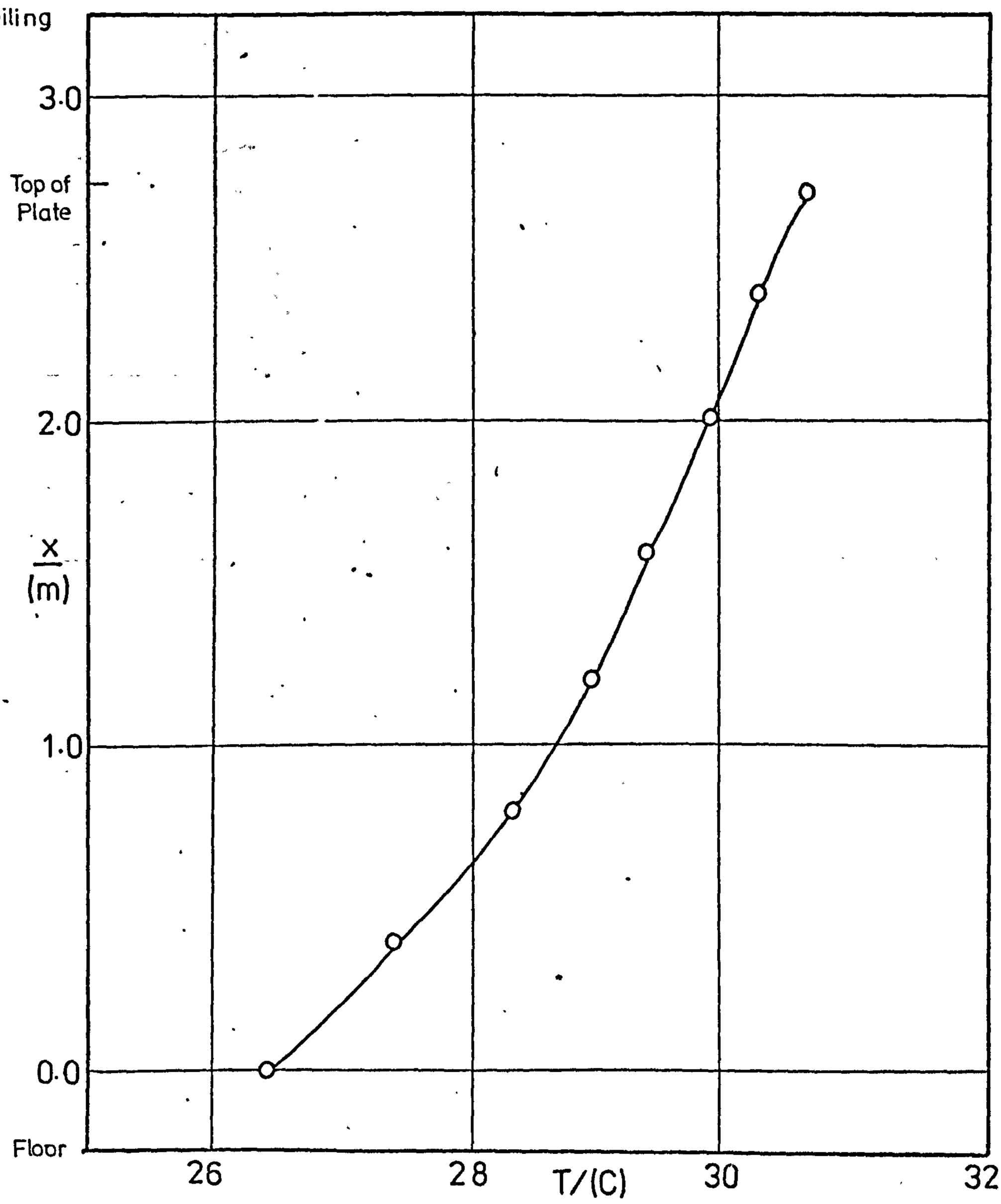

Figure 7.1 Typical Vertical Temperature Distribution in the Laboratory

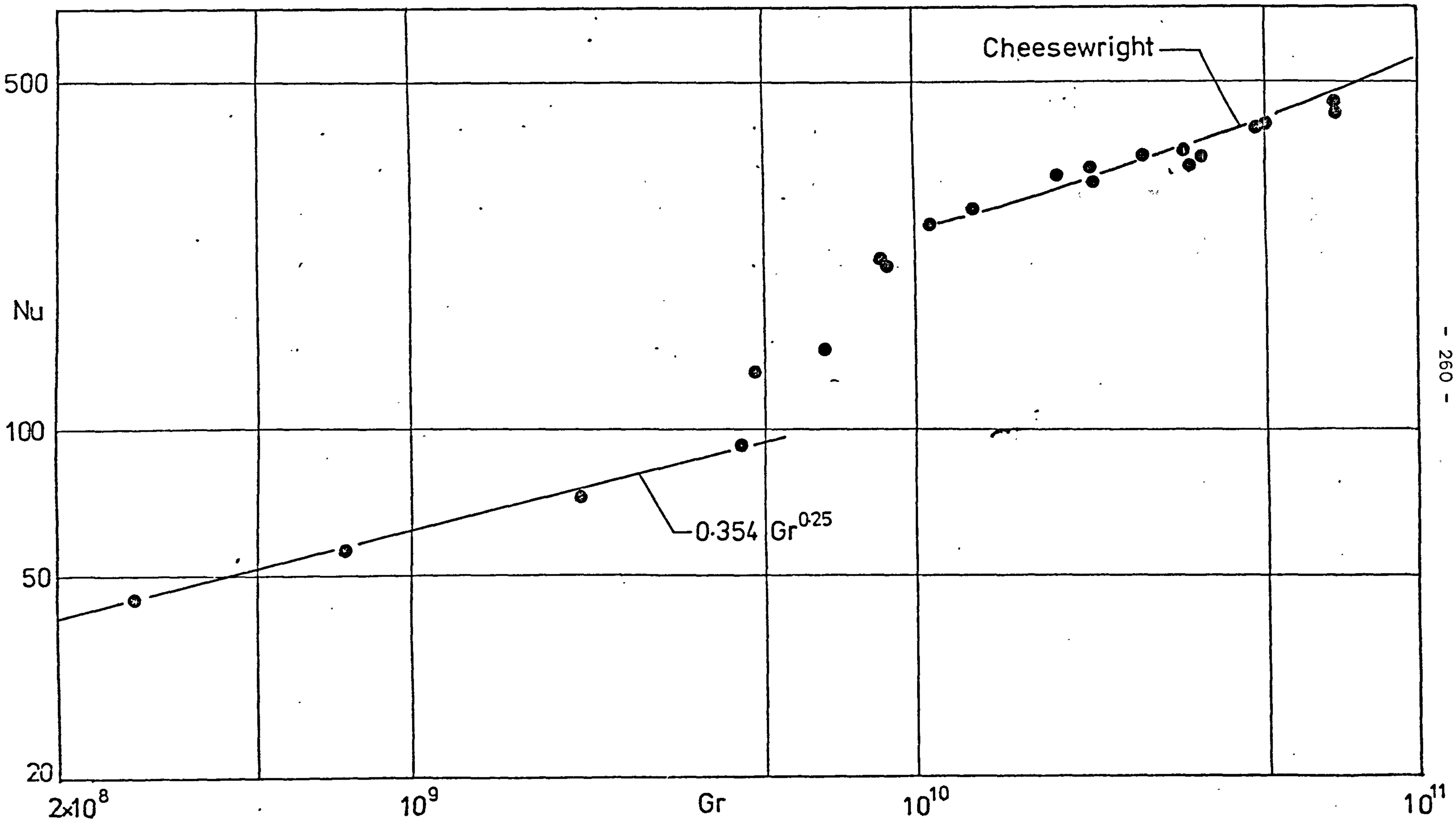

Fig. 8.1 Streamwise development of Nusselt number

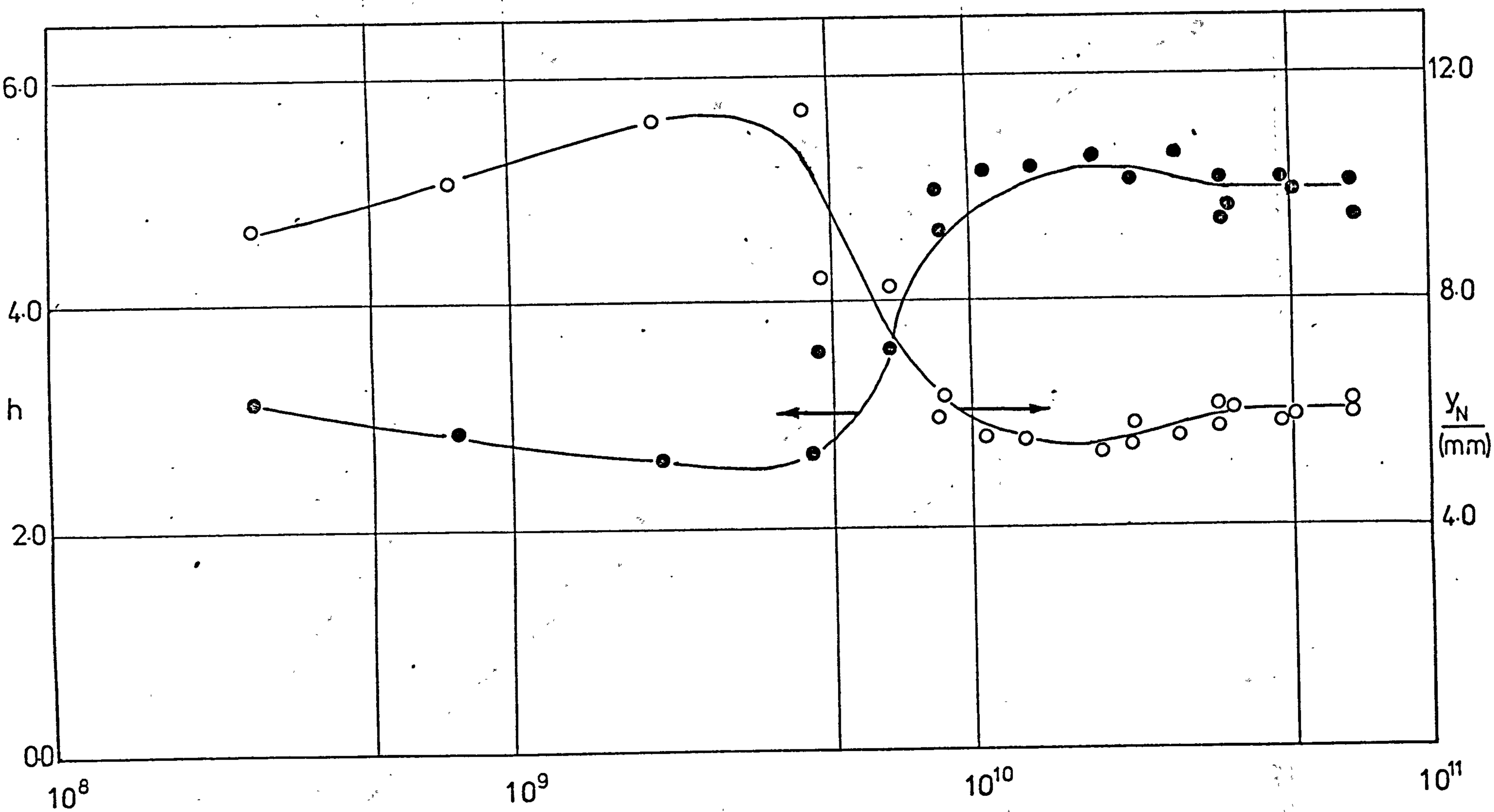

Fig. 8.2 Streamwise development of heat transfer coefficient and y_N.

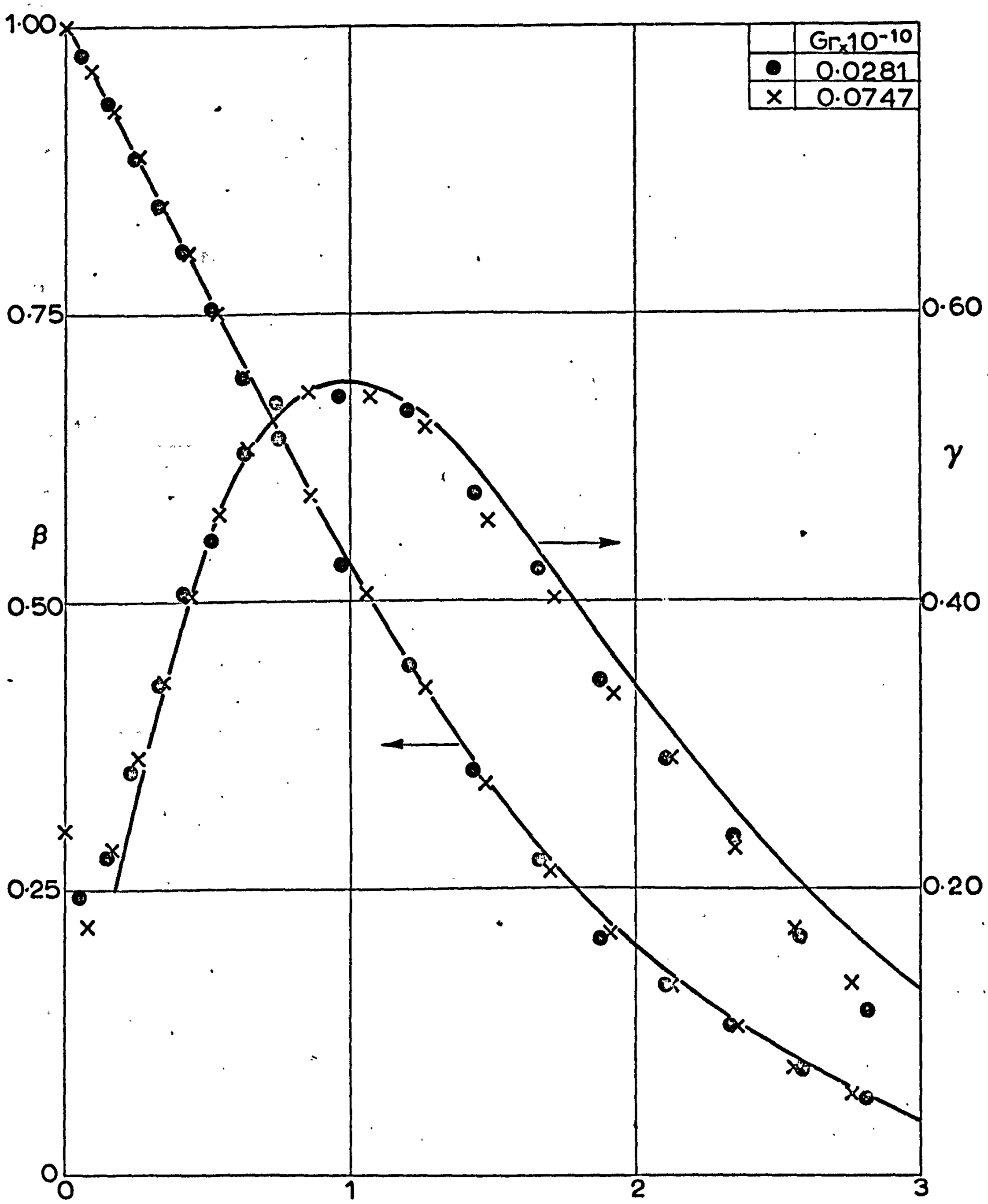

Fig.8·3 Mean temperature and velocity profiles across a laminar boundary layer

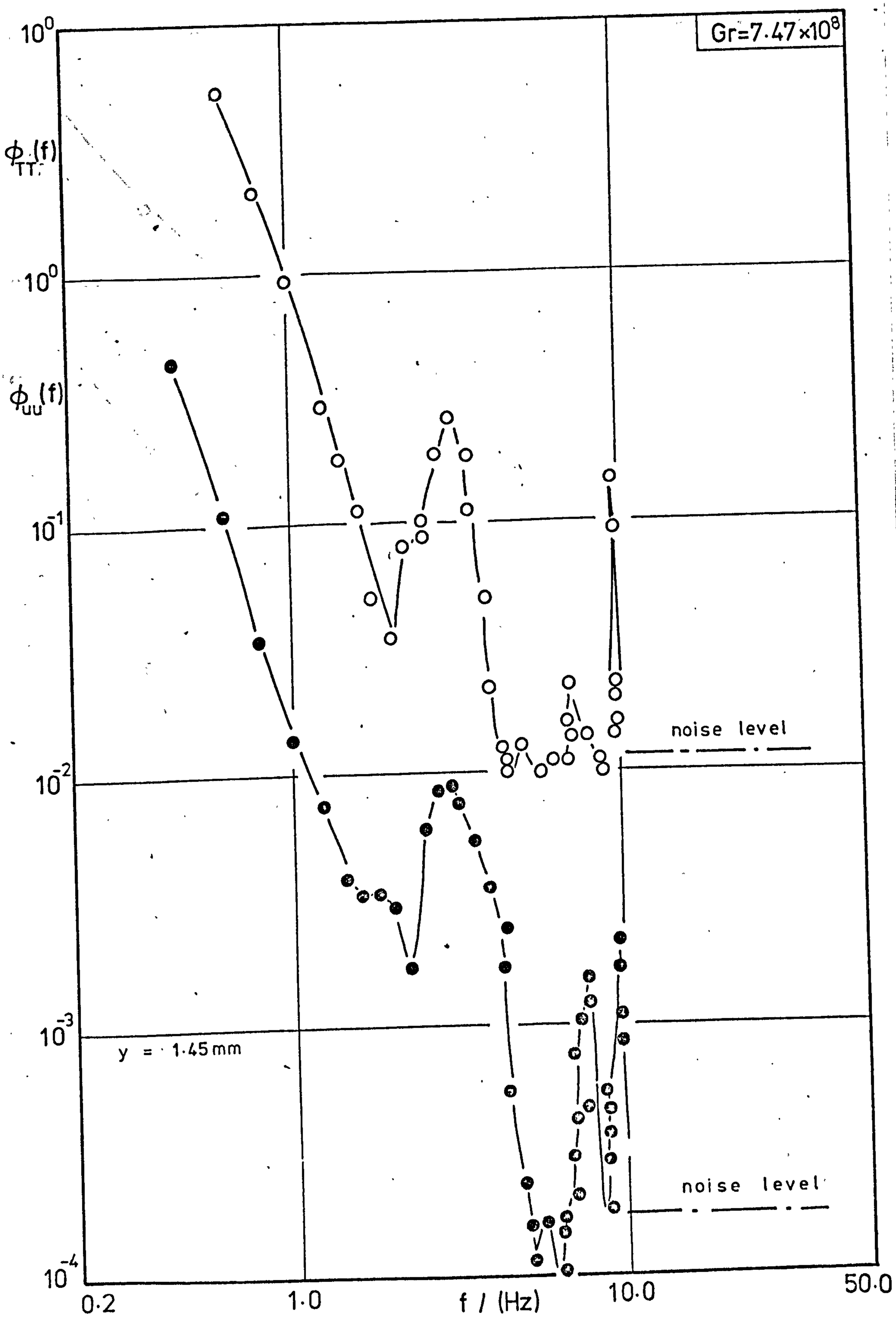

Fig. 8.4 Power spectra distributions

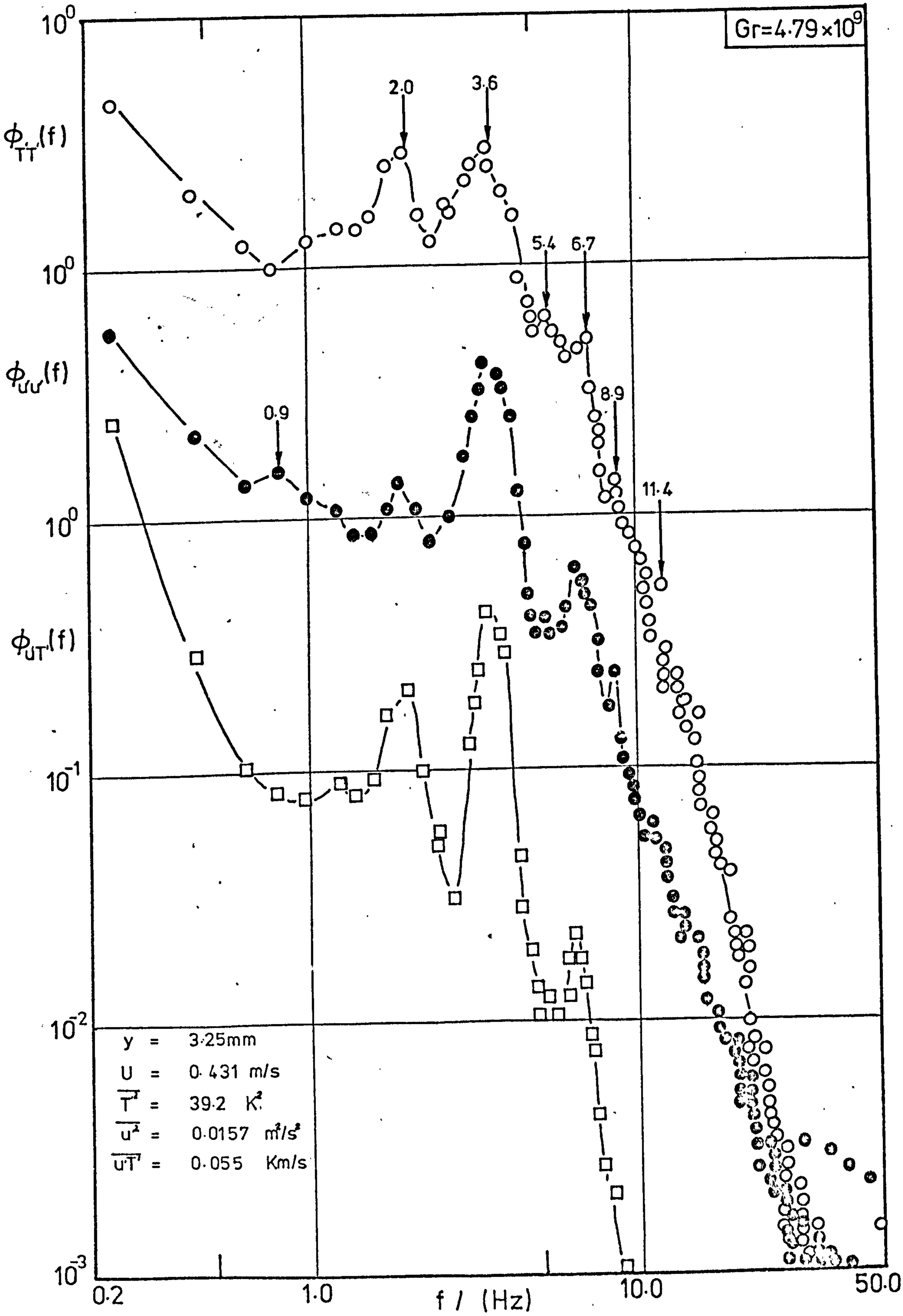

Fig. 8·5 Power spectra distributions

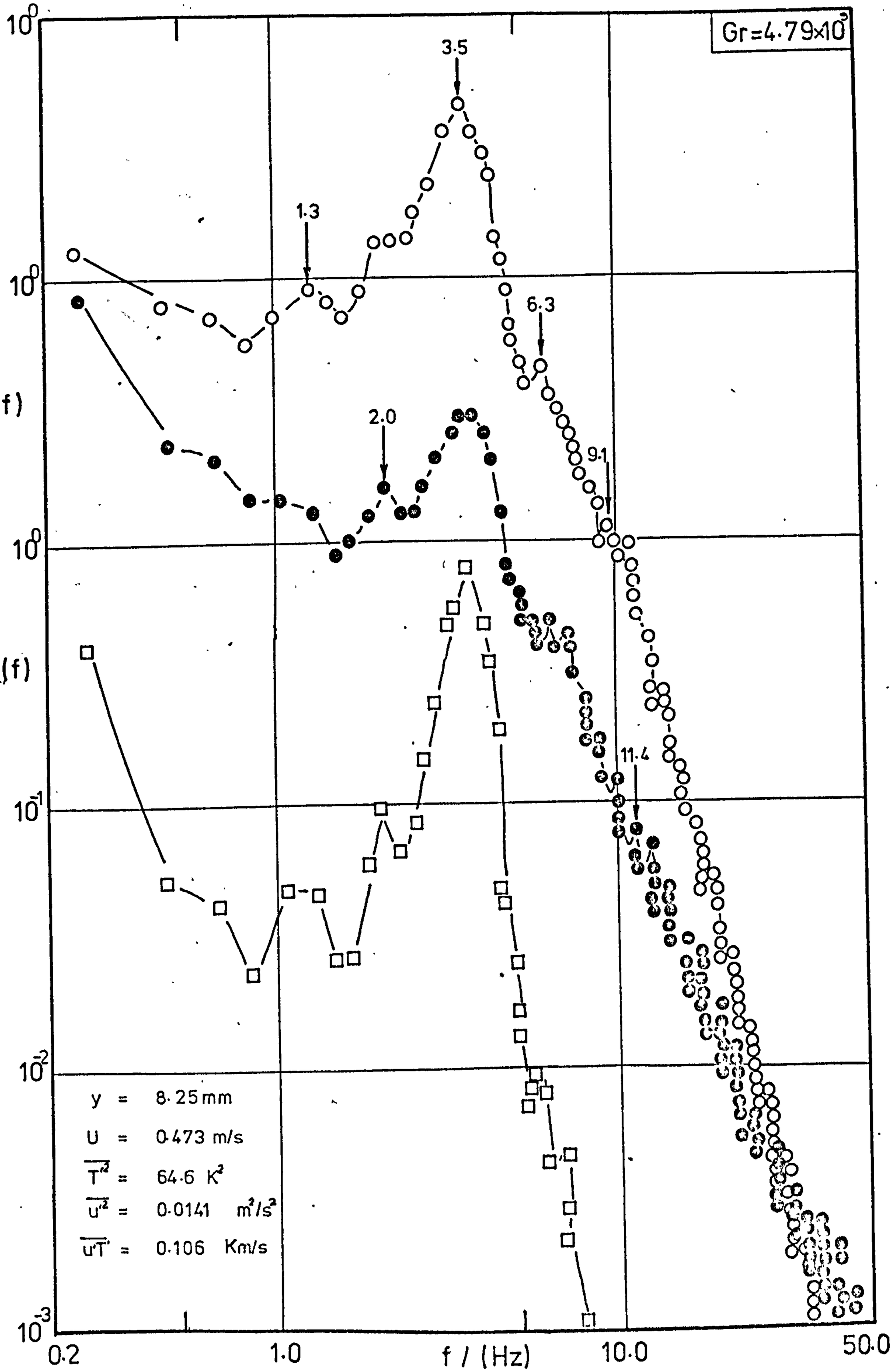

Fig. 8.6 Power spectra distributions

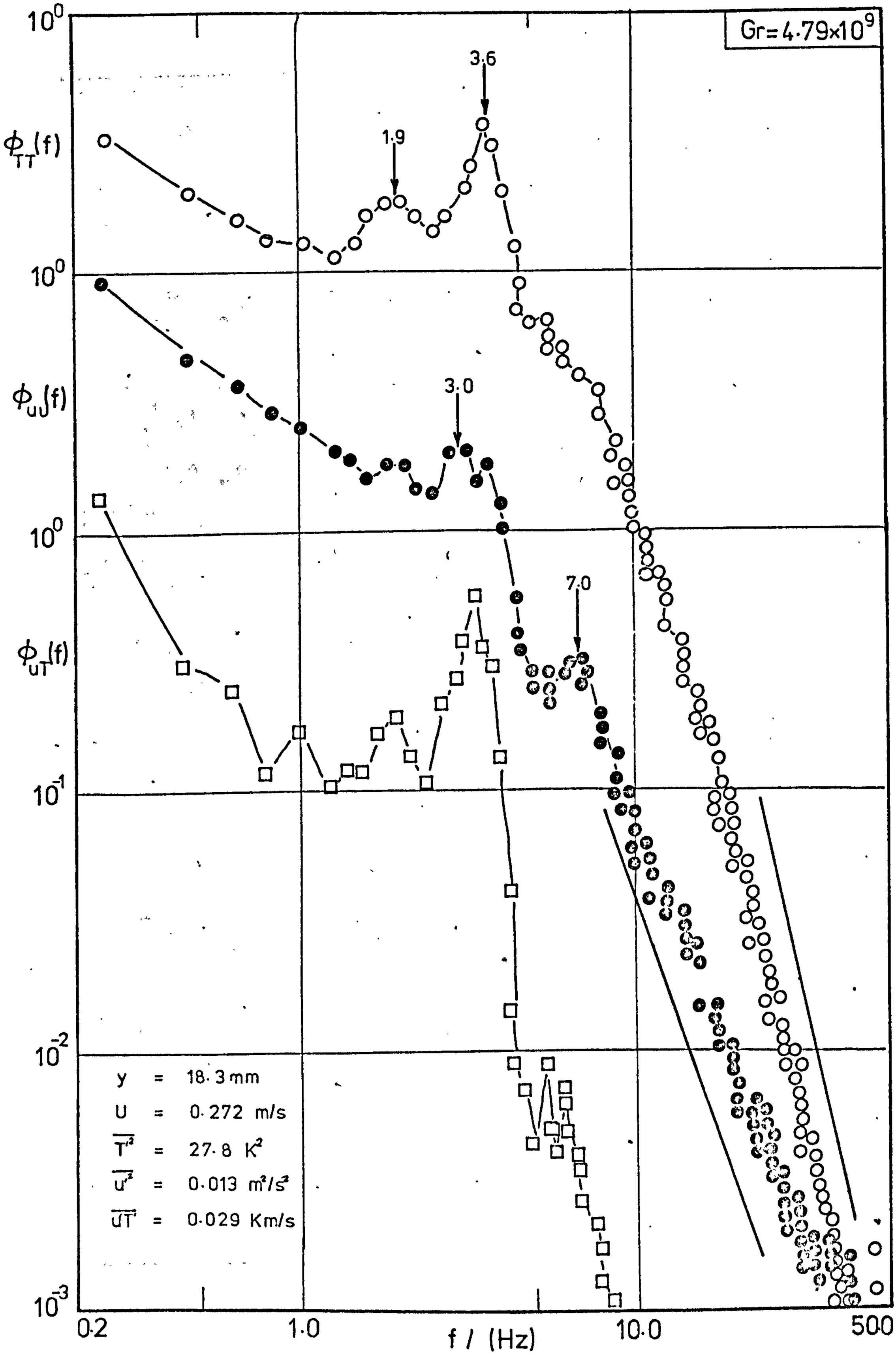

Fig. 8.7 Power spectra distributions

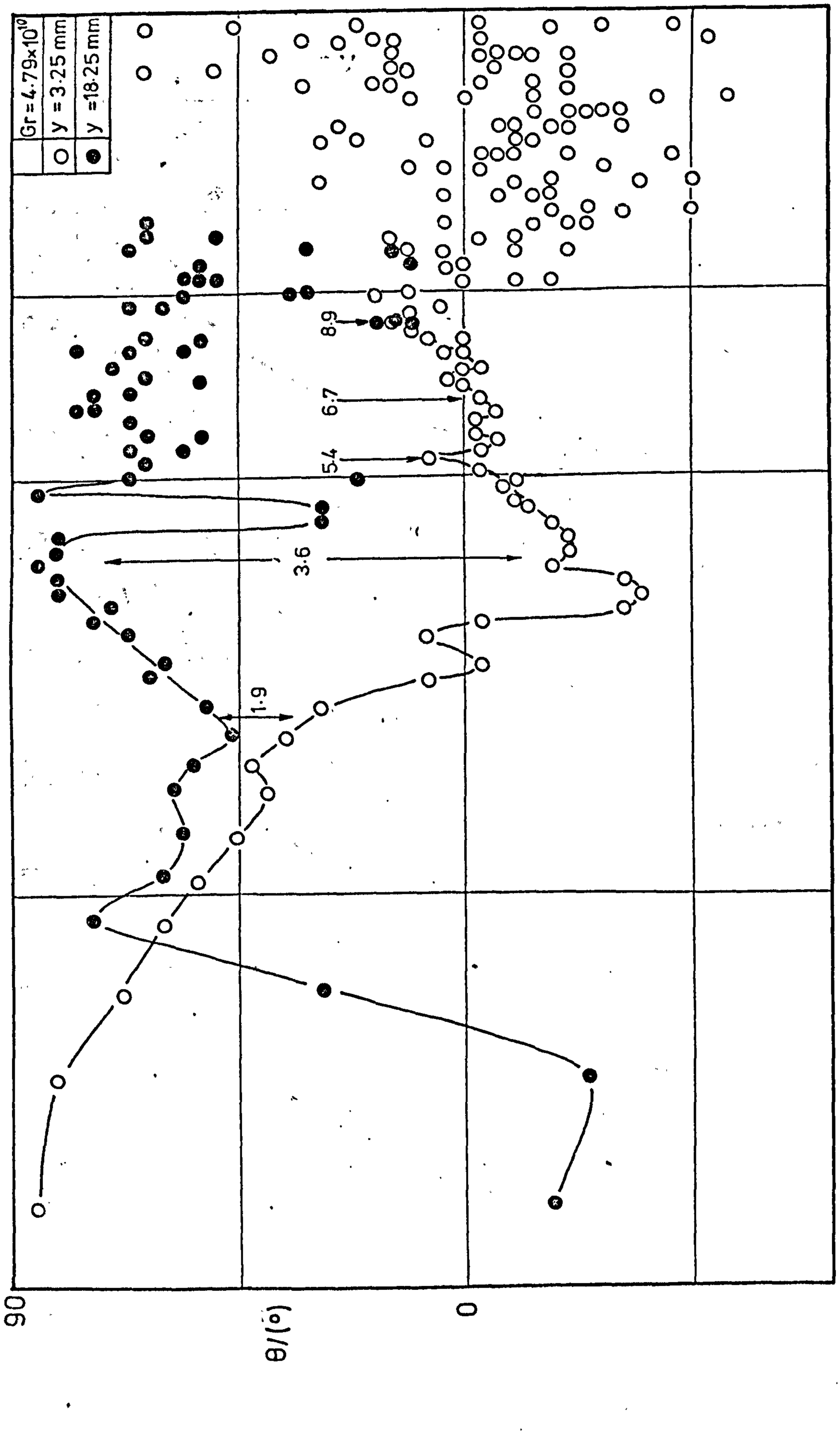

Figure 8.8 Phase Angle Distribution of $\overline{u'T'}$

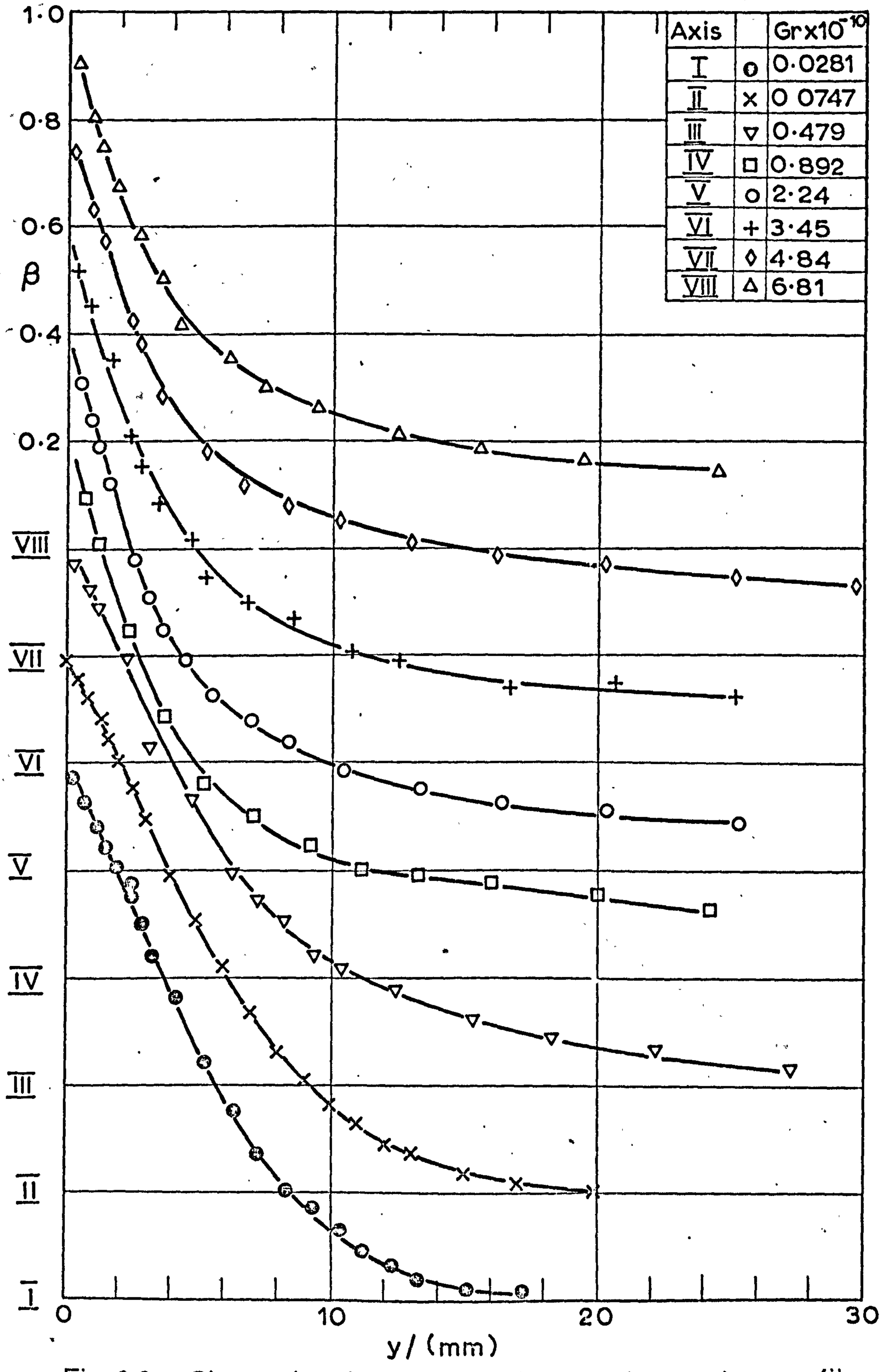

Fig. 8.9 Streamwise development of mean temperature profiles

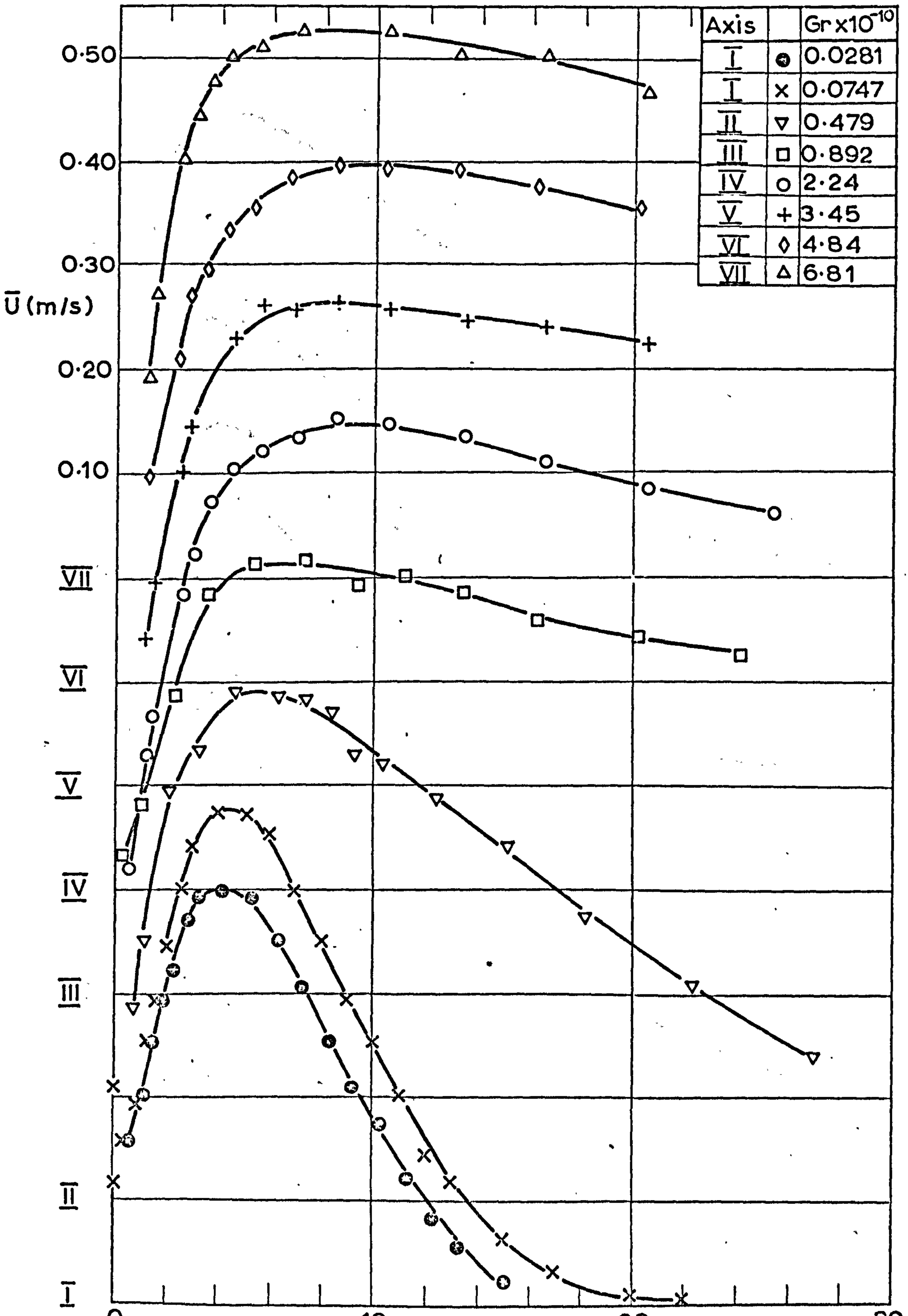

Fig. 8.10 Streamwise development of mean velocity profiles

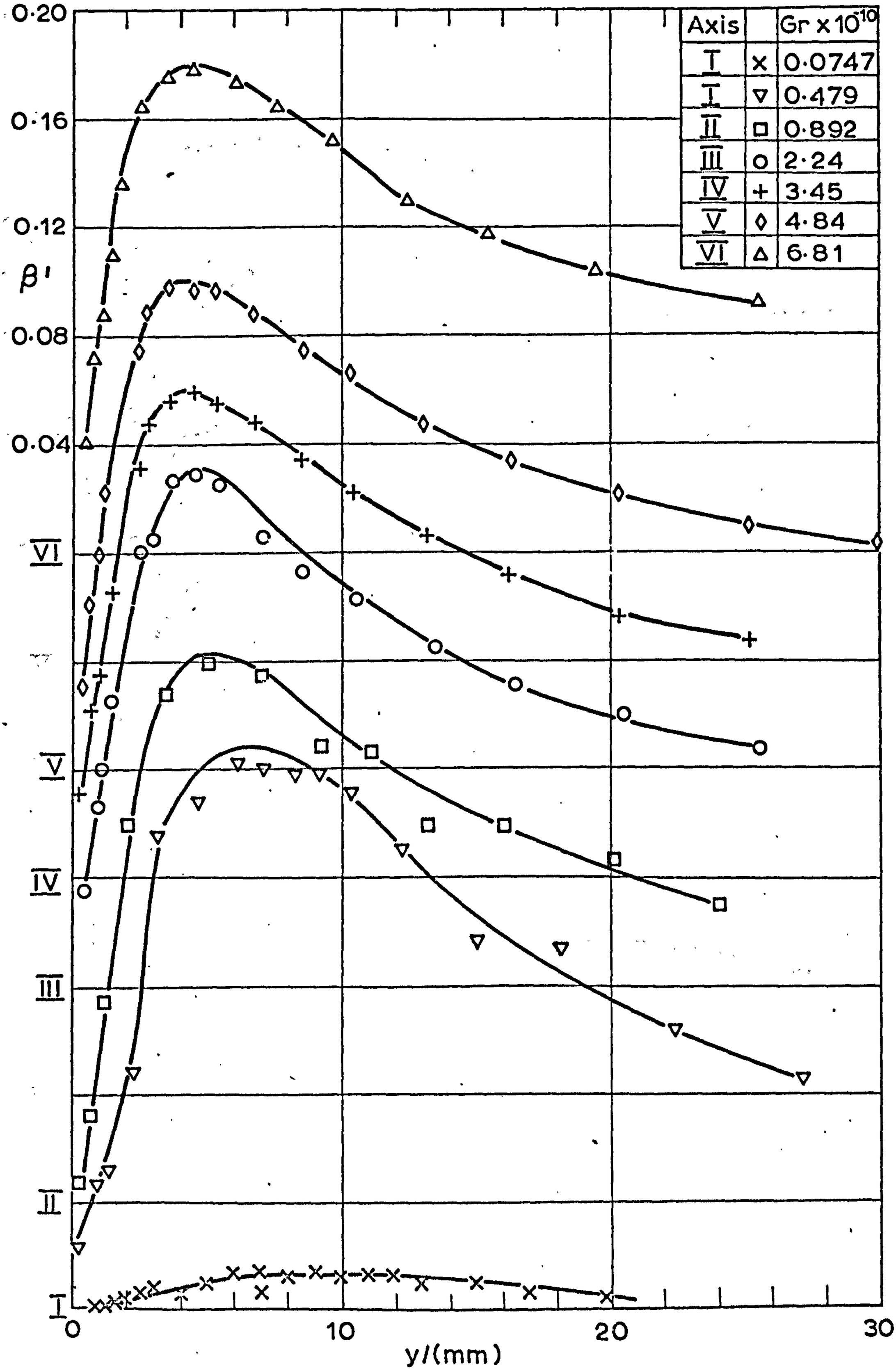

Fig. 8.11 Streamwise development of β' profiles

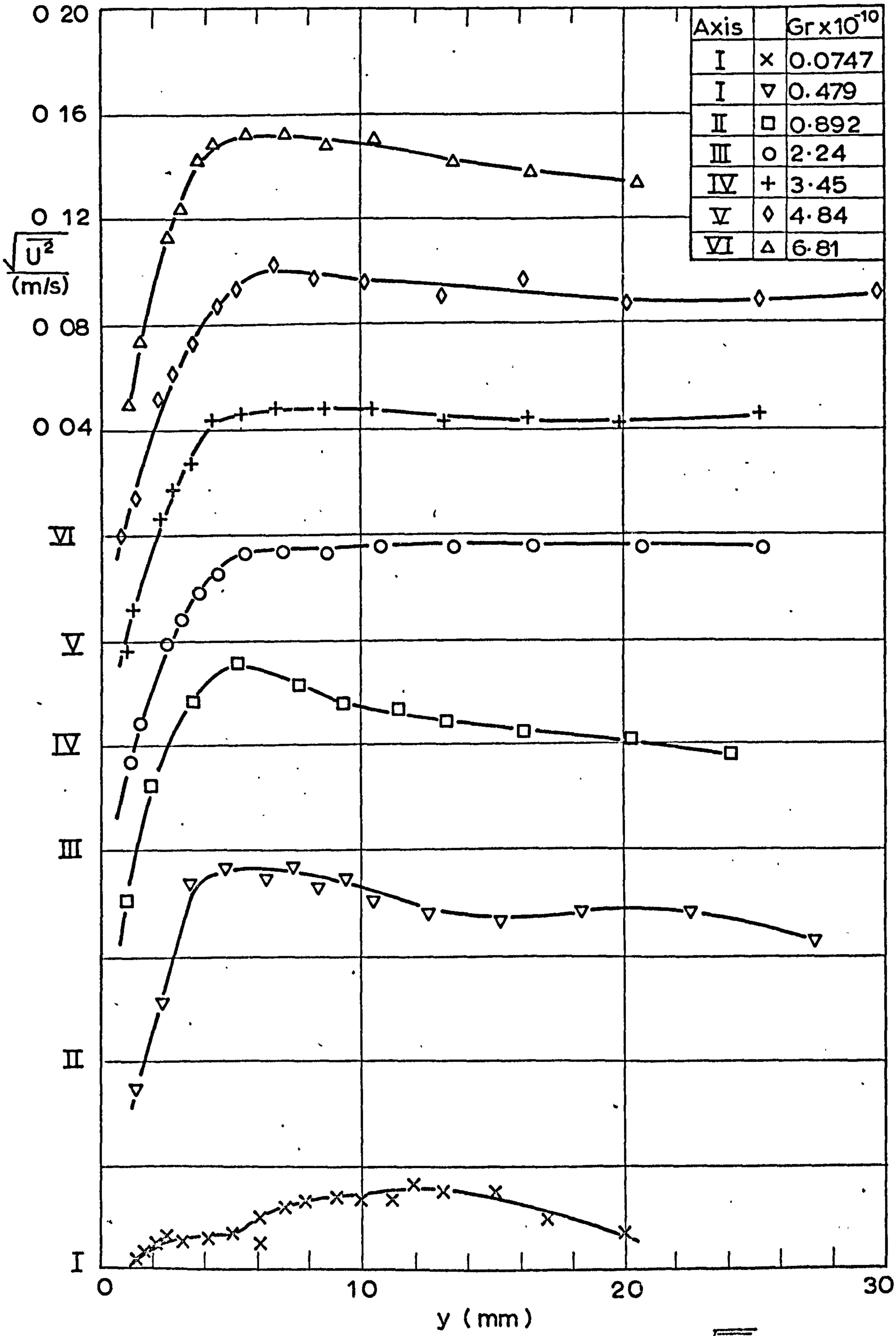

Fig. 8.12 Streamwise development of $\sqrt{\overline{u'^2}}$ profiles

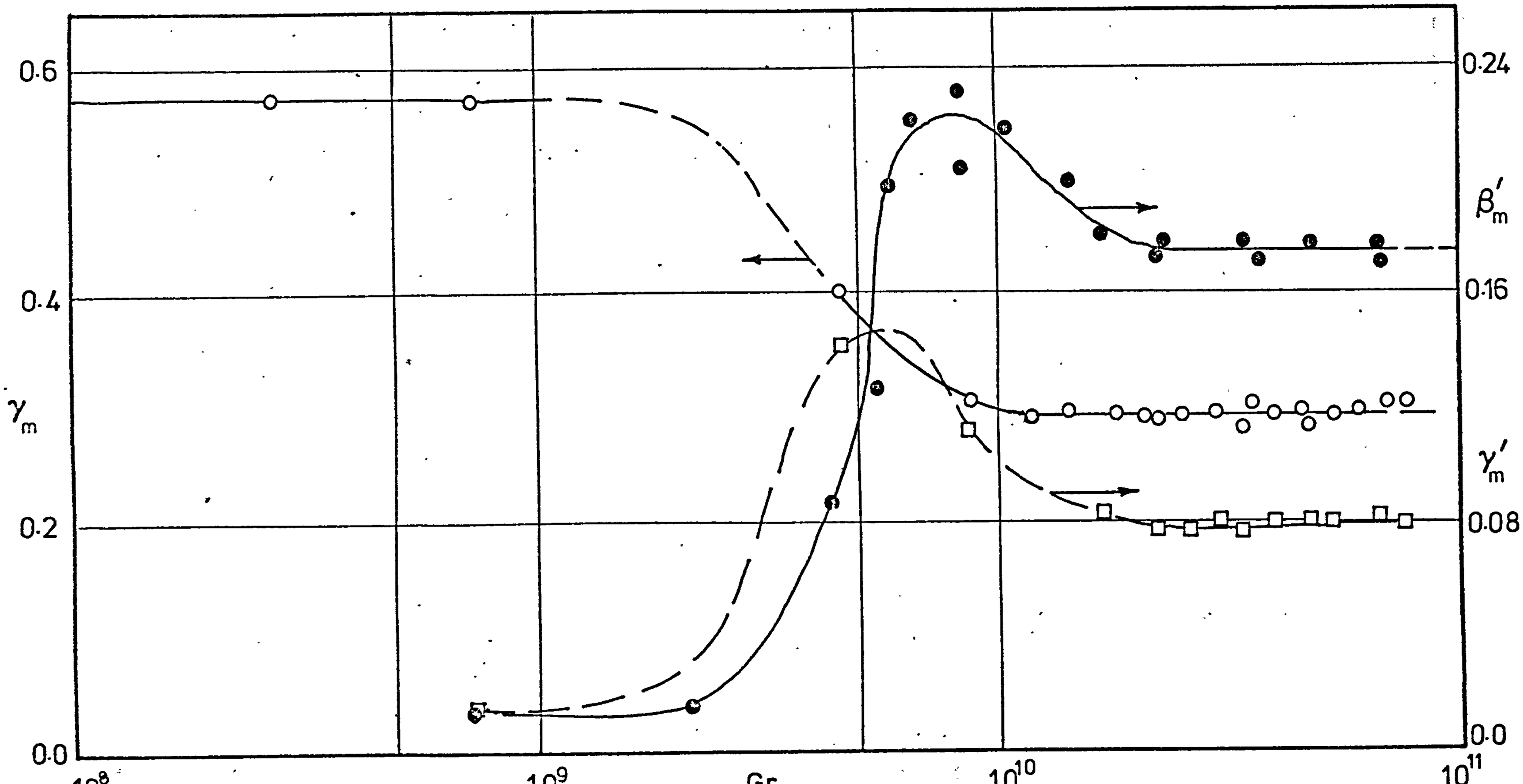

Figure 8.13 Streamwise Flow Development of γ_m, γ'_m and β'_m

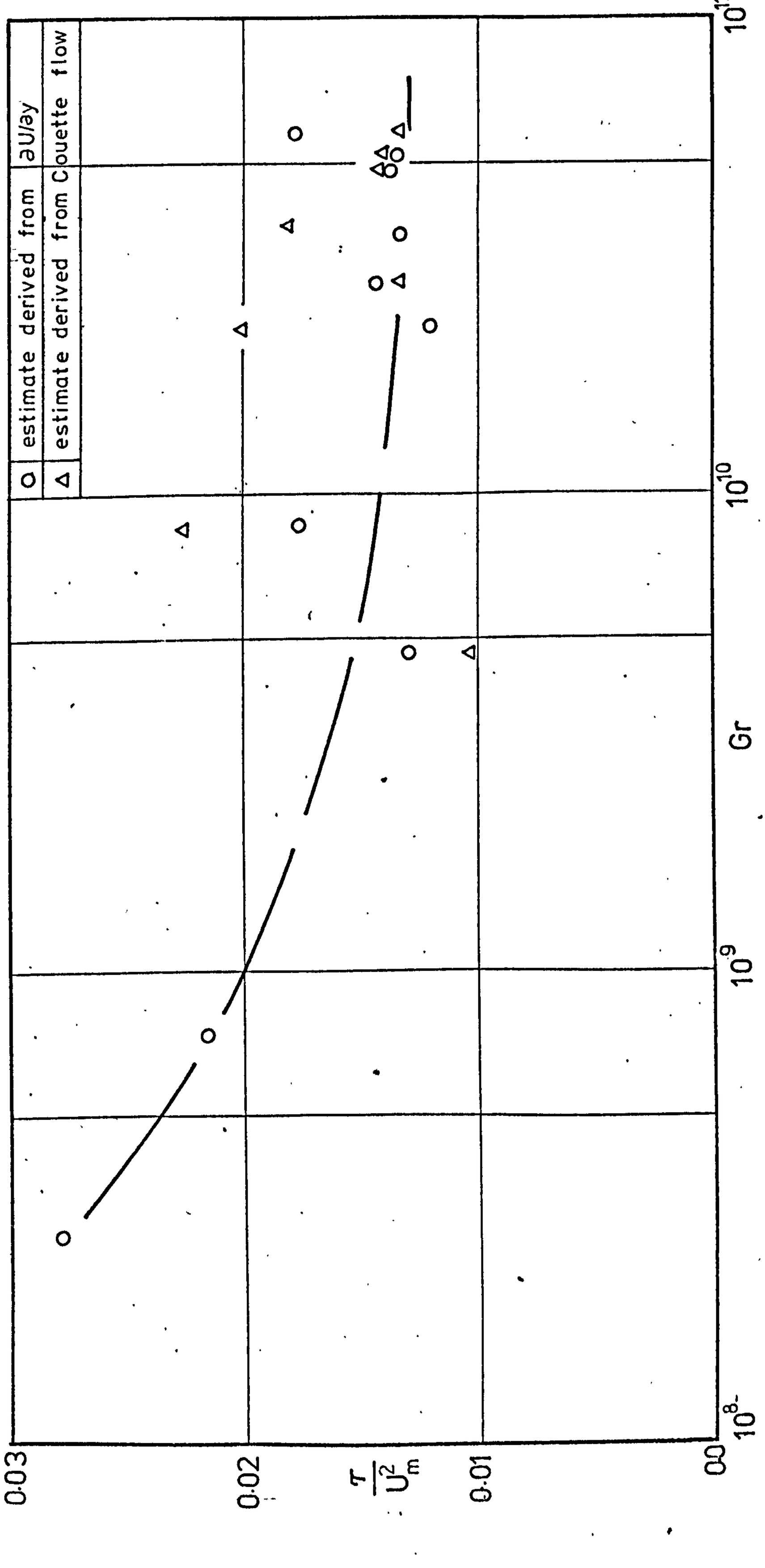

Fig. 8.14a Streamwise distribution of wall shear stress

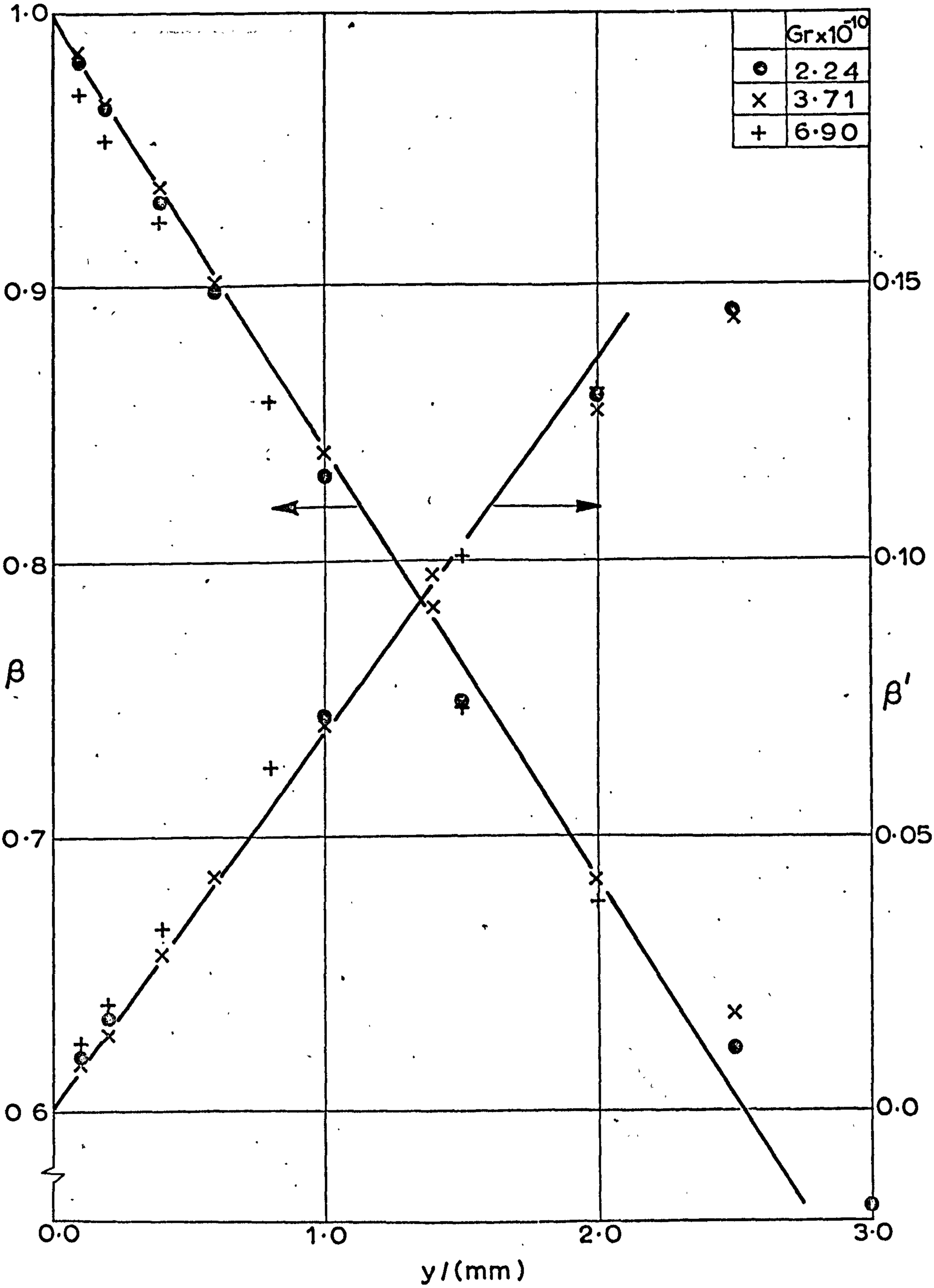

Fig. 8.14b β and β' profiles very near the plate

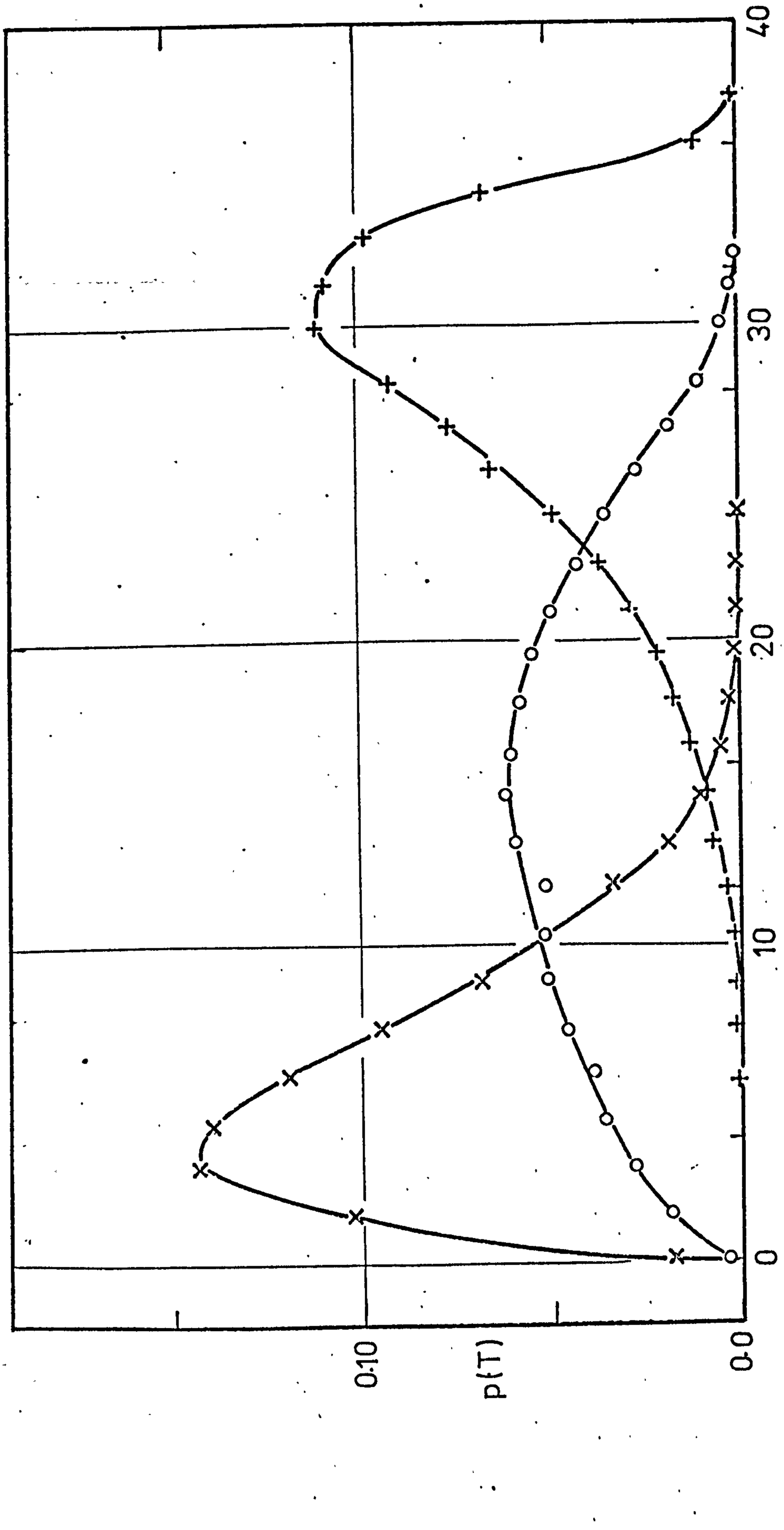
Representative probability density distributions of temperature
T / (K)
p(T)
0
10
20
30
40
0.0
0.10

Fig. 8.15

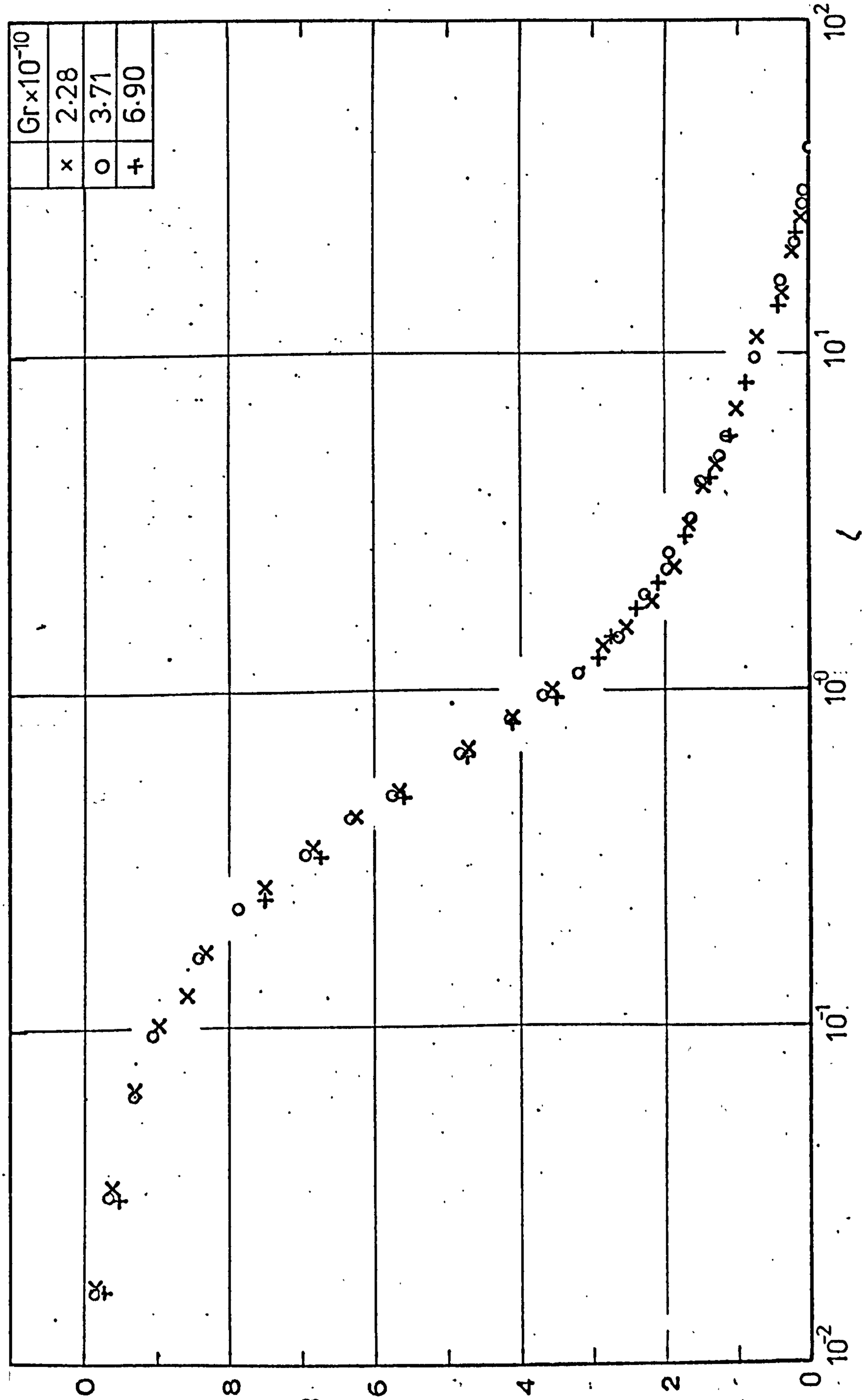
Gr×10⁻¹⁰
x 2.28
o 3.71
+ 6.90
1.0
0.8
0.6
0.4
0.2
0
β
10²
10¹
10⁰
10⁻¹
10⁻²
ζ
Mean temperature profiles across the boundary layer

Fig. 8.16

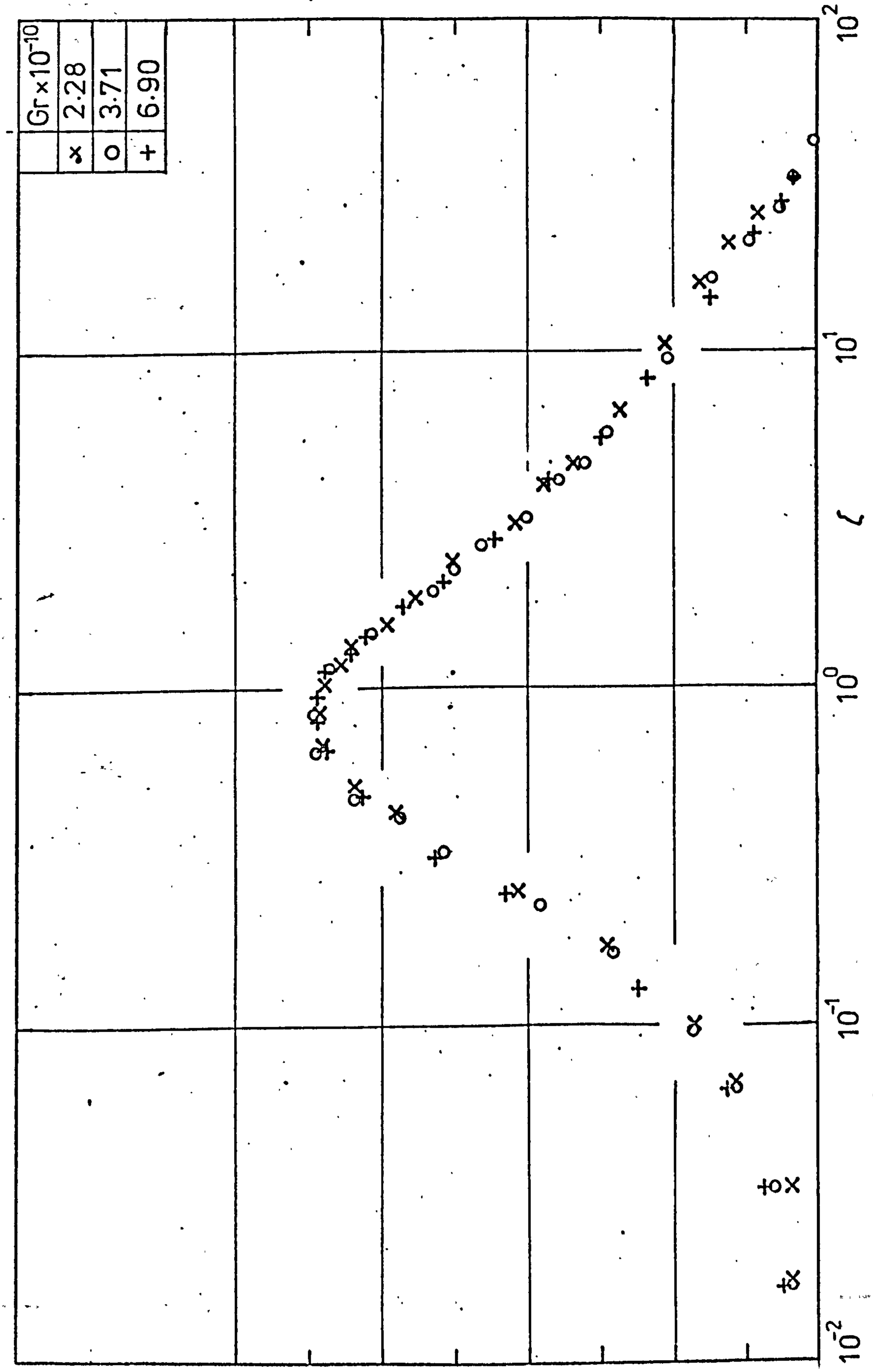
Gr x10^-10
x 2.28
o 3.71
+ 6.90
β' profiles across the boundary layer
β'
ζ
0.20
0.15
0.10
0.05
10^2
10^1
10^0
10^-1
10^-2

Fig. 8.17

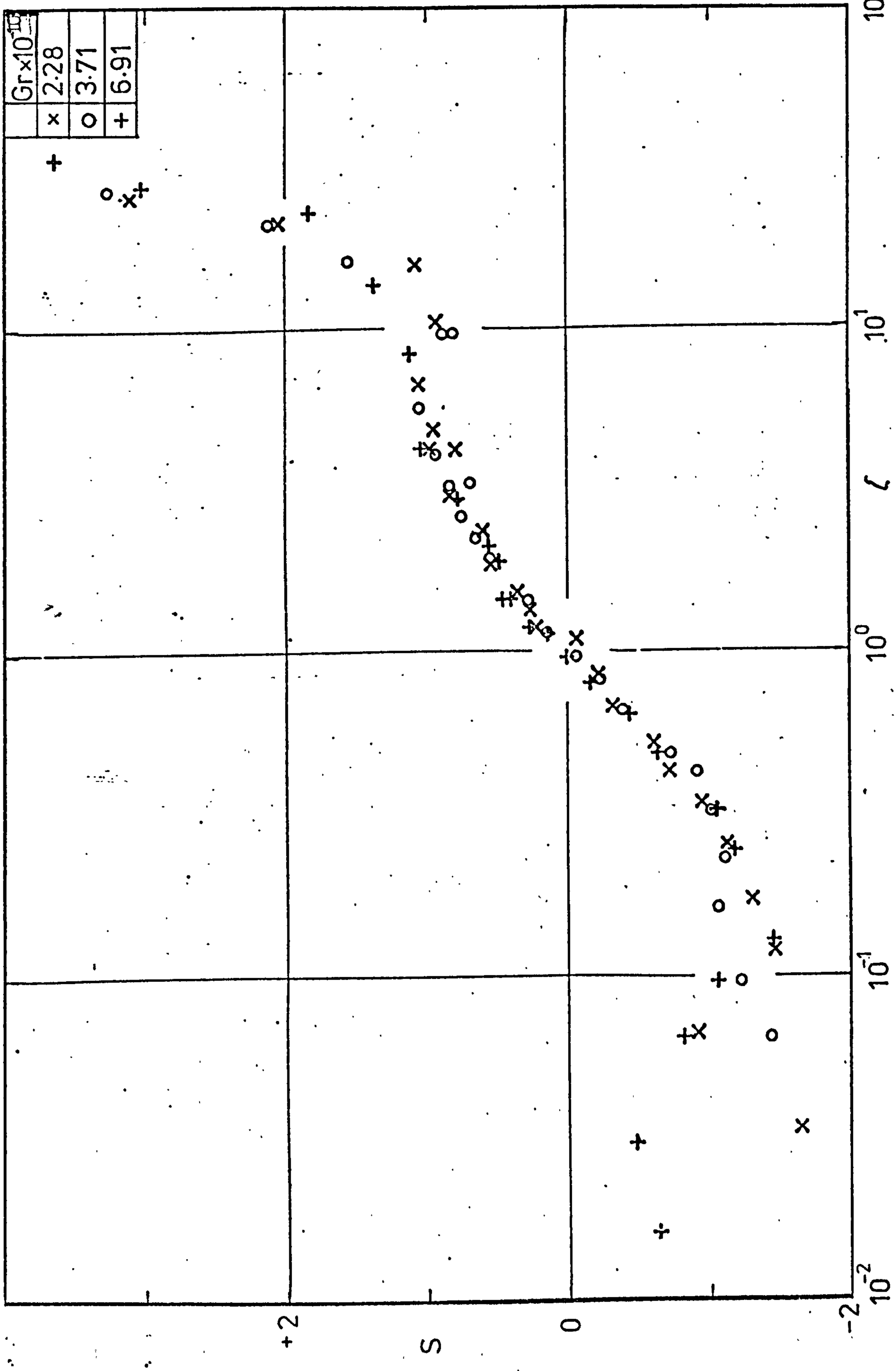
Gr×10⁻¹⁰
x 2.28
o 3.71
+ 6.91
10²
10¹
10⁰
10⁻¹
10⁻²
ζ
Skewness factor profiles across the boundary layer
+2
S
0
-2

Fig. 8.18

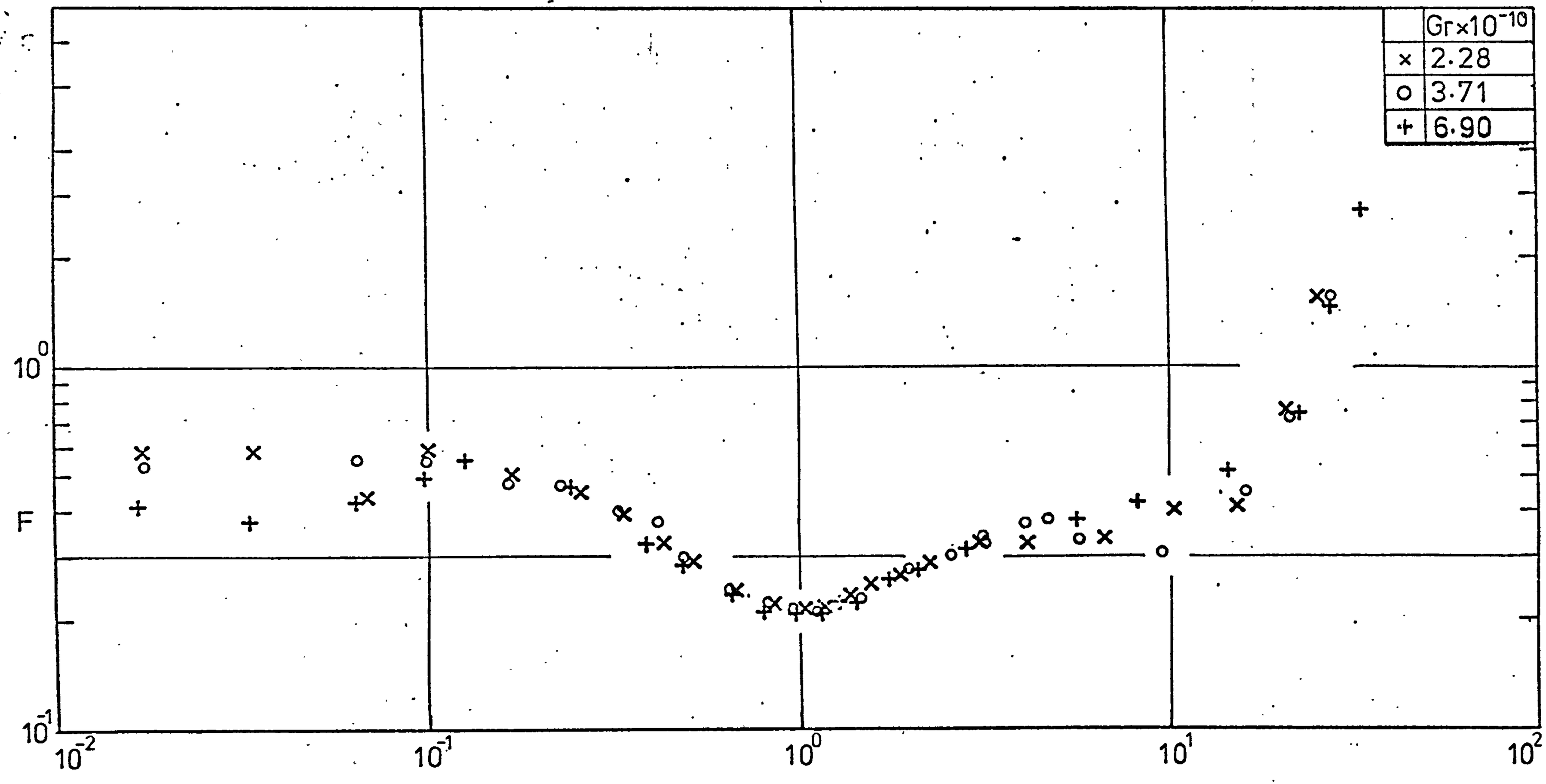

Fig.8.19 Flatness factors (F) profiles across the boundary layer

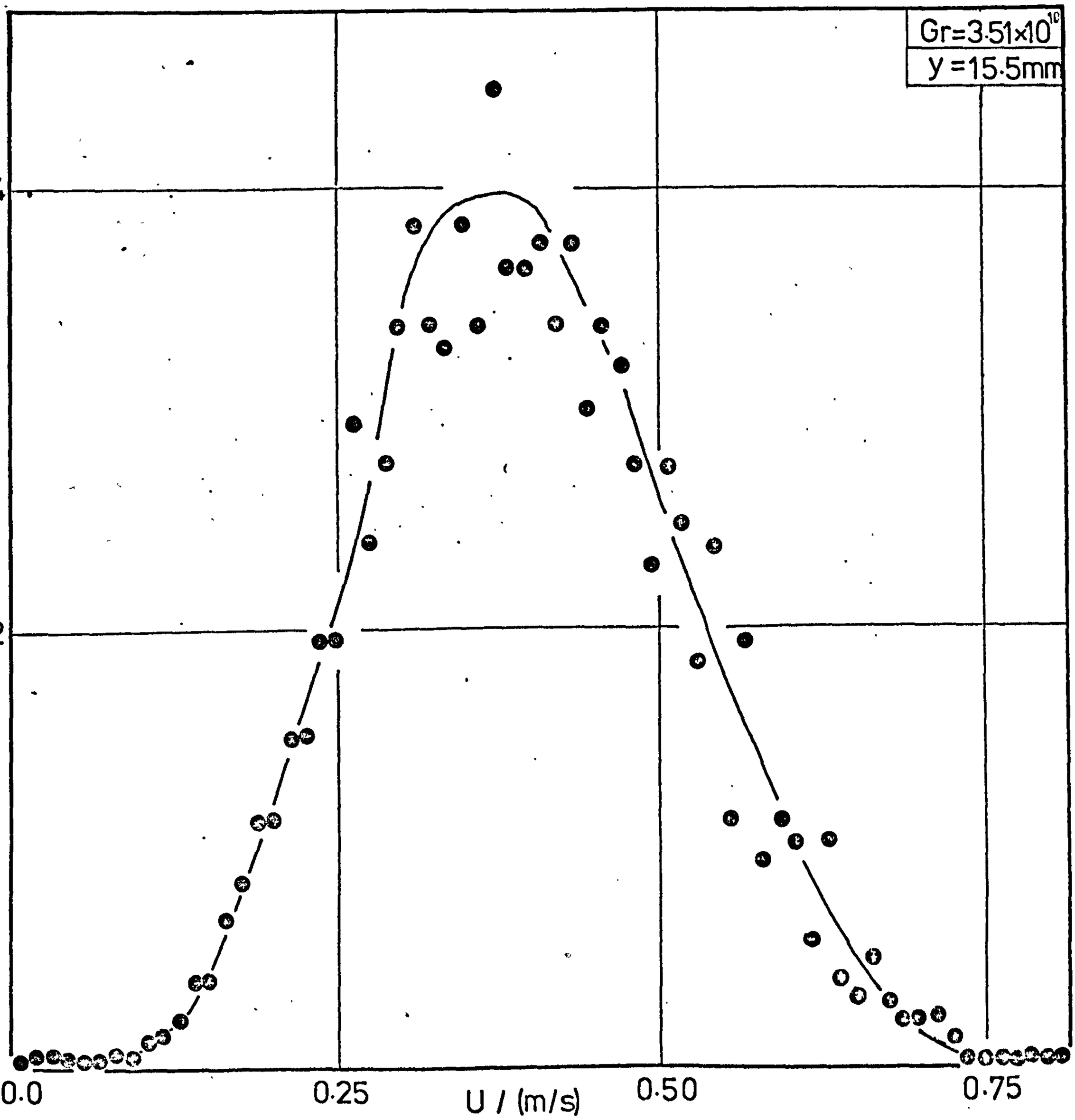

Fig.8.20 Representative probability density distribution of velocity

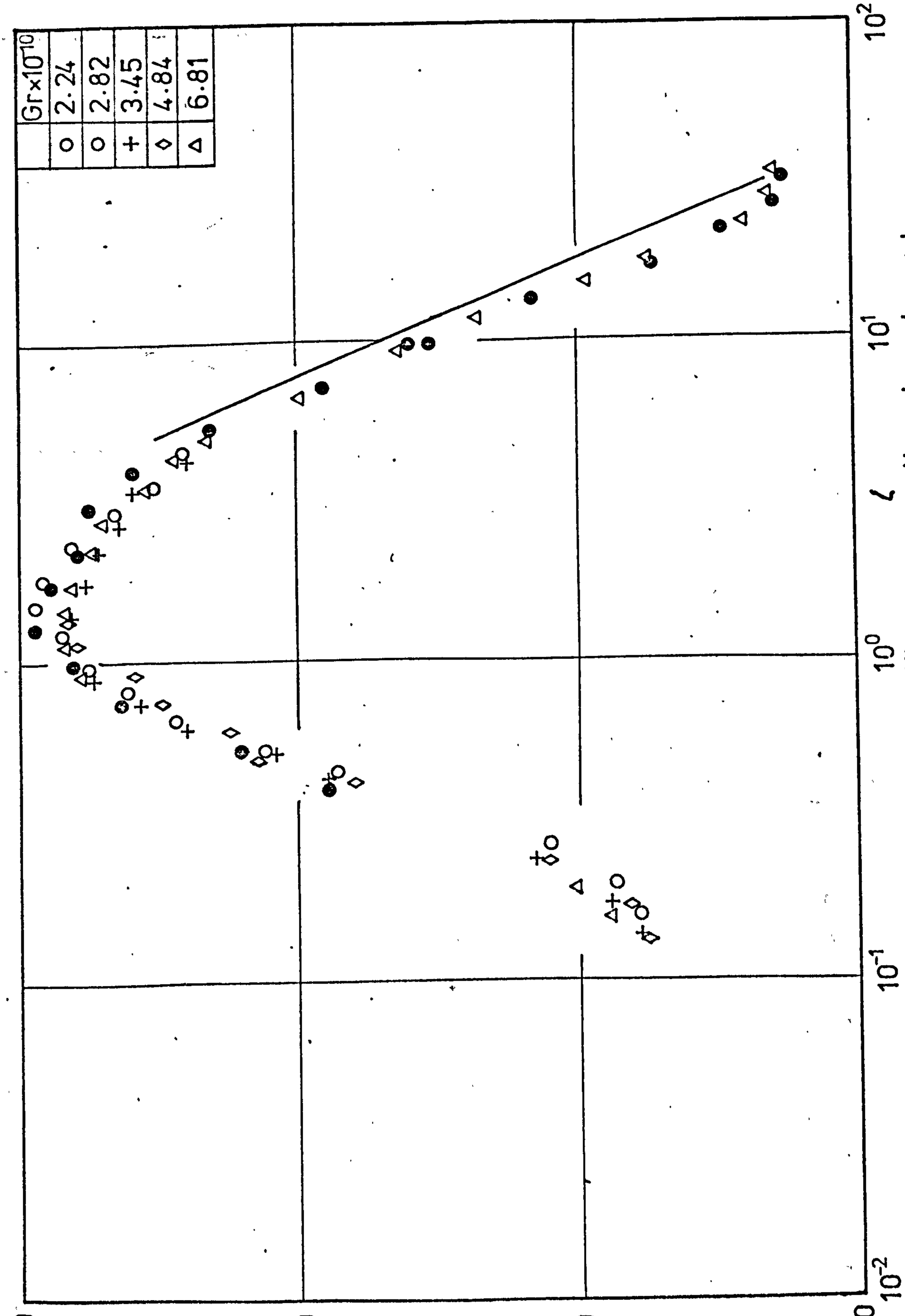

Fig. 8.21 Mean Velocity P

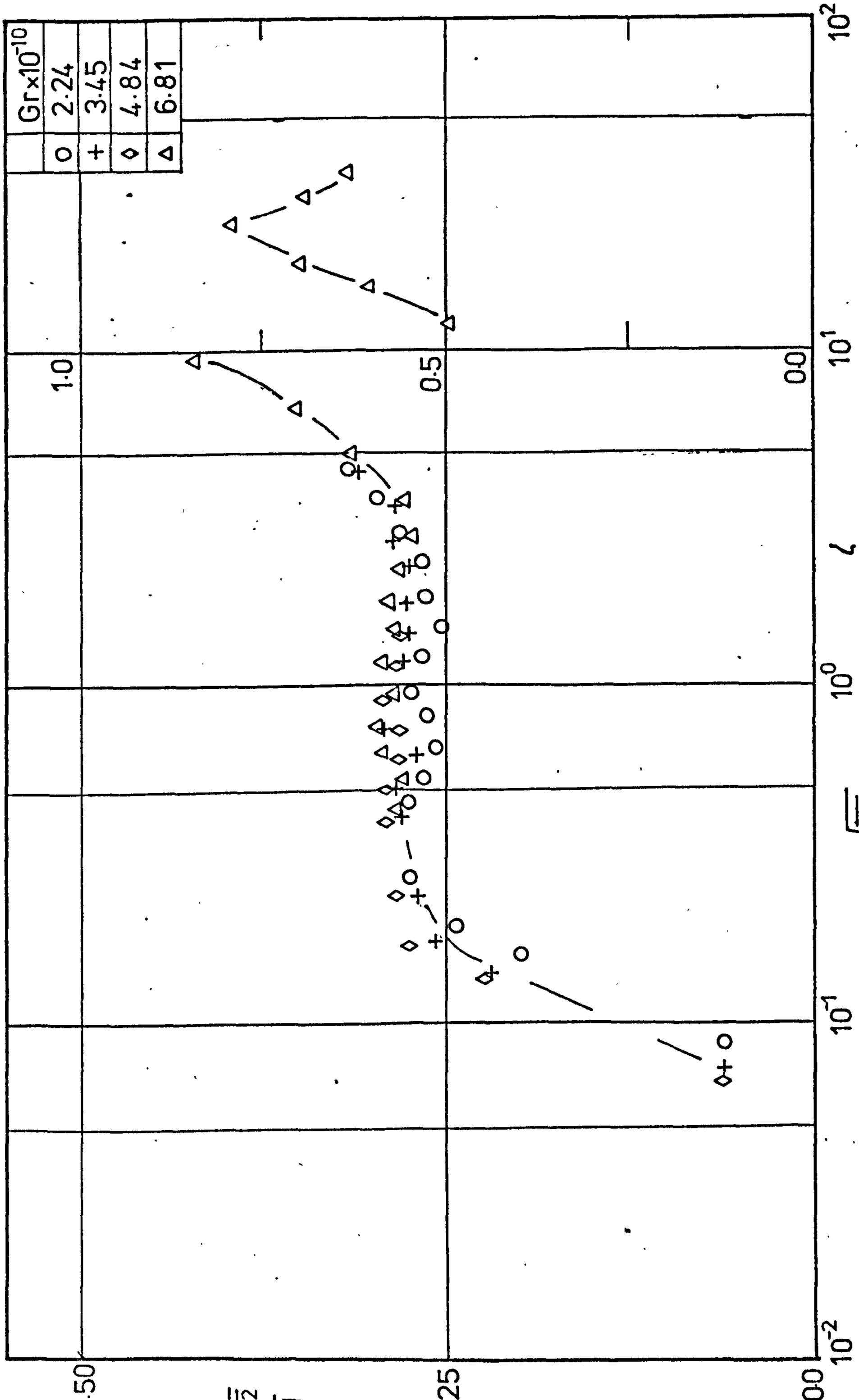
Gr×10⁻¹⁰
2.24
3.45
4.84
6.81
o
+
◇
△
1.0
0.5
0.0
0.50
0.25
0.0
10²
10¹
10⁰
10⁻¹
10⁻²
√u'²/U
ℓ
√u'²/U, profiles across the boundary layer

Figure 8.22

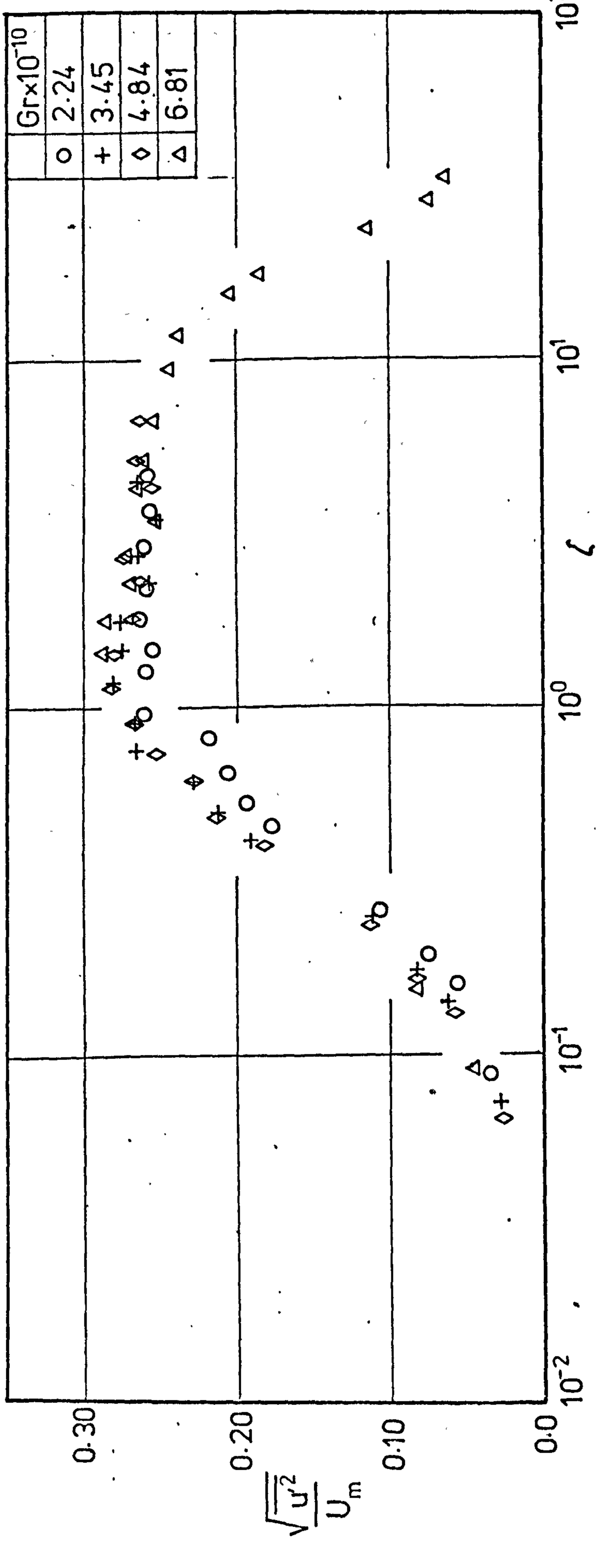

Fig. 8.23 $\frac{\sqrt{\overline{u'^2}}}{U_m}$ profiles across the boundary layer

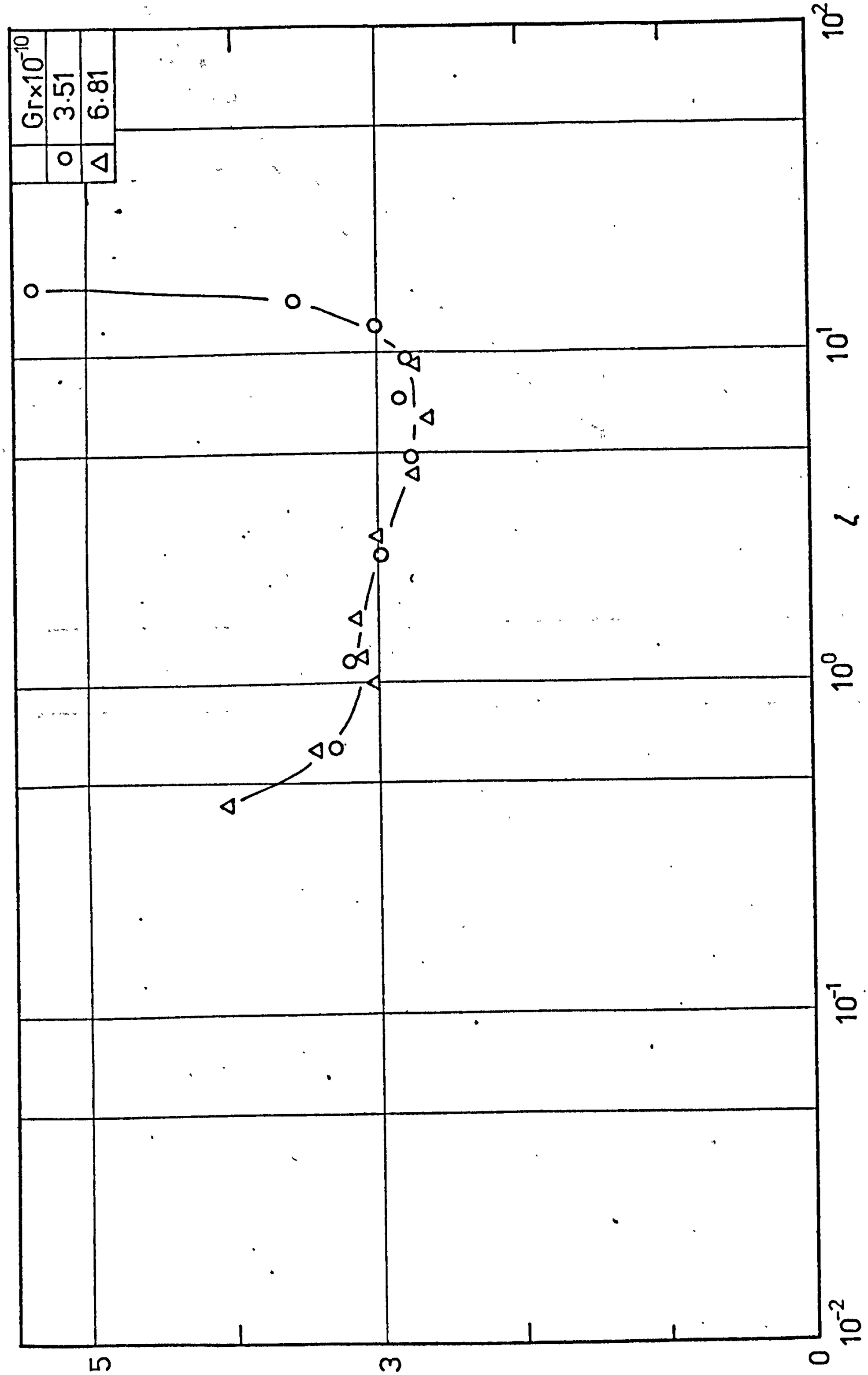

Fig 8.24 Flatness Factor profiles across the boundary layer

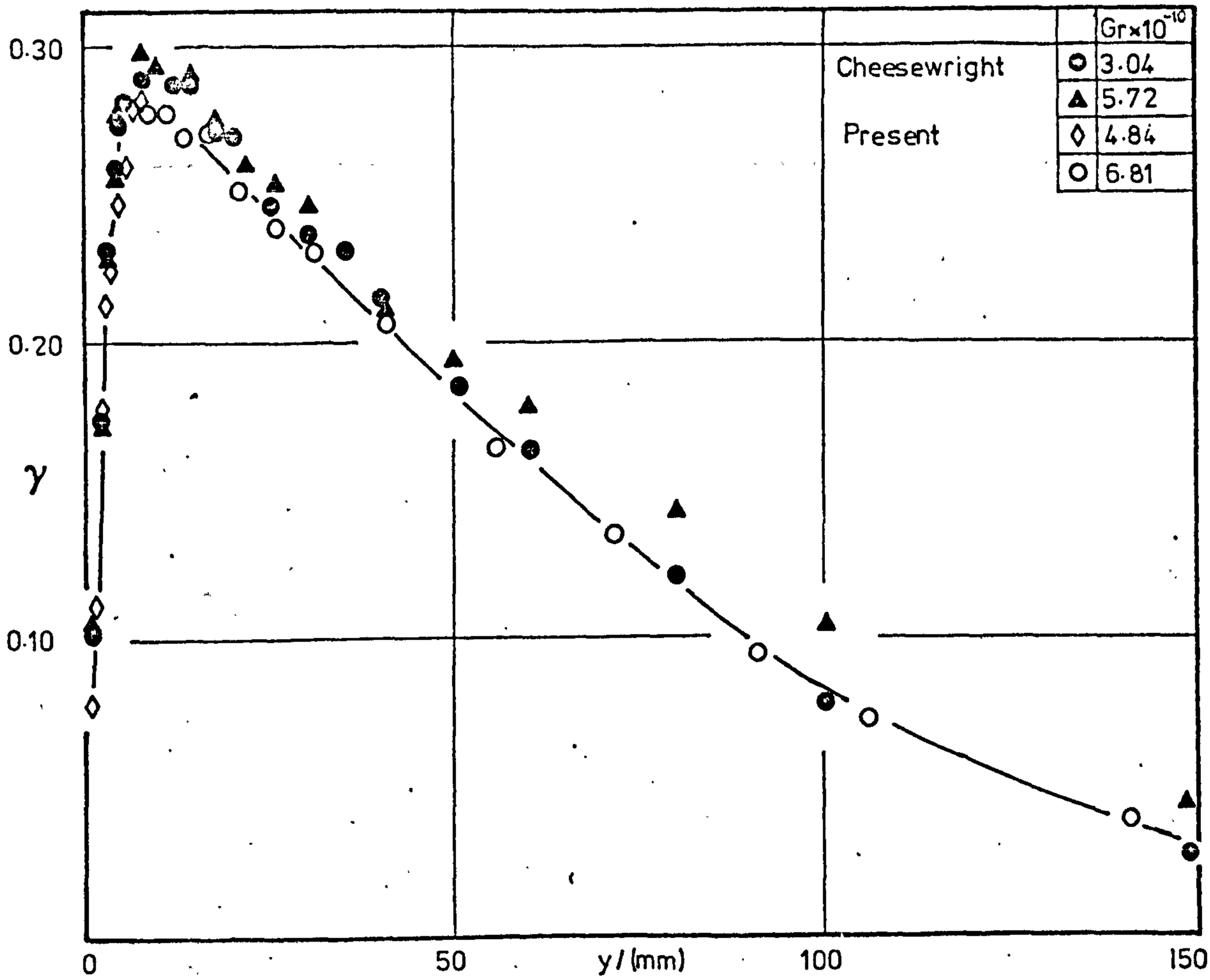

Fig. 8-25 Comparison of mean velocity data

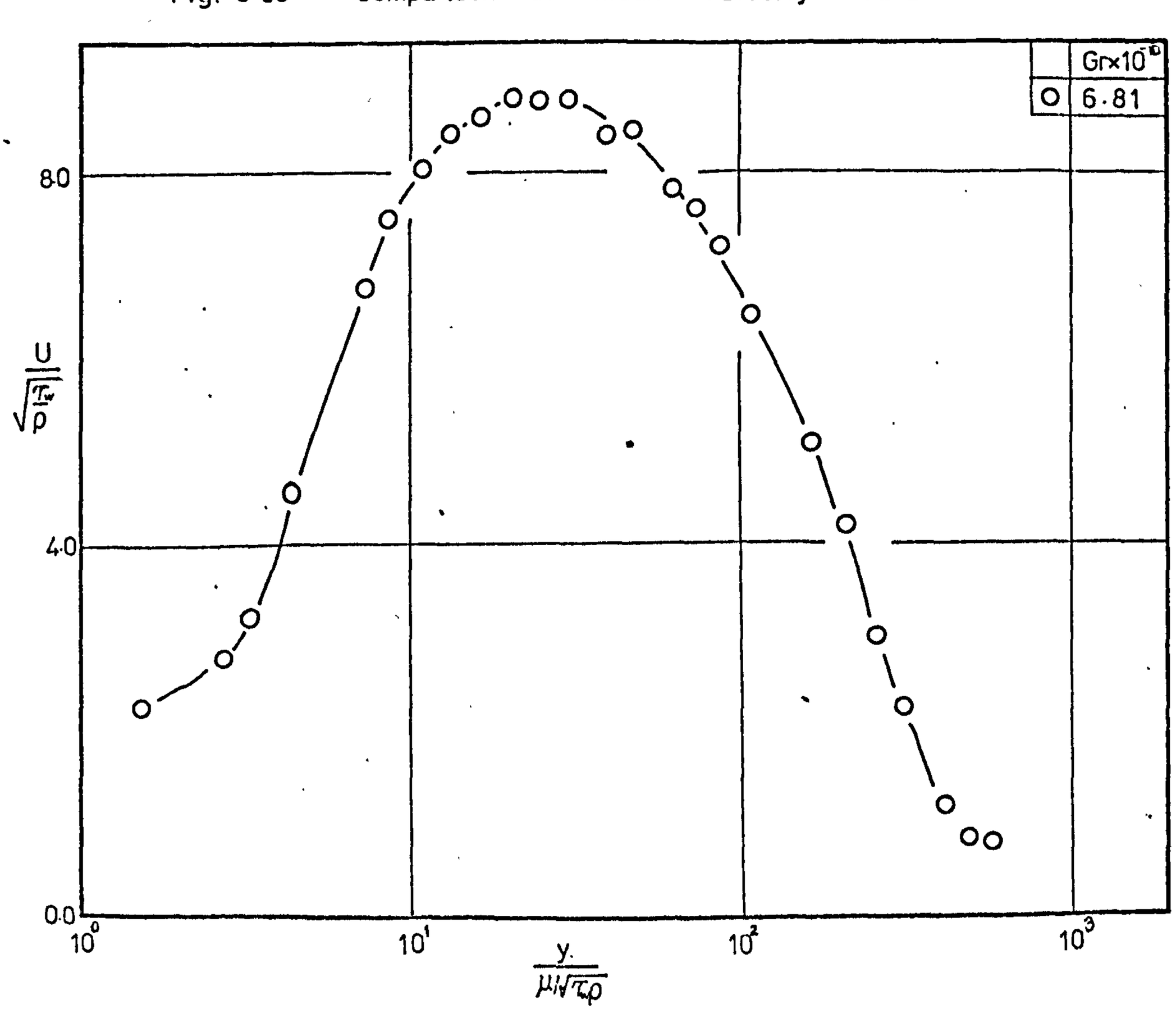

Fig. 8-26 Mean velocity profile across the boundary layer

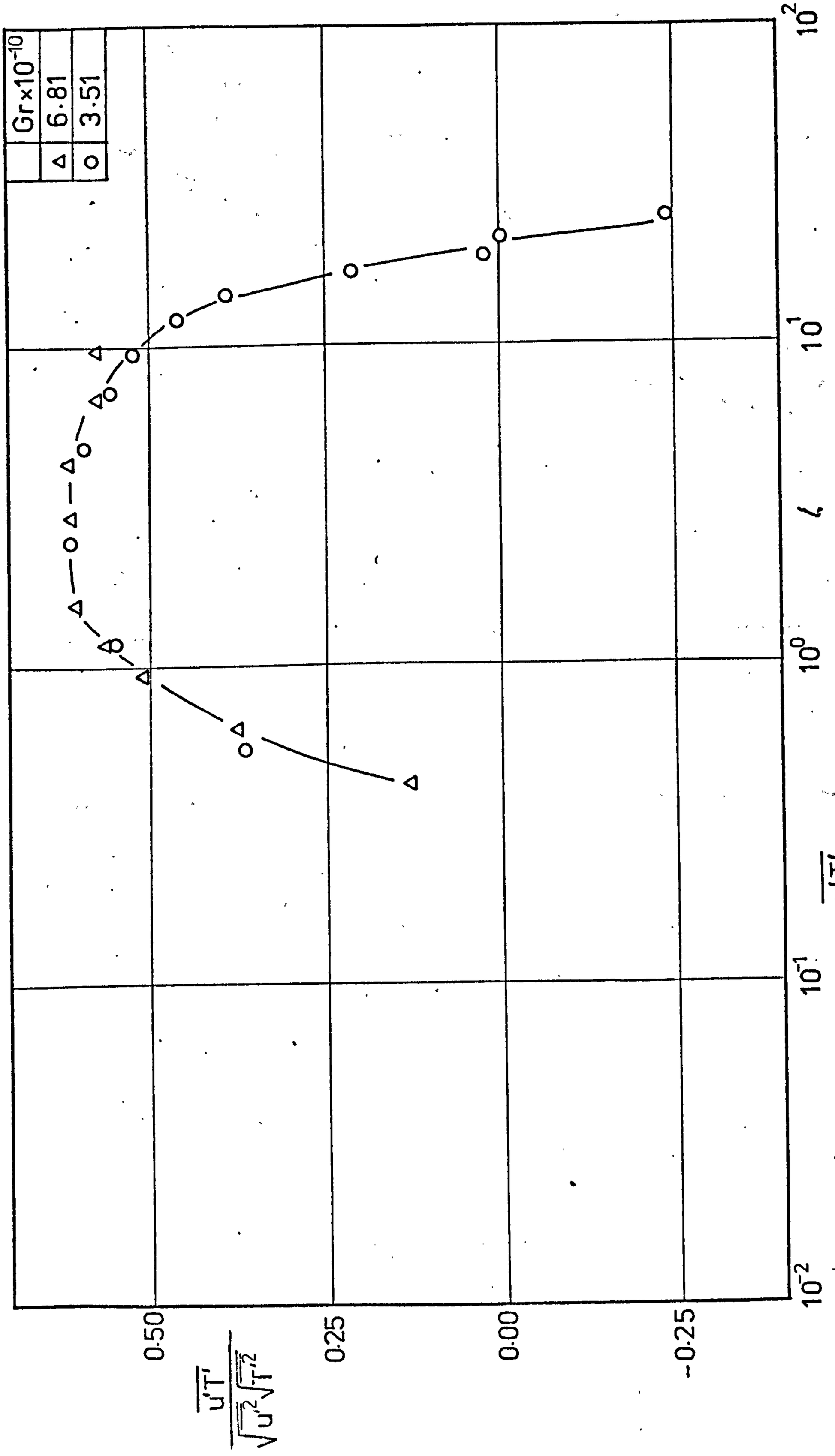
Gr×10⁻¹⁰
6.81
3.51
0.50
0.25
0.00
-0.25
$\frac{\overline{u'T'}}{\sqrt{\overline{u'^2}}\sqrt{\overline{T'^2}}}$
10^{-1}
10^{0}
10^{1}
10^{2}
10^{-2}
ℓ
profiles across the boundary layer

Fig. 8.27

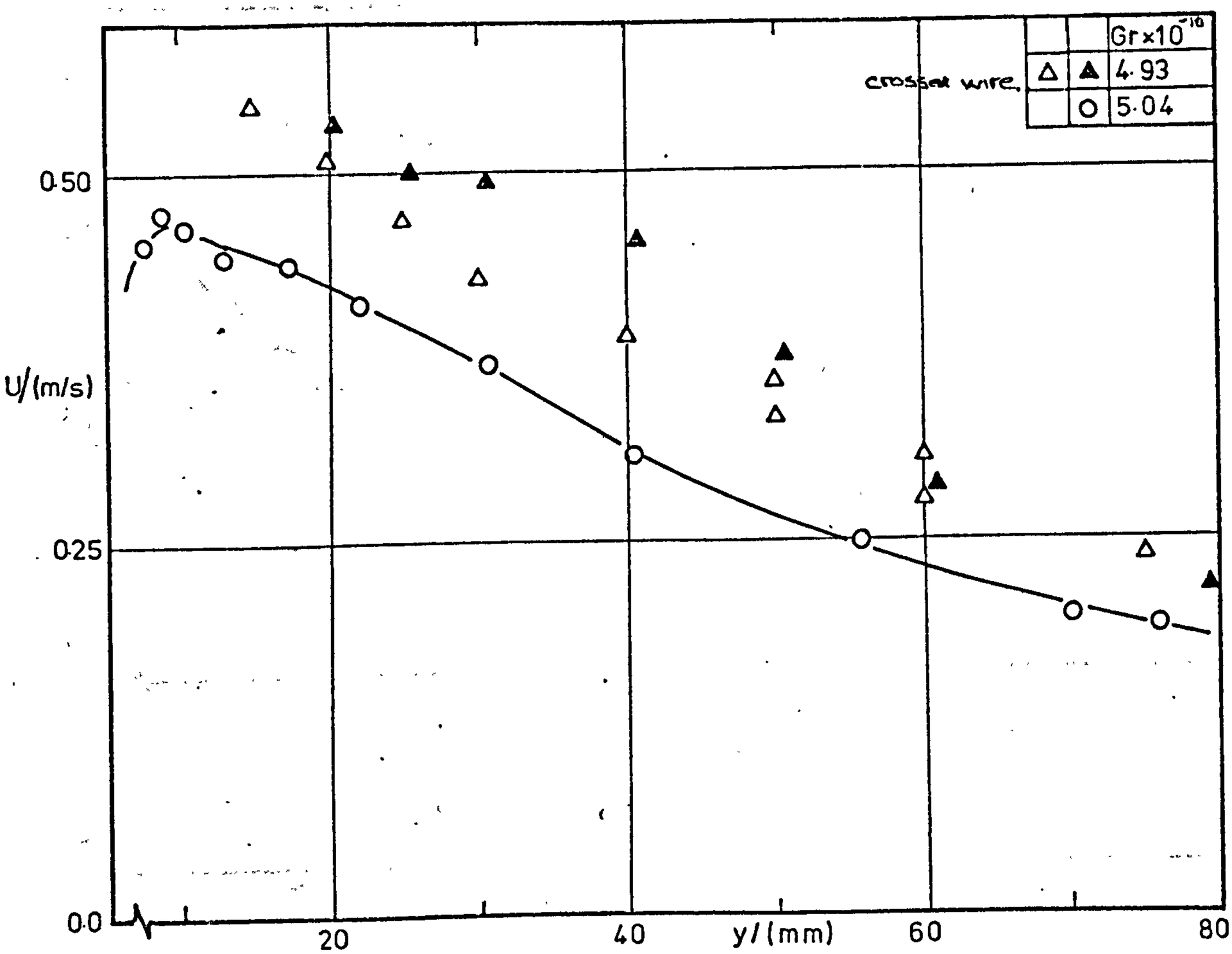

Fig. 8·28 Mean - streamwise velocity profiles across the boundary layer

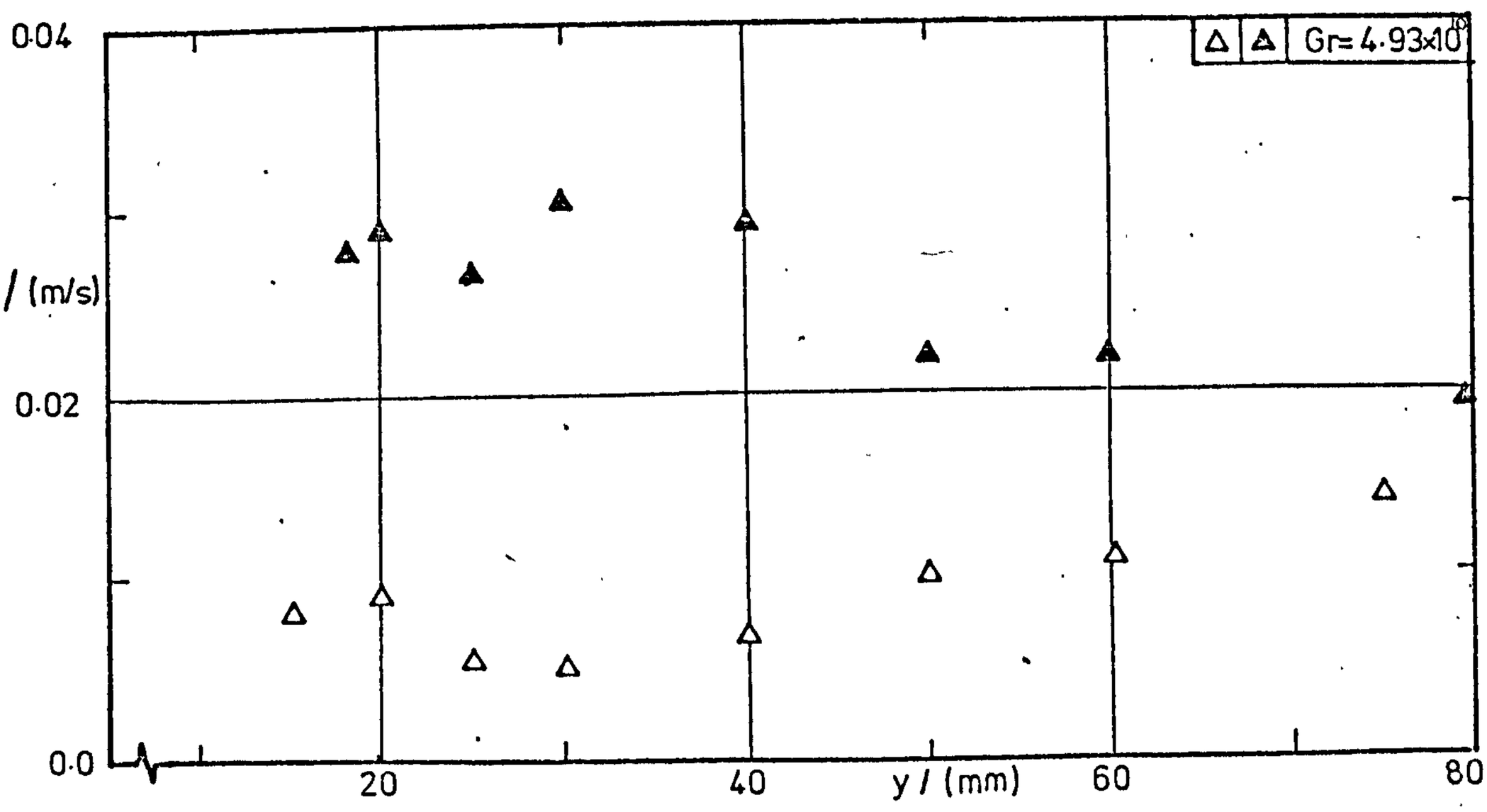

Fig. 8·29 Mean lateral velocity profiles across the boundary layer

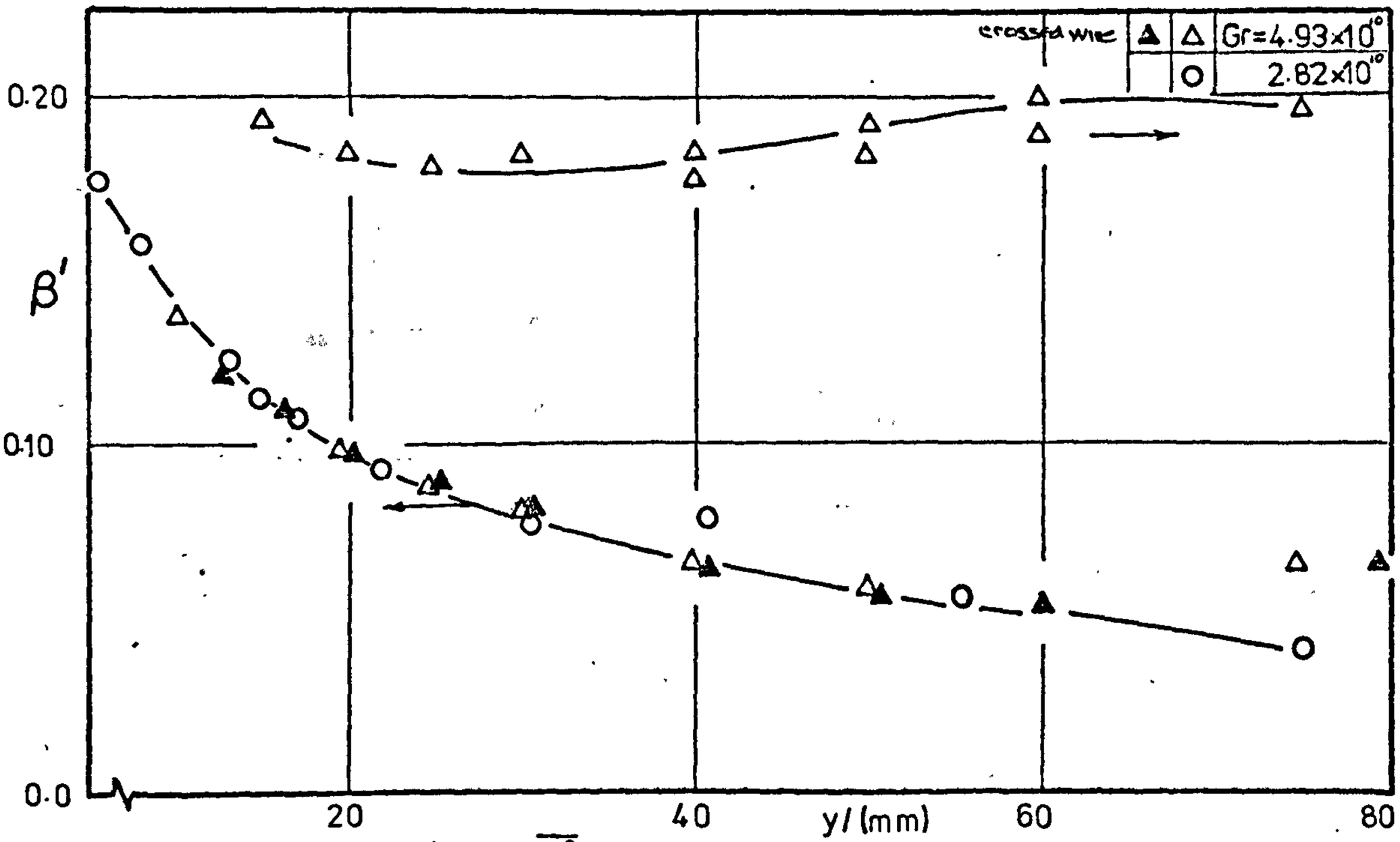

Fig 8.30 β' and $\frac{\overline{u'^2}}{\overline{v'^2}}$ profiles across the boundary layer

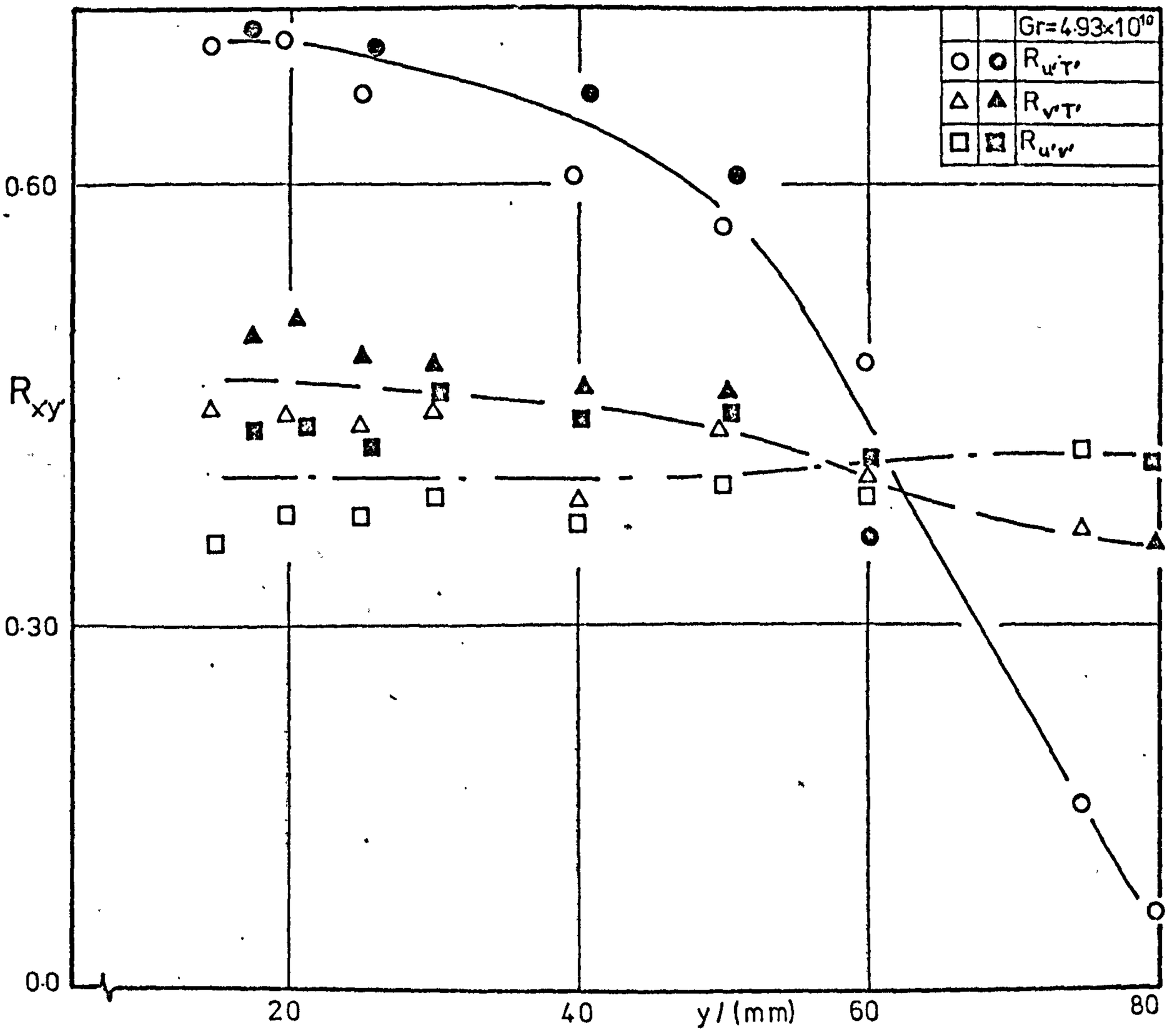

Fig. 8.31 Correlation coefficient profiles across the boundary layer

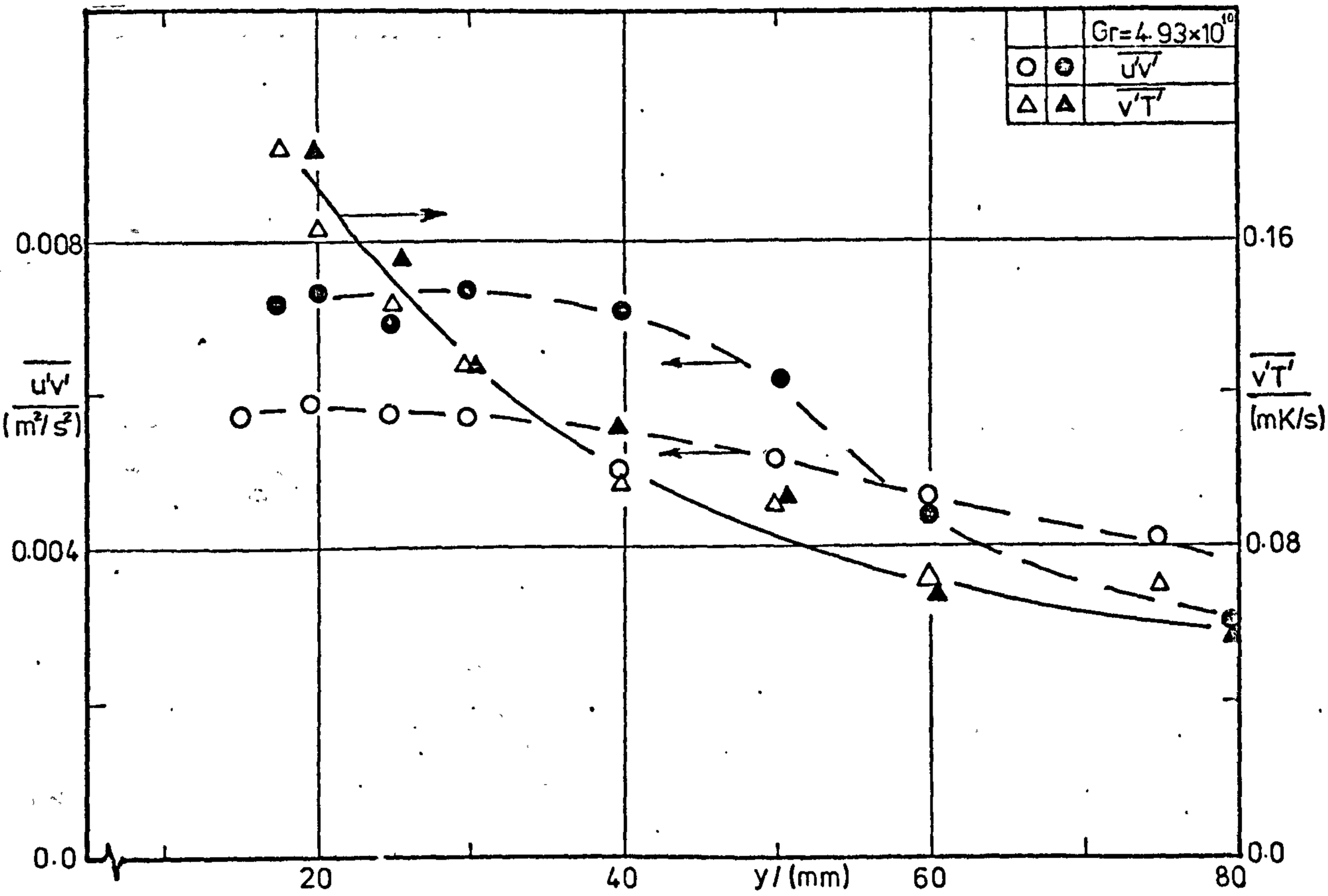

Fig 8.32 $\overline{u'v'}$ and $\overline{vT'}$ profiles across the boundary layer

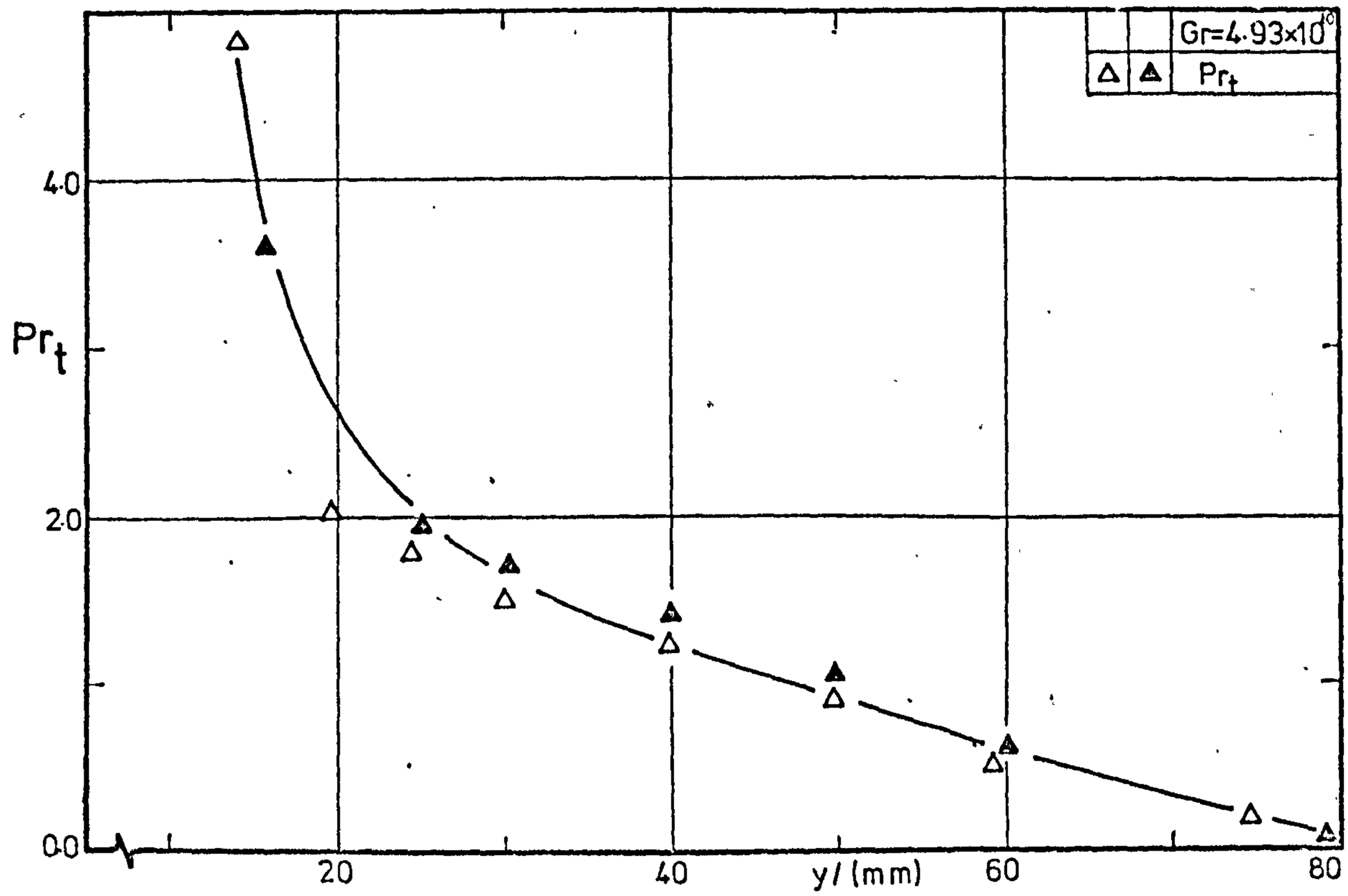

Fig. 8.33 Turbulent Prandtl number profile across the boundary layer

Fig. 8·34 Power spectra distributions

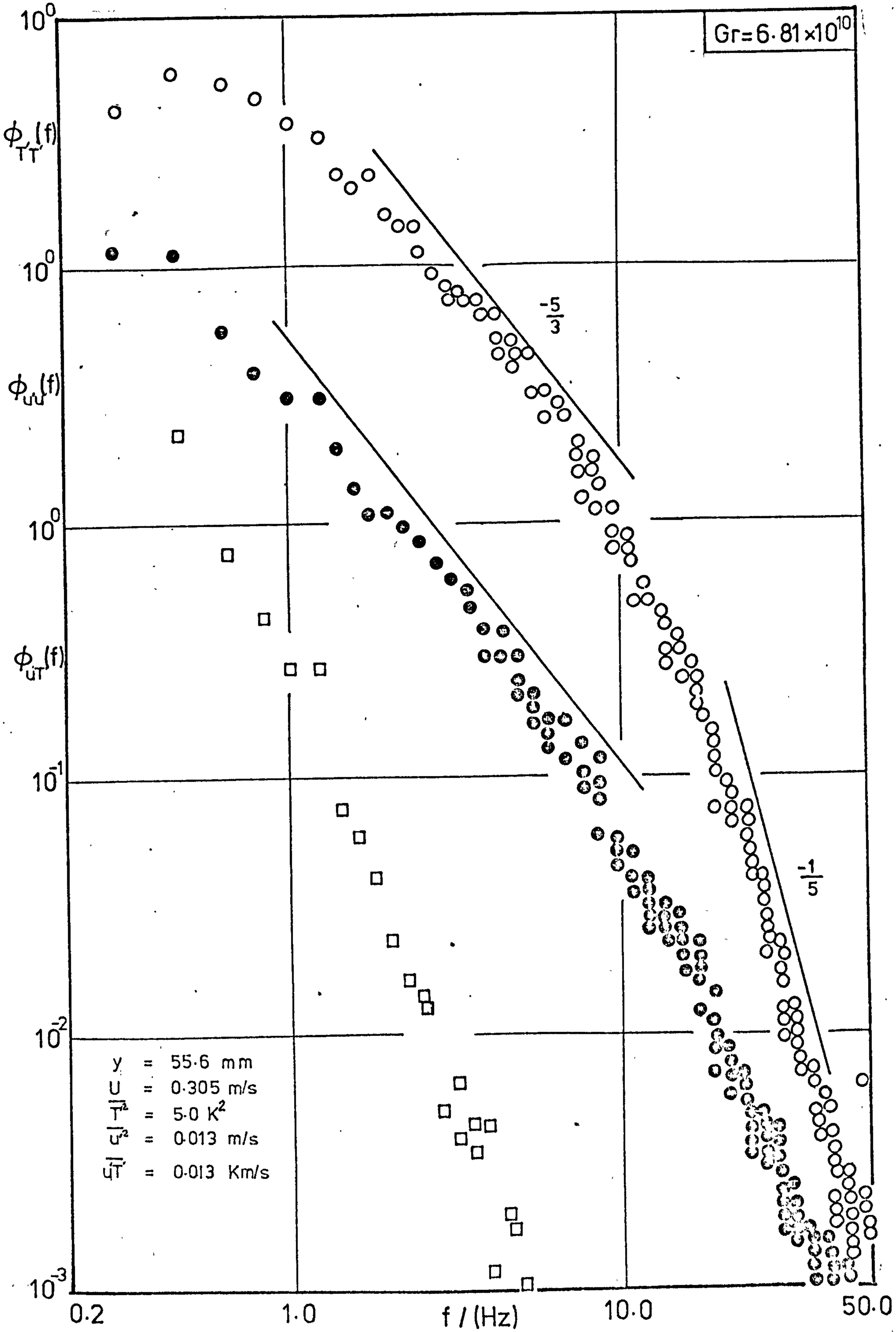

Fig.8·35 Power spectra distributions

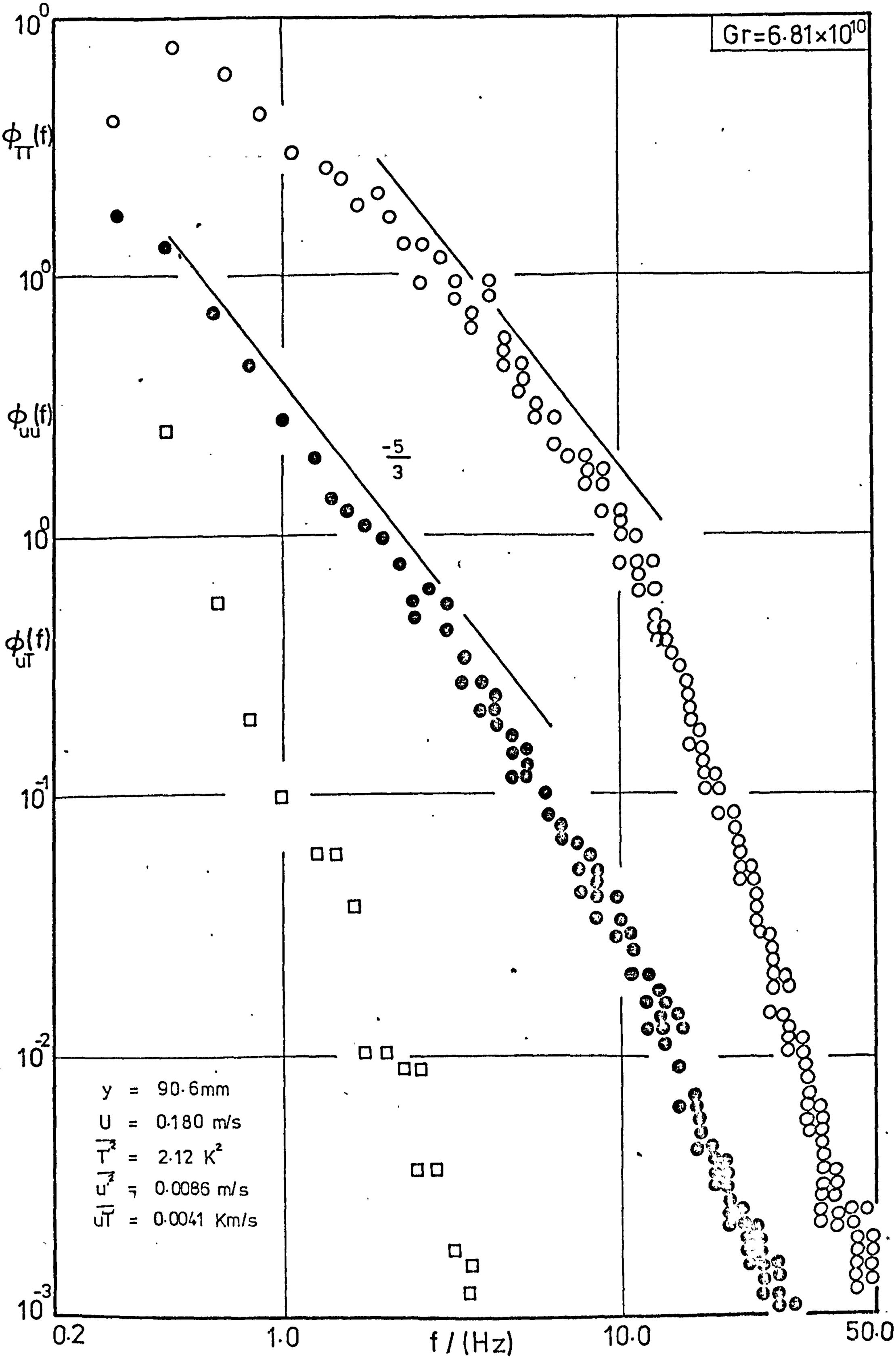

Fig. 8.36 Power spectra distributions

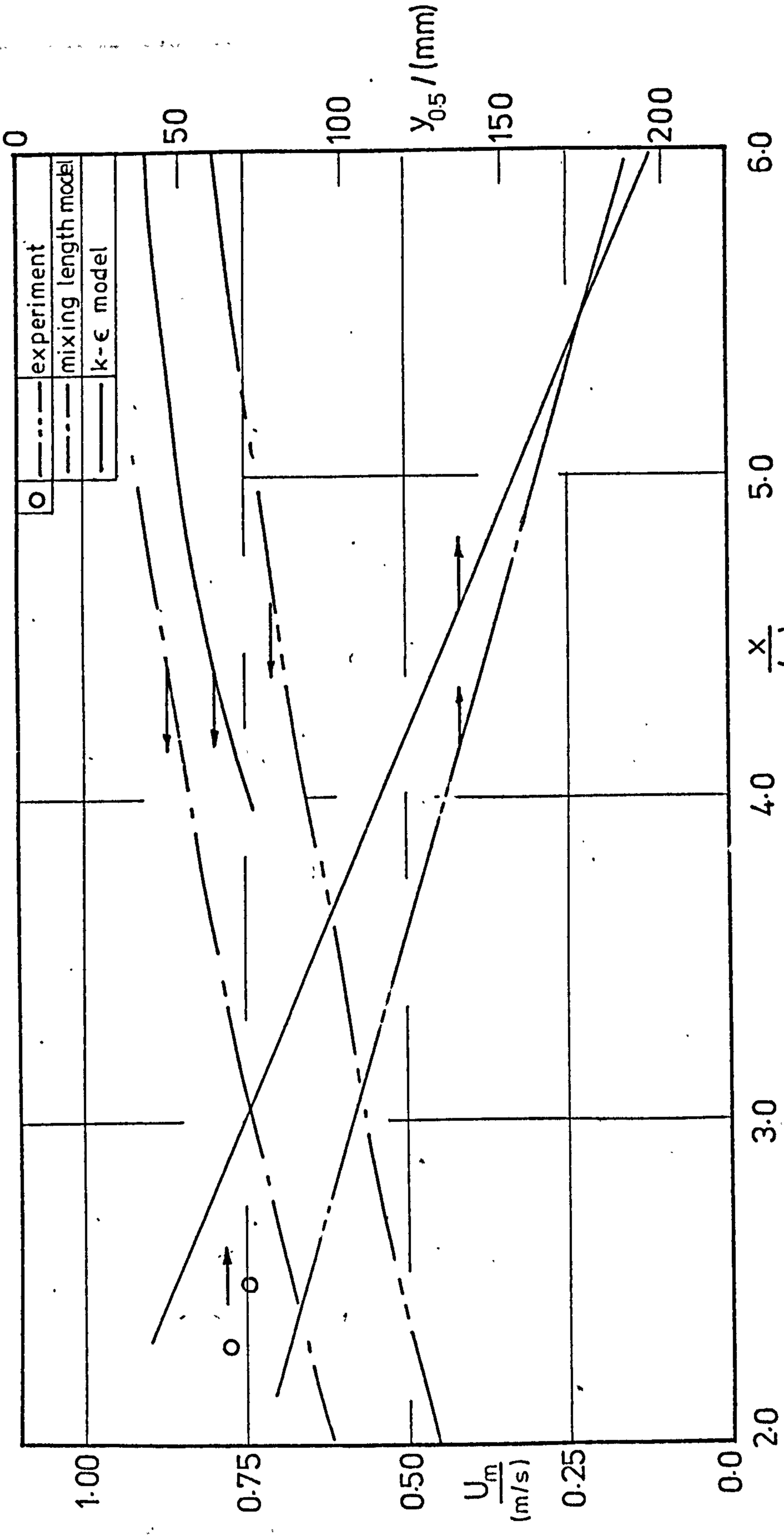

Fig. 10.1 Comparison of streamwise development of U_m and $y_{0.5}$

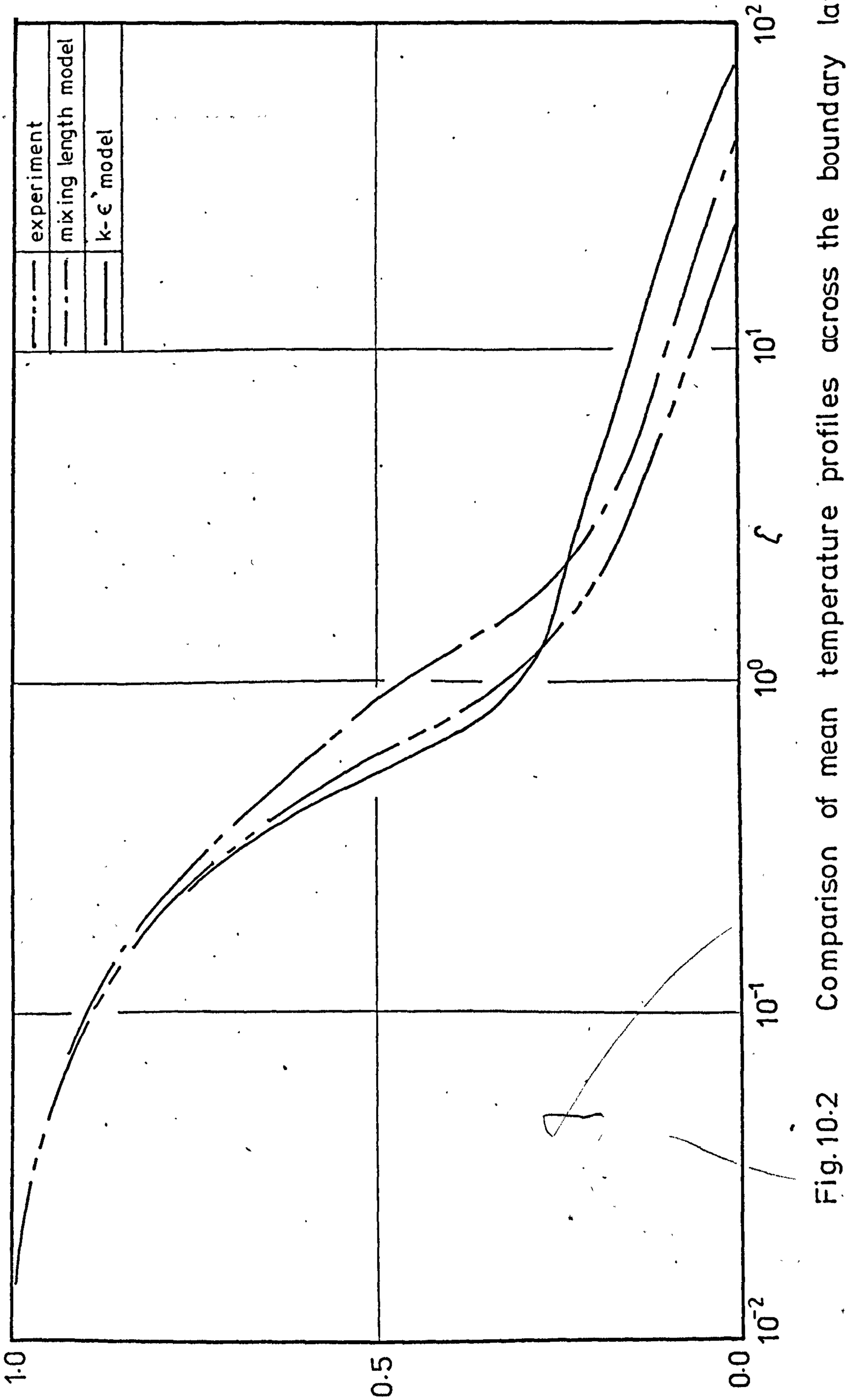

Comparison of mean temperature profiles across the boundary layer

Fig. 10.2

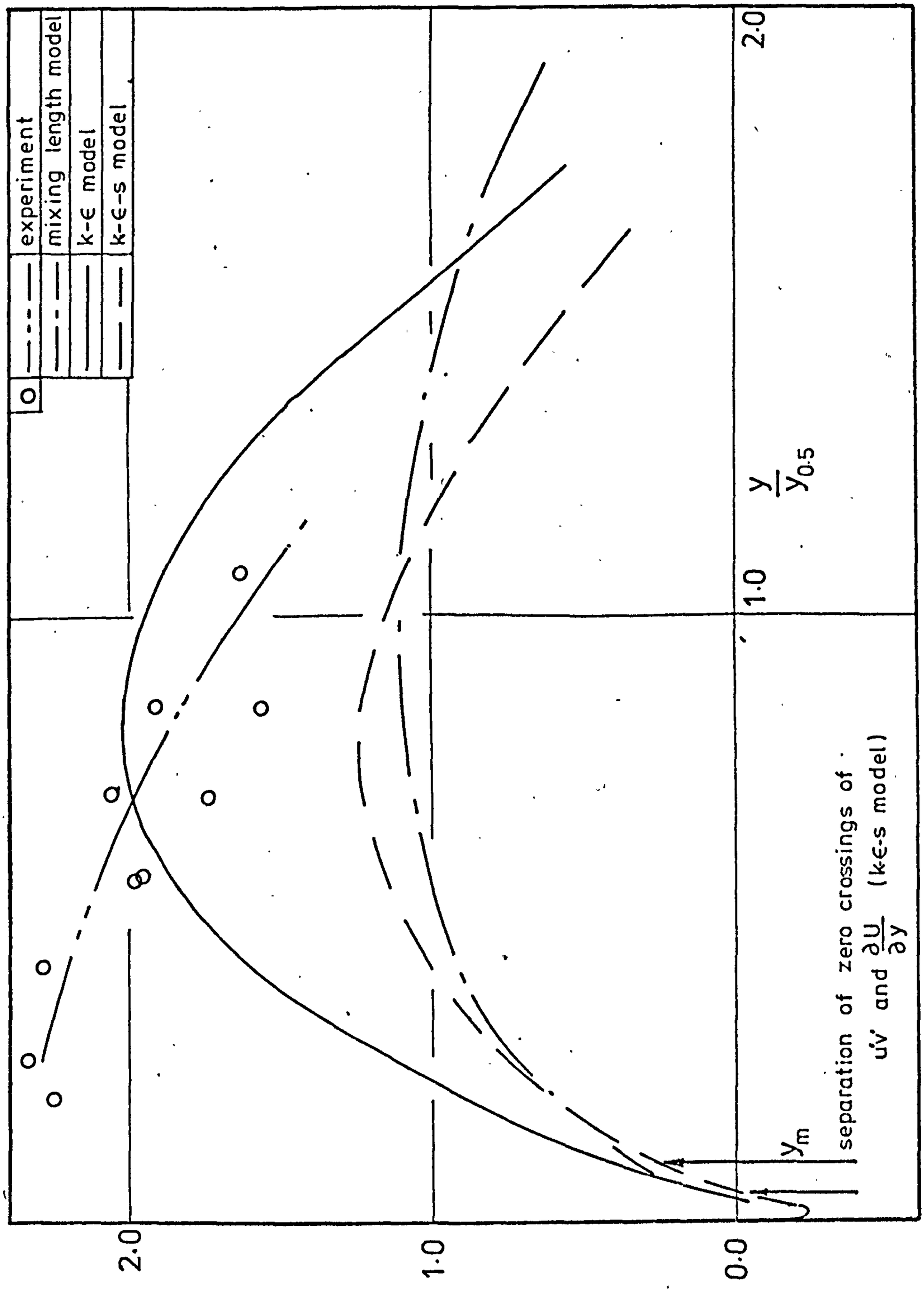

Fig. 10.3 Comparison of $\frac{\overline{u_1'u_2'}}{U_m^2}$ profiles across the boundary layer

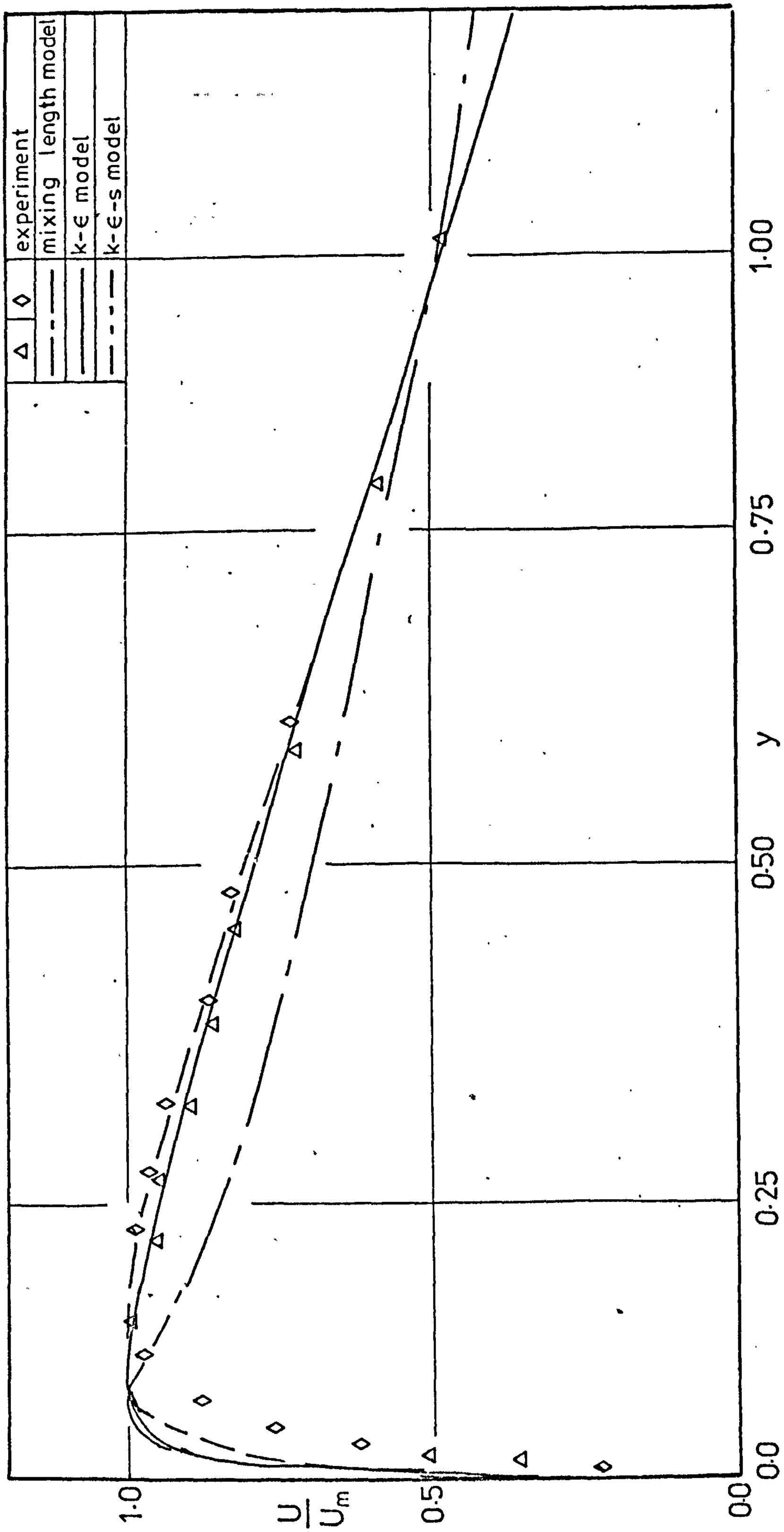

Fig. 10.4 Comparison of $\frac{U}{U_m}$ profiles across the boundary layer

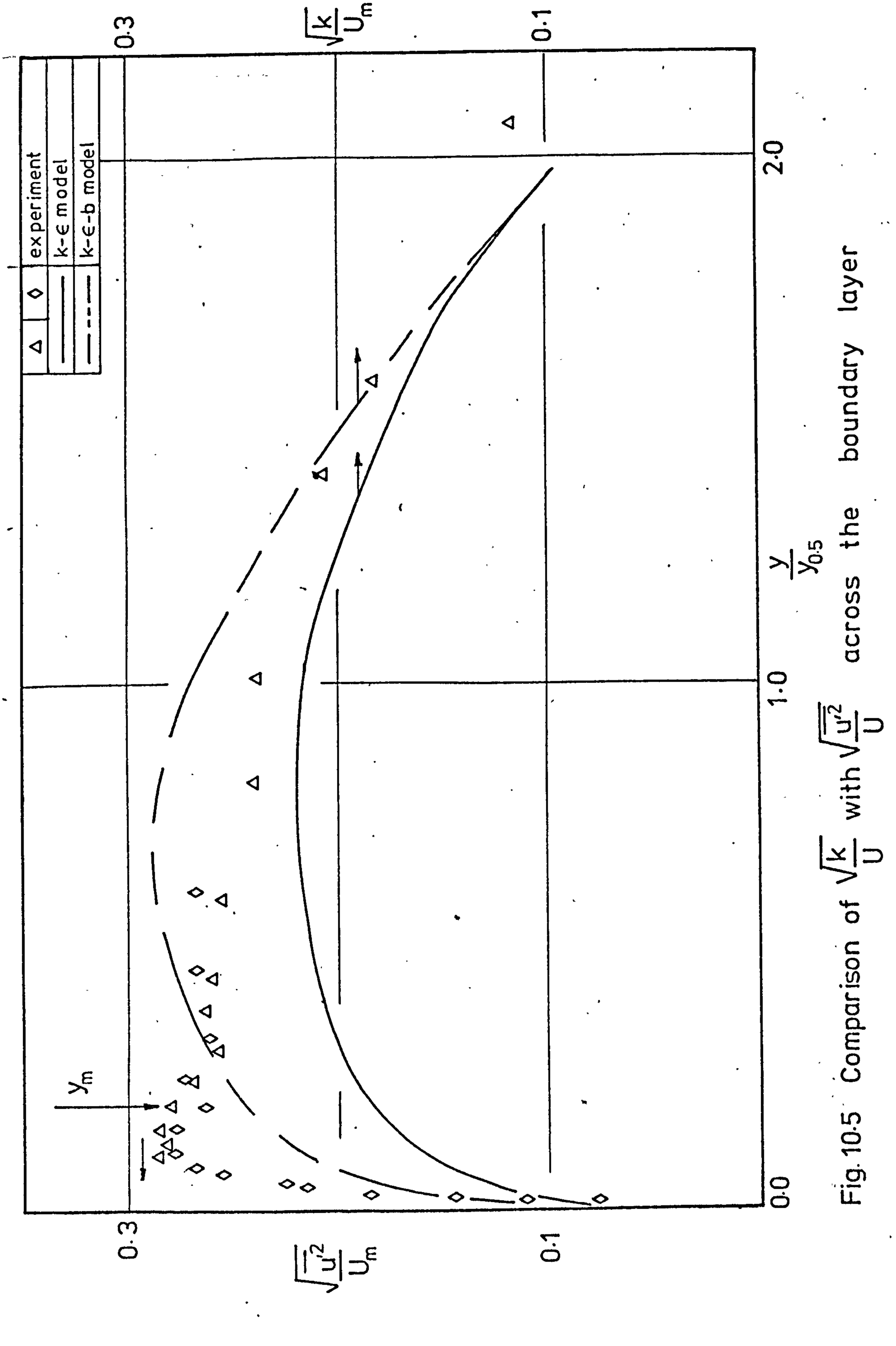

Fig. 10.5 Comparison

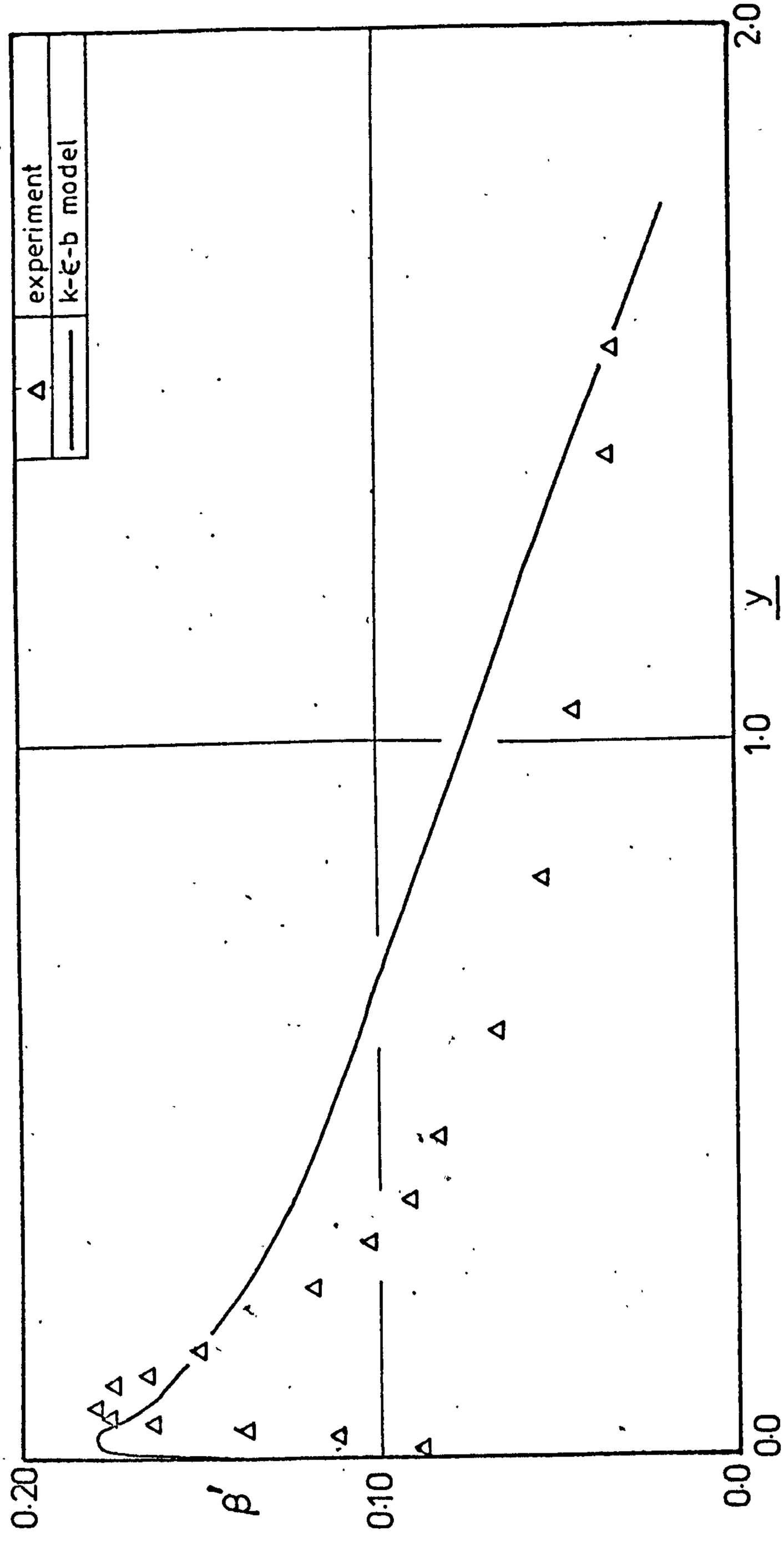

Fig. 10.6 Comparison of β' profiles across the boundary layer

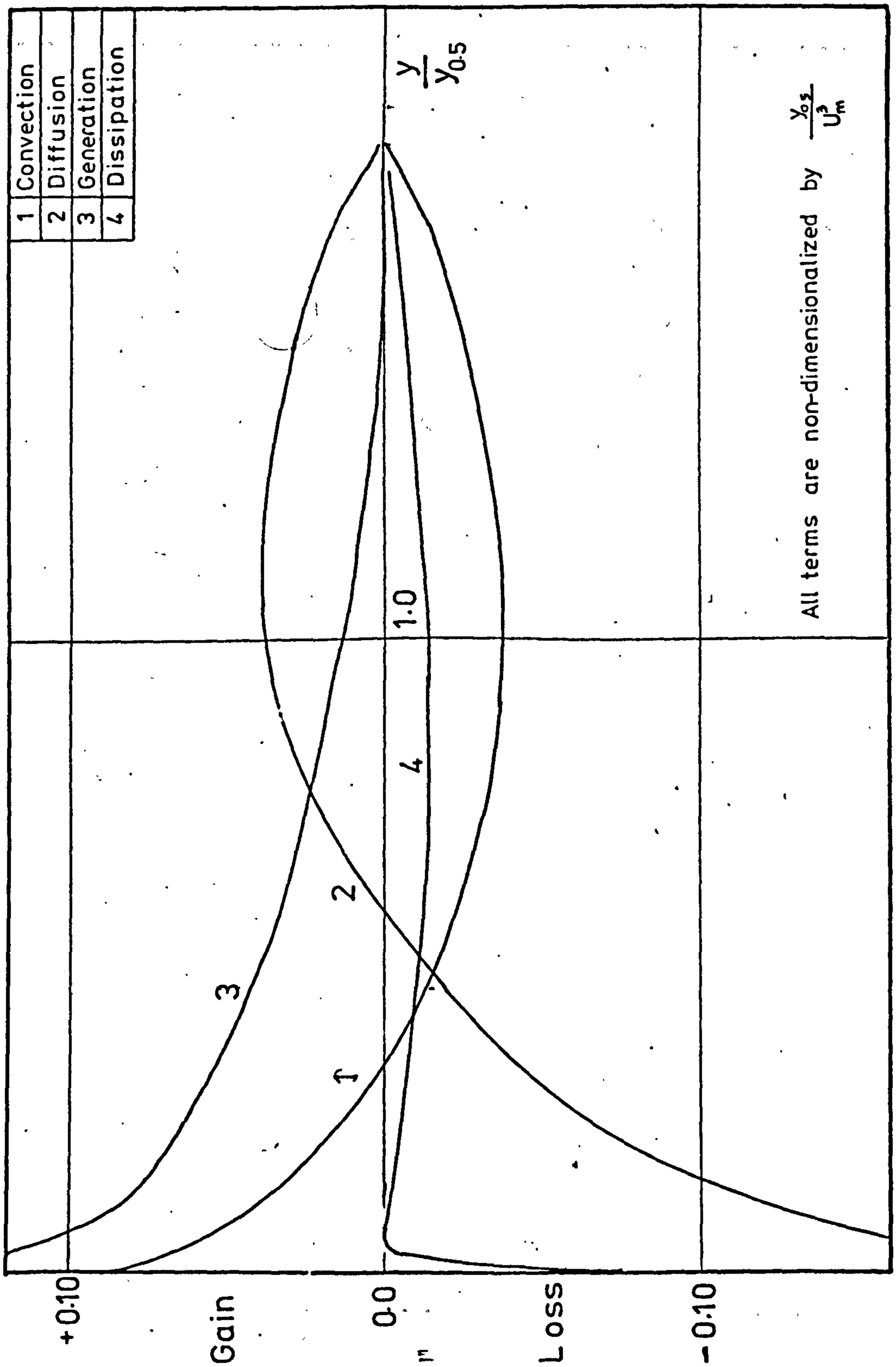

Fig. 10.7 Predicted mean kinetic energy balance

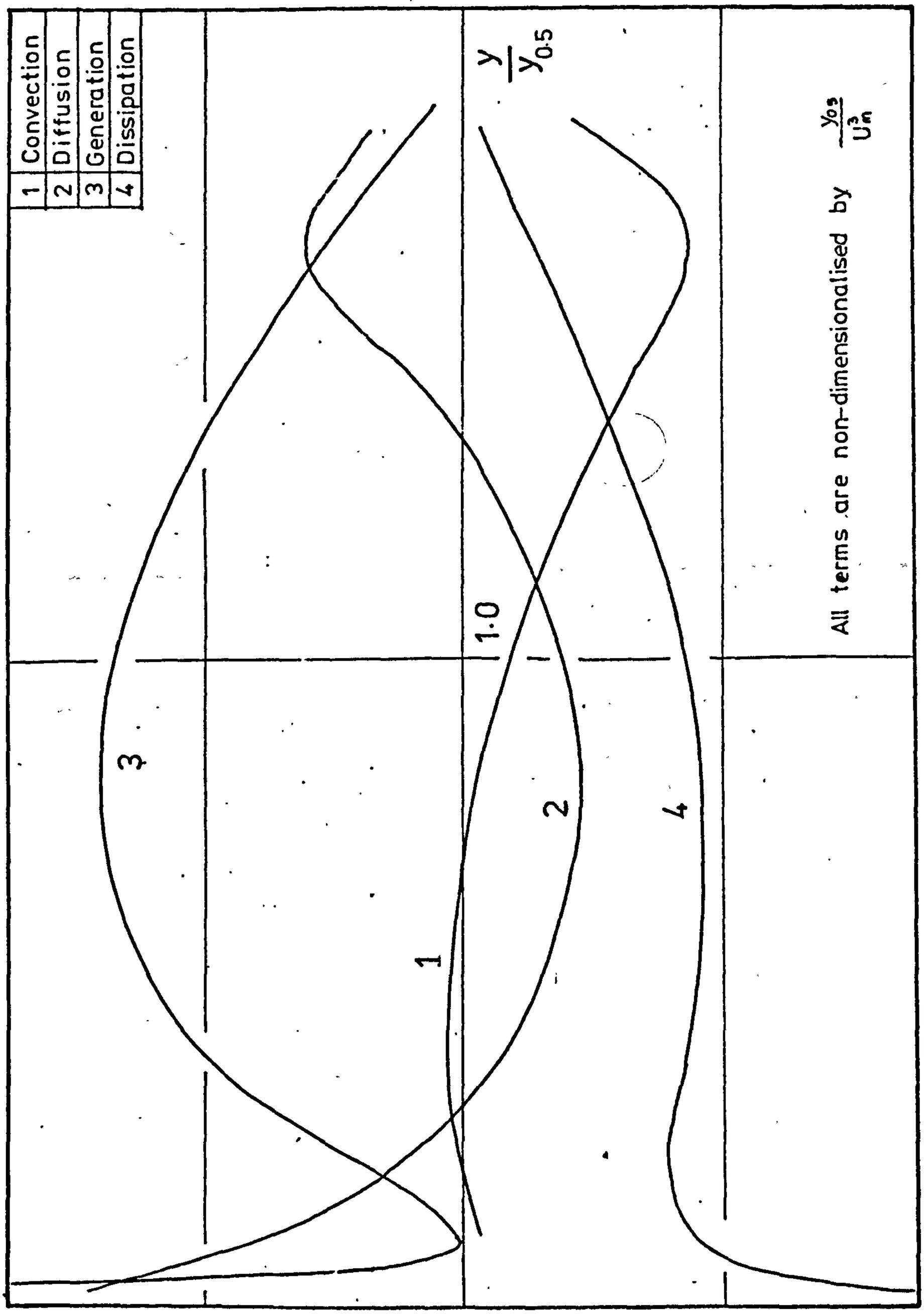

Predicted balance of turbulence kinetic energy.

Fig.10.8

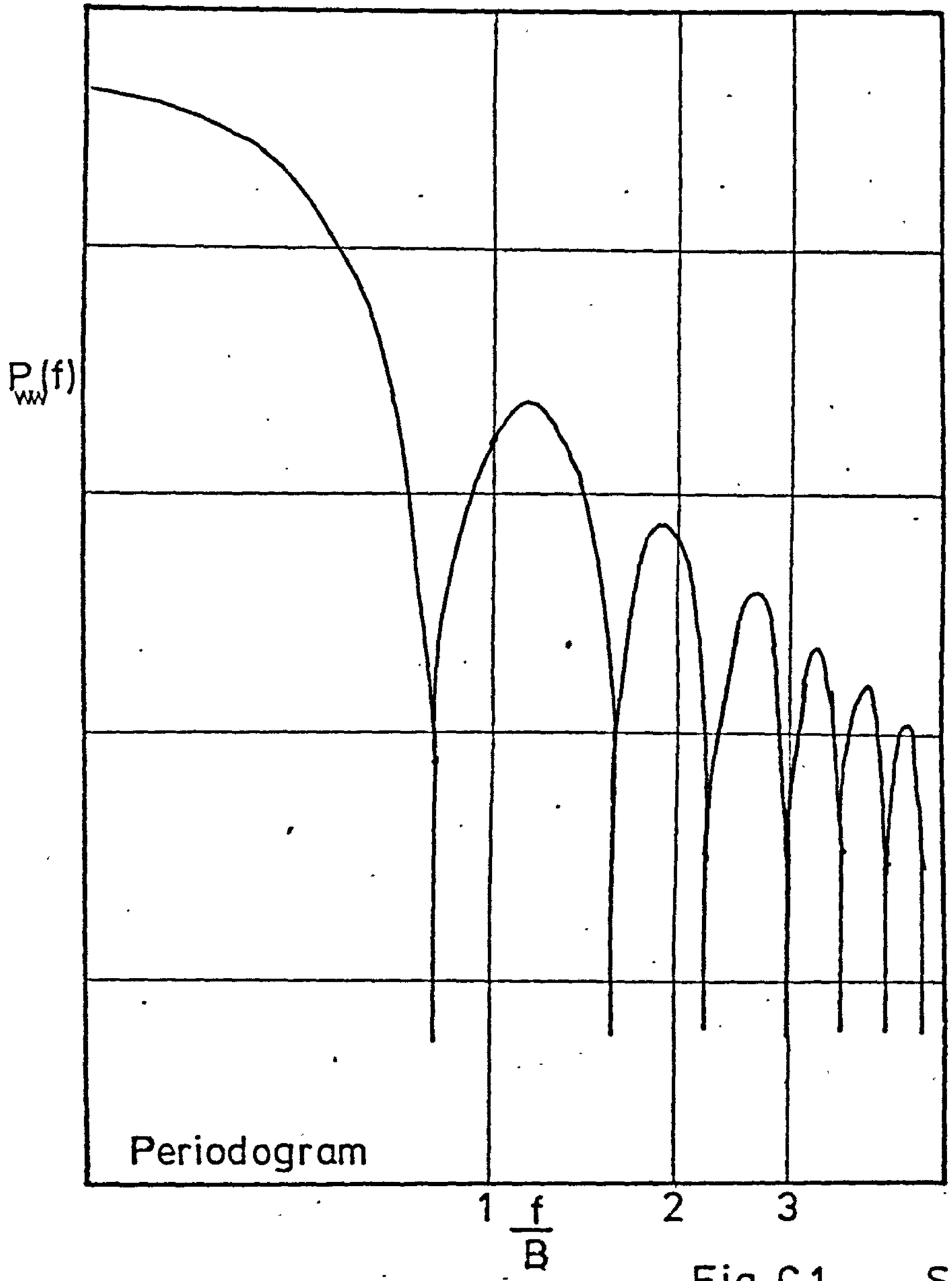

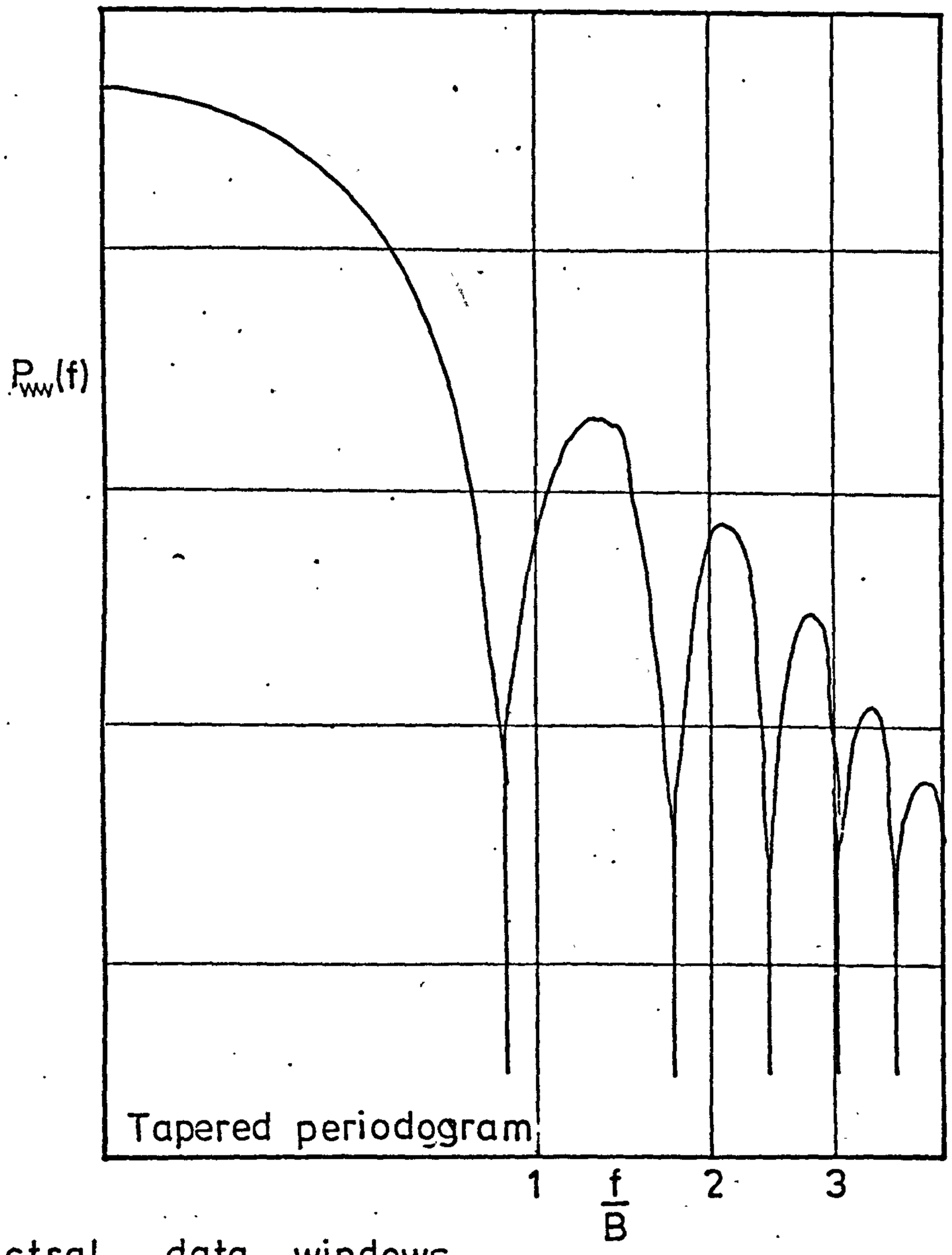

Fig. C.1 Spectral data windows

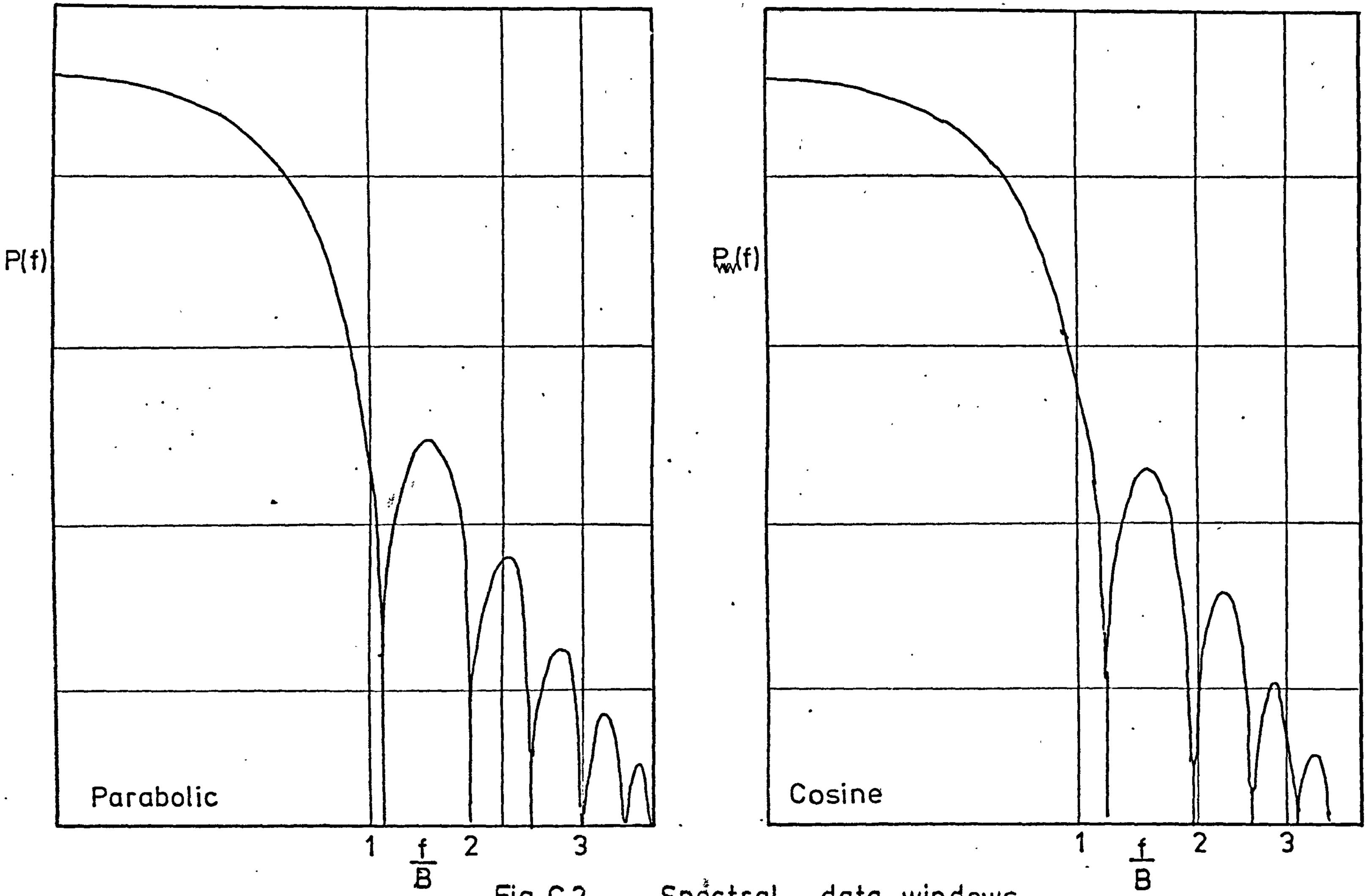

Fig. C-2 Spectral data windows